MCEER
LTIDISCIPLINARY CENTER FOR EARTHQUAKE ENGINEERING RESEARCH
lational Center of Excellence in Advanced Technology Applications

SN 1520-295X

PB2000-105994

Design and Retrofit Methodology for Building Structures with Supplemental Energy Dissipating Systems

by

Gokhan Pekcan, John B. Mander and Stuart S. Chen
University at Buffalo, State University of New York
Department of Civil, Structural and Environmental Engineering
Ketter Hall
Buffalo, New York 14260-4300

Technical Report MCEER-99-0021

December 31, 1999

This research was conducted at the University at Buffalo, State University of New York and was supported in whole or in part by the National Science Foundation under Grant No. CMS 96-16624.

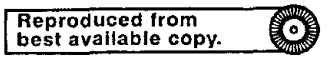

NOTICE

This report was prepared by the University at Buffalo, State University of New York as a result of research sponsored by the Multidisciplinary Center for Earthquake Engineering Research (MCEER) through a grant from the National Science Foundation and other sponsors. Neither MCEER, associates of MCEER, its sponsors, University at Buffalo, State University of New York, nor any person acting on their behalf:

a. makes any warranty, express or implied, with respect to the use of any information, apparatus, method, or process disclosed in this report or that such use may not infringe upon privately owned rights; or

b. assumes any liabilities of whatsoever kind with respect to the use of, or the damage resulting from the use of, any information, apparatus, method, or process disclosed in this report.

Any opinions, findings, and conclusions or recommendations expressed in this publication are those of the author(s) and do not necessarily reflect the views of MCEER, the National Science Foundation, or other sponsors.

MULTIDISCIPLINARY CENTER FOR EARTHQUAKE ENGINEERING RESEARCH
A National Center of Excellence in Advanced Technology Applications

Design and Retrofit Methodology for Building Structures with Supplemental Energy Dissipating Systems

by

Gokhan Pekcan[1], John B. Mander[2] and Stuart S. Chen[2]

Publication Date: December 31, 1999
Submittal Date: June 16, 1999

Technical Report MCEER-99-0021

Task Number 97-5000

NSF Master Contract Number CMS 96-16624
and
University at Buffalo Foundation Contract Number UBFS-9103-374825

1 Post Doctoral Research Associate, Department of Civil, Structural and Environmental Engineering, University at Buffalo, State University of New York
2 Associate Professor, Department of Civil, Structural and Environmental Engineering, University at Buffalo, State University of New York

MULTIDISCIPLINARY CENTER FOR EARTHQUAKE ENGINEERING RESEARCH
University at Buffalo, State University of New York
Red Jacket Quadrangle, Buffalo, NY 14261

Preface

The Multidisciplinary Center for Earthquake Engineering Research (MCEER) is a national center of excellence in advanced technology applications that is dedicated to the reduction of earthquake losses nationwide. Headquartered at the University at Buffalo, State University of New York, the Center was originally established by the National Science Foundation in 1986, as the National Center for Earthquake Engineering Research (NCEER).

Comprising a consortium of researchers from numerous disciplines and institutions throughout the United States, the Center's mission is to reduce earthquake losses through research and the application of advanced technologies that improve engineering, pre-earthquake planning and post-earthquake recovery strategies. Toward this end, the Center coordinates a nationwide program of multidisciplinary team research, education and outreach activities.

MCEER's research is conducted under the sponsorship of two major federal agencies: the National Science Foundation (NSF) and the Federal Highway Administration (FHWA), and the State of New York. Significant support is derived from the Federal Emergency Management Agency (FEMA), other state governments, academic institutions, foreign governments and private industry.

The Center's NSF-sponsored research is focused around four major thrusts, as shown in the figure below:

- quantifying building and lifeline performance in future earthquake through the estimation of expected losses;
- developing cost-effective, performance based, rehabilitation technologies for critical facilities;
- improving response and recovery through strategic planning and crisis management;
- establishing two user networks, one in experimental facilities and computing environments and the other in computational and analytical resources.

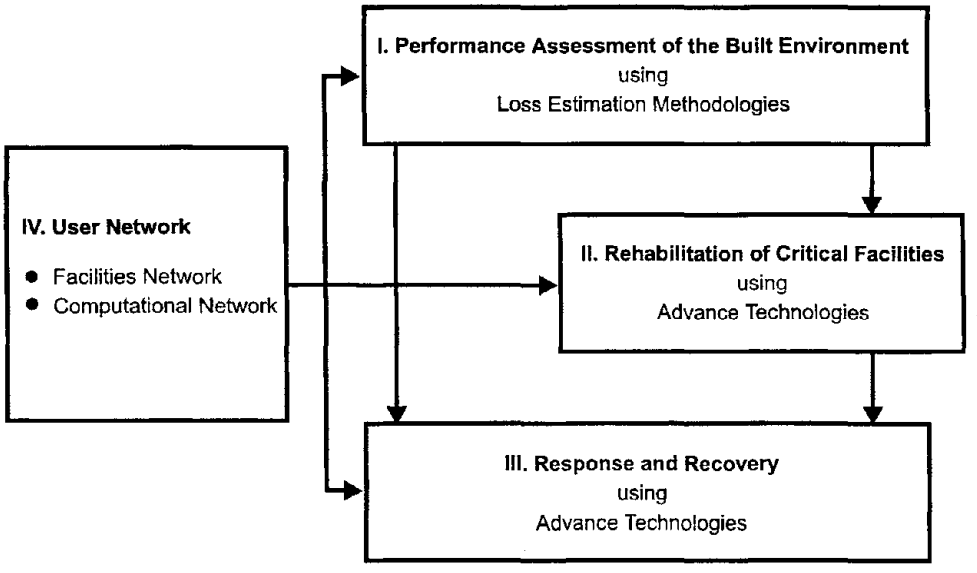

 Preceding Page Blank

The study described in this report focuses on fundamental issues related to the design and use of supplemental damping devices in building structures. The principle objective is to develop a generic/ practical analysis and design methodology for structures that considers structural velocities and equivalent viscous damping of the devices. These two issues are explored in depth. Tools to transform the spectral velocity to an actual relative structural velocity are provided, and a simple design procedure which incorporates power equivalent linear damping based on actual structural velocities is presented. The effectiveness of the design methodology is demonstrated with a retrofit design example using a supplemental load balancing tendon configuration.

ABSTRACT

This report considers two issues related to the design of nonlinear viscous dampers: structural velocities and equivalent viscous damping. As the effectiveness of non-linear viscous dampers is highly dependent on operating velocities, it is important to have reliable estimates of the true velocity in the device. This estimate should be based on the *actual* relative structural velocity and not the commonly misused spectral velocity. This is because spectral velocities are based on design displacements ($S_v=\omega_o S_d$) and are thus fundamentally different from the *actual* relative structural velocity. The difference between these two velocities is examined, and based on an extensive study of historical earthquake motions, empirical relations that permit the designer to transform the well-known spectral velocity to an *actual* relative structural velocity for use in design are proposed.

Nonlinear static analysis procedures recommended in current guidelines for the design of structural systems with supplemental damping devices are based on converting rate-dependent device properties into equivalent viscous damping properties based on an equivalent energy consumption approach. Due to the nonlinear velocity dependence of supplemental devices, an alternative approach for converting energy dissipation into equivalent viscous damping is advanced paper that is based upon *power consumption* considerations. The concept of a *normalized damper* capacity (ε) is introduced and a simple design procedure which incorporates power equivalent linear damping based on *actual* structural velocities is presented.

Based on these studies, general step-by-step retrofit/design algorithms are presented for building structures with supplemental damping systems. An overall strategy is presented for the various phases of the design process. This includes facets of conceptual and preliminary design as well as the final design verification process. The efficacy of the preliminary design phase is improved by a well-conceived SDOF idealization of the structural system. This is followed by a brief overview of performance objectives. The general normalized design parameters for the supplemental system are then transformed for the MDOF system based on the specific configuration details. Finally, the design of a nine-story building is presented as an example of the applicability of proposed design algorithms and alternative system configurations.

ACKNOWLEDGEMENTS

Financial support was primarily provided by Jarret Inc. of Cannonsburg, PA. Funding under the "Year 11" program was also provided by the Multidisciplinary Center for Earthquake Engineering Research (MCEER). Both sources of support are gratefully acknowledged.

TABLE OF CONTENTS

LIST OF FIGURES

LIST OF FIGURES – CONT'D

LIST OF FIGURES – CONT'D

LIST OF TABLES

SECTION 1

INTRODUCTION

1.1 BACKGROUND

As modern structures become taller, more slender and lighter with the advent of new structural materials, the quest for enhanced design and economical construction techniques becomes more pronounced. In particular, the control of seismic excitations and/or wind effects is essential to the well being of a structure. In the past, many design and analysis methods for structures subjected to seismic excitations have been proposed based on extensive analytical and experimental research. Most of the conventional seismic design and construction approaches rely on system ductility. Conventional ductile design requires that structures passively resist earthquakes through a combination of strength, deformability and energy dissipation. Lateral strength to the structure is provided to resist seismic loads in the form of moment resisting frames, shear walls, concentric and eccentric braces or a combination of these. To prevent collapse during severe earthquake excitation and to achieve an economical design for frame structures, shear walls are permitted to crack and yield, concentric braces are permitted to buckle and eccentric brace-shear links are designed to yield so as to reduce the inertia forces during earthquake shaking. Hence, inelastic deformations take place in the form of localized and/or spread plasticity in hinges that result in increased flexibility and energy dissipation. These inelastic actions, however, result in damage to the structural members.

It is now well know that supplemental damping through the use of mechanical energy dissipating devices improves the seismic performance of structures by reducing deformations and forces in the structural members. Supplemental damping devices dissipate earthquake-induced energy through yielding of metals, sliding friction, viscous and visco-elastic action, etc. However, the amount of response reduction varies depending not only on the supplemental damping provided but also on the inherent mass, stiffness and damping characteristics of the parent structure. A comprehensive review of the characteristics of various devices and their implementation in building structures can be found in Constantinou et al. (1998).

The increasing number of building structures that are either retrofitted or designed using energy dissipation devices, however, requires a simple, yet accurate design methodology that

eliminates rigorous analysis. Much research has been done to investigate various kinds of supplementary damping systems. Preliminary design guidelines have been suggested based on the results obtained from numerous experimental and analytical studies. Whittaker (1992) was first to propose general guidelines for the design of structures incorporating energy dissipating systems. Currently, several documents, specifications and guidelines provide building design formulations that are based on available research findings. In fact, various simplified linear and nonlinear analysis and design procedures have recently been suggested in *NEHRP Guidelines for the Seismic Rehabilitation of Buildings* (FEMA 273) and its *Commentary* (FEMA 274). These documents contain the most up-to-date analysis and design guidelines for buildings that incorporate energy dissipating as well as seismic isolation systems. The capacity-demand spectral approach is employed for one of the nonlinear static procedures in which the structural response is found at the intersection of capacity and demand curves. The reduced demand is determined as a function of the available damping in the structural system such as: inherent and hysteretic (if any) damping, and/or supplemental devices (if any). The added damping associated with the supplemental energy dissipating devices is approximated with an "effective" damping based on equivalent linear viscous properties. Hence, five percent-damped demand spectra is modified to account for the total effective damping in the structure.

Various other design methods for building structures with supplementary damping systems have been suggested by Shen and Soong (1996), and Gluck et al. (1996). Shen and Soong proposed a design method for multistory reinforced concrete structures that is based on the concept of damage control. In their study, they used equivalent SDOF system properties in determining a damage index recommended by Park and Ang (1985) and included the effect of energy dissipating devices implicitly through maximum deformation and hysteretic energy quantities. Gluck et al. adopted optimal control theory using a linear quadratic regulator to design linear viscous or visco-elastic devices. It was proposed that the gain matrix obtained by minimizing a performance index that ensures optimality can be used to determine the damping system properties in terms of constant stiffness and damping coefficients.

1.2 Objectives and Scope

This study focuses on fundamental issues related to the design of supplemental damping devices for building structures. In general, various techniques and approaches adopted in current

guidelines for the design of damping devices are based on equivalent linear properties, namely, equivalent linear damping and stiffness properties of the device under consideration. These simplified procedures are approximate due to the assumptions involved in the equivalent linear presentation of nonlinear properties of the structure and the supplemental damping system. It must be noted that the accuracy of design and retrofit methods for building structures may largely depend on the "quality" of the linearized (approximate) parameters versus their actual values. In fact, traditionally, equivalent damping is determined based on the equivalent energy consumption approach. However, in this study, the development of equivalent linear properties based on the notions of power consumption equivalent between a viscously damped system and a system possessing nonlinear [viscous nature] dampers is proposed (Pekcan et al. 1999a).

Furthermore, it must be noted that the general behavior of viscous devices is governed by the structural velocities. To successfully use the spectral design methodologies such as the capacity-demand spectral approach, it is essential that actual structural velocities be used in all of the equivalent damping formulations. This is because if the spectral velocities based on design displacements ($S_v = \omega_o S_d$) are used, errors are introduced as the two velocities are not equivalent across the spectrum. Hence, simplified design formulations are given for the proposed transformations to actual velocities.

Finally, the principal objective of this study is to propose a generic/practical analysis and design methodology for supplemental damping devices, which address the issues mentioned above along with the uncertainties involved in the assessment of the seismic demand. The effectiveness of the design methodology is demonstrated with a retrofit design example using an innovative supplemental load balancing tendon configuration, previously introduced by Pekcan et al. (1999b, 2000).

1.3 Organization of this Report

Section 2 presents an overview of the capacity-demand spectral design approach. Various steps involved in the pushover analysis to determine the structural capacity are described and an alternative elasto-plastic analysis approach is introduced. Section 3 focuses on the fundamental considerations for the design of supplemental damping systems. The design formulations for a pseudo-actual velocity transformation are given following a discussion of the differences between the two quantities. Also discussed in this section is the proposed equivalent

linear damping for the nonlinear [viscous nature] devices based on the equivalent power consumption approach. Finally, various phases involved in designing supplemental systems for building structures are introduced in Section 4. Design steps for two alternative device configurations are given. Section 5 presents the retrofit design example of a nine-story flexible steel building and discusses the performance of these two alternative configurations. Conclusions are drawn and recommendations are made in Section 6.

SECTION 2

CAPACITY-DEMAND SPECTRAL DESIGN APPROACH

2.1 INTRODUCTION

In this section, capacity-demand spectral design approach is reviewed in detail. First, techniques used to evaluate the structural capacity to form so-called capacity spectrum are discussed. A simplified elasto-plastic approach is introduced to determine the structural capacity of building structures. This approach consists of an elastic analysis step to determine the initial elastic period of the structural system. In the second step, a generalized plastic analysis is formulated to evaluate the ultimate base shear capacity. Finally, various sources of uncertainties involved in the assessment of the seismic demand are discussed and quantified through a statistical analysis on 36 earthquake ground motions and their components.

2.2 BACKGROUND

Linear elastic analysis and design methods are in general not permitted or appropriate for inelastic structures with or without supplemental damping systems. A significant departure from linear elastic analysis has been the adoption of nonlinear methods of analysis over the last decade. Dramatic advancements in the development of computational tools have made nonlinear time history analysis methods easily accessible to the practicing engineers. This took place almost concurrently with the establishment of the capacity design principles as the preferred design methodology. Engineers had the opportunity to design their structures and check the validity of their designs using sophisticated computer programs (DRAIN-2DX, IDARC, etc.). However, this meant that analysis became more involved and significant attention had to be paid to detail every aspects of the computer model of the actual nonlinear structure. Hence, there have been extensive studies focused on simplified nonlinear static procedures that are utilized in developing design methods.

As will be discussed in the subsequent sections, response spectrum analysis is a well-known method to evaluate the seismic response of structures. Elastic as well as inelastic response spectra can be generated for many different types of ground motions. Furthermore, approximate inelastic spectra can be obtained from elastic response spectra performing appropriate adjustments that are based on the system ductility (Newmark and Hall, 1982). It

must be noted that, in applying response spectra methods for the analysis and design of structures, it is generally necessary to idealize the multi-degree-of-freedom (MDOF) system with an equivalent single-degree-of-freedom (SDOF) system.

An alternative and attractive representation of structural response is to use a composite capacity-demand spectral approach which monitors the acceleration and displacement response simultaneously. Freeman et al. (1975) and Freeman (1978) first suggested the so-called Capacity-Spectrum Method. This type of spectral representation (Capacity-Demand Curves) of the maximum inertia forces vs. the maximum displacement response was used for the evaluation of elastic as well as inelastic structures by Kircher (1993), Freeman (1994) and Mahaney et al. (1993). The Capacity Spectrum Method is the preferred method in this study. In fact, it is a nonlinear static procedure that provides a graphical representation of the global force-displacement, *capacity* curve of the structure (which is referred as "pushover") and compares it to the response spectrum representations of the earthquake *demand.* It must be noted that *demand* is a representation of the earthquake ground motion hazard whereas *capacity* is the resistance exhibited during the dynamic response as a reaction to the inertial and damping forces.

The capacity spectrum method estimates the peak response by expressing both the structural capacity and seismic demand in terms of spectral accelerations and displacements. The response of a nonlinear structure can be estimated graphically as the point where the capacity curve of the structure intersects the elastic demand curve that corresponds to the available damping in the structural system. Hence, one of the steps in capacity spectrum method is the determination of the pushover capacity of the structural system via pushover analysis. The theoretical background, formulations and various issues related to the evaluation of pushover capacity (lateral strength) are discussed in detail in the following sections.

In the second step of the capacity-demand spectral design approach, demand curves for various effective damping within the structural systems are generated using demand reduction factors. The amount of reduction of 5% damped demand spectra associated with a specific effective damping is based on the median spectral amplification factors proposed by Newmark and Hall (1982). These factors vary depending on the effective period of the system at the performance point. In general, both effective period and effective damping are amplitude dependent. Up to yield, effective period is the same as the initial period calculated based on the elastic pushover stiffness of the structure. Corresponding effective damping is equal to inherent

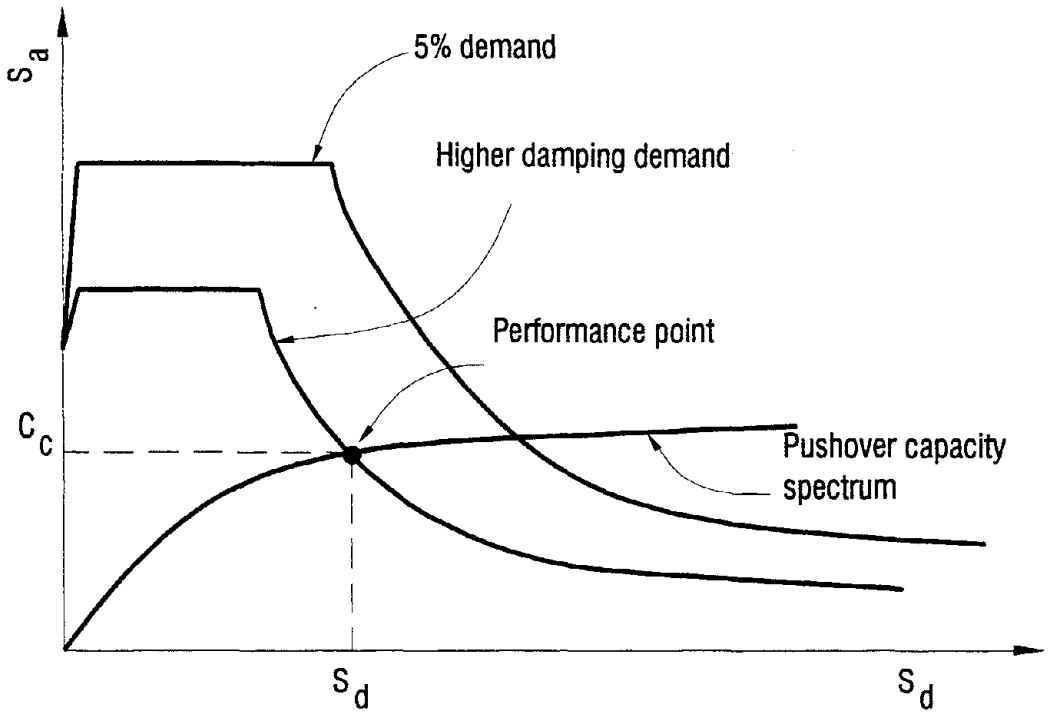

Figure 2-1 Graphical Interpretation of the Capacity Spectrum Method

structural damping (usually 2 to 5%). After yield, effective period lengthens and effective damping increases as inelastic deformations take place.

The capacity spectrum method is graphically shown in figure 2-1.

2.3 Evaluation of Structural Capacity

In general pushover analysis explicitly incorporates the nonlinear behavior of the structure in a quasi-dynamic fashion. The structure is subjected to assumed lateral loads of specified distribution (pushover mode) and analyzed for increments of loads. Corresponding base shear is plotted versus the deformation at a specified node. Pushover curve of the structural system is then converted to an equivalent capacity curve using appropriate transformations.

2.3.1 Pushover Analysis

One of the key elements in Capacity Spectrum Method is to establish the capacity of the structure under consideration through an appropriate pushover analysis. This can be achieved by plotting force-displacement curve for the structure by tracking the base shear and roof displacement. This curve so obtained is called the "pushover capacity". It becomes almost a trivial task during the design process when a nonlinear structural analysis program is used, such as DRAIN-2DX, IDARC etc. For a displacement-controlled pushover analysis, a target displacement profile is specified and applied in increments to the structure. In general, modal values that define the first mode shape can be used as unit load factors at the corresponding floor levels. The nonlinear pushover analysis is then carried out by applying incremental displacements in the direction of applied unit loads and calculating the corresponding structural force response for each instant of deformation increments. However, a force-controlled analysis is usually preferred since so-called displacement profile is generally not known *a priori*. In force-controlled pushover analysis, a mathematical model of the structure is subjected to a predefined lateral force distribution. The distribution of lateral forces mimics the distribution of maximum inertial loads induced at location of lumped story masses in case of a ground shaking and depends mostly on the dominant mode shape. In either case, the structural displacement at a predefined control node (e.g. roof displacement) is plotted against the total base shear to form the pushover curve as shown in figure 2-1.

The lateral load pattern can be determined using a code type equation:

$$F_x = \frac{w_x h_x^k}{\sum_{i=1}^{n} w_i h_i^k} V_b \tag{2-1}$$

in which w_i = portion of the total building weight (W), $w_{x\ (or\ i)}$ = portion of the total building weight (W) located on floor x, $h_{i\ (or\ x)}$ = height from the base to level i (or x), k = constant that determines the shape of the load pattern, and V_b = design base shear. Shape constant determines the shape of the load pattern and can take values between 1 and 2 as:

$$1 < k = 1 + \frac{T - 0.5}{2} < 2 \tag{2-2}$$

where T = considered fundamental period of vibration of the structure. If the shape constant k = 1, the corresponding load pattern is an inverted triangle which emphasizes the dominant first mode response.

The static pushover analysis has no rigorous theoretical background. It is based on the premise that the response of a MDOF structure is essentially governed by a single mode that remains constant through out the time history analysis. Accordingly, if the equation of motions is expressed as

$$M\ddot{X} + C\dot{X} + KX = -M\{1\}\ddot{x}_g \tag{2-3}$$

where M = mass, C = damping and K = stiffness matrices, $\{1\}$ = unit vector and $\ddot{x}_g$ = ground acceleration. Using the modal analysis approach where the displacement matrix X is expressed as a product of mode shape matrix Φ and a vector of generalized modal coordinates $\{Y\}$, the equation (2-3) can be rewritten as

$$M\Phi\{\ddot{Y}\} + C\Phi\{\dot{Y}\} + K\Phi\{Y\} = -M\{1\}\ddot{x}_g \tag{2-4}$$

where $\Phi = [\phi_1 \quad \phi_2 \quad \dots \quad \phi_m \quad \dots \quad \phi_N]$ column matrix of mode shape vectors and $\{Y\} = \{y_1 \quad y_2 \quad \dots \quad y_m \quad \dots \quad y_N\}^T$ modal coordinates. If it is assumed that only mth mode is dominant then the above equation (2-4) can be modified as

$$M\phi_m\ddot{y}_m + C\phi_m\dot{y}_m + K\phi_m y_m = -M\{1\}\ddot{x}_g \tag{2-5}$$

Pre-multiplying both sides of the above equation with ϕ_m^T

$$\phi_m^T M\phi_m\ddot{y}_m + \phi_m^T C\phi_m\dot{y}_m + \phi_m^T K\phi_m y_m = -\phi_m^T M\{1\}\ddot{x}_g \tag{2-6}$$

From which

$$m_n^*\ddot{y}_m + 2\xi_m\omega_m m_n^*\dot{y}_m + \omega_m^2 m_n^* y_m = -L_m\ddot{x}_g \tag{2-7}$$

where $m_m^* = \phi_m^T M\phi_m$= generalized m^{th} modal mass, $\xi_m = m^{th}$ modal damping, ω_m = generalized m^{th} modal frequency and $L_m = m^{th}$ modal excitation factor. Equation (2-7) can be solved as a SDOF system from which

$$\max y_m = \frac{L_m}{m_m^*} S_d(\omega_m, \xi_m) \tag{2-8}$$

where $S_d(\omega_m, \xi_m)$ = spectral displacement corresponding to damping ξ_m and frequency ω_m. Multiplying both sides of the above equation by the magnitude of the m^{th} mode shape at the n^{th} location ϕ_{nm}, one obtains

$$x_{nm} = \phi_{nm} \cdot \max y_m = \phi_{nm} \frac{L_m}{m_m^*} S_d(\omega_m, \xi_m) \tag{2-9}$$

where x_{nm} = displacement at the n^{th} location for the m^{th} mode shape. Using equation (2-9) the spectral displacement can be solved as

$$S_d = \frac{x_{nm}}{\phi_{nm}} \frac{m_m^*}{L_m} = \frac{x_{nm}}{\alpha_1} \tag{2-10}$$

in which

$$\alpha_1 = \phi_{nm} \frac{\sum_{i=1}^{N} w_i \phi_{im}}{\sum_{i=1}^{N} w_i \phi_{im}^2} \tag{2-11}$$

with w_i = tributary weight at the location i varying from1 to N through n with N being the total number of discrete weight/pushover mode shape locations. Also the maximum shear for the m^{th} mode shape can be obtained from the solution of equation (2-7) as

$$\max \{f_s\}_m = M\phi_m \frac{L_m^*}{m_m} S_a(\omega_m, \xi_m) \tag{2-12}$$

where $S_a(\omega_m, \xi_m)$ = spectral acceleration corresponding to damping ξ_m and frequency ω_m. The base shear capacity can be obtained by adding all the terms of the shear force vector. Thus

$$V = \sum_{i=1}^{N} f_{sim} = \alpha_2 S_a W \tag{2-13}$$

where

$$\alpha_2 = \frac{\left[\sum_{i=1}^{N} w_i \phi_{im}\right]^2}{W \sum_{i=1}^{N} w_i \phi_{im}^2} \tag{2-14}$$

in which W = total seismic weight. Thus spectral acceleration can be solved as

$$S_a = \frac{V}{\alpha_2 W} \tag{2-15}$$

From the above formulation it becomes clear that given the base shear vs. displacement at any location in a MDOF system subjected to any arbitrary chosen distribution of lateral forces, it is possible to convert them to an S_a vs. S_d format by using the transformation suggested by equations (2-9) and (2-15).

2.3.2 Elasto-Plastic Analysis Approach

Pushover analysis is basically a step-by-step plastic analysis for which the lateral loads are applied to a structure and progressively increased until a target displacement is reached. It provides information on many response characteristics and gives an overall picture of the structural system behavior. These benefits however come at the cost of additional analysis effort associated with incorporating all of the important characteristics of the structural elements and performing incremental inelastic analysis.

As will be discussed later in this section, one of the performance objectives in designing supplemental systems for building structures is to keep the seismic response within its elastic limits for the design basis earthquake. Moreover, plastic hinge rotations are limited such that structural collapse is prevented for maximum considered earthquake. While the pushover capacity curve (as obtained from a pushover analysis) contains all relevant information for design purposes, a three-stage elasto-plastic analysis can be used to obtain an approximate bilinear pushover capacity of a given building structure (figure 2-2) designed (or retrofitted) with one of the alternatives introduced in Pekcan et al (1999).

The building structure shown in figure 2-2 comprises exterior-lateral load resisting moment frames and interior-gravity load carrying frames that generally have simple beam-column connections. For the purpose of two-dimensional analysis, two frames can be modeled with rigid links as shown in the figure. Three stages involved in the elasto-plastic analysis to obtain the approximate pushover capacity are i) elastic analysis that will give the elastic response, hence the initial period, of the structure ii) plastic analysis of the moment frame that will give the ultimate strength of the structural system, iii) truss action analysis that will take stiffness contribution of the supplemental system into account. These stages and the generation of pushover capacity curve are depicted in figure 2-3.

2.3.2.1 Determination of Initial Elastic Period

In order to establish the initial elastic response, a period estimation for the building under consideration is needed. This can be achieved using a code-based empirical formulation (FEMA 273) as follows

$$T = C_t h_n^{3/4} \qquad \textbf{(2-16)}$$

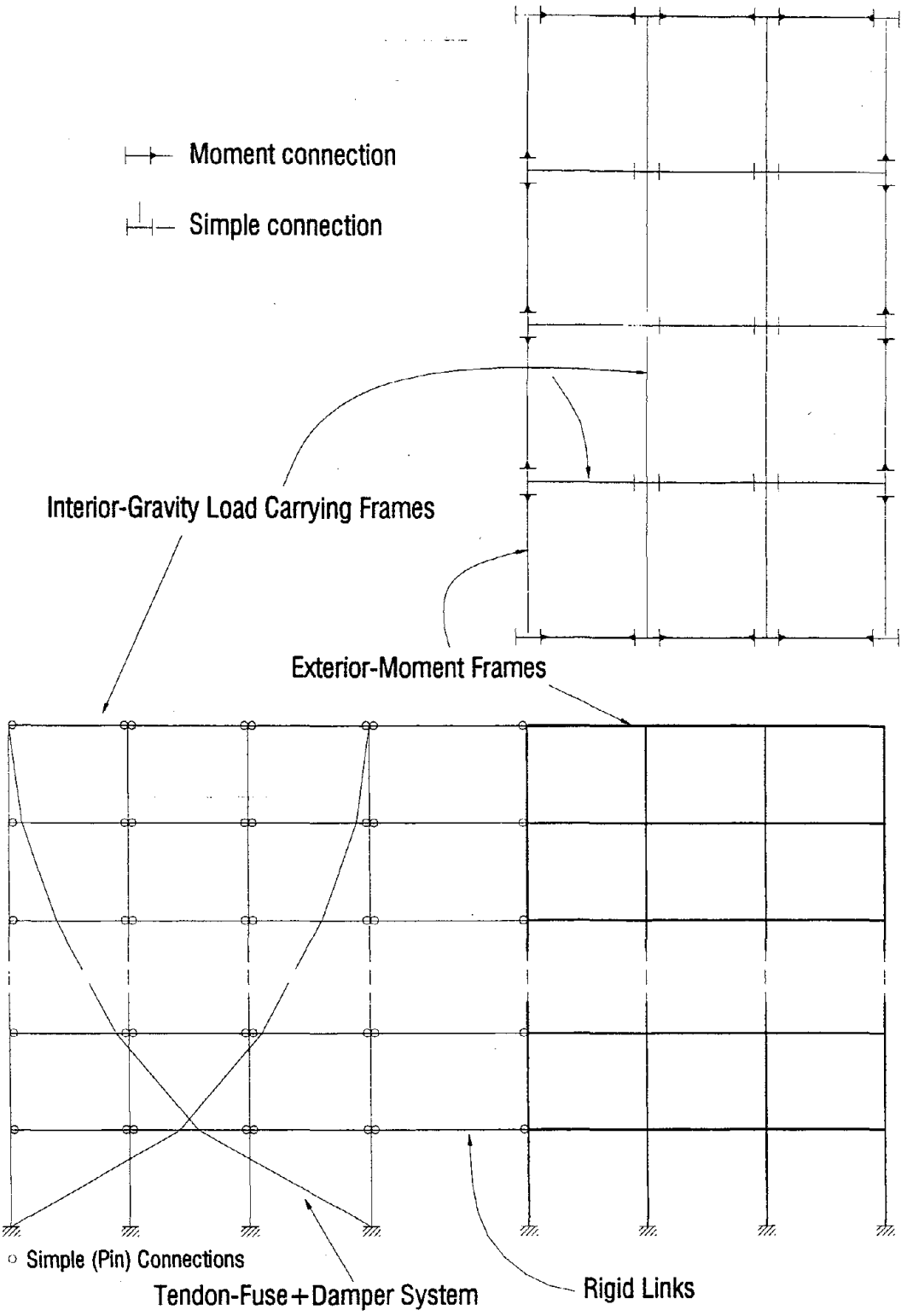

Figure 2-2 Plan View and Elevation of a Typical Building with Supplemental System

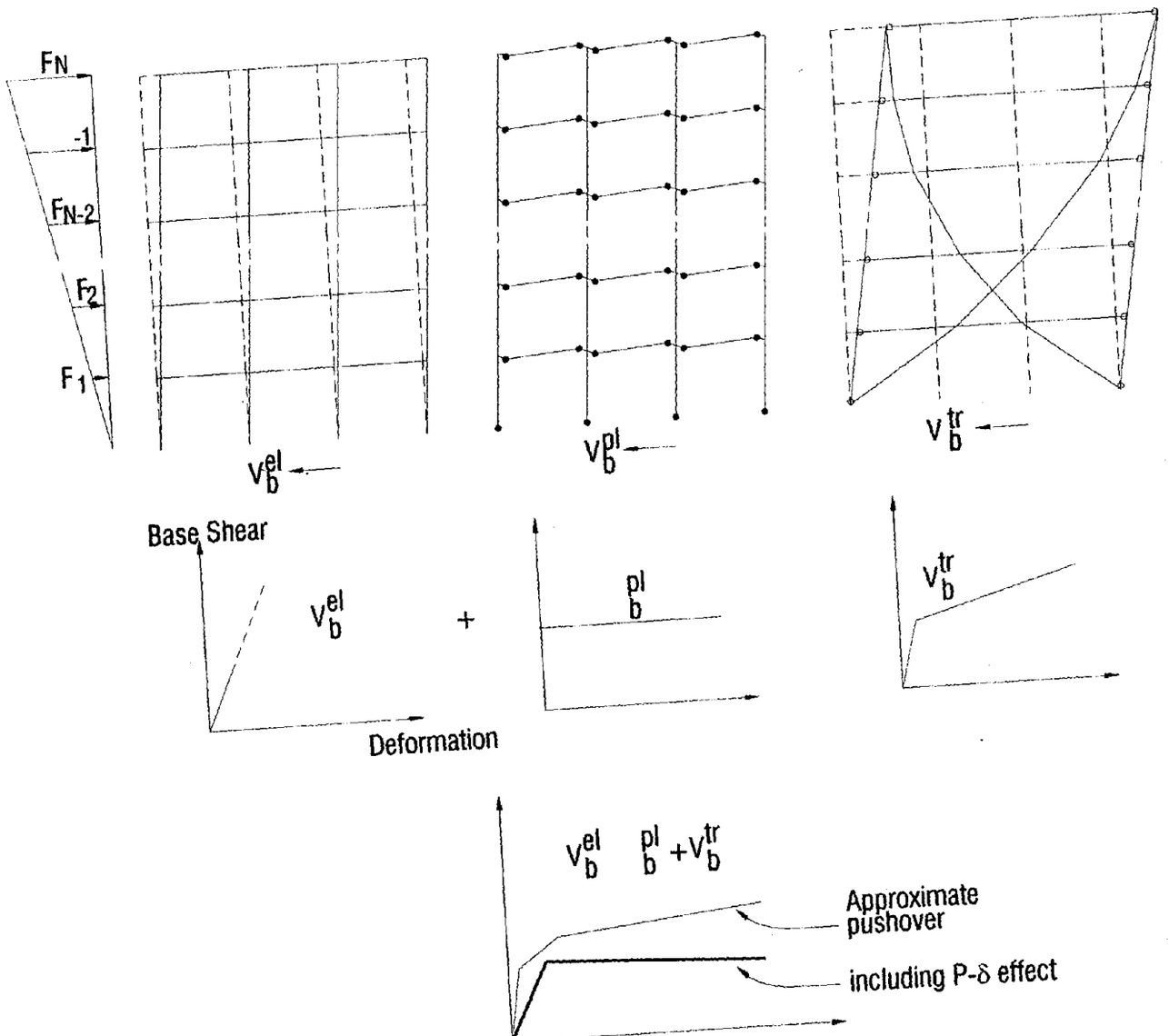

Figure 2-3 Idealized Representation of Pushover Capacity

where T = fundamental period of vibration, C_t = 0.007 for moment-resisting concrete frames, 0.005 for moment-resisting steel frames, h_n = height above the base to the roof level in meters. Therefore, a relationship between elastic capacity and spectral displacement can be established as

$$C_{c,el}^{str} = \frac{4\pi^2}{g}\frac{S_d}{T^2} \tag{2-17}$$

2.3.2.2 Determination of Ultimate Strength Using Plastic Analysis

The ultimate base shear capacity, $C_{c,pl}^{str}$ of the building structure shown in figure 2-2 and 2-3 can be determined based on the well-established rules of plastic analysis. For this purpose a lateral seismic force distribution is assumed in the shape of an inverted triangle. Hence, using the upper bound method of plastic analysis general equations for the internal and external work done due to a beam sidesway mechanism become

$$EWD = F_1\Delta_1 + F_2\Delta_2 + \ldots + F_i\Delta_i \tag{2-18}$$

in which $\Delta_i = \theta_c h_i$ is the horizontal deformation at the i^{th} level.

Similarly internal work done can be written in terms of plastic moment capacities of the beam and column elements

$$IWD = \sum M_{pbi}\theta_{pb} + \sum M_{pci}\theta_{pc} \tag{2-19}$$

Note that hinge rotations at the beam end (θ_{pb}) are related to the column rotation (θ_{pc})

$$\theta_{pb} = \frac{L}{L_b}\theta_{pc} \tag{2-20}$$

in which L_b = the beam length, L = is the width of a typical bay.

Now equating the external work done to internal work done and simplifying using equation (2-20), the overturning moment capacity of the structure can be determined as

$$OTM = \sum F_i h_i = \sum M_{pbi}\theta_{pb} + \sum M_{pci}\theta_{pc} \tag{2-21}$$

The total base shear capacity is then determined by summing all the lateral loads (ΣF_i) that correspond to the plastic mechanism.

It must be noted that several plastic mechanisms should be considered to determine the minimum base shear corresponding to a specific plastic failure mechanism. Most conventional building structures are nowadays designed based on the so-called "strong column-weak beam" concept. Therefore, a generic plastic collapse mechanism of the type shown in figure 2-4 can be assumed for preliminary analysis purposes. This mechanism assumes that plastic hinges form at all the beam ends up to a certain height ($h_{pl} = n_{sp}h$). Plastic hinges are required at the column ends located at the ground level and at top level of the plastic portion of the structure, as shown in figure 2-4. The virtual work method of plastic analysis can be used to determine the base shear capacity (V_b) in terms of unknown plastic structure height h_{pl}. Total internal work done due to plastic hinge rotations is

$$IWD = (IWD)_{beam} + (IWD)_{column} \tag{2-22}$$

where

$$\begin{aligned}(IWD)_{beam} &= 2n_b M_{pb}(n_{pl} - 1)\theta_{pb} \\ (IWD)_{column} &= 2(n_b + 1)M_{pc}\theta_{pc}\end{aligned} \tag{2-23}$$

in which M_{pb}, M_{pc} = plastic moment capacity of beams and columns respectively, θ_{pb}, θ_{pc} = plastic rotation at the beam and column ends respectively, n_b = number of bays, n_{sp} = number of stories participating in the plastic mechanism (figure 2-4).

From figure 2-5 and 2-6, geometry requires that

$$\theta_{pb} = \frac{L}{L_b}\frac{\Delta_p}{n_{sp}h} \tag{2-24}$$

where Δ_p = plastic drift at the roof level and h = story height which is assumed to be constant in this formulation (although this is not a general restriction).

Therefore equation (2-22) can be re-written as

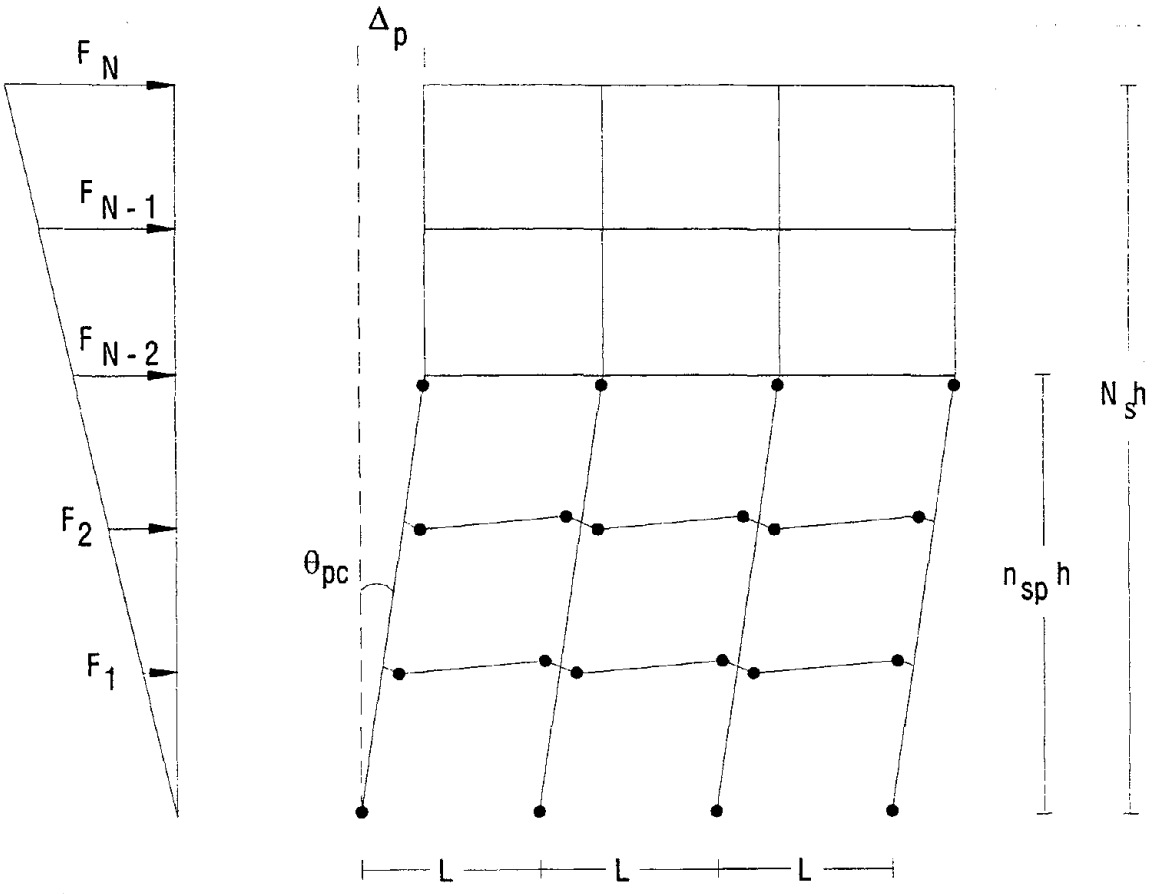

Figure 2-4 Idealized Plastic Mechanism for a MDOF Structure

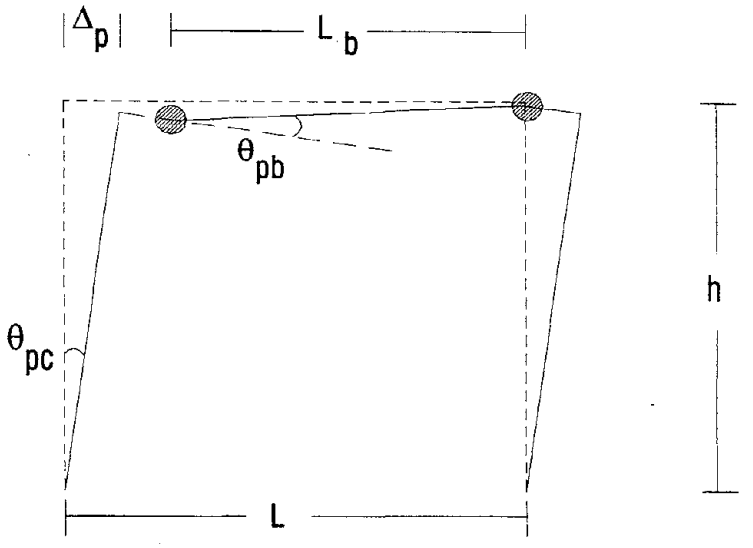

Figure 2-5 Relationship between Plastic Drift and Plastic Hinge Rotation

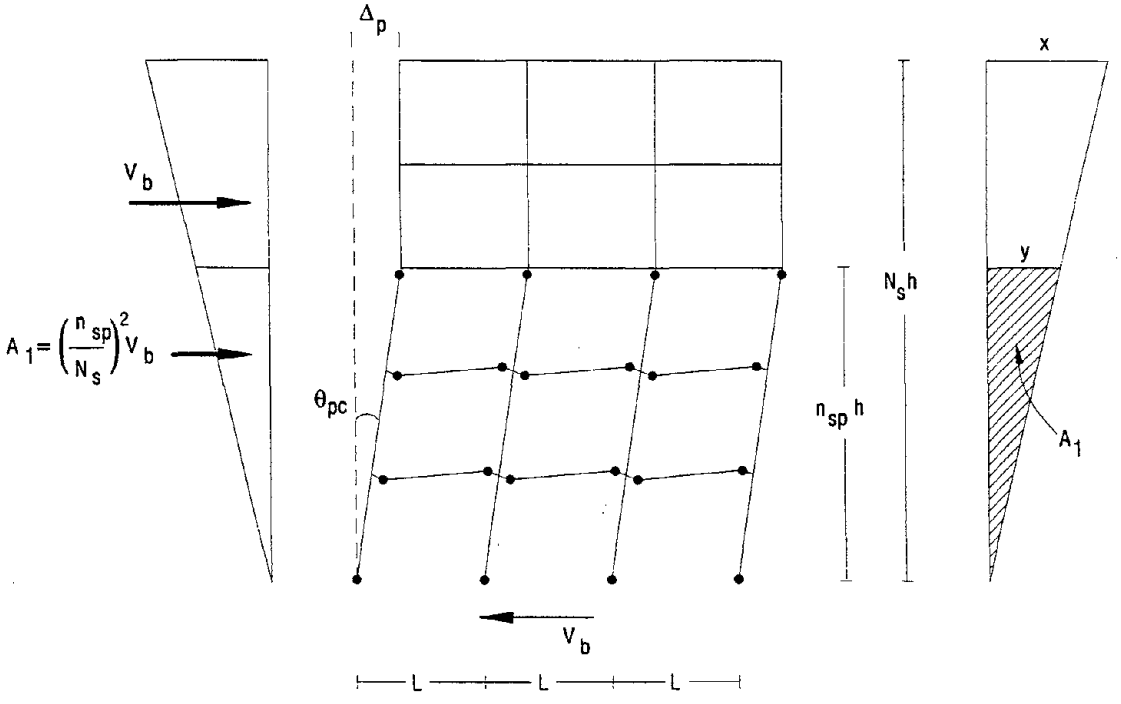

Figure 2-6 Idealized Plastic Mechanism and Corresponding Base Shear

$$IWD = \frac{2\Delta_p}{n_{sp}h}\left(n_b(n_{sp}-1)M_{pb}L/L_b + (n_b+1)M_{pc}\right) \tag{2-25}$$

The total external work done (EWD) can be written in terms of the total base shear V_b (figure 2-6) as

$$EWD = \left(1-\frac{1}{3}\left(\frac{n_{sp}}{N_s}\right)^2\right)V_b\Delta_p \tag{2-26}$$

where N_s = total number of stories.

Equation 2-26 and 2-26 can be equated and solved for V_b as

$$V_b = \frac{2\left(n_b(n_{sp}-1)M_{pb}L/L_b + (n_b+1)M_{pc}\right)}{n_{sp}h\left(1-\frac{1}{3}\left(\frac{n_{sp}}{N_s}\right)^2\right)} \tag{2-27}$$

Note that this is a general mixed mechanism solution that also gives two of the most commonly assumed specific mechanism that are (i) beam sidesway mechanism when $n_{sp} = N_s$, and (ii) column sidesway mechanism when $n_{sp} = 1$.

The correct number of stories in the critical mechanism will occur when the energy is minimized. This can be found by minimizing equation (2-27) with respect to the number of stories in the plastic substructure n_{sp}. Therefore,

$$\frac{dV_b}{dn_{sp}} = 0 \quad \Rightarrow \quad \frac{2/3n_{sp}^3}{(1+1/n_b)(L_b/L)(M_{pc}/M_{pb})-1} + n_{sp}^2 - N_s^2 = 0 \tag{2-28}$$

Once the above cubic equation is solved for n_{sp}, the corresponding base shear can be calculated using equation (2-27).

2.3.2.3 Truss Action Analysis

Supplemental systems in general increase the stiffness of the parent structure and hence modify the pushover capacity. The stiffening effect on the pushover capacity can be easily taken

into account by means of a simple truss-action analysis. For the tendon system shown in figure 2-2, stiffening effect of the system with supplemental damping devices can be determined provided that its stiffness characteristics are known. However, preliminary design (sizing) of the supplemental devices does not require the effect of the supplemental system on the overall capacity of the structure. As will be discussed later in Section 4, normalized "total" supplemental system capacity can be iteratively determined based on a SDOF idealization of the MDOF system, approximate capacity of the bare structure and target design performance (i.e. target design displacement X_{max} and total effective damping ξ_{eff}^{total}).

2.3.2.4 P-δ Effect on the Structural Capacity

It is also possible to include so-called P-δ effects on the capacity of a building frame. The P-δ effect on a structural system is to reduce the lateral force that can be resisted by the structure. As shown in figure 2-7, the simple cantilever model (idealized SDOF) is subjected to lateral force F, and the resulting horizontal displacement lead to additional overturning moments due to the weight of the structure (W). Hence, in addition to the overturning moments induced by lateral loads, the secondary moment $W\ \delta$ should also be resisted causing additional lateral displacements. Therefore available capacity of the structural system to resist the lateral forces reduces as the displacement increases. Reduced capacity at a given horizontal displacement can be derived from the basic equilibrium condition as shown in figure 2-7:

$$\Delta C_{P-\delta} = \frac{\delta}{h_e} \tag{2-29}$$

where $\Delta C_{P-\delta}$= reduced capacity, W_e = effective weight of the structure, h_e = equivalent height of the SDOF system.

A target design displacement, X_{max} must lie on the above-mentioned capacity spectrum, in order to represent the structural performance. However, the point that corresponds to the target displacement must also be located on a demand curve which quantifies the demand, C_d that is imposed on the structural system, as a function of the target design displacement, X_{max} and total effective damping ξ_{eff}^{total}. Construction of demand curves is discussed in what follows.

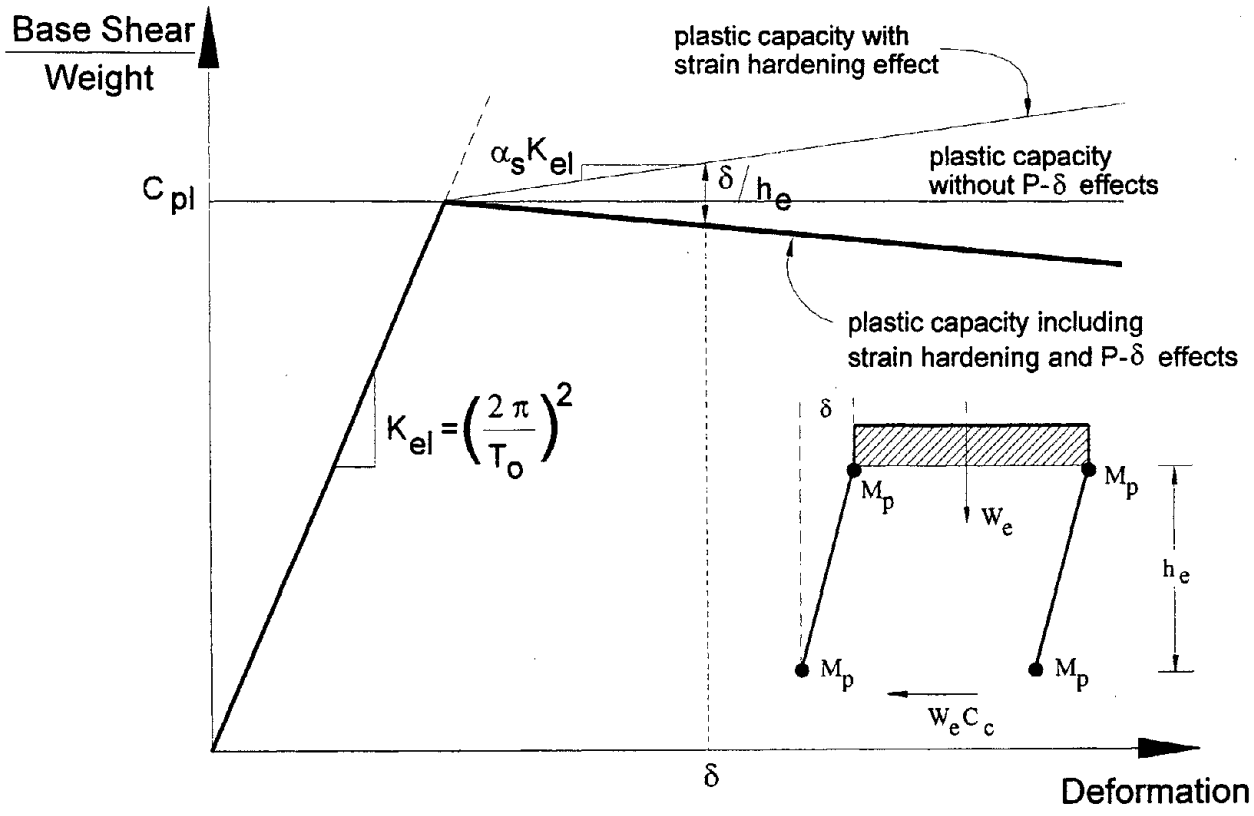

Figure 2-7 P-δ Effect on the Structural Capacity

2.4 ASSESSMENT OF SEISMIC DEMAND

The second step in the capacity spectrum method is the construction of demand curves as a function of the target displacement, X_{max} and total effective damping ξ_{eff}^{total}. The maximum base shear V_b and corresponding SDOF displacement S_d, can be obtained from a series of time-history analyses for various equivalent viscous damping ratios. As a result, site specific demand curves can then be plotted as S_d vs. C_d (V_b=W) for the damping level considered as mentioned above.

Alternatively, code-based relationships can be used. In publications ATC-33 and ATC-40, Applied Technology Council proposed the construction of a 5% damped elastic demand spectrum as shown in figure 2-8. In this figure, C_a and C_v are the seismic coefficients. The coefficient C_a represents the effective peak ground acceleration, PGA.

The modified demand spectrum for higher damping values can be obtained as shown in figure 2-8. The amount of reduction is based on the mean spectral amplification factor given by Newmark and Hall (1992) and listed in table 2-1. These factors are different for short (B_s) and long period ranges (B_l) as shown in figure 2-8 and 2-9. A regression analysis is performed on the Newmark-Hall values to obtain analytical expressions. Regression results are also listed in table 2-1 in comparison with Newmark-Hall values and plotted on figure 2-9. Following the regression analysis the following relationships may be derived (Cheng, 1997):

$$B_s = \left(\frac{\xi_{eff}^{total}}{0.05}\right)^{0.5} \quad and \quad B_l = \left(\frac{\xi_{eff}^{total}}{0.05}\right)^{0.3} \tag{2-30}$$

The demand spectra can then be transformed into demand curve by calculating the corresponding spectral displacements, S_d associated with demand C_d as follows

$$S_d = C_d g T^2 / 4\pi^2 \tag{2-31}$$

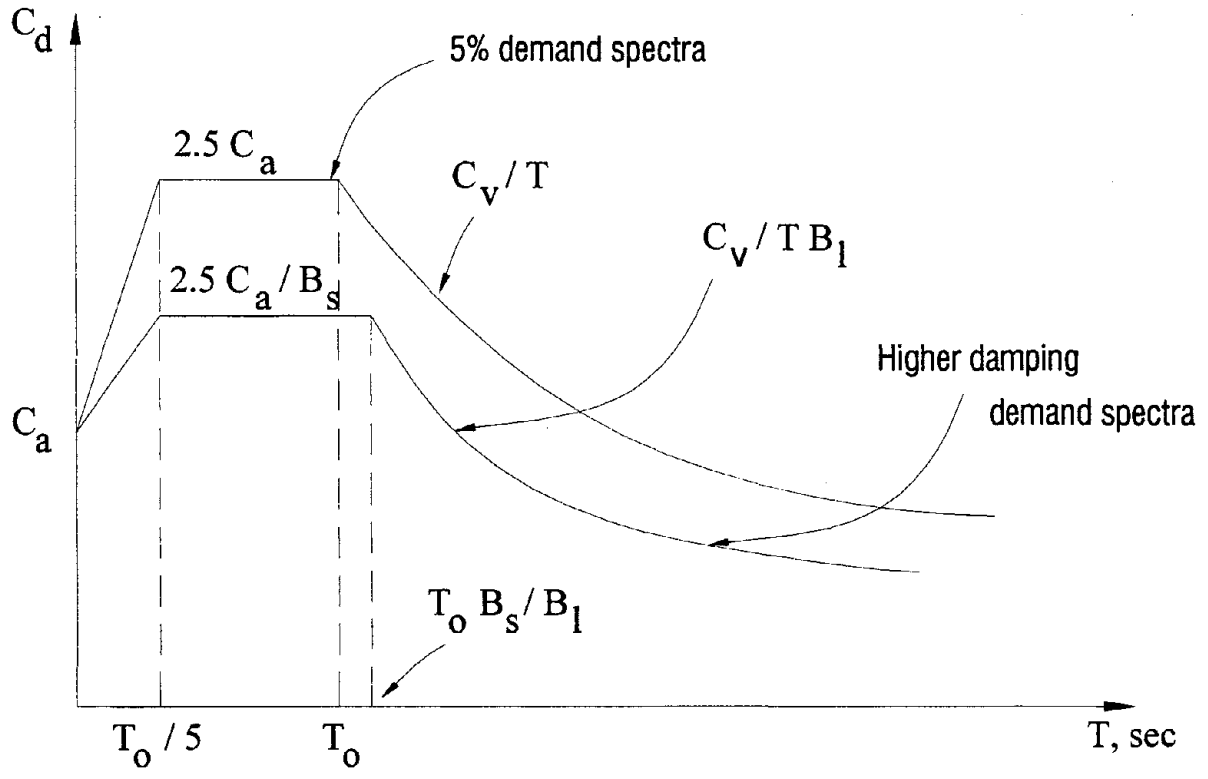

Figure 2-8 Construction and Modification of 5% Damped Spectrum for Higher Damping (ATC-40)

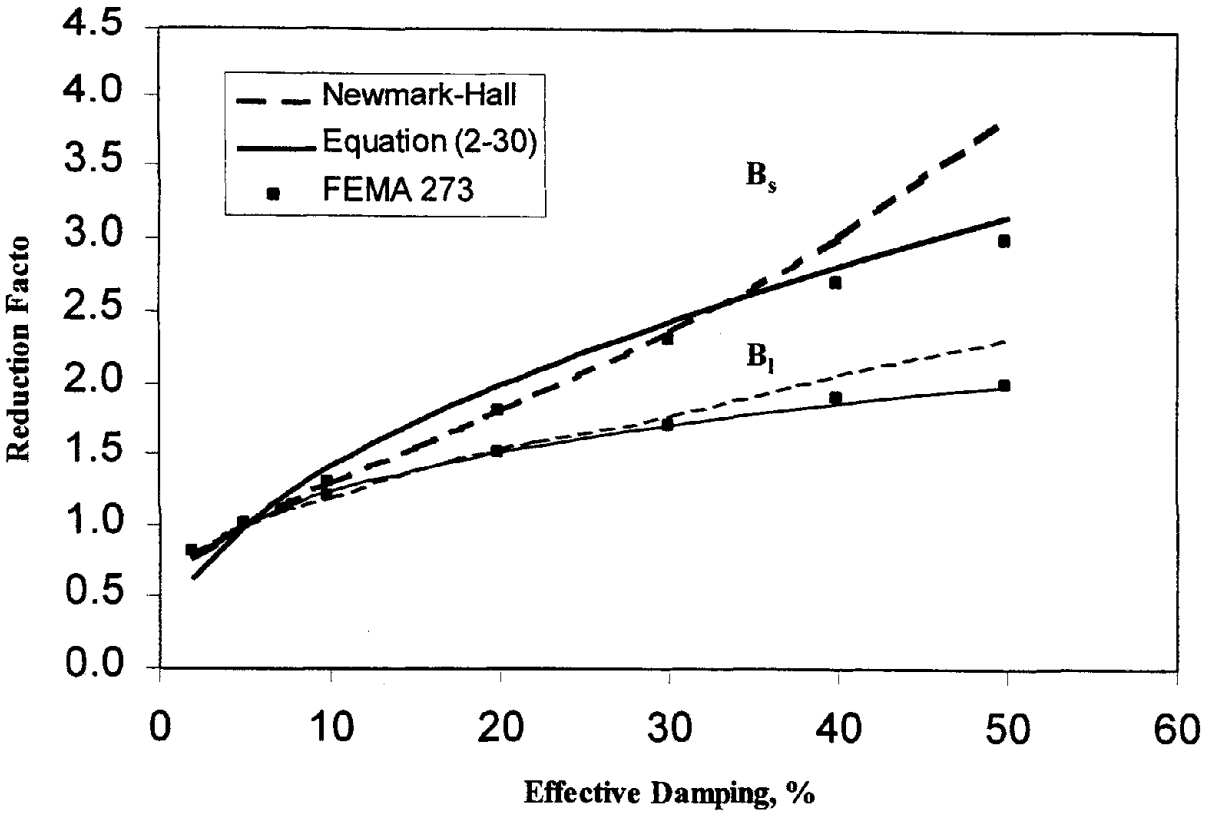

Figure 2-9 Long and Short Period Demand Reduction Factors

Table 2-1 Demand Spectra – Damping Reduction Factors

ξ_{eff}^{total}, %	Short Period Factors, B_s			Long Period Factors, B_l		
	Newmark-Hall	FEMA 273	Eq. (2-30)	Newmark-Hall	FEMA 273	Eq. (2-30)
2	0.78	0.80	0.63	0.81	0.8	0.76
5	1.00	1.00	1.00	1.00	1.00	1.00
7	1.12	-	1.18	1.09	-	1.11
10	1.30	1.30	1.41	1.20	1.20	1.23
15	1.54	-	1.73	1.39	-	1.39
20	1.82	1.80	2.00	1.54	1.50	1.52
30	2.38	2.30	2.45	1.79	1.70	1.71
40	3.03	2.70	2.83	2.08	1.90	1.87
50	3.85	3.00	3.16	2.33	2.00	2.00

2.4.1 Effective Hysteretic Damping, ξ_{eff}^{str}

In the capacity spectrum method, the total effective damping (ξ_{eff}^{total}) is defined by the equivalent viscous damping at a given deformation on the capacity curve. Hence, total effective damping represents all energy dissipation mechanisms of the structure, including inherent viscous damping ξ_o, damping associated with inelastic action, ξ_{hy}^{str} and supplemental damping system ξ_d, (if any) etc. The most common method for defining the equivalent damping is to equate the energy dissipated in a response cycle of the actual structure to that of an equivalent viscous system as (Chopra, 1995)

$$\xi_{hy}^{str} = \frac{1}{4\pi}\frac{E_D}{E_S} \tag{2-32}$$

where

$$E_D = 4X_y X_{\max}(K_o - K_{eff}) \tag{2-33}$$

$$E_S = K_{eff} X_{\max}^2 / 2 \tag{2-34}$$

in which effective stiffness can be written in terms of ductility ratio μ as

$$K_{eff} = K_o(\alpha_s + (1-\alpha_s)/\mu) \tag{2-35}$$

Therefore, assuming an overall bilinear pushover response as shown in figure 2-10a, effective damping due to hysteresis can be calculated by substituting equations (2-33) through (2-35) into (2-32) and rearranging

$$\xi_{eff}^{str} = \xi_o + \xi_{hy}^{str} = \xi_o + \frac{2}{\pi}\eta\frac{(1-\alpha_s)(1-1/\mu)}{(1-\alpha_s+\mu\alpha_s)} \tag{2-36}$$

where $\mu = X_{max}/X_y$ is the displacement ductility, α_s= post yield to initial stiffness ratio, and η = efficiency factor defined as the ratio of the actual area enclosed by the hysteresis loop to that of the assumed bilinear hysteresis (figure 2-10b). The efficiency factor is influenced by bond slip or

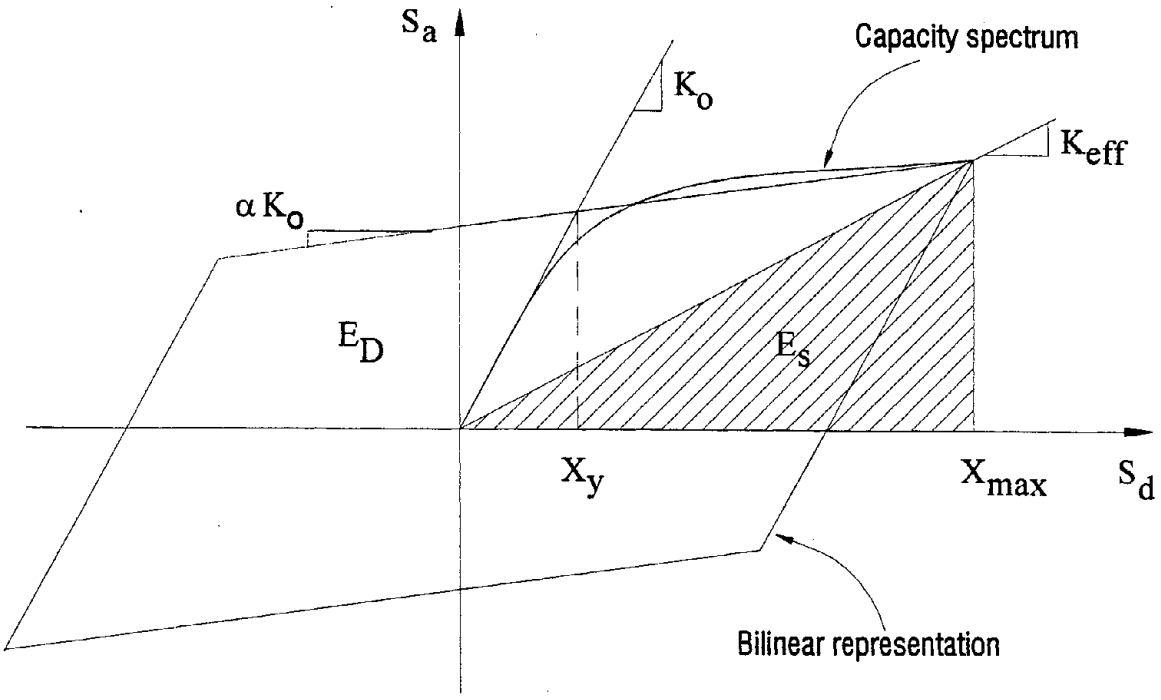

Figure 2-10a Bilinear Representation of Capacity Spectrum and Effective Hysteretic Damping

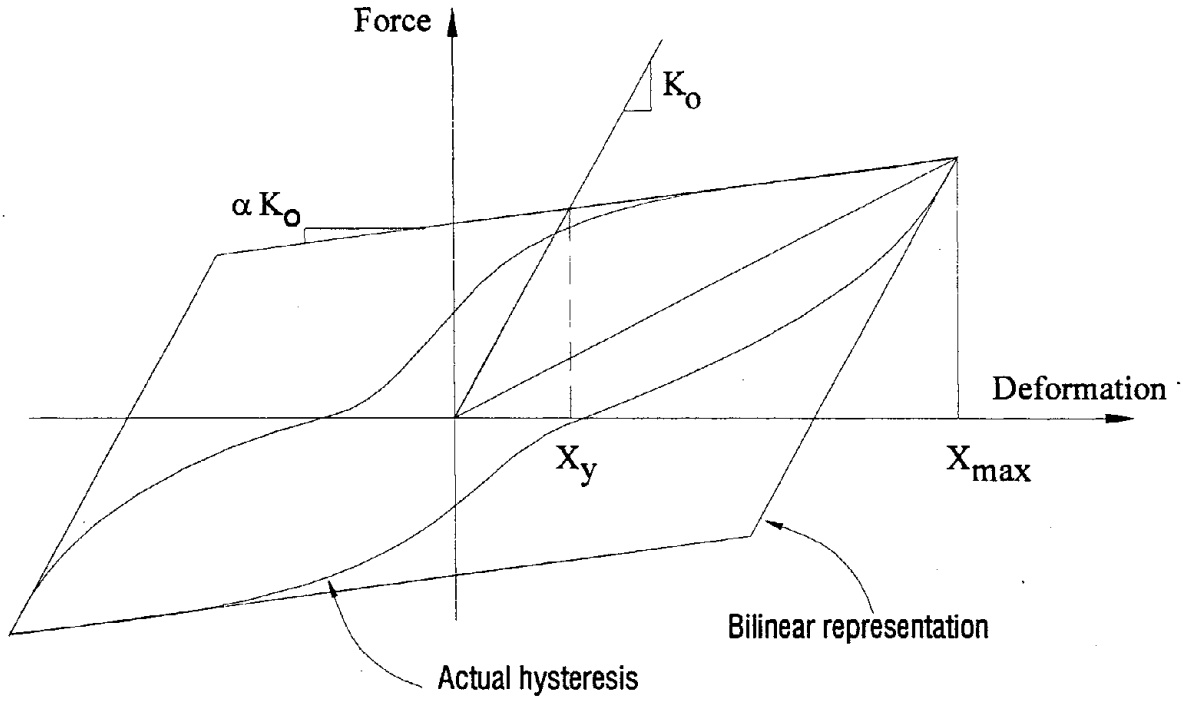

Figure 2-10b Definition of Efficiency Factor, η

pinching effect in reinforced concrete and by the Bauschinger effect in steel structures as well as the type of construction. Typical values range between 0.2 and 0.6 for concrete and steel structures, respectively.

2.5 Uncertainties Involved in the Evaluation of Ground Motion Demand

The uncertainty of the ground motion demand as well as the structural capacity has a direct relationship to the reliability of engineering structures. Therefore, it is necessary to pursue an analysis that takes into account the possible uncertainties in both capacity and demand. If these uncertainties are not accounted for, the computed response represents only one result in a set of possibilities. One commonly used method for quantifying the randomness in a given problem is to treat the so-called random variable as a statistical quantity. In this part of the study, peak acceleration response of various SDOF systems subjected to the ground motions listed in table 2-2 were used to form the sets of *statistical data* in an attempt to identify the confidence intervals from the demand point of view. Spectral accelerations for 5% and 20% viscous damping were calculated at T_o = 0.2, 0.3, 1.0 and 2.0 sec as these damping ratios are typical for steel and reinforced concrete structures. Average (mean) spectra are plotted together with the corresponding range of specific data points on figure 2-11. A considerable scatter in the data is evident. Nevertheless, the response, which is random due to the vagaries of the ground motion input, can be described by a probability density function. An analysis of these results show that the distribution of spectral acceleration response can be best described by using a lognormal probability density function (PDF). This two-parameter PDF can be described by the following equation:

$$f(S_a) = \frac{1}{S_a \beta \sqrt{2\pi}} \exp\left[-\frac{1}{2} \left(\frac{\ln(S_a / \theta_{S_a})}{\beta} \right)^2 \right] \qquad \textbf{(2-37)}$$

in which S_a = spectral acceleration, β = standard deviation of normally distributed variable, i.e. $\ln S_a$, θ_{Sa} = median of lognormally distributed variable S_a ($= \exp(m_{\ln S_a})$). It must be noted that for a normally distributed random variable, mean and median are equal due to the symmetry (figure 2-12).

Equation (2-37) can be written in terms of the standard normal variant z, as,

Table 2-2 Earthquake Ground Motions

Ground motion	Station	Direction	PGA, g	PGV, m/s	PGD, m
Tabas, Sep 78	Tabas/Iran	N/A	0.812	0.856	0.430
Loma Prieta, 89	Los Gatos P.C.	N/A	0.717	1.728	0.646
Loma Prieta, 89	Lex. Dam	N/A	0.686	1.787	0.566
C. Mendocino, 92	Petrolia	N/A	0.655	0.929	0.414
Erzincan, 92	Erzincan/Turkey	N/A	0.432	1.192	0.421
Landers, 92	Lucerne	N/A	0.713	1.359	1.566
Northridge, 94	Rinaldi R.St.	N/A	0.889	1.746	0.383
Northridge, 94	Sylmar, Olive	N/A	0.732	1.219	0.305
Kobe, 95	Kobe, JMA	N/A	1.088	1.698	0.402
Kobe, 95	Takatori	N/A	0.786	1.738	0.560
Imperial Valley, 79	Array 5	N230	0.374	0.880	0.541
Imperial Valley, 79	Array 5	N140	0.527	0.438	0.246
Imperial Valley, 79	Array 6	N140	0.376	0.627	0.275
Imperial Valley, 79	Array 6	N230	0.436	1.061	0.578
Imperial Valley, 79	Array 7	N140	0.333	0.447	0.208
Imperial Valley, 79	Array 7	N230	0.462	1.063	0.418
Imperial Valley, 79	Bounds Corner	N140	0.587	0.437	0.131
Imperial Valley, 79	Bounds Corner	N230	0.785	0.485	0.151
San Fernando, 71	Pacoima Dam	S16E	1.170	1.156	0.561
San Fernando, 71	Pacoima Dam	S74W	1.070	0.590	0.156
Northridge, 94	Sylmar CH.	360 deg	0.843	1.291	0.313
Northridge, 94	Sylmar CH.	90 deg.	0.604	0.776	0.188
Northridge, 94	Santa Monica	360 deg	0.369	0.250	0.074
Northridge, 94	Santa Monica	90 deg.	0.883	0.411	0.129
Northridge, 94	Tarzana	360 deg	0.989	0.778	0.334
Northridge, 94	Tarzana	90 deg.	1.778	1.064	0.289
Northridge, 94	Newhall F.S.	360 deg	0.589	0.952	0.393
Northridge, 94	Newhall F.S.	90 deg.	0.583	0.741	0.187
Northridge, 94	Arleta F.S.	360 deg	0.308	0.231	0.112
Northridge, 94	Arleta F.S.	90 deg.	0.344	0.396	0.162
Kobe, 95	Kobe, KOB/Japan	NS	0.833	0.918	0.214
Kobe, 95	Kobe, KOB/Japan	EW	0.629	0.757	0.238
Imperial Valley, 40	El Centro	S00E	0.348	0.396	0.169
Imperial Valley, 40	El Centro	S90W	0.214	0.489	0.150
Kern County, 52	Taft L. Tunnel	N21E	0.156	0.181	0.080
Kern County, 52	Taft L. Tunnel	S69E	0.179	0.175	0.100
AVERAGE	-	-	0.629	0.844	0.327

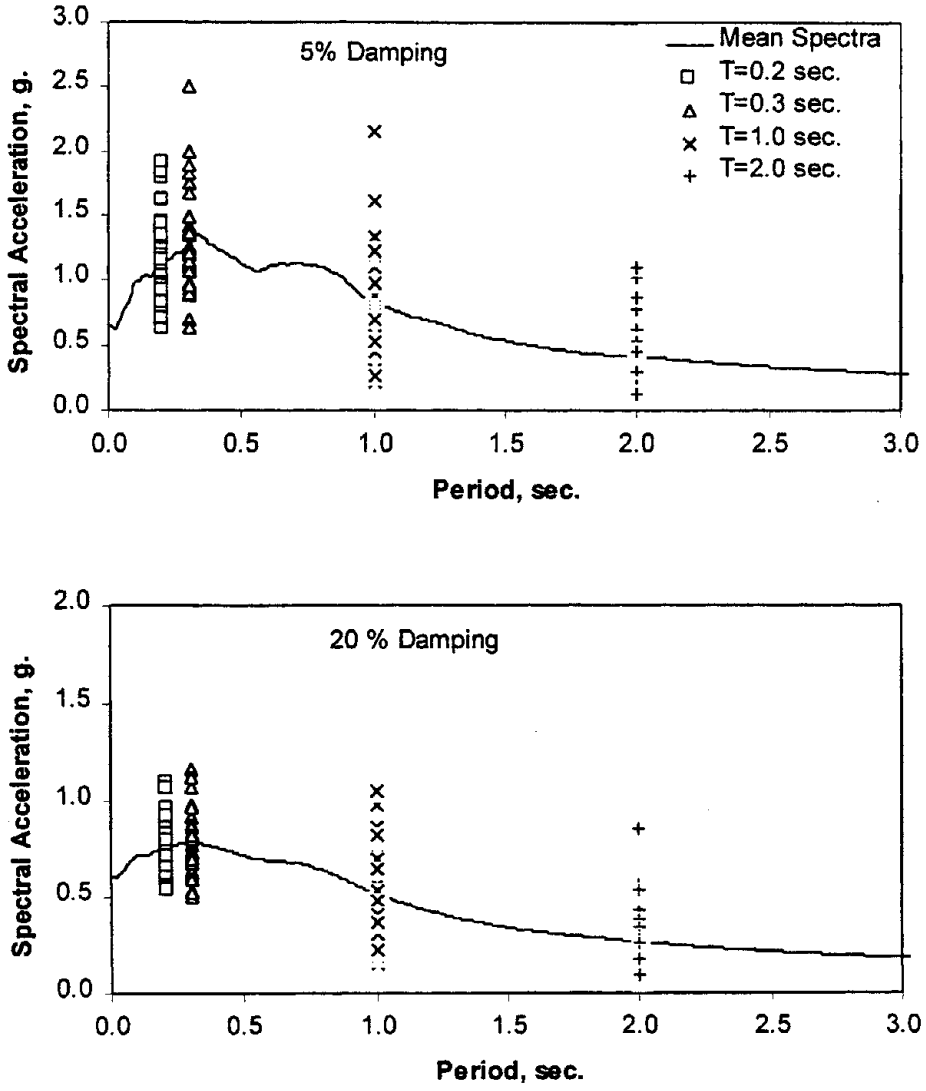

Figure 2-11 Mean Spectral Accelerations and Distribution at Various Periods

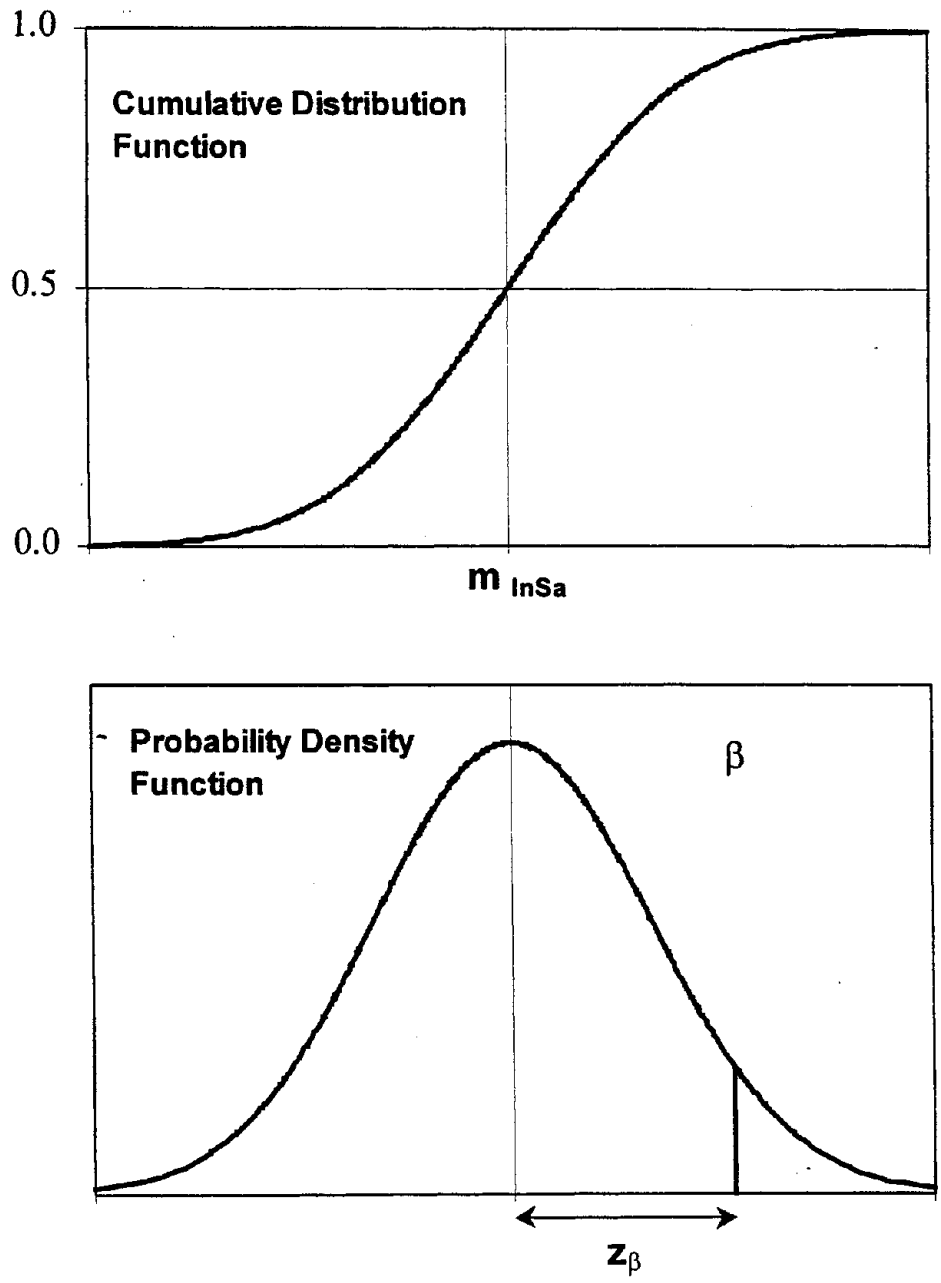

Figure 2-12 Probability Density and Cumulative Distribution Functions of a Normally Distributed Random Variable

Table 2-3 Scaled Standard Deviations of the Mean Spectral Accelerations

Damping	5% damping				20% damping			
Period (sec.)	T=0.2	0.3	1.0	2.0	T=0.2	0.3	1.0	2.0
Mean S_a, $\bar{S}_a$ (g)	1.12	1.27	0.83	0.41	0.76	0.78	0.52	0.26
Standard Dev., β	0.29	0.28	0.51	0.55	0.18	0.21	0.48	0.58

$$f(S_a) = \frac{1}{S_a \beta} f(z) \tag{2-38}$$

where $z = \frac{1}{\beta} \ln\left(\frac{S_a}{\theta_{Sa}}\right)$ and $f(z)$ = PDF of the standard normal variant with a zero mean and standard deviation of 1, which is widely tabulated.

Corresponding cumulative distribution function (CDF) can then be determined in terms of z as,

$$F_z(z) = P[S_a \le x] = F\left(\frac{1}{\beta} \ln\left(\frac{S_a}{\theta_{Sa}}\right)\right) \tag{2-39}$$

where the interval represents the probability that the random variable (S_a) take on a value in that interval and F is the standard cumulative distribution function.

Figure 2-13 presents results of the present analysis. First, in figure 2-13(a) and (b), the field observed CDF's are respectively plotted for damping ratios of 5% and 20%. Secondly, the theoretical lognormal distributions in accordance with equation (2-37) are shown for the two damping ratios in figure 2-13(c) and (d). The parameters used for fitting these distributions are given above in table 2-3.

From the results in table 2-3, it is evident that there is a measure of consistency in the distribution factors β for the short periods ($T = 0.2$ *and* $0.3\,\text{sec.}$, $\beta = 0.18 \sim 0.29$) and long periods ($T = 1.0$ *and* $2.0\,\text{sec.}$, $\beta = 0.51 \sim 0.58$). Figure 2-14 further normalizes the field observed

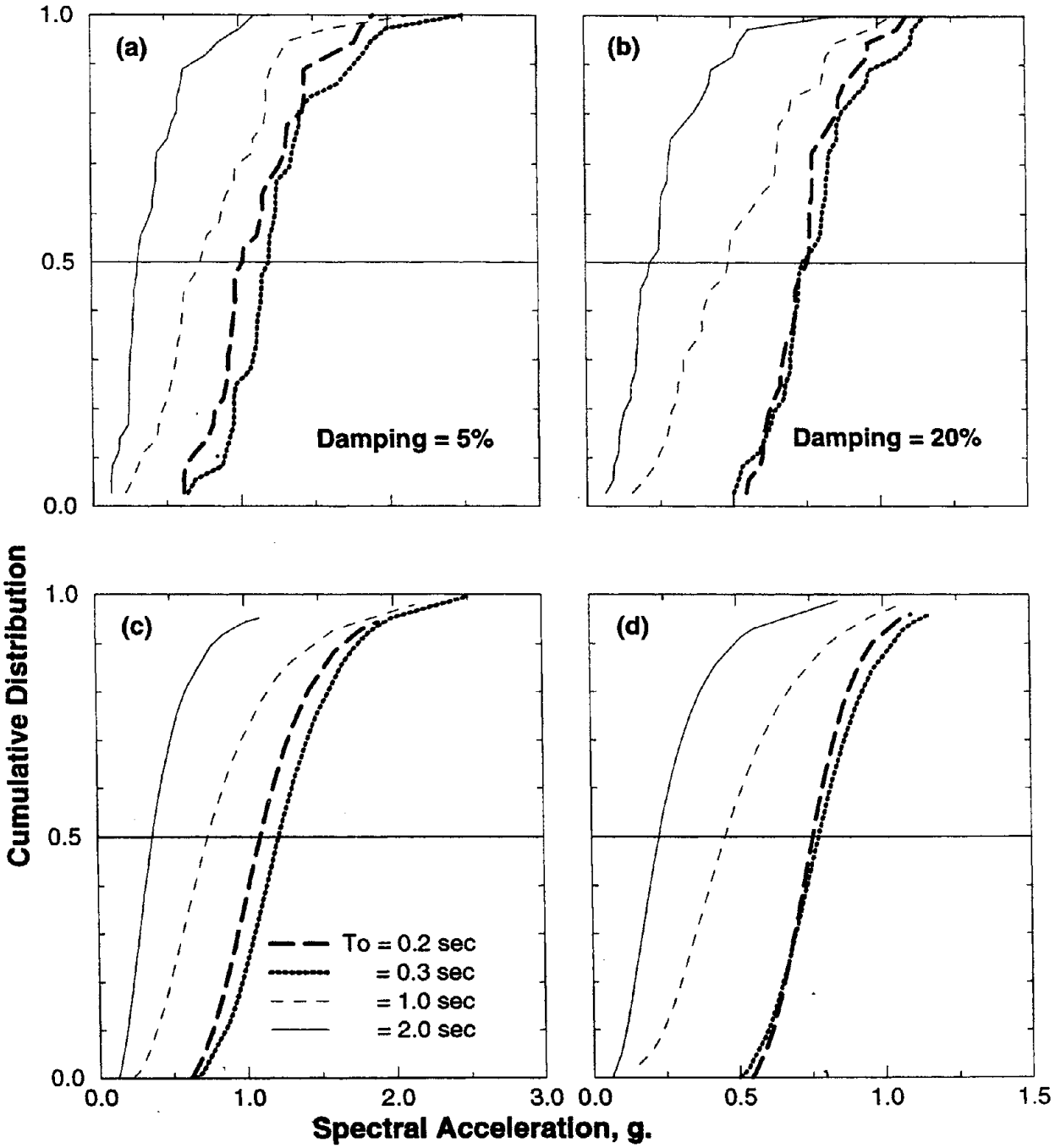

Figure 2-13 Lognormally Distributed Random Variables

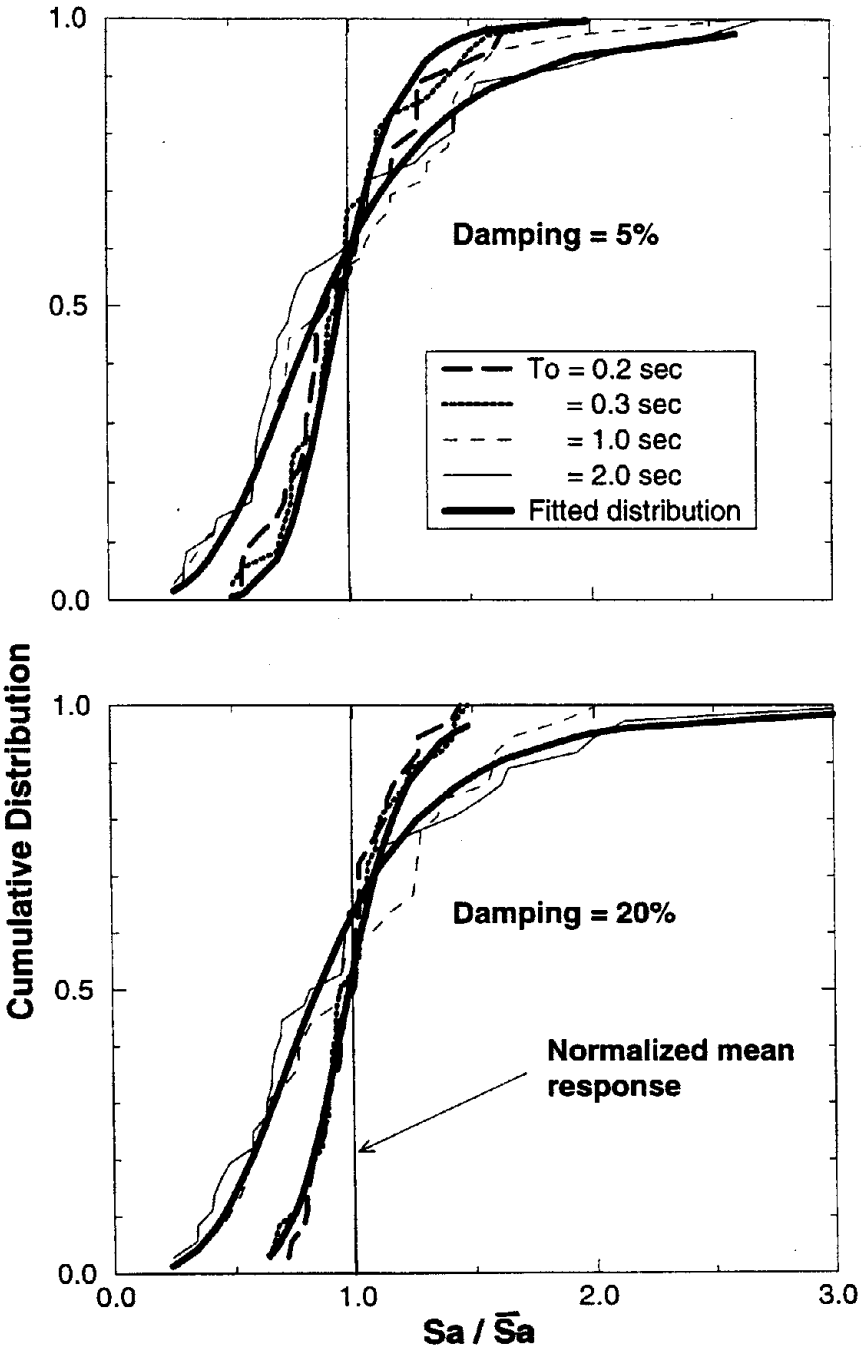

Figure 2-14 Normalized Cumulative Distributions

results in terms of the mean spectral acceleration response $\bar{S}_a$ for each given period and damping factor. This clearly shows the grouping of the data sets. For subsequent convenience (for design purposes) it is proposed to adopt single β values for short and long period motions as follows

$$\begin{aligned} \beta_s &= 0.20 \qquad \textit{for short period} \\ \beta_l &= 0.50 \qquad \textit{for long period} \end{aligned} \tag{2-40}$$

The theoretical lognormal distributions using these values are overplotted (with thick heavy line) in figure 2-14. It is evident from the results that this form of simplification is justified. It must be noted here that the suggested values in equation (2-40) are representatives of higher damping ratios (when compared to those in table 6-3). However, it is believed that the so-called uncertainties become more critical for the higher damping ratios. In fact, most structural systems with supplemental systems as well as yielding structures possess higher damping (>10~20%).

The results of this study can be extended to develop the probability ranges for the ground motion demand in terms of well-known amplification factors. The probabilistic values for the amplification factors was determined as those that bound the 90-percentile range around the mean 5%-damped acceleration response for the lognormal distribution as follows

$$\begin{aligned} \lambda_s^{up} &= e^{z\beta_s} \quad \textit{and} \quad \lambda_l^{up} = e^{z\beta_l} \qquad \textit{for upper bound} \\ \lambda_s^{lo} &= e^{-z\beta_s} \quad \textit{and} \quad \lambda_l^{lo} = e^{-z\beta_l} \qquad \textit{for lower bound} \end{aligned} \tag{2-41}$$

where λ_s and λ_l = are the short and long period amplification factors respectively, β = 0.2 or 0.5 depending on the period range, z = standard normal variant (= 1.64 for 45%-percentile range), and superscripts *up* and *lo* designate the upper or lower bound amplification factor respectively.

Therefore upper and lower bounds of 5%-damped spectra can be obtained as

$$2.0\lambda_s C_a \le \lambda_l \frac{C_v}{T} \tag{2-42}$$

with a corner period determined as the ratio

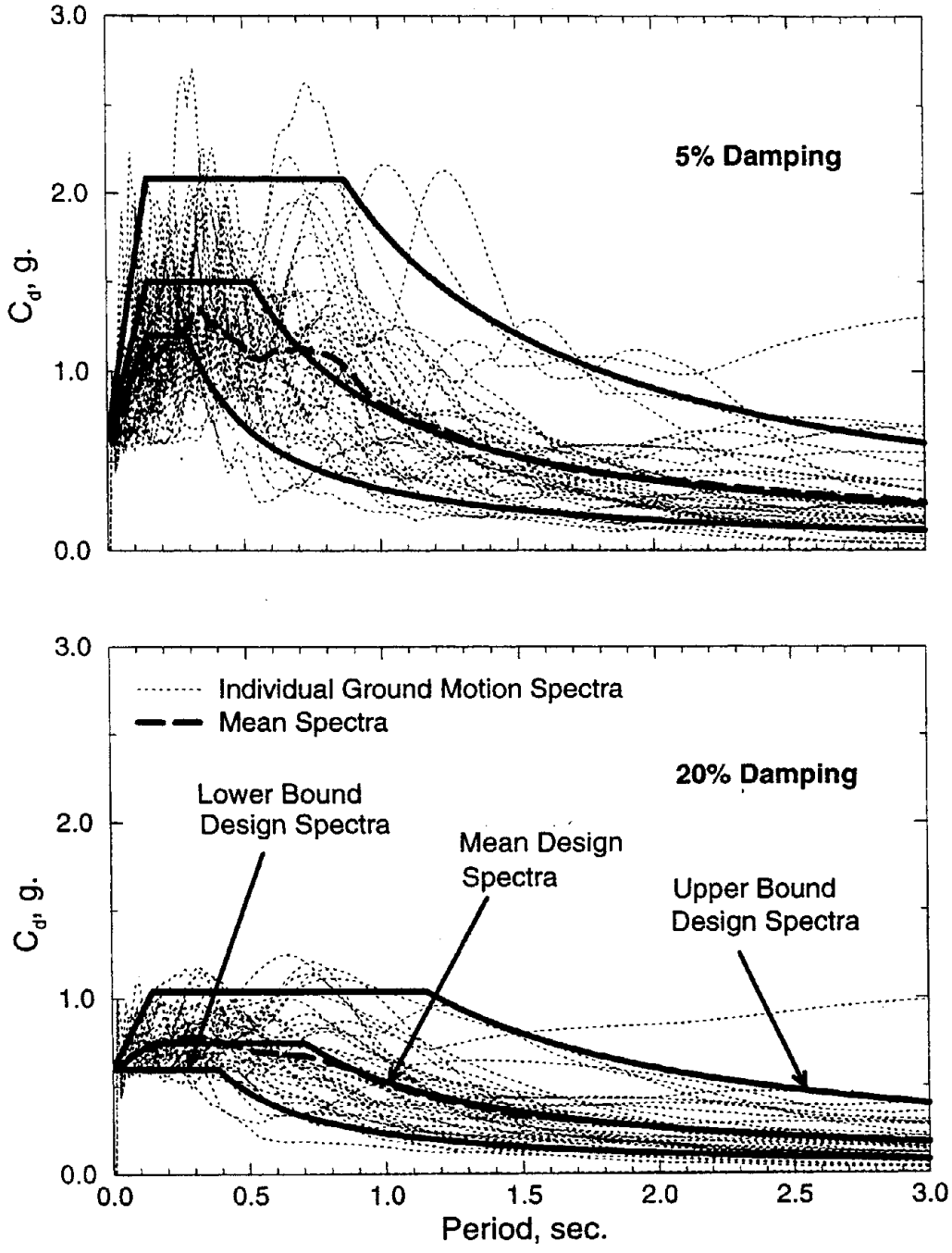

Figure 2-15 90-Percentile Ranges for the 5% and 20%-Damped Design Spectra

$$T_o = \frac{\lambda_1 C_v}{2.0\lambda_s C_a} \tag{2-43}$$

where C_a and C_v = are the peak ground acceleration and the peak ground velocity (0.6g and 0.8 m/sec for the ground motions used in this study).

It must be noted that an amplification factor of 2.5 is used initially in order to fit the common design spectra to the mean response spectra as shown in figure 2-15. So obtained 90%-percentile demand curves are also plotted in figure 2-15 together with the 5% and 20%-damped mean demand and individual ground motion response curves. Finally, following amplification factors, which bound the 90-percentile range around the mean demand spectra, are suggested.

$$\begin{aligned} \lambda_s^{up} &= 1.39 \qquad \lambda_1^{up} = 2.27 \\ \lambda_s^{lo} &= 0.72 \qquad \lambda_1^{lo} = 0.44 \end{aligned} \tag{2-44}$$

2.6 SUMMARY AND CONCLUSIONS

In this section, a brief review of current seismic design and retrofit philosophy was given. This was followed by a summary of the capacity-demand spectral design approach. An alternative elasto-plastic analysis approach was used to derive, in a direct fashion, the lateral strength (pushover) curve that is intended to be used in the preliminary stages of the design. The technique presented provides a straightforward alternative to somewhat time consuming inelastic pushover analysis. It must be noted that it yields very good approximations to pushover analysis especially for regular MDOF systems. However, caution must be exercised when applying this method for irregular frame systems as the dominant response may not be governed by the first mode and may result in erroneous structural capacity predictions.

The assumptions built-in the capacity-demand spectral design method are that both capacity and demand curves are known a priori without any associated uncertainty. However, in a real scenario, such an assumption can lead to gross errors because both capacity and demand will have some form of probabilistic variations as shown in figure 2-16. If this is neglected, then the answer obtained will be one among the many possibilities. Alternatively, if it is assumed that both capacity and demand are probabilistically known in the form of some distribution, then the PGA corresponding to a particular response level will also be known in the form of probability

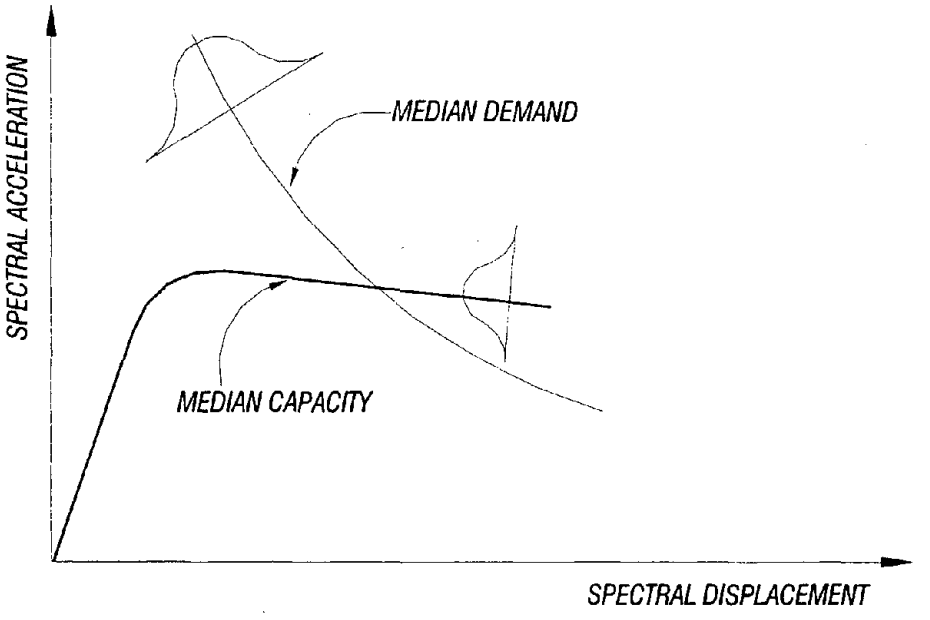

Figure 2-16 Probabilistic Variations of Demand and Capacity

distribution within certain limits of confidence. The uncertainty associated with the final answer will be as a result of the uncertainty in both demand and capacity. The uncertainty in the demand arising from the fact that there can be an array of ground motions with associated response spectra, which are being generalized to follow a code-specific spectrum. Consequently, it was noted that uncertainties involved in determining the ground motion demand on structures can be identified by means of a statistical analysis. This type of analysis was performed for the set of 36 scaled ground motions used in this study. A set of normalized standard deviations was proposed for the assessment of uncertainties within the short and long period ranges.

SECTION 3

FUNDAMENTAL CONSIDERATIONS FOR THE DESIGN OF SUPPLEMENTAL DAMPING SYSTEMS

3.1 INTRODUCTION

This section focuses on the two fundamental issues related to the design of nonlinear [viscous] dampers. In general, various techniques and approaches adopted in the current guidelines for the design of such damping devices, are based on the equivalent linear properties, namely equivalent linear damping of the device under consideration. Traditionally, equivalent linear damping is determined based on the equivalent energy consumption approach. However, in the following paragraphs, the development of equivalent linear properties based on notions of power consumption equivalence between a viscously damped system and a system possessing nonlinear [viscous] dampers is proposed. It is then noted that the general behavior of viscous devices is governed by the structural velocities. To successfully use spectral design methodologies such as capacity-demand spectrum, it is essential that actual structural velocities be used in all of the equivalent damping formulations. This is because if spectral velocities based on design displacements ($S_v = \omega_o S_d$) are used, errors are introduced, as the two velocities are not equivalent across the spectrum. Simplified design formulations are given for the proposed transformation to exact velocity. Normalized damper capacity (ε) is introduced in design formulations and a simple design procedure which incorporates the power equivalent linear damping is presented.

3.2 DETERMINATION OF ACTUAL STRUCTURAL VELOCITY

In this part of the study, it is realized that the accuracy of design/retrofit methods for building structures may largely depend on the "quality" of linearized (approximated) parameters versus their exact values. This becomes more important in the design of supplemental damping systems whose characteristics are primarily function of velocity. Therefore, it is desirable to use the actual maximum structural velocity in order to obtain consistent and more accurate estimations of damping system characteristics in terms of linearized quantities. Consequently, any attempt to predict the behavior of such systems, in general, should be based on the actual response parameters. However, actual velocity response is usually not readily available since

response spectra are typically available only for spectral deformation (S_d), pseudo spectral velocity (S_v) and pseudo spectral acceleration (S_a). Therefore, this section first describes the important characteristics of response spectra, and then derives an empirical spectral approach to estimate the actual maximum velocity response from the pseudo velocity spectra.

3.2.1 Characteristics of Response Spectra

As mentioned previously, response spectra have become a standard design tool to characterize the frequency content of an earthquake and the effective demands on a structure. Response spectra provide concise information that enables one to apply the knowledge of structural dynamics to structural design. Response spectra can be generated for various viscous damping ratios and presented by plotting the maximum value of the absolute displacement D (or S_d), relative velocity V, and acceleration A, obtained by solving the equations of motion of the linear single-degree-of-freedom (SDOF) system for various natural periods, T_o. However, it has been a common practice to use the pseudo-relative velocity S_v ($= \omega_o S_d$) and pseudo-acceleration S_a ($= \omega_o^2 S_d = \omega_o S_v$) instead of their actual counterparts, as these quantities can be directly calculated from the corresponding spectral displacements for the range of natural frequencies (ω_o in rad/sec.) considered on a spectra plot. Moreover, the three spectral values thus calculated can be conveniently plotted simultaneously on a tripartite log-log scale graph. More specifically, response spectra values are defined as follows:

$$\begin{aligned} S_d &= D = |x(t)|_{\max} \\ V &= |\dot{x}(t)|_{\max} \\ A &= |\ddot{x}(t)|_{\max} \\ S_v &= \omega_o S_d \\ S_a &= \omega_o S_v = \omega_o^2 S_d \end{aligned} \qquad \textbf{(3-1)}$$

in which $x(t), \dot{x}(t), \ddot{x}(t)$ are the displacement, velocity and acceleration response time histories, respectively, $|.|_{\max}$ designates maximum absolute value of the enclosed quantity, and $\omega_o = 2\pi / T_o$ is the natural circular frequency of the SDOF system.

Each of the pseudo spectral values contain the same information and are inter-related via the natural period of vibration, T_o. However, they each provide direct relationships to different

physically meaningful quantities. The pseudo acceleration spectra are directly related to the maximum forces in the structure, whereas pseudo relative velocity is related to the peak strain energy stored during ground shaking. The fact that these three quantities can be interrelated (approximately) and presented on a single plot makes it very desirable from an elastic design point of view. However, it can be shown that large variations of the shape and hence the characteristics of the response spectra exist. Some of the geological factors that have an effect on the response spectra are source mechanism, epicentral distance, focal depth, and soil conditions. The former factor is generally considered to be more significant than the rest. Due to the fact that these factors cannot be identified quantitatively, most of the studies have used approximate stochastic methods to generate site specific response spectrum curves which are functions of soil type and the critical viscous damping ratio.

Response spectra can be divided into various period ranges for which distinct observations can be made. The characteristics of each of these regions become very important when deriving the design response spectra. In general, it can be observed that in the short period (high frequency) range (which implies a stiff structure), pseudo acceleration approaches the maximum ground acceleration as the system deforms very little and the mass moves with the ground. This observation is valid for all damping values. Similarly, in the long period (low frequency) range (flexible structures), the maximum displacement response is practically equal to the maximum ground displacement whereas in the medium period range the displacement response is somewhat amplified beyond the ground displacement. However, in this period range, there is a near constant amplification factor for pseudo acceleration response for a given viscous damping ratio. This amplification factor becomes smaller for higher damping ratios. A nearly constant velocity response is observed in the medium period range.

At this point of the discussion, some of the important aspects of pseudo vs. actual response will be given in the following.

The maximum displacement response S_d of a SDOF system subjected to a ground acceleration $p(t)$ may be expressed by the well-known *Duhamel* integral as:

$$S_d = \left| \frac{1}{\omega_o} \int_0^t p(\tau) \sin \omega_d (t-\tau) \exp(-\xi_o \omega_o (t-\tau)) d\tau \right|_{max} \qquad \textbf{(3-2)}$$

when small critical viscous damping is assumed ($\omega_d = \omega_o\sqrt{1-\xi^2} \cong \omega_o$). The displacement response can be differentiated with respect to time to obtain the corresponding velocity response from which the maximum response can be calculated as:

$$V = \left| \int_0^t p(\tau)\cos\omega_o(t-\tau)d\tau \right|_{\max} \tag{3-3}$$

It must be noted that viscous damping ratio ξ_o, is assumed to be zero in the above expression for simplicity. Moreover, using equation (3-2) with $\xi_o = .0$, the pseudo relative velocity can be written as:

$$S_v = \left| \int_0^t p(\tau)\sin\omega_o(t-\tau)d\tau \right|_{\max} \tag{3-4}$$

It is clear from equations (3-3) and (3-4) that the actual spectral velocity and pseudo velocity are *different* even for zero damping, since the latter involves a *cosine* term whereas pseudo velocity expression has a *sine* term. It can be shown that the difference between the two response values becomes more pronounced for long period systems as well as for high damping ratios. In general, pseudo-relative velocity spectra values are consistently higher than the actual-relative velocity spectra in the low period range, and become nearly the same in the medium period range for low damping values. The lower and upper period limits of this region depend on the frequency content of the velocity trace of the ground motion. In other words, the broader the band of frequencies involved, the broader is the range of natural periods over which the pseudo and actual velocities are similar. Furthermore, pseudo-relative velocity (S_v) is unconservative in the high period region as the actual-relative velocity (V) approaches the maximum ground velocity (v_g) while pseudo velocity approaches zero as $T_o \rightarrow \infty$.

Following a similar discussion, it can be shown that the pseudo acceleration is the same as the maximum acceleration when there is no damping in the system. However, for higher damping values, pseudo acceleration starts to diverge from the maximum acceleration. The pseudo acceleration is typically less than the maximum acceleration. Constantinou et al. (1998) have proposed an approximate relationship between the maximum and pseudo acceleration by

assuming that during the cycle of maximum response, the analyzed SDOF system undergoes harmonic motion of frequency ω_o:

$$A = (f_1 + 2\xi f_2)S_a \tag{3-5}$$

in which $f_1 = \cos[\tan^{-1}(2\xi)]$ and $f_2 = \sin[\tan^{-1}(2\xi)]$

The difference between maximum and pseudo acceleration, however, has less significance from the design point of view, since current seismic design codes specify the earthquake excitation in the form of an acceleration response spectra with amplification factors that indirectly consider the above mentioned pitfall. This is the case for the difference between pseudo and exact velocities, but only for classically damped systems. If the system damping is of linear viscous type and does not change with time and loading, it will be referred as "classically damped". When system damping is of classical type, the desired responses are the induced deformations and the forces in the system by the ground shaking. Therefore the response spectra needed are those for maximum relative velocity. In previous applications of spectral analysis and design approaches to non-classically damped systems, the spectral values of relative velocity were approximated by the corresponding pseudo velocity values. While it may lead to results of reasonable accuracy under certain conditions, this approximation is clearly not generally valid. Hence, there is a need to re-examine the issues involved in the application of the analysis and design methods to non-classically damped systems such as those with nonlinear rate-dependent devices (nonlinear viscous, $\alpha < 1.0$).

3.2.2 Relationship Between Actual and Pseudo Relative Velocity Spectrum

Based on the above observations, a general relationship between pseudo and actual maximum velocity is analytically derived using a series of earthquake ground motions. Each record was scaled such that the maximum ground velocity is $v_{gmax} = 1m/sec$. This is in order to facilitate direct comparison of results. The ground motions used are previously listed in table 2-2, with some selected acceleration time histories plotted in figure 3-1. Mean pseudo and actual relative velocity spectra are plotted on log-log scale velocity-period graphs in figures 3-2 through 3-10 for T_o = 0 to 10 sec. and viscous damping ratios, ξ of 5, 10, 20, 30, 40, 50, 60, 70 and 80%. The following set of relationships are proposed for three different period ranges mentioned above:

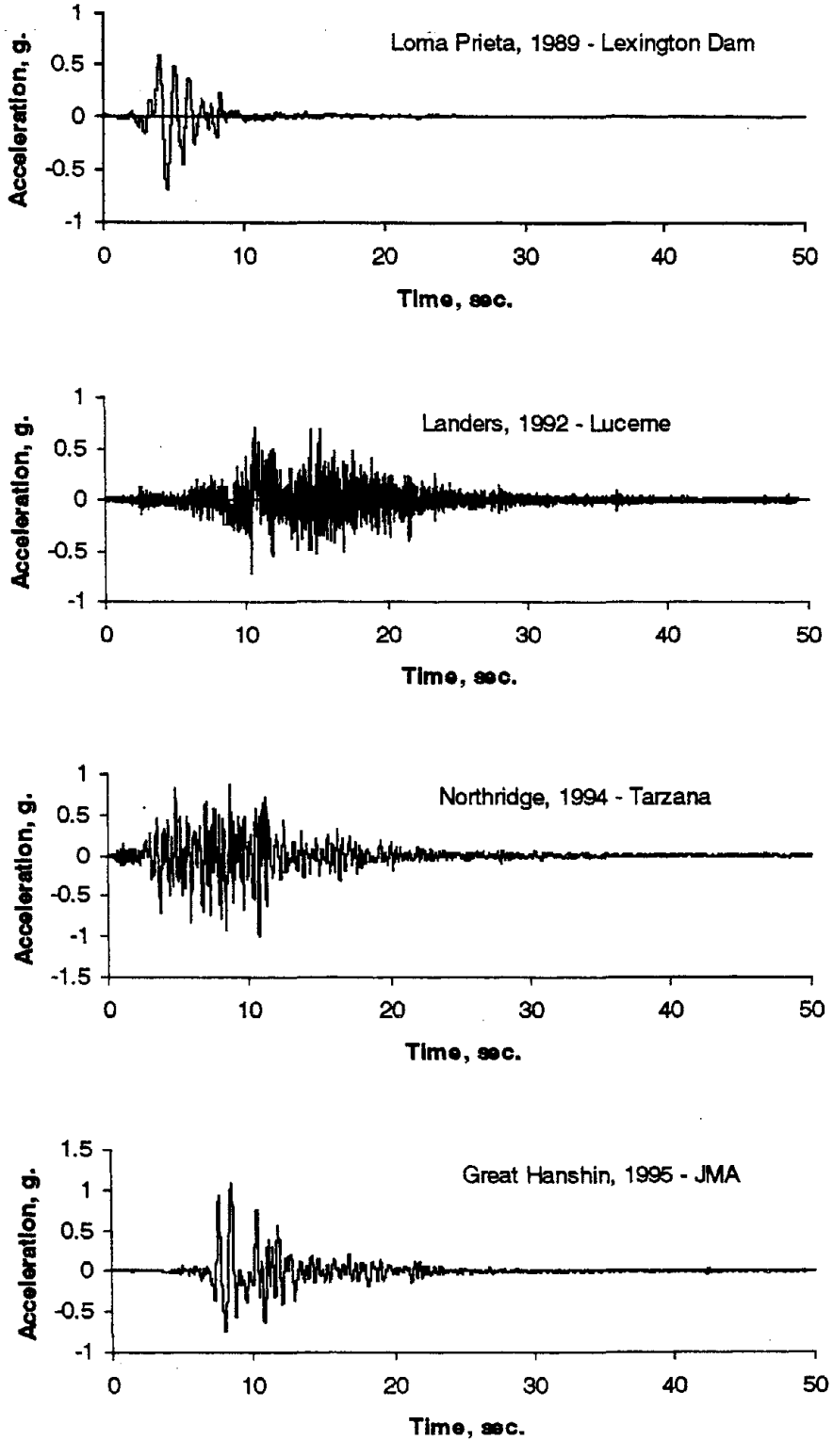

Figure 3-1 Selected acceleration time histories

Table 3-1 Regression Results

Parameter Definition	Equation	r^2
Upper Limit Period, T_u	$T_u = 3.149\xi + 3.112$	**0.98**
Medium Limit Period, T_m	$T_m = -0.064\xi + 0.756$	**0.96**
Lower Limit Period, T_l	$T_l = -0.042\xi + 0.113$	**0.96**
Exponent, α_u	$\alpha_u = -0.489\xi + 0.607$	**0.99**
Exponent, α_m	$\alpha_m = 0.455\xi + 0.132$	**0.98**
Exponent, α_l	$\alpha_l = -0.450\xi + 0.729$	**0.99**

$$V = S_v \begin{cases} \left(\frac{T_o}{T_l}\right)^{\alpha l}\left(\frac{T_o}{T_m}\right)^{\alpha m} & 0 < T_o < T_l \\ \left(\frac{T_o}{T_m}\right)^{\alpha m} & T_l \le T_o \le T_u \\ \left(\frac{T_o}{T_m}\right)^{\alpha m}\left(\frac{T_o}{T_u}\right)^{\alpha u} & T_o > T_u \end{cases} \qquad \textbf{(3-6)}$$

A least square regression analysis was used to establish the parameters in equation (3-6). Results of this analysis are presented figure 3-11 and in table 3-1 along with the respective correlation coefficients, r^2. Note that for perfect agreement $r^2 = 1$. Using the relationships proposed in equation (3-6), the graphs of exact and theoretical maximum velocity spectra are plotted in figures 3-2 to 3-10. It is evident that excellent agreement is obtained throughout the entire range of periods from $T_o = 0.01$ to 10 sec.

3.2.3 Design Formulation for Pseudo-Exact Relative Velocity Transformation

The above-mentioned (table 2-2) ground motions were scaled to a maximum PGA = 0.6 m / sec^2 and linear response spectra were generated for 5, 10, 20, 30 and 40% viscous damping ratio. A period range of T_o = 0 to 3 *sec.* was chosen, since it covers the period range that is most relevant to most of the building structures. Corresponding design acceleration spectra (S_a-T) were plotted together with those generated in figure 3-12. Also plotted in the figure are the corresponding demand curves (C_d-S_d).

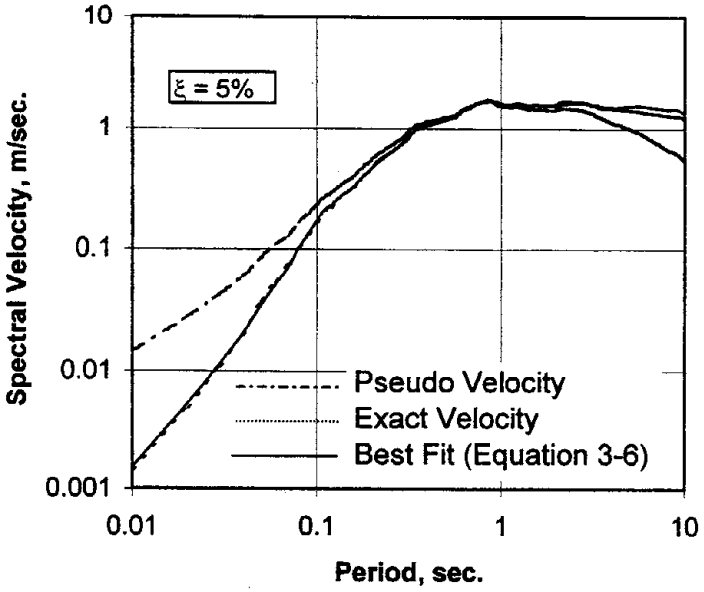

Figure 3-2 Average Relative Velocity Spectra, ξ=5%

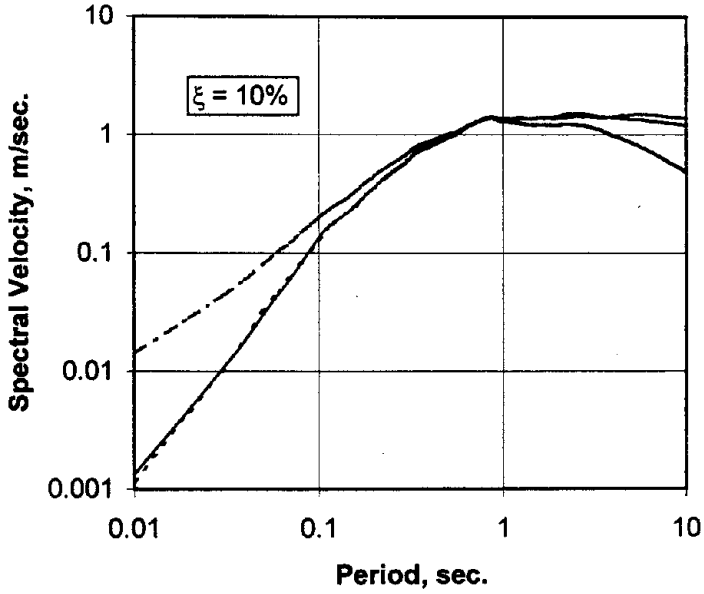

Figure 3-3 Average Relative Velocity Spectra, ξ=10%

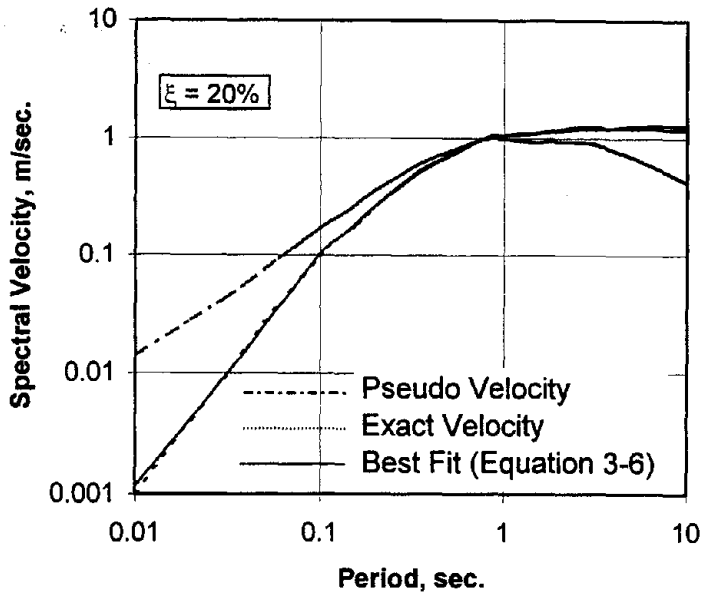

Figure 3-4 Average Relative Velocity Spectra, ξ=20%

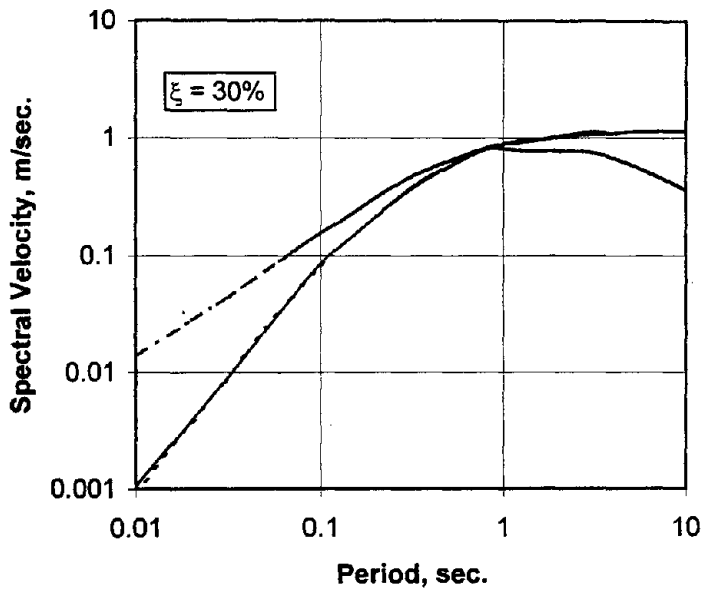

Figure 3-5 Average Relative Velocity Spectra, ξ=30%

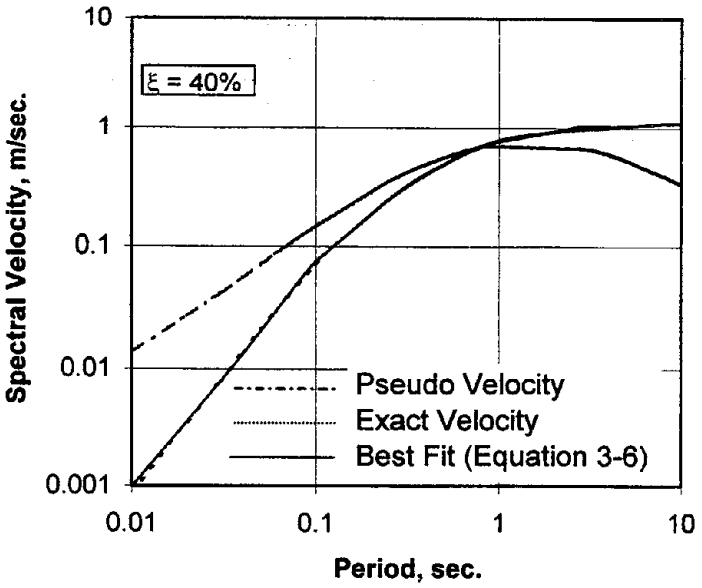

Figure 3-6 Average Relative Velocity Spectra, ξ=40%

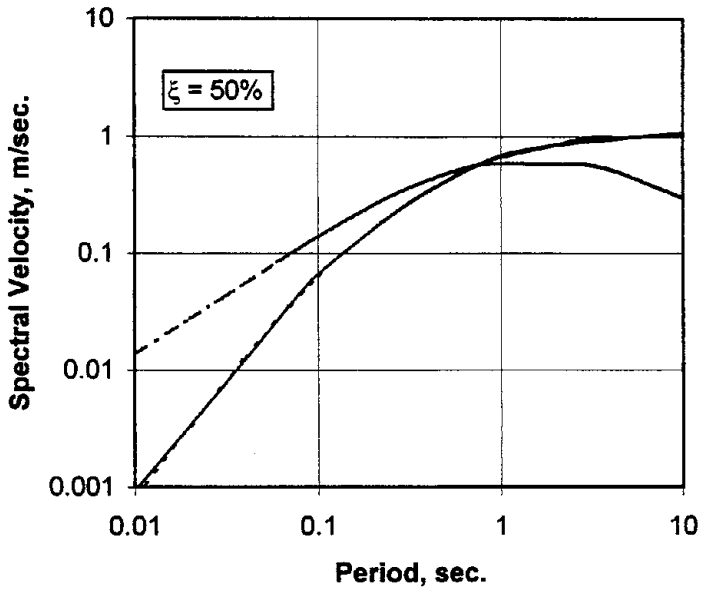

Figure 3-7 Average Relative Velocity Spectra, ξ=50%

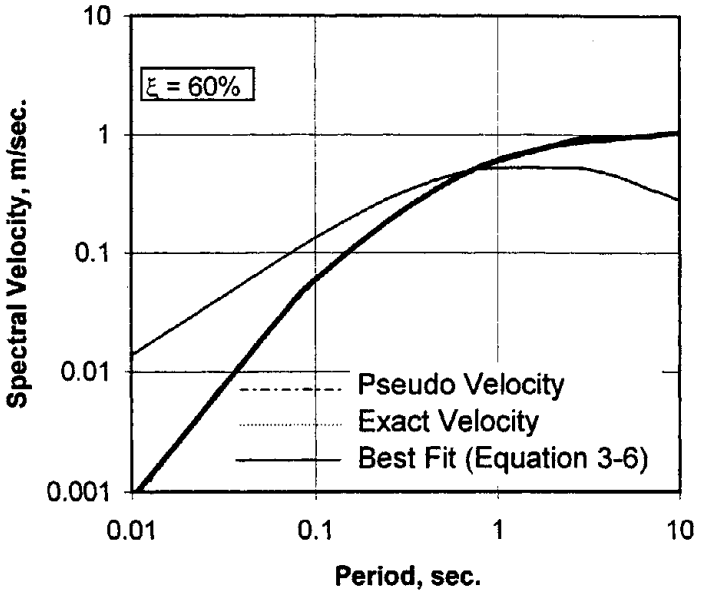

Figure 3-8 Average Relative Velocity Spectra, ξ=60%

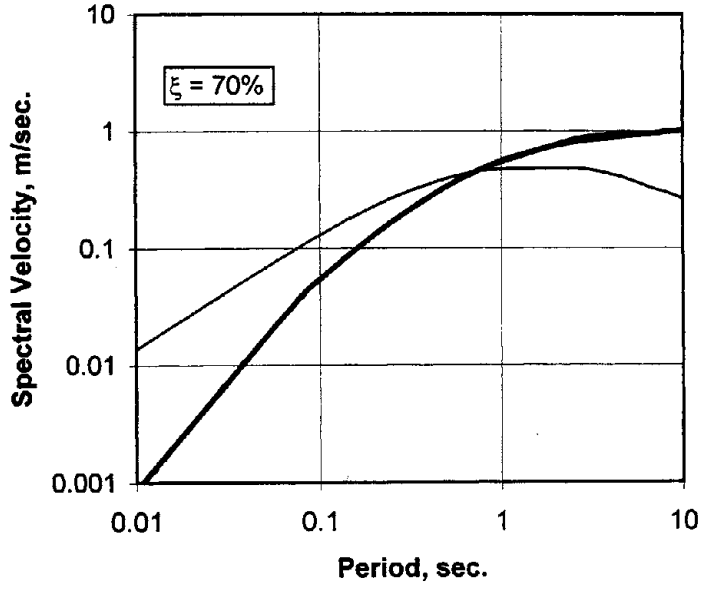

Figure 3-9 Average Relative Velocity Spectra, ξ=70%

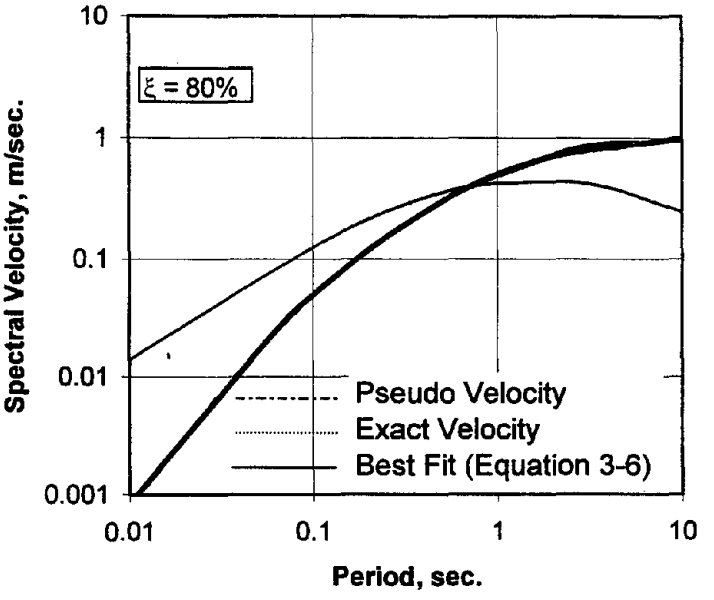

Figure 3-10 Average Relative Velocity Spectra, ξ=80%

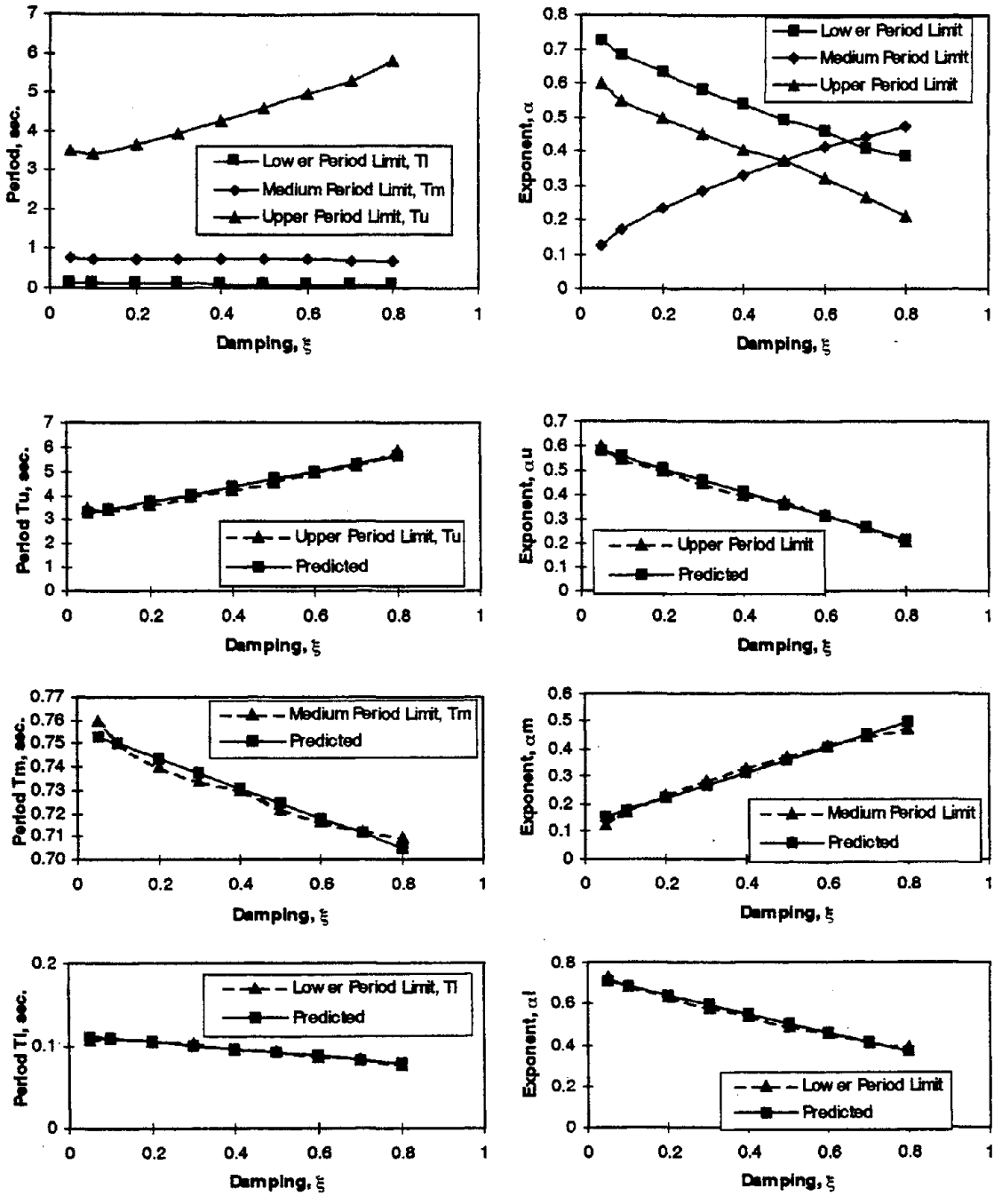

Figure 3-11 Variation of Parameters defined in equation 3-6 and Regression Results

Pseudo relative velocity ($S_v = T_o S_a / 2\pi$) spectra are plotted in figure 3-13 together with corresponding actual velocities. The difference between actual and pseudo velocities as mentioned in the previous section can also be seen in these figures. Following transformation is proposed for 5% damping based on the general expression given in equation (3-6) and for the period range considered:

$$V^{5\%} = S_v^{5\%} \left(\frac{T}{0.75} \right)^{0.15} \qquad 0 \le T_o \le 3\ sec. \tag{3-7}$$

Approximate actual velocity spectra for higher damping values can be determined using the same B_s and B_1 factors (equation 2-30) used for the spectral acceleration spectra as shown in figure 3-13 with proper adjustment for the corner period 0.75 sec. as

$$V_\xi = \left(\frac{T}{0.75} \right)^{0.15} \begin{cases} \dfrac{S_v^{5\%}}{B_s} & 0 \le T_o \le T_{sl} \\ \dfrac{S_v^{5\%}}{B_l} & 0.75 \dfrac{B_s}{B_l} \le T_o \le 3\ sec. \end{cases} \tag{3-8}$$

It must be noted that equations (3-7) and (3-8) are not valid for the period range $T_{sl} = C_v / 2.5C_a < T < 0.75(B_s / B_l)$, instead, a linear relationship is assumed for this intermediate region.

As mentioned in the previous subsections, response spectra approaches using appropriate equivalent linear properties are nowadays used in the design of structures. It was also noted that this approach could be easily implemented in a design procedure that involves supplemental damping systems, particularly if the relevant nonlinear properties of such systems can be reliably linearized. Therefore, in the following subsections, a simple linearization technique is described for nonlinear damping systems following a brief review of various other techniques.

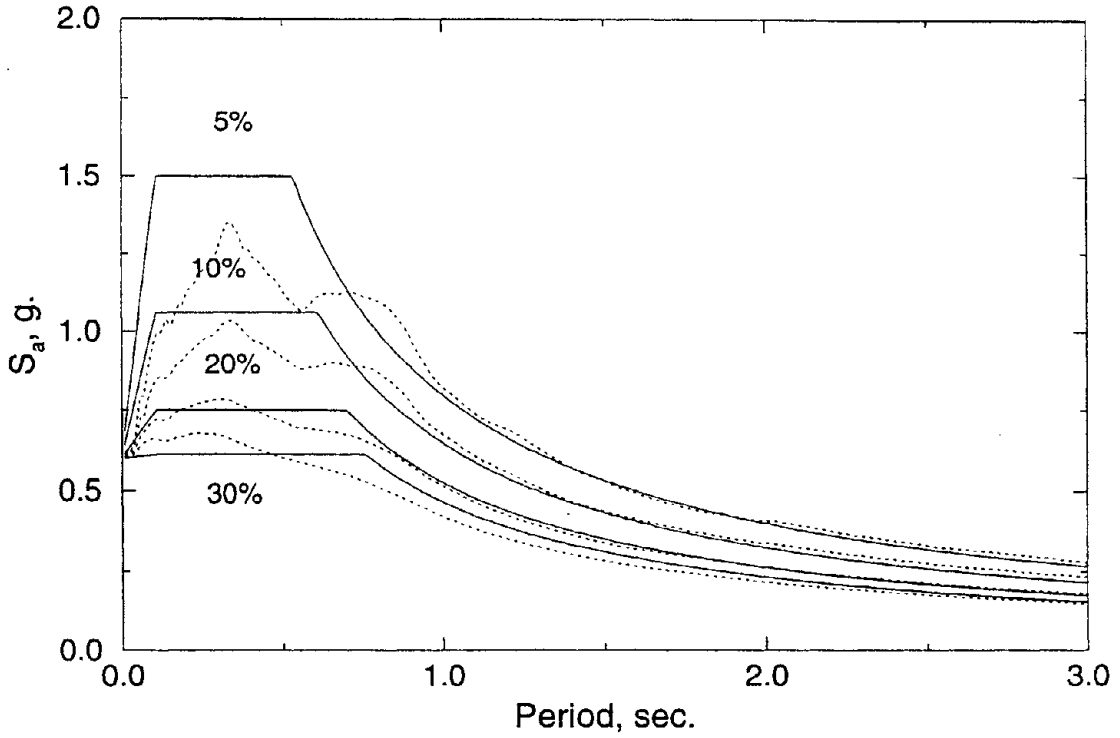

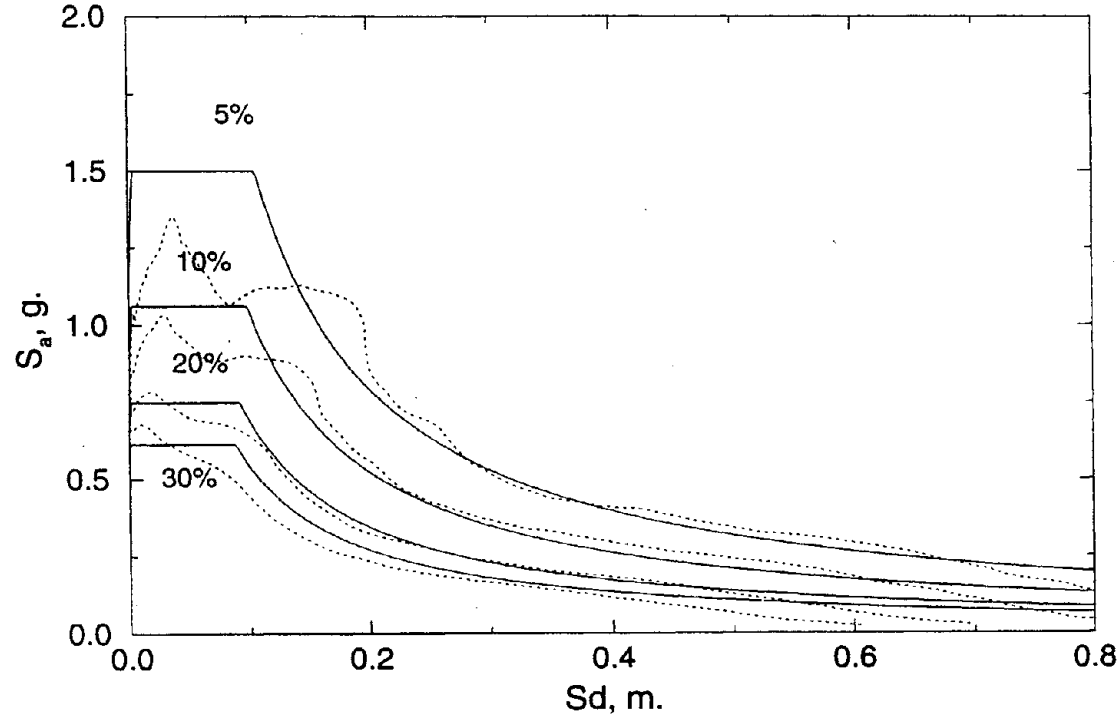

Figure 3-12 Spectral Acceleration and Demand Curves

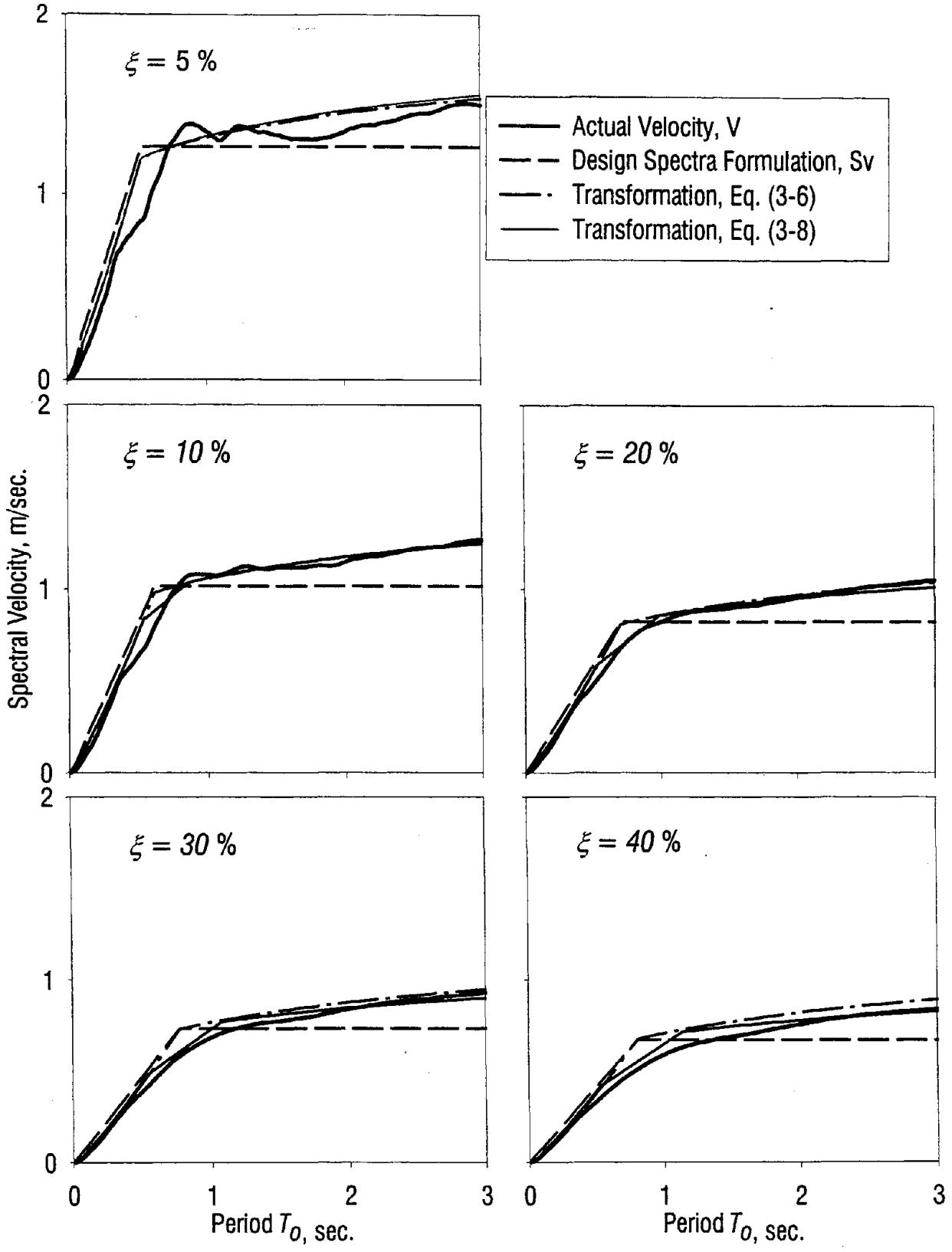

Figure 3-13 Pseudo-Actual Relative Velocity Transformations

3.3 LINEARIZATION OF NONLINEAR ($\alpha \neq 1$) DAMPING

Equivalent linear models facilitate the analysis and design of corresponding nonlinear models. Therefore, it is very important that reliable linearized models be studied and be implemented at least in the preliminary stages of design.

Jacobsen (1930) first proposed to use an equivalent viscous damping coefficient for a nonlinear system. Many other approximate linearization methods were then studied and applied to analyze and to design various nonlinear dynamic structural systems. These include methods based on harmonic linearization, energy balance, resonant amplitude matching, dynamic mass, constant critical damping, geometric stiffness, and geometric energy, just to name a few. Although these methods are based on the assumption that the earthquake response of a structural system is quasi-harmonic, there are also methods that consider the random nature of the earthquake response, namely, stationary random equivalent linearization, average period and damping, average stiffness and energy etc.

Caughey (1959a, 1959b) first proposed application of equivalent linearization techniques to stochastic systems. In his studies, Caughey proposed the replacement of a nonlinear SDOF oscillator by a linear one for which the coefficients of linearization can be found from a mean-square criterion. Foster (1968), Iwan and Yang (1972) and Atalik and Utku (1976) have generalized this method for multi-degree-of-freedom (MDOF) systems. A brief description of these methods is given by Iwan and Gates (1979).

Among the above mentioned methods, harmonic equivalent linearization and energy balance methods are the most widely accepted and are used by many researchers. Both of these methods are similar in that they attempt to define an equivalent linear force-deformation relation for the nonlinear system. The equivalent damping coefficient c_{eq}, and equivalent stiffness k_{eq}, are sought such that the two equations of motion yield similar solutions:

$$m\ddot{x} + c\dot{x} + kx + F(x,\dot{x}) \approx m\ddot{x} + c_{eq}\dot{x} + k_{eq}x \qquad \textbf{(3-9)}$$

where $x, \dot{x}, \ddot{x}$ = displacement, velocity and the acceleration of the system, respectively, m= mass, c = viscous damping, k = stiffness of the system, and $F(x,\dot{x})$ = a nonlinear function of velocity and displacement.

In the method of harmonic equivalent linearization the difference between the exact nonlinear equation of motion and the equivalent linear equation of motion is minimized with

respect to the equivalent linear parameters over one cycle of sinusoidal response. In the method of energy balance, the work per cycle of oscillation for the nonlinear restoring force is equated to that of the equivalent linear restoring force. It can easily be shown that both methods yield identical results.

In the following paragraphs, the classical energy balance method, which is customarily employed in linearization studies and adopted in FEMA 273/274, is reviewed. A new approach based on considering power consumption equivalence between viscously damped system and system possessing nonlinear devices is proposed. An average empirical transformation between actusl and pseudo spectral velocities is described and utilized in the linearization. The equivalent energy approach and proposed power approach are then compared with exact time history predictions for a number of earthquake ground motions for a linear SDOF system.

3.3.1 Equivalent Energy Consumption Approach

One of the most common methods for defining equivalent viscous damping is to equate the energy dissipated in a vibration cycle of the actual nonlinear system and equivalent viscous system. Applying the energy balance method to nonlinear viscous damping devices which can be modeled using equation (3-10):

$$F_V = \mathrm{sgn}(\dot{x}_D) c_\alpha |\dot{x}_D|^\alpha \tag{3-10}$$

Constantinou (Soong and Constantinou, 1994) has shown that the work done (dissipated energy) in one cycle of sinusoidal loading can be written as:

$$W_d = \int_0^{T_o} F_V \dot{x}_D dt \tag{3-11}$$

where $T_o = 2\pi / \omega_o$ and $x_D = x_o \sin\omega_o t$. Equation (3-11) can then be integrated to give:

$$W_d = 4.2^\alpha \frac{\Gamma^2(1+\alpha/2)}{\Gamma(2+\alpha)} c_\alpha x_o^{1+\alpha} \omega_o^{\alpha} \tag{3-12}$$

where $\Gamma(\ )$ is the gamma function. Therefore the equivalent damping is calculated by equating equation (3-12) and the energy dissipated in equivalent viscous damping:

$$4\pi\xi_{eq}\omega_o E_S = W_d \tag{3-13}$$

in which strain energy $E_S = kx_o^2/2$. Solving equation (3-13) for equivalent damping ratio:

$$\xi_{eq} = \frac{2^{1+\alpha} c_\alpha x_o^{\alpha-1} \omega_o^{\alpha-2} \Gamma^2(1+\alpha/2)}{\pi M \quad \Gamma(2+\alpha)} \tag{3-14}$$

in which M = mass of the system, x_o = amplitude of harmonic motion at the undamped natural frequency ω_o. It must be noted here that due to the viscous nature of this type of device, it is conveniently assumed that they possess only equivalent viscous damping characteristics.

3.3.2 Proposed Equivalent Power Consumption Approach

In this study, it is contended that for velocity dependent systems such as viscous dampers, consideration of the *rate* of energy dissipation—that is power (rather than energy)—becomes more important in seeking the equivalent linear properties for these systems. A simple method for making the transformation from the nonlinear damper behavior to equivalent viscous damping is described in what follows.

Power, by definition, is the *rate* of energy dissipation. The time-average power consumption over one cycle of sinusoidal loading can be approximated as the area under the force-velocity response curve, as shown in figure 3-14 and given as

$$\overline{P} \approx \frac{F_{Do}\dot{x}_{Do} + F_{Dn}\dot{x}_{Dn}}{2} \approx \frac{1}{2}\sum_{i=1}^{T_o/\Delta t}(F_{D_{i+1}} + F_{D_i})(\dot{x}_{D_{i+1}} - \dot{x}_{D_i}) = \int_0^{T_o} F_D d\dot{x}_D \tag{3-15}$$

in which $\overline{P}$ = average power consumption over one cycle of sinusoidal response, F_{Do}, F_{Dn} = damper force at the beginning and at the end of the time history, respectively, $\dot{x}_{Do}$, $\dot{x}_{Dn}$ = corresponding damper velocities, F_{D_i} = damper force, $\dot{x}_{D_i}$ = damper velocity.

Thus, average power consumption over one cycle of oscillation (area under the force-velocity curve) for the nonlinear damper (c_α) is equated to that for the equivalent linear damper (c_{eq}) with $\alpha = 1$:

$$\begin{aligned} &\overline{P}_\alpha = \overline{P}_{eq} \\ &\frac{1}{1+\alpha} c_\alpha \dot{x}_o^{\alpha+1} = \frac{1}{2} c_{eq} \dot{x}_o^2 \end{aligned} \tag{3-16}$$

Solving the above equation (3-16) for c_{eq} gives:

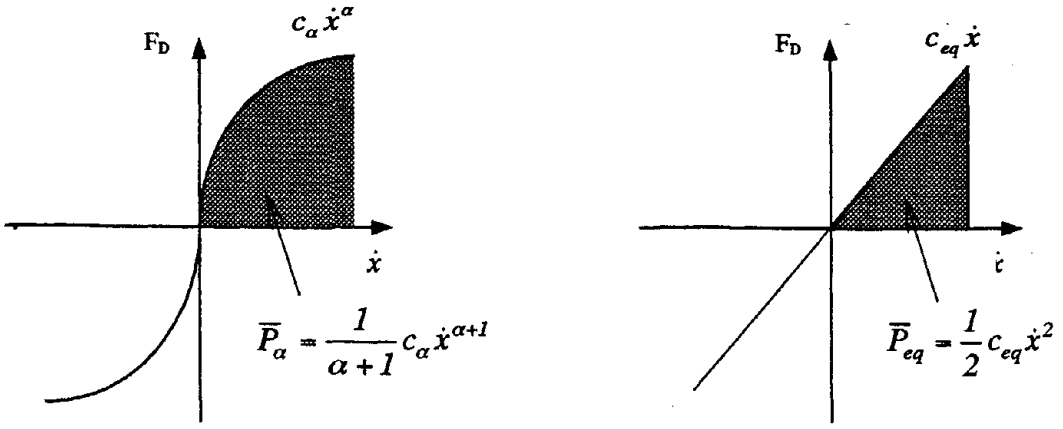

Figure 3-14 Equivalent Power Formulation

$$c_{eq} = \frac{2}{1+\alpha} c_\alpha \dot{x}_o^{\alpha-1} \tag{3-17}$$

Given the customary definition of damping ratio (ξ) obtained from $c_{eq} = 2\xi_{eq}\omega_o m$, then equation (3-17) can be expressed in terms of:

$$\xi_{eq} = \frac{1}{1+\alpha} \frac{c_\alpha x_o^{\alpha-1} \omega_o^{\alpha-2}}{M} \tag{3-18}$$

The proposed theory can also be applied to determine the equivalent linear properties of elastomeric spring dampers (ESD) (Pekcan et al., 1995a, 1995b). However, the stiffness contribution for this class of damper should also be considered in the formulation; the effective stiffness ($\omega_e^2 = K_e / M$) of an ESD can be calculated as the secant stiffness at the maximum displacement response. It is further assumed that in terms of absolute maximum response quantities (displacement and velocity):

$$c_\alpha \dot{x}^\alpha \left(\frac{x_m}{x_R}\right)^\beta \approx c_\alpha \dot{x}_m$$

Finally, equivalent viscous damping of ESD can be determined from equation (3-18) using $\omega_o = \omega_e$.

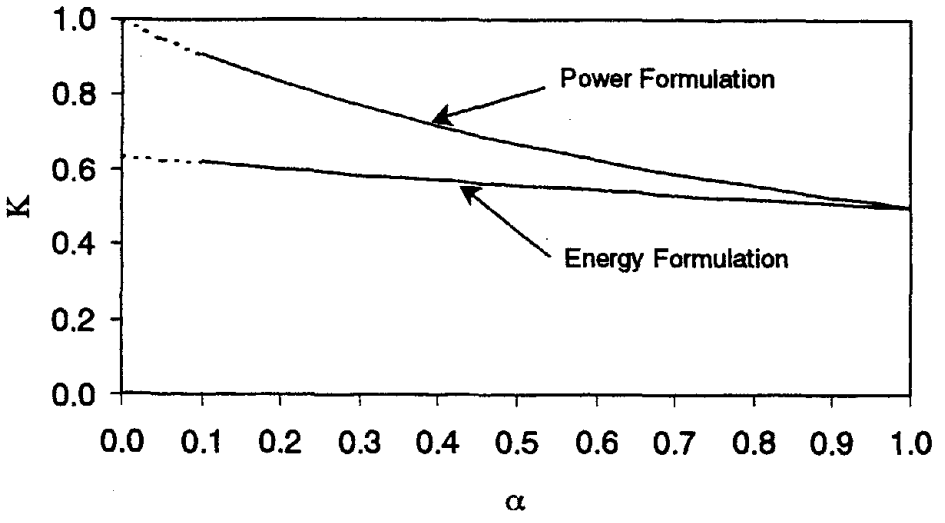

Figure 3-15 Comparison of Equivalent Damping Formulations

In the derivations of equations (3-14) and (3-18), maximum velocity response $\dot{x}_o$ is assumed to be equal to the product of natural circular frequency ω_o and, the maximum displacement response x_o. However, exact maximum velocity is used herein to obtain more consistent and more accurate estimations of equivalent damping, as the actual behavior of the devices is a function of the "actual" velocity. In fact, any attempt to predict the behavior, in general, should be based on the exact response parameters. Therefore, firstly response spectra for a series of ground motions were generated using both energy based and proposed power equivalent approaches and compared with those obtained from exact analyses. Secondly, the effect of pseudo-exact velocity transformation on the equivalent response spectra based on power equivalent approach is presented.

3.3.3 Comparison of Proposed and Energy Based Methods

In the previous subsection an approximate relationship between pseudo and actual relative maximum velocity is established. The motivation behind this part of the study is the fact that more accurate predictions of the nonlinear viscous damper behavior under the earthquake ground motions can be made using actual relative velocity response of the systems rather than the pseudo relative velocities. Therefore, this section is designed mainly to compare the commonly used energy based equivalent linear model for nonlinear viscous dampers with proposed power equivalent method. The effect of using pseudo versus exact velocity response in power equivalent formulation is demonstrated and the results are compared.

Equations (3-14) and (3-18) that are used to determine equivalent linear damping ratios are both in the form of:

$$\xi_{eq} = \kappa \left(\frac{c_\alpha x_o^{\alpha-1} \omega_o^{\alpha-2}}{M} \right) \tag{3-19}$$

where

$\kappa = \kappa_{EN} = \frac{2^{1+\alpha}}{\pi} \frac{\Gamma^2(1+\alpha/2)}{\Gamma(2+\alpha)}$ for the energy approach and

$\kappa = \kappa_{PO} = \frac{1}{1+\alpha}$ for the power approach.

These coefficients are plotted for various α values and compared in figure 3-15. As can be seen from the figure, the power equivalent approach predicts higher damping values (17 % more for $\alpha = 0.5$ and values 28 % more for $\alpha = 0.2$) in general as the two curves converge to 0.5 for $\alpha = 1$. One must be cautious using any of the above formulations for small α powers, since the mechanism of the devices changes from viscous (velocity dependent) to Coulomb friction type. A more detailed comparison using specific ground motions and levels of critical damping ratios is given in the following paragraphs.

The equation of motion of a linear SDOF system with various nonlinear viscous dampers was numerically solved to generate response spectra. For the present study, elastic response spectra are generated for five different ground motions, namely 1940 Imperial Valley - El Centro N-S, 1971 San Fernando - Pacoima Dam S16E, 1994 Northridge - Sylmar County Hospital, 1995 Hanshin – Kobe (JMA) and 1992 Landers- Lucerne. Peak ground accelerations of these ground motions are scaled to 1.0 g in order to facilitate direct comparison of the results. The inherent viscous damping of the parent structure is assumed to be a standard value of $\xi_o = 5\%$. The non-dimensional damper capacity ε is defined as:

$$\varepsilon = \frac{c_\alpha \dot{x}_{ref}^{\alpha}}{W} \tag{3-20}$$

in which W = total weight of the system, and $\dot{x}_{ref} = 1m/\text{sec}$ which is a standard testing velocity for viscous dampers (Note for some manufacturers standard testing velocity is 2 m/sec). Introducing the non-dimensional damper capacity ε into equations (3-14) and (3-18) and rearranging:

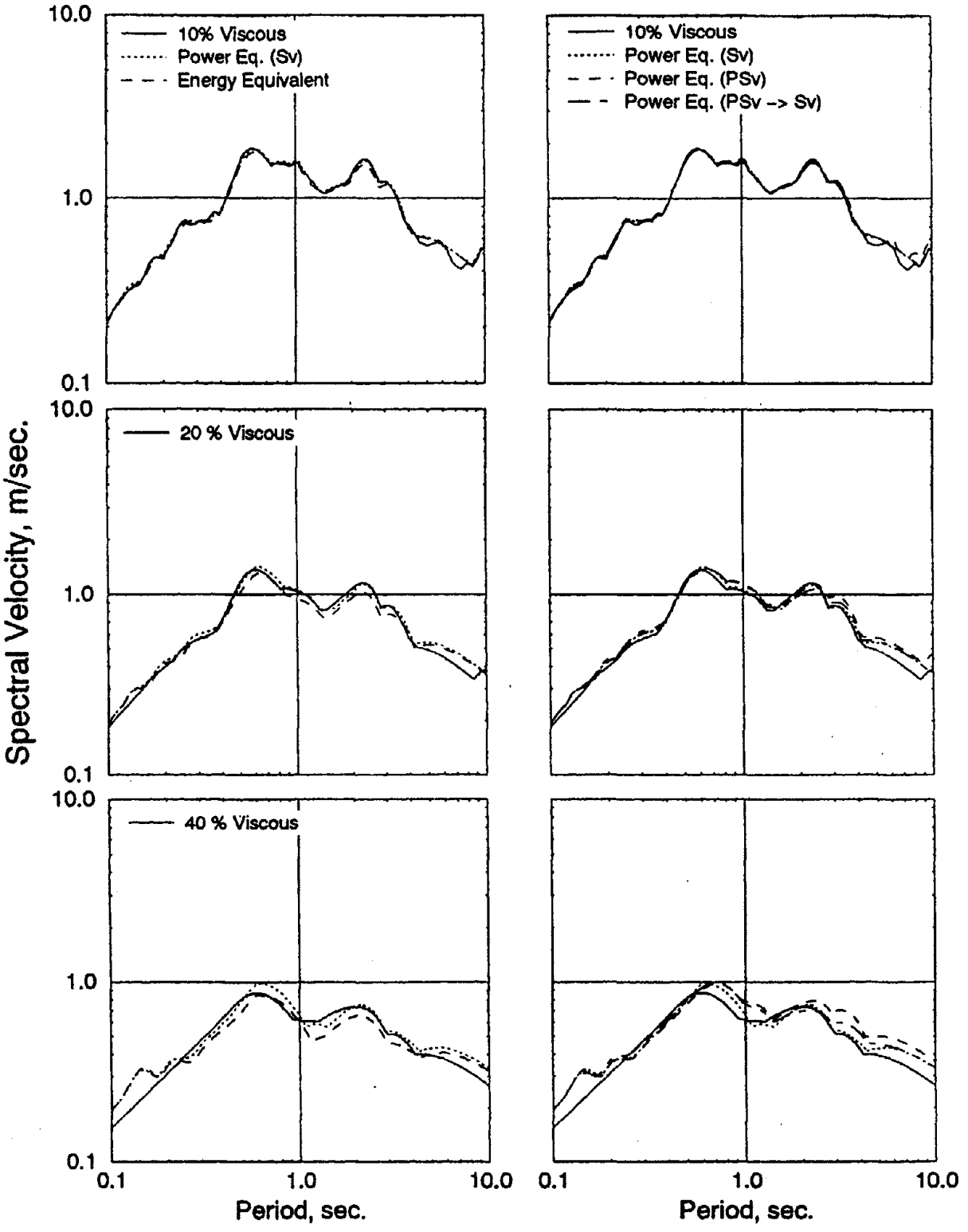

Figure 3-16 Comparison of Energy and Power Approach –El Centro, α=0.5

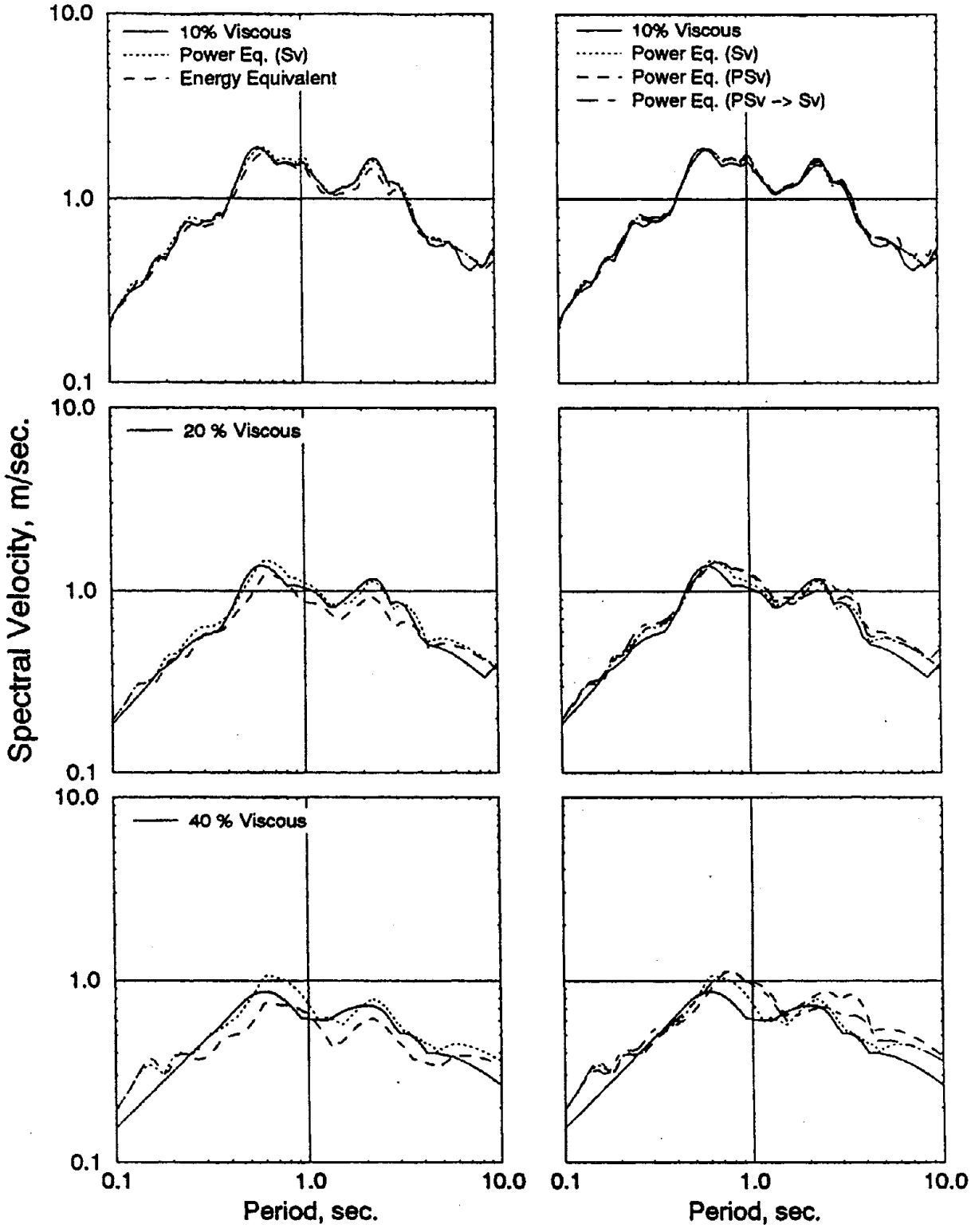

Figure 3-17 Comparison of Energy and Power Approach – El Centro, α=0.2

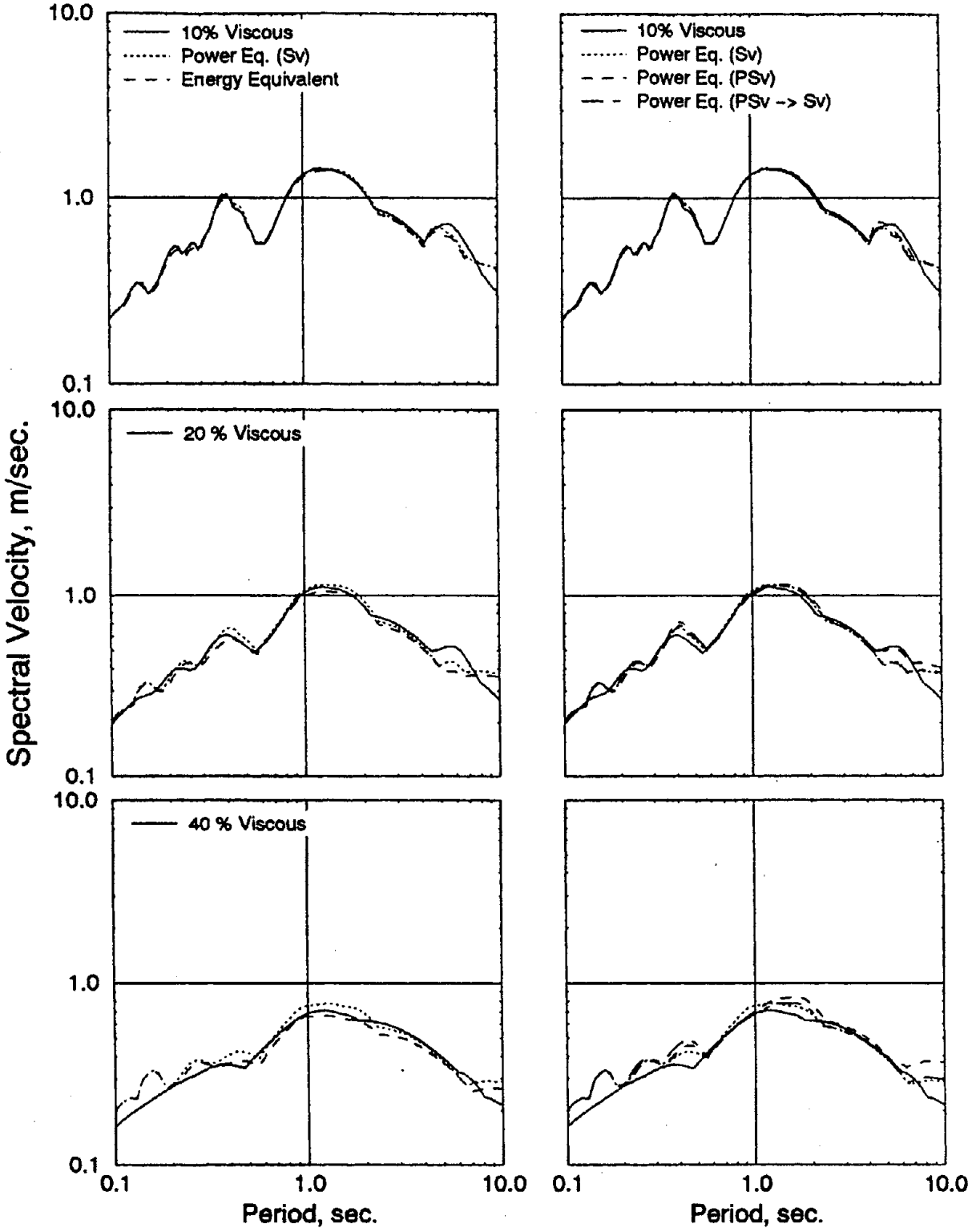

Figure 3-18 Comparison of Energy and Power Approach – Pacoima Dam, α=0.5

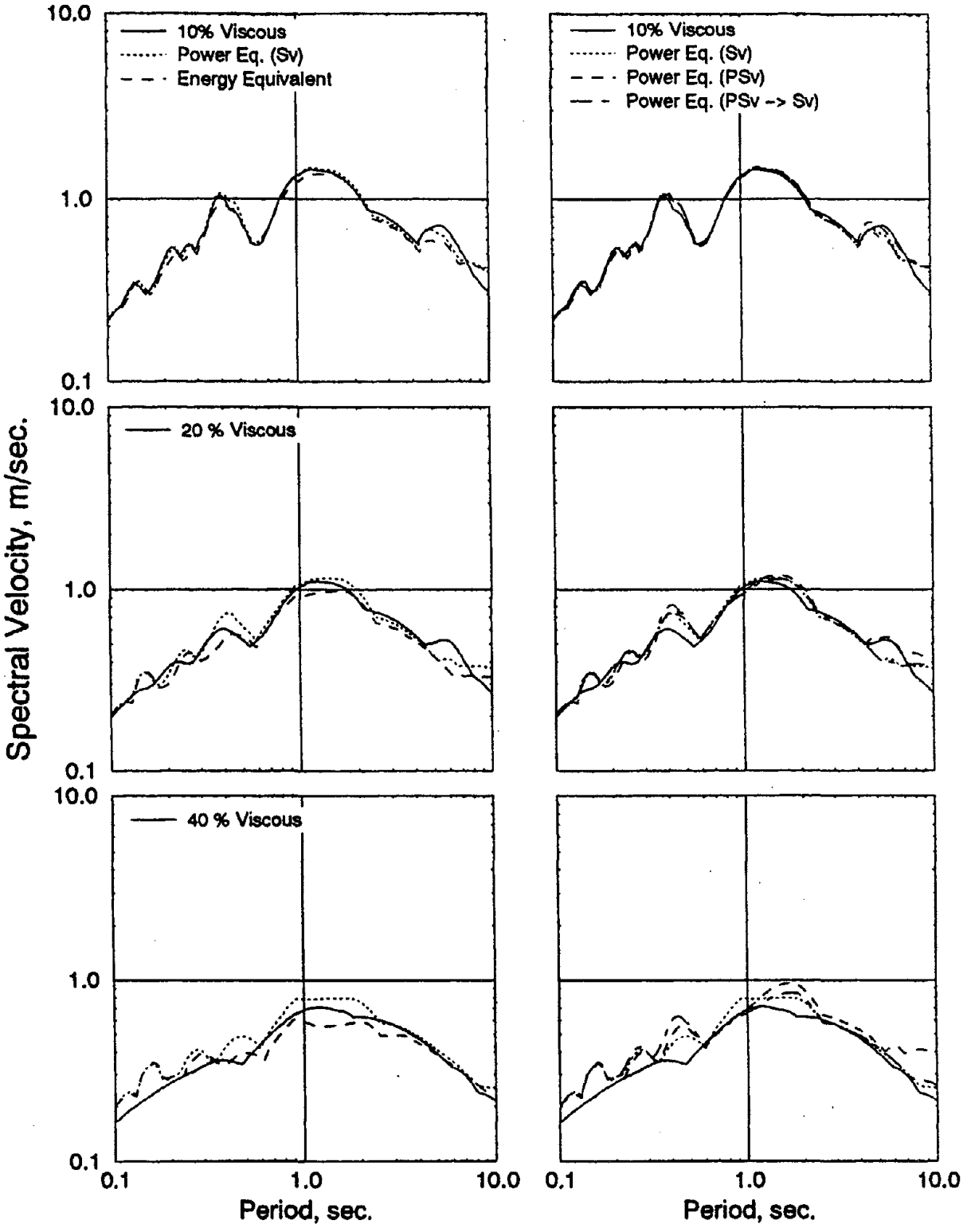

Figure 3-19 Comparison of Energy and Power Approach – Pacoima Dam, α=0.2

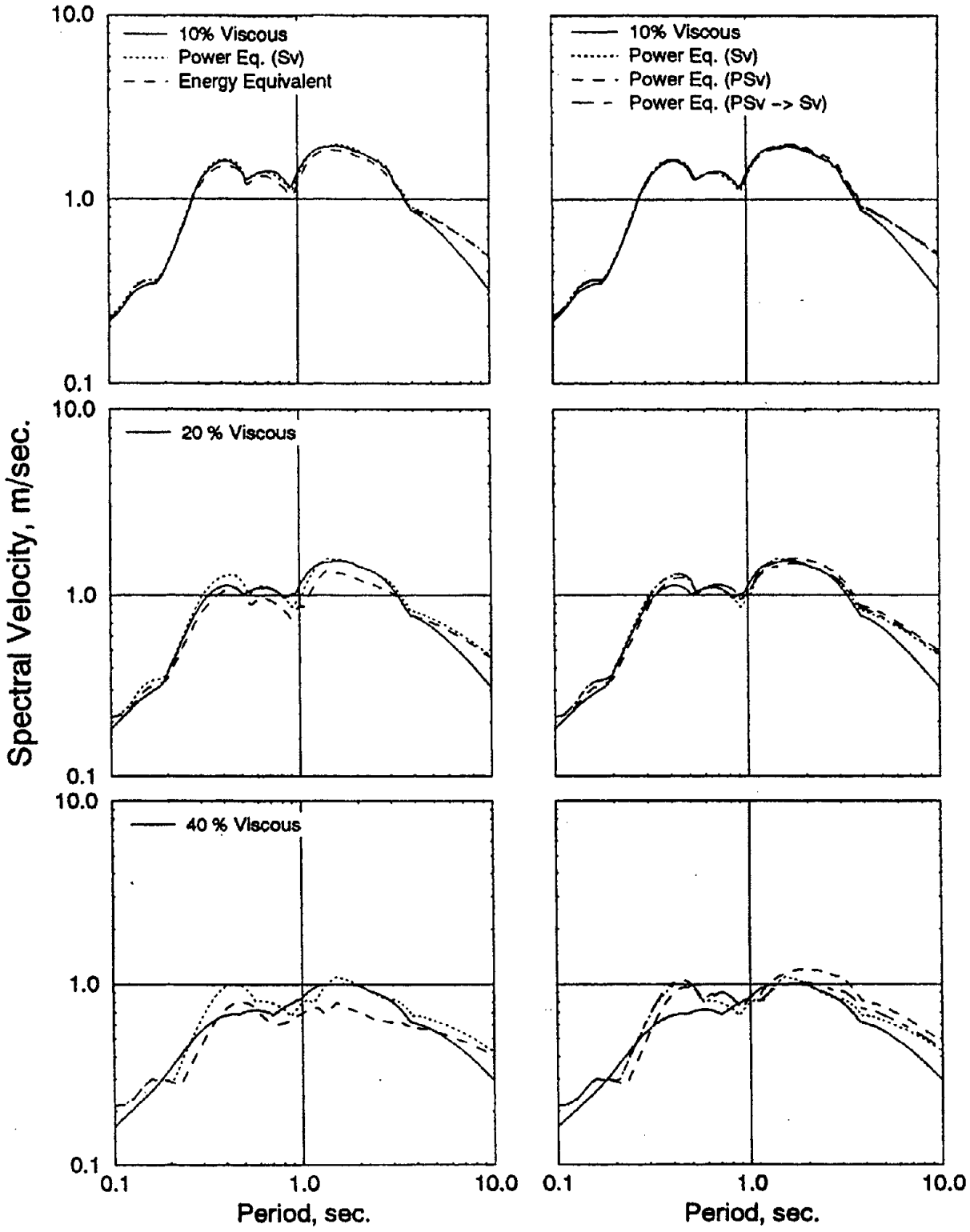

Figure 3-20 Comparison of Energy and Power Approach – Sylmar C.H., α=0.5

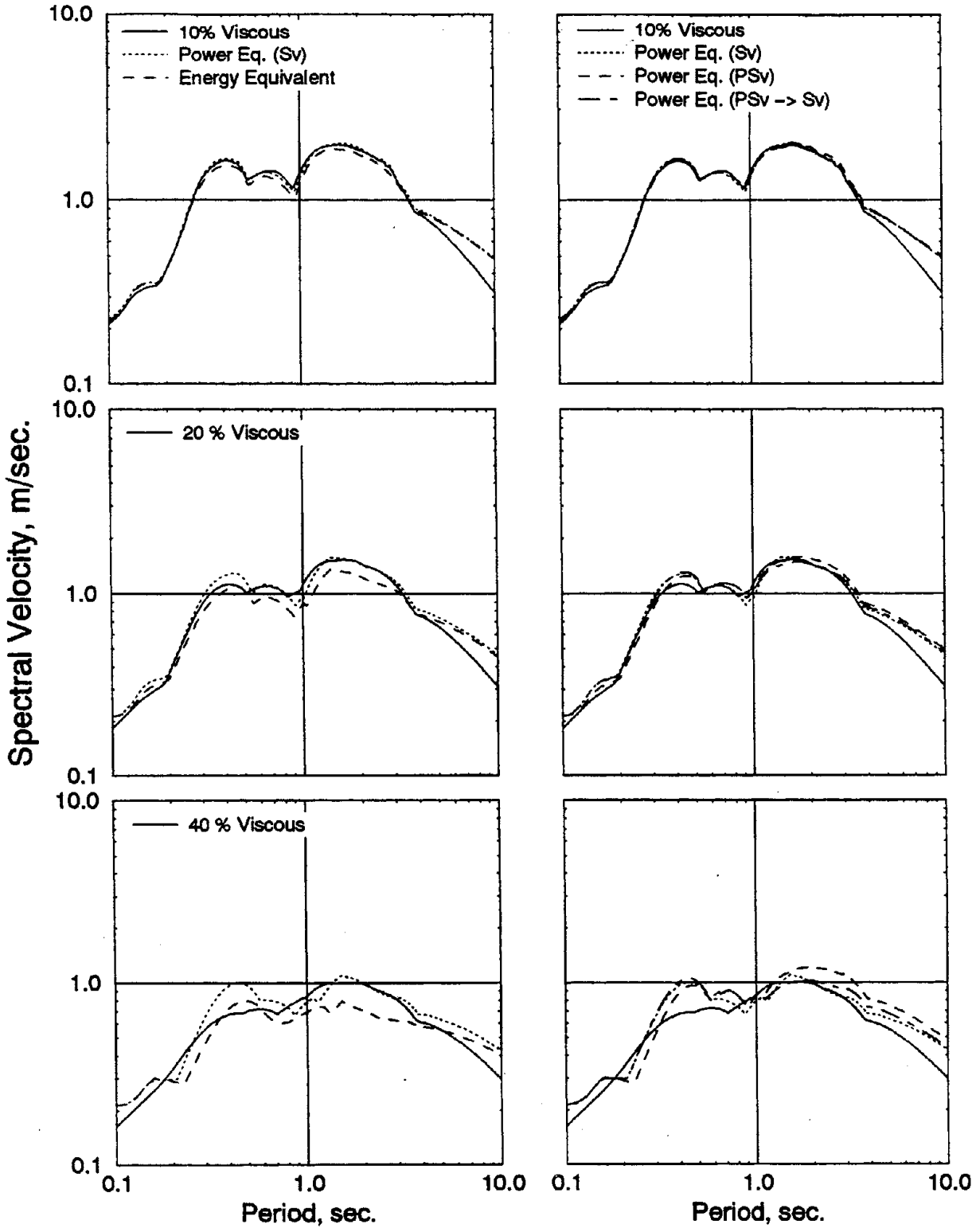

Figure 3-21 Comparison of Energy and Power Approach – Sylmar C.H., α=0.2

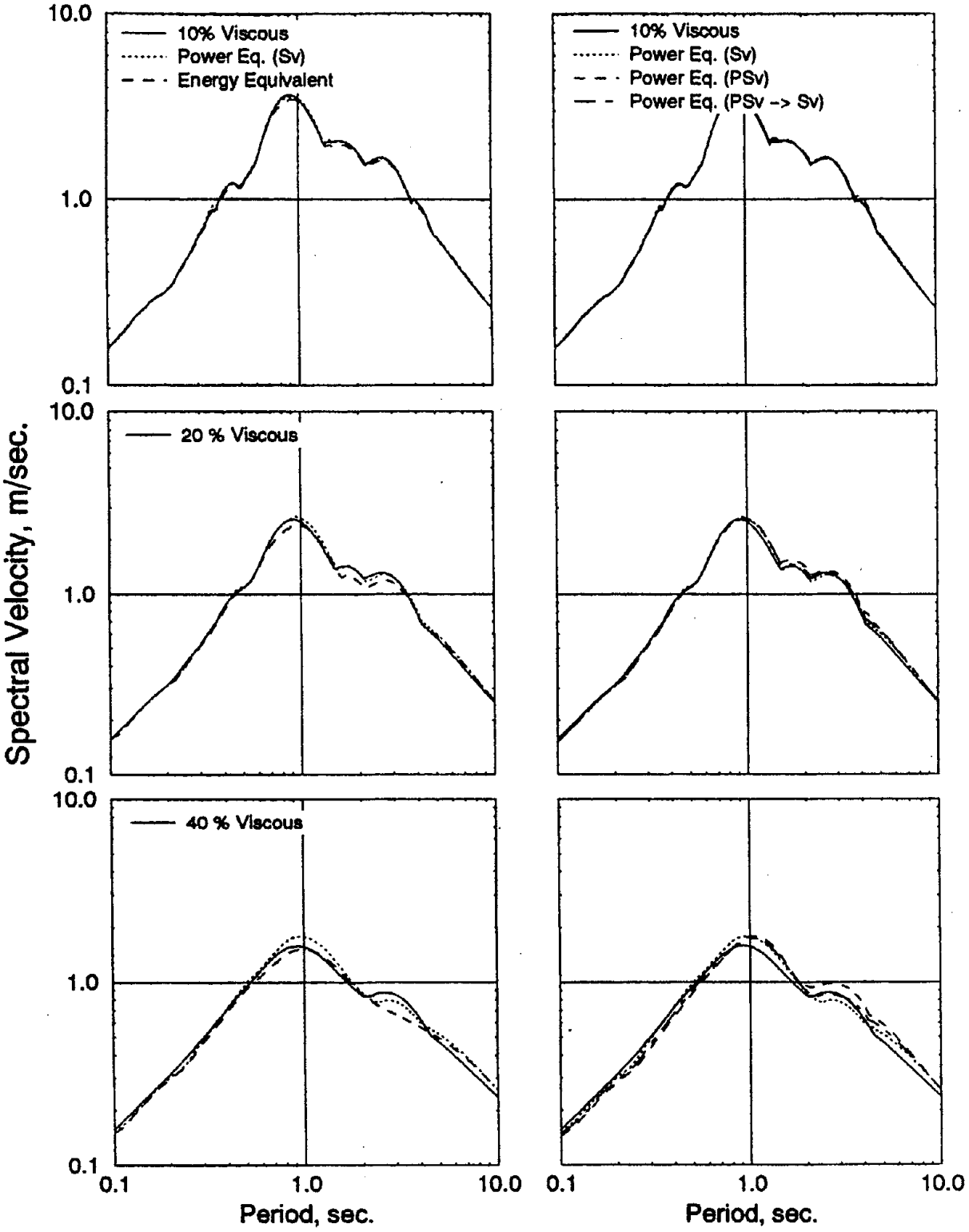

Figure 3-22 Comparison of Energy and Power Approach – Kobe, α=0.5

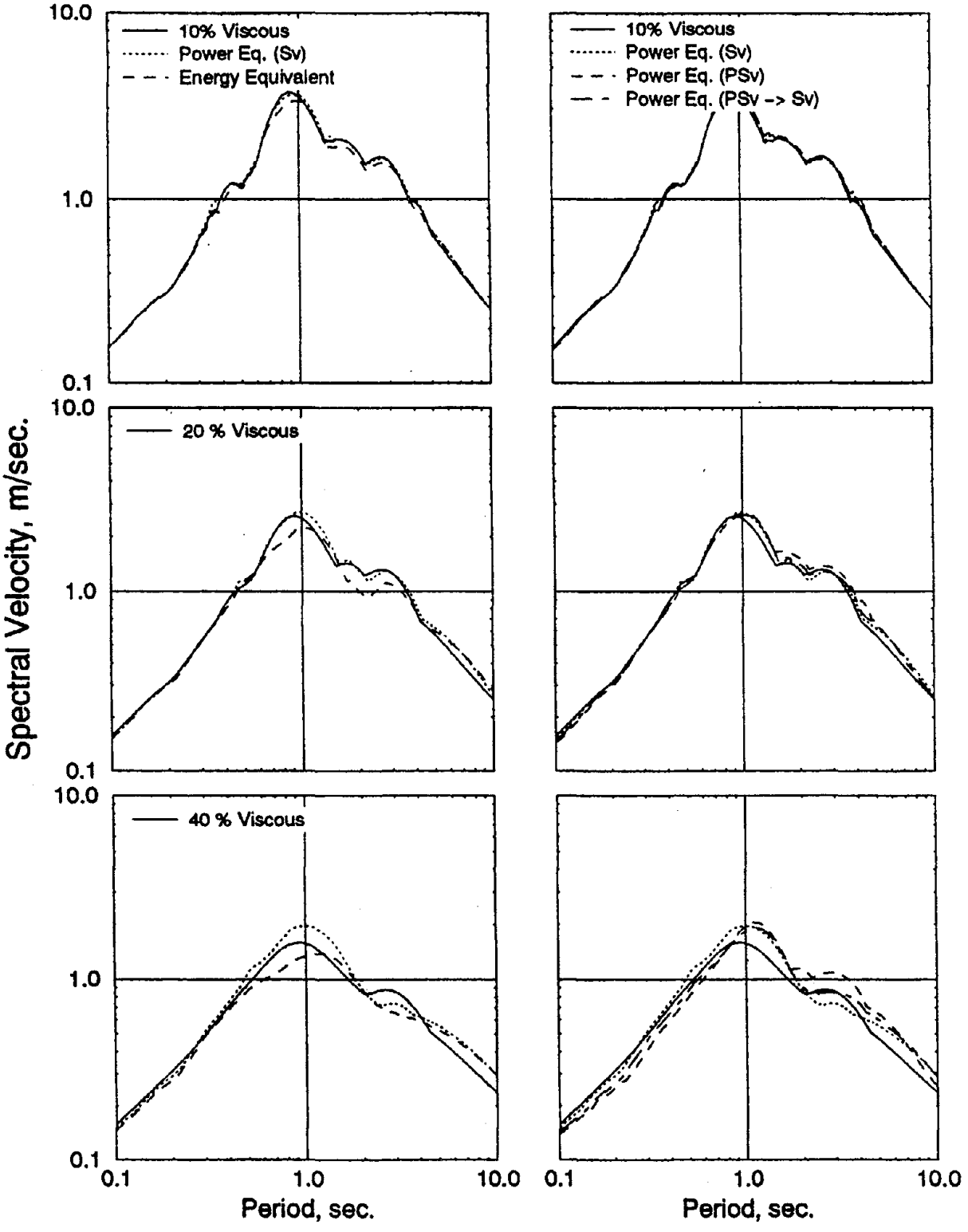

Figure 3-23 Comparison of Energy and Power Approach – Kobe, α=0.2

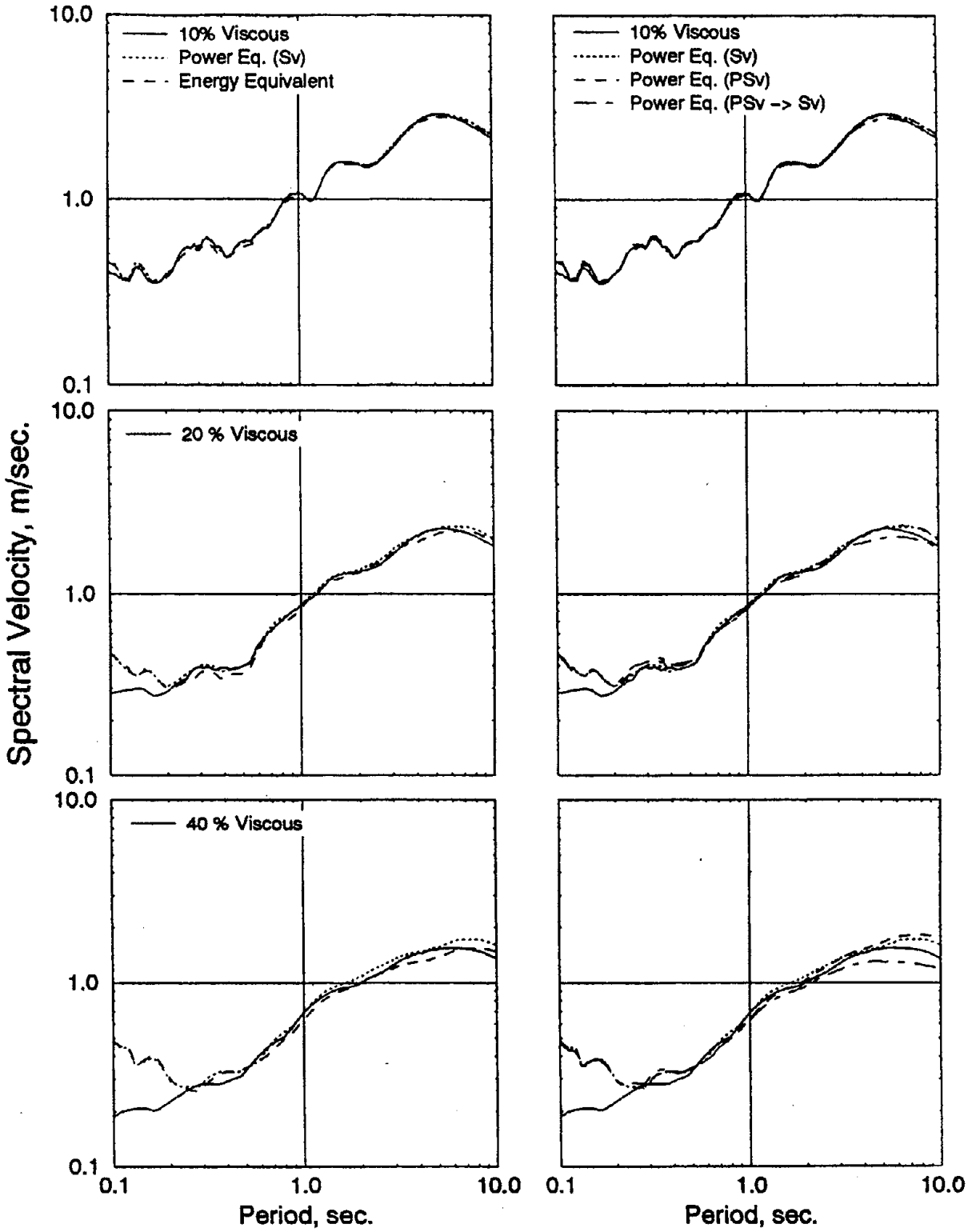

Figure 3-24 Comparison of Energy and Power Approach – Lucerne, α=0.5

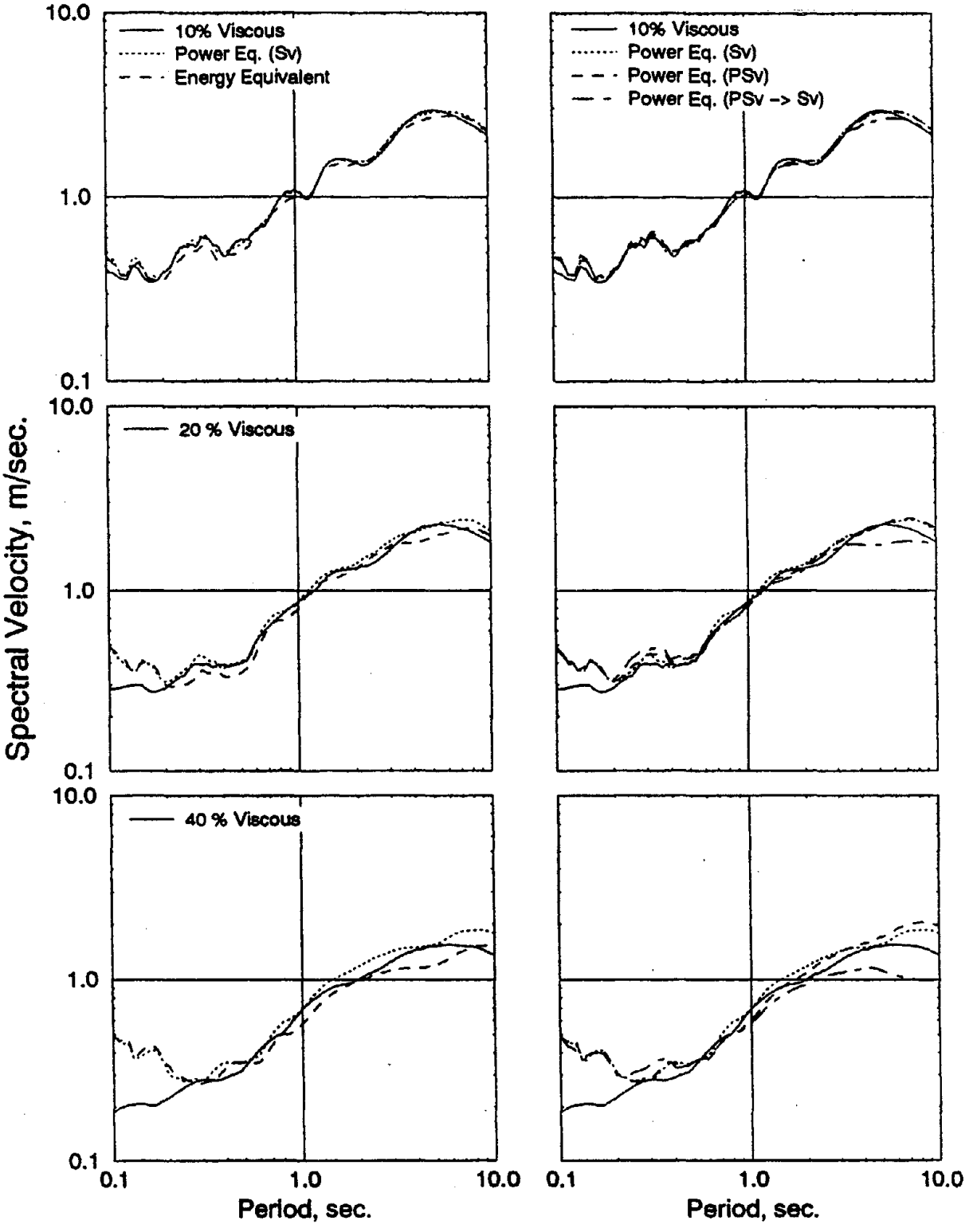

Figure 3-25 Comparison of Energy and Power Approach – Lucerne, α=0.2

$$\varepsilon_{EN} = \xi_{eq}\left(\frac{\pi}{2^{1+\alpha}g}\frac{\Gamma(2+\alpha)}{\Gamma^2(1+\alpha/2)}\dot{x}_{\xi_t}{}^{1-\alpha}\omega_o\right) \tag{3-21}$$

$$\varepsilon_{PO} = \xi_{eq}\left(\frac{1+\alpha}{g}\dot{x}_{\xi_t}{}^{1-\alpha}\omega_o\right) \tag{3-22}$$

in which $\dot{x}_{\xi_t}$ = exact velocity response of a system with total effective damping ξ_t and ω_o = natural frequency of vibration.

Damper capacity ε is calculated for equivalent damping values ξ_{eq} = 5, 15 and 35%. Since the inherent viscous damping ξ_o of the SDOF system is assumed to be 5%, pseudo (or actual) velocity values that correspond to 10, 20 and 40% total viscous damping ξ_t are used to calculate the corresponding damper capacities given in equations (3-21) and (3-22). The equation of motion including the nonlinear viscous dampers with α = 0.5 and 0.2 is solved numerically to obtain the exact response. Comparisons are given in figures 3-16 through 3-25 for the five ground motions listed above. On the left hand side column, pseudo spectral velocity response is compared for the natural period of vibrations, T_o up to 10 sec. as the damper capacities (ε) were determined from equations (3-21) and (3-22) for energy and power equivalent cases, respectively. On the right hand side column, results of four different cases are plotted, i.e. the damper capacities were calculated using a) actual velocity response (V), b) pseudo velocity response (S_v), c) the transformation from the pseudo to actual velocity (S_v -> V), of the equivalent linear system.

As can be seen from these plots, power equivalent approach gives predictions either better than or comparable to the energy approach. Analysis results based on the velocity transformation give (in general) better predictions compared to the predictions based on the pseudo spectral velocity. Although approximations in all of the cases are unconservative (i.e. overestimates the exact response) for periods T_o>4 sec., they are acceptable within the range ($0 \le T_o \le 4\,sec.$) as far as the seismic design of building structures concerned.

3.3.4 Added Damping in terms of Normalize Damper Capacity and Design Implications

The normalized damper capacity, ε previously defined in equation (3-20) and the proposed velocity transformation (3-8) allow one to express the added damping due to both linear ($\alpha = 1.0$) and nonlinear ($\alpha < 1.0$) viscous [nature] dampers in terms of spectral quantities,

i.e. spectral displacement, S_d and demand, C_d. Hence, equation (3-8) can be used to determine the actual velocity in equation (3-22), which in turn is solved for the equivalent (added) damping to give:

$$\xi_d = \frac{\varepsilon}{1+\alpha}\left(\frac{2\pi}{0.75}\right)^{0.15(\alpha-1)} g^{0.5(0.85\alpha+0.15)} S_d^{0.5(1.15\alpha-0.15)} C_d^{0.5(0.85\alpha-1.85)} \quad \textbf{(3-23)}$$

in which ξ_d = added damping and α = the damper power. Note that for a linear viscous damper ($\alpha = 1.0$ and $g = 9.81\, m/s^2$), equation (3-22) takes the simple form:

$$\xi_d = 13\,\varepsilon\sqrt{\frac{S_d}{C_d}} \quad \textbf{(3-24)}$$

Equation (3-23) can be efficiently utilized in the preliminary as well as final design stages involved in designing a wide variety of viscous dampers for structures. The relationship given in equation (3-23) is in fact very suitable for the recommended design procedures recently introduced in NEHRP (1997). These procedures mainly employ in the Capacity Spectrum Method introduced in section 2.

In the capacity spectrum method, the total effective damping is defined by the equivalent viscous damping at a given deformation on the capacity curve. Hence, total effective damping represents all energy dissipation mechanisms of the structure, including inherent viscous damping ξ_o, damping associated with inelastic action, ξ_{hy} and supplemental damping system ξ_d, (if any) etc. In general, the effective (secant) period and the hysteretic damping for a structure are amplitude dependent. The effective period is the same as the initial period up to the yield response and the effective hysteretic damping is equal to the assumed inherent viscous damping (usually 5% critical). After yield, the effective period lengthens and the effective damping typically increases as the inelastic deformations take place. However, in all cases, a unique value of total effective damping can be calculated for each spectral displacement on the capacity curve.

The damping due to structural yielding ξ_{hy}^{str}, hence the total effective (structural) damping can be determined using equation (2-36) given in section 2.4.1 and repeated here for convenience,

$$\xi_{eff} = \xi_o + \xi_{hy} = \xi_o + \frac{2}{\pi}\eta\frac{(1-\alpha_s)(1-1/\mu)}{(1-\alpha_s+\mu\alpha_s)} \quad (3\text{-}25)$$

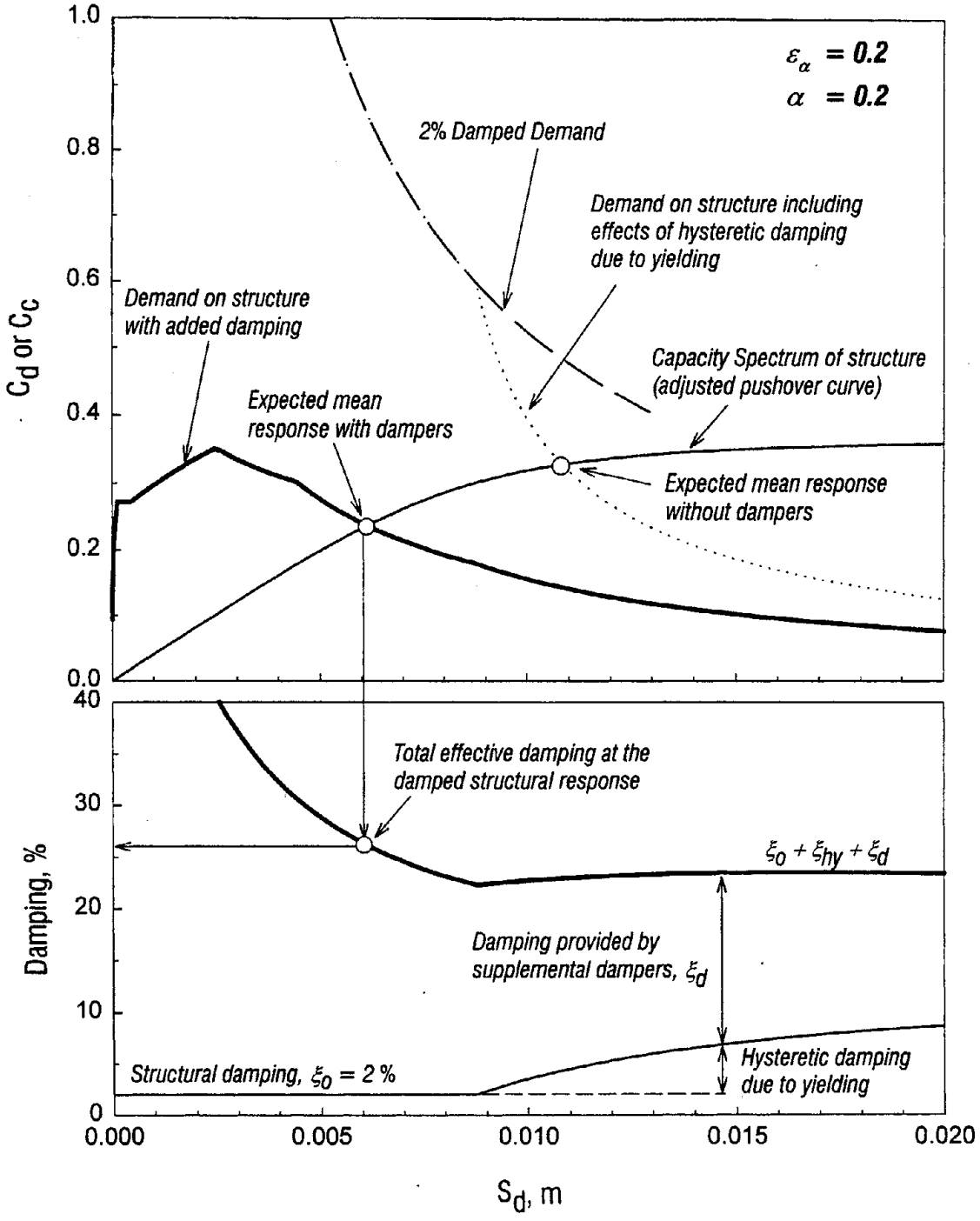

Figure 3-26 Graphical Interpretation of Design Procedure

where ξ_o = inherent damping, ξ_{hy} = hysteretic damping, $\mu = X_{max} / X_y$ is the displacement ductility, α_s= post yield to initial stiffness ratio, and η = efficiency factor defined as the ratio of the actual area enclosed by the hysteresis loop to that of the assumed perfect bilinear hysteresis.

Similarly, added damping due to supplemental viscous dampers can be taken into account using equation (3-23). The graphical procedure described above is depicted on figure 3-26. The corresponding *reduced* demand curves for undamped and for one particular damper capacity ε_α = 0.2 (α = 0.2) is plotted for the modified structural (due to added supplemental damping). In this figure, it is assumed that the stiffness properties of the structure (structural capacity) are not affected due to supplemental viscous devices. This procedure yields a single demand curve, which intersects the capacity curve at the performance point as shown in the figure. A desired damper capacity can thus be determined graphically depending on the performance objectives.

3.4 Summary and Conclusions

In this section, importance of accurate linear approximation techniques was discussed and due to the apparent velocity dependent behavior, it was recommended that actual spectral velocities should be used in the design of such supplemental damping devices. For this purpose, 36 ground motions and their components were used to generate average pseudo and actual velocity spectra. Emprical expressions were obtained that enable transformations between pseudo and actual velocities as a function of damping, which were then simplified and employed in design formulations.

Simplified velocity transformations were utilized in the proposed equivalent power consumption approach to determine the equivalent viscous properties of nonlinear viscous dampers. It was shown that the equivalent power consumption formulation gives improved agreement to the exact solution compared to the equivalent energy formulation, particularly for the periods of interest for structures ranging from 0.5 to 4.0 sec. Moreover, equivalent power consumption approach provides a more direct and reliable relationship that can be easily incorporated in the preliminary as well as final design stages. This was demonstrated via the use of a normalized damper capacity term (ε) which is expressed as the maximum [nonlinear] viscous damper force at a reference velocity as a percentage of the structural weight. The graphical design procedure, which is in fact an extension to the capacity-demand spectrum approach, may considerably facilitate the design of viscous devices.

SECTION 4

GENERAL DESIGN THEORY FOR MDOF STRUCTURAL BUILDING SYSTEMS WITH SUPPLEMENTAL ENERGY DISSIPATION DEVICES

4.1 INTRODUCTION

In this section, step-by-step design algorithms are presented for the two supplemental damping system configurations, namely: the damping system to oppose shear forces (the truss solution) and the load-balancing damping system (tendon-fuse+damper solution). These solutions were introduced by Pekcan et al. (1999b). An overall strategy is presented for the various phases of the design process. This includes facets of conceptual and preliminary design as well as the final design verification process. The efficacy of the preliminary design phase is improved by a well-conceived SDOF idealization of the structural system. This is followed by a brief overview of performance objectives. The general normalized design parameters for the supplemental system are then transformed for the MDOF system based on the specific configuration details. Finally, the design of a nine-story building is presented as an example of the applicability of the proposed design algorithms and system configurations.

4.2 RETROFIT /DESIGN STRATEGIES AND PERFORMANCE OBJECTIVES

Improved dynamic response can be achieved by either: a) adding damping, b) structural strengthening, c) enhancing ductility or d) a combination of the three. As a result of strengthening, the size of the structural elements may increase, but structural deformations such as interstory drift reduce, thus decreasing damage. However, strengthening is commonly associated with stiffening, which in turn increases the seismic demand, and therefore may lead to increased damage potential. Careful detailing of structural members and connections may provide improved ductility. However, strengthening, stiffening or ductility improvements may not be desirable due to high cost and other constructional complexities.

One may consider the overall seismic design objective complying with the following:

$$SEISMIC\ CAPACITY \geq SEISMIC\ DEMAND$$

The above-mentioned design alternatives target improved capacity, i.e. "*left-hand-side of the equation*". As an alternative design/retrofit strategy the demand on the structural system *(right-hand side of the equation)* can be reduced by providing supplementary energy dissipation devices. It must be noted here that this reduction in demand is usually accompanied by some stiffening of the structural system due to either addition of the supporting components for the supplementary system or inherent characteristics of the supplemental damping devices. These aspects should be carefully considered in the design process.

As a structure responds to an earthquake ground motion, it experiences lateral displacements. For moderate to high levels of ground shaking, inelastic response is likely to occur and the structure will experience damage. Performance objectives for a specific level of design (or retrofit) prescribe the deformation limits for a desired performance level. Therefore the structural system should be provided with a lateral load resisting system that is capable of fulfilling these performance requirements.

The principal design objective is generally set by specifying the desired level of performance for a given ground motion. Depending on intensities, ground motions are categorized into two main groups (FEMA 273), namely, Maximum Considered Earthquake (MCE) and Maximum Assumed Earthquake (MAE). FEMA 273 defines MCE as the level of ground shaking that has a 2 percent chance of being exceeded in a 50-year period. Similarly, MAE is the ground shaking that has a 10 percent chance of being exceeded in 50-year period but not more than 2/3 of the MCE. However, ATC-40 gives slightly different names and definitions; Maximum Earthquake (ME) and Design Earthquake (DE). Maximum Earthquake (ME) in ATC-40 is defined as the ground shaking that has a 5 percent chance of being exceeded in 50-year period. ATC-40 gives a third level of ground shaking namely Service Earthquake (SE) which has typically 50% less intensity than that of (DE). The former terms (MCE and MAE) will be adopted herein.

The desired performance objective for a MAE is that the structure remains elastic (no damage) at all times during a ground shaking; some minor damage to nonstructural elements is permitted. However, the structure is allowed to yield without collapse (with damage to the structural elements) for MCE. The desired performance level for the MAE can be achieved by proper distribution of added damping (supplemental devices, design/retrofit) and stiffening or

strengthening as required (retrofit) of the structural elements. Since there will be some amount of yielding under MCE, collapse should be avoided by properly designing the structural elements and the supplemental devices to accommodate the deformation demands. Yielding, in general, means permanent deformation. This can be avoided by providing damping devices with re-centering capabilities.

Another key element for the desired performance objective is the identification of probable seismic load path. This is mainly a function of the structural configuration in terms of distribution of stiffness, mass distribution and the type of framing (shear wall, braced frame, moment frame etc). However, a preferred seismic load path can be attained by carefully designing a supplemental system.

4.3 Phases Involved in Designing Supplementary Systems for Structures

A generic flow-chart of phases involved in the design of supplementary systems for structures is given in figure 4-1. These phases are briefly discussed in what follows.

Phase I: SDOF Idealization

Based on the discussion presented in section 2, it is evident that a well-conceived SDOF idealization of the MDOF system can considerably facilitate the overall design process of supplementary systems. Therefore, this task is considered as Phase I of the design process. Structural dynamic properties of the MDOF system are determined, which are then used to transform the MDOF system into an equivalent SDOF system. Approximate methods may be adopted to determine the dynamic properties in the absence of an analysis tool. Such an approximation for the period of vibration can be obtained by a code equation for the specific structural system or any method that can be readily found in the literature (Clough and Penzien 1993, Chopra 1995). Similarly, the first mode shape may be assumed to be proportional to the story height (height from foundation to the floor level) vector. Consequently, the elasto-platic structural capacity can be determined as described previously in section 2.

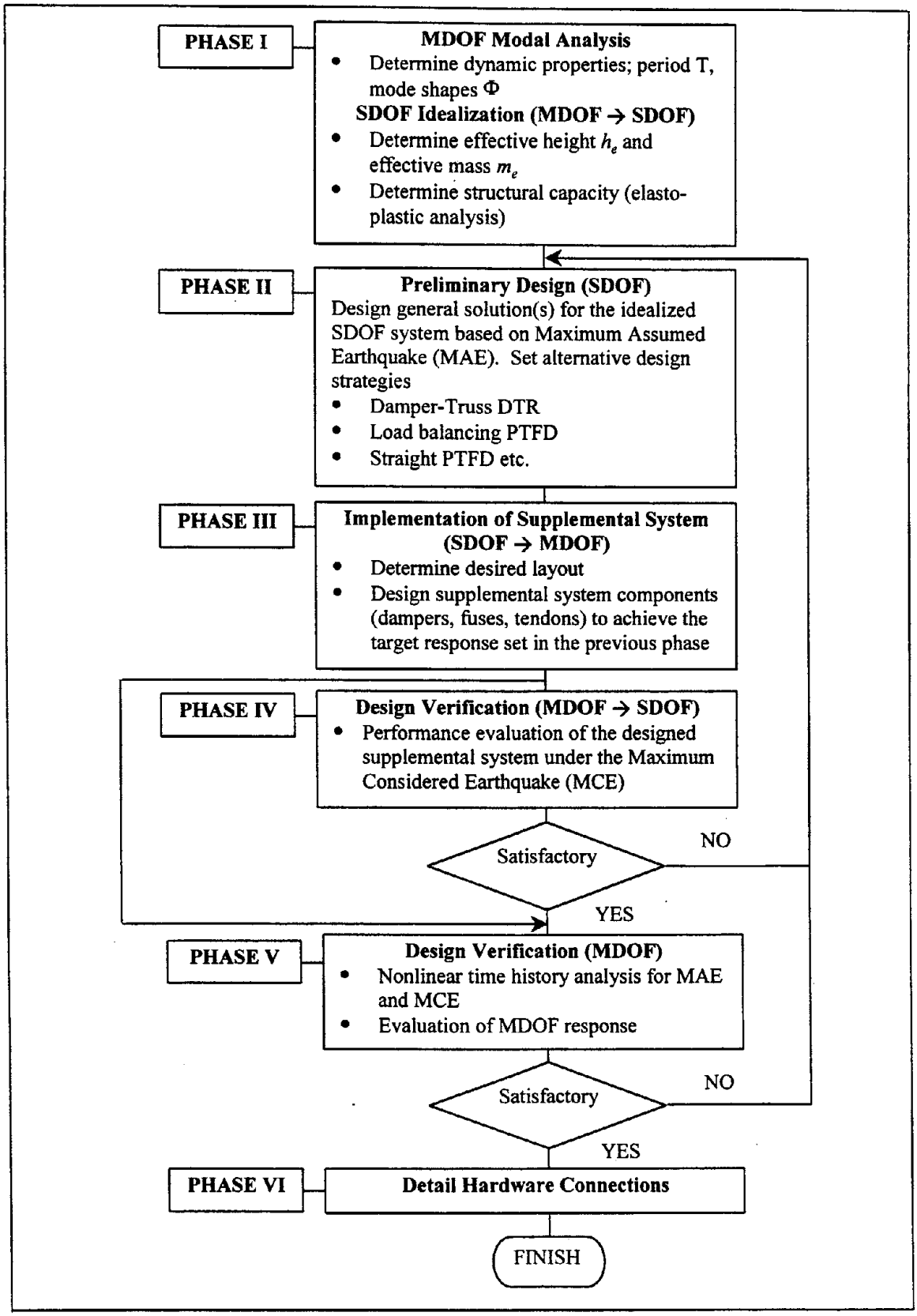

Figure 4-1 Designing Supplemental Systems for Structures: Design Phases

Phase II: Preliminary Design

In the preliminary design phase, lateral forces imposed on the structural system are quantified based on the design ground motion (MAE) and the target design response. At this stage of the design, the uncertainty factors that were proposed in section 3 can be adopted. Accordingly, supplemental systems should be designed for

$\lambda_s C_d$ for short period

$\lambda_l C_d$ for long period

where $\lambda_s = 1.2$ and $\lambda_l = 1.5$.

An iterative preliminary design is then carried out to determine the normalized supplemental system capacity for the deficiency between structural capacity and imposed ground motion demand on the structure. In other words, a target design displacement at the effective height of the MDOF system is chosen and the required normalized supplemental capacity and corresponding added damping to achieve the target response is iteratively calculated. Various design alternatives should be explored at this stage before proceeding to the next phase.

Phase III: Design Implementation

This may be considered to be the final design phase in which the normalized design parameters for the equivalent SDOF system are implemented in the MDOF system through appropriate transformations. These include the modifications of the normalized supplemental system capacities to account for the layout geometry. The relationships that enable these transformations were presented previously by Pekcan et al. (1999b) for the damper-truss solution (DTR) and the load balancing prestressed tendon-fuse+damper solution (PTFD).

Phase IV: Simplified Design Verification

As was mentioned in section 4.2, the performance objective usually targets "*no structural damage (elastic response)*" under MAE conditions. However, the performance of the supplemental system as well as the parent structure should also be examined under MCE conditions to ensure that; i) the damage (if any) to the structural members are within acceptable limits, and ii) the supplemental system is designed for the possible maximum reserved

deformation capacity which may be encountered under such events. This phase requires an updated idealized SDOF system, which exhibits the characteristics of the supplemental system (designed in phase III). The effect of the supplemental system on the overall pushover capacity can be taken into account using the methods described in Section 6.

Phase V: Comprehensive Design Verification

The design process consists of a more comprehensive design verification in which analytical tools are utilized to model the MDOF with all its members to reflect the realistic force-deformation characteristics together with the supplemental system as implemented in the structure. It must be noted here that depending on how complex the MDOF system is, one might choose to skip phase IV as both phases IV and V are for verification purpose as shown on figure 4-1.

Phase VI: Design Detailing

If the system performance is found to be satisfactory after the previous phase, the supplemental system components can be detailed and the design process is terminated. Otherwise, other design alternatives should be considered for either economical feasibility or better structural performance.

These design phases are discussed in detail and a design example of a nine-story steel structure is presented in the following sections.

4.4 PRELIMINARY RETROFIT/DESIGN WITH SUPPLEMENTARY DAMPING SYSTEMS

One of the most important and challenging phases in the design of supplemental damping systems for structures is the preliminary sizing of the supplemental system based on the performance objectives. Initially, there is usually only information pertaining to the bare (undamped) structure. However, the performance of the structure with supplemental system is modified due to the added damping and/or stiffness by the supplemental system whose properties are in fact a function of the overall system response. Therefore, the following questions should be addressed:

(i) *What is the capacity of the bare (undamped) structure?*

(ii) *What is the effect of the supplemental system on the stiffness/strength characteristics?*

(iii) *What is the effect of added damping on the seismic performance of the overall structural system?*

It should be realized that the answers to the above questions should be sought for considering the demand imposed on the structural system by the design ground motion. A typical capacity-demand representation of an idealized SDOF structure is shown in figure 4-2.

As previously mentioned in section 3, the effective (secant) period and hysteretic damping for a structure are amplitude dependent. The effective period is the same as the initial period up to the yield response and the effective hysteretic damping is equal to the assumed inherent viscous damping (usually 5% of critical). After yield, the effective period lengthens and the effective damping typically increases as inelastic deformation of the structure increases. However, in all cases, a unique value of effective damping can be calculated for each spectral displacement on the capacity curve using equation (3-24) and repeated here for convenience,

$$\xi_{eff} = \xi_o + \xi_{hy} = \xi_o + \frac{2}{\pi}\eta\frac{(1-\alpha_s)(1-1/\mu)}{(1-\alpha_s+\mu\alpha_s)} \tag{4-1}$$

Demand reduction factors (B_s and B_l) can then be determined based on the values of the effective damping and corresponding demand can be calculated. This procedure yields a single demand curve, which intersects the capacity curve at the performance point as shown in figure 4-2.

Similarly, the effect of damping on the structural performance due to supplemental system can be studied in terms of the normalized damper capacity previously given in equation (3-22) and repeated herein,

$$\xi_d = \frac{\varepsilon}{1+\alpha}\left(\frac{2\pi}{0.75}\right)^{0.15(\alpha-1)} g^{0.5(0.85\alpha+0.15)} S_d^{0.5(1.15\alpha-0.15)} C_d^{0.5(0.85\alpha-1.85)} \tag{4-2}$$

in which ξ_d = added damping and α = the damper power.

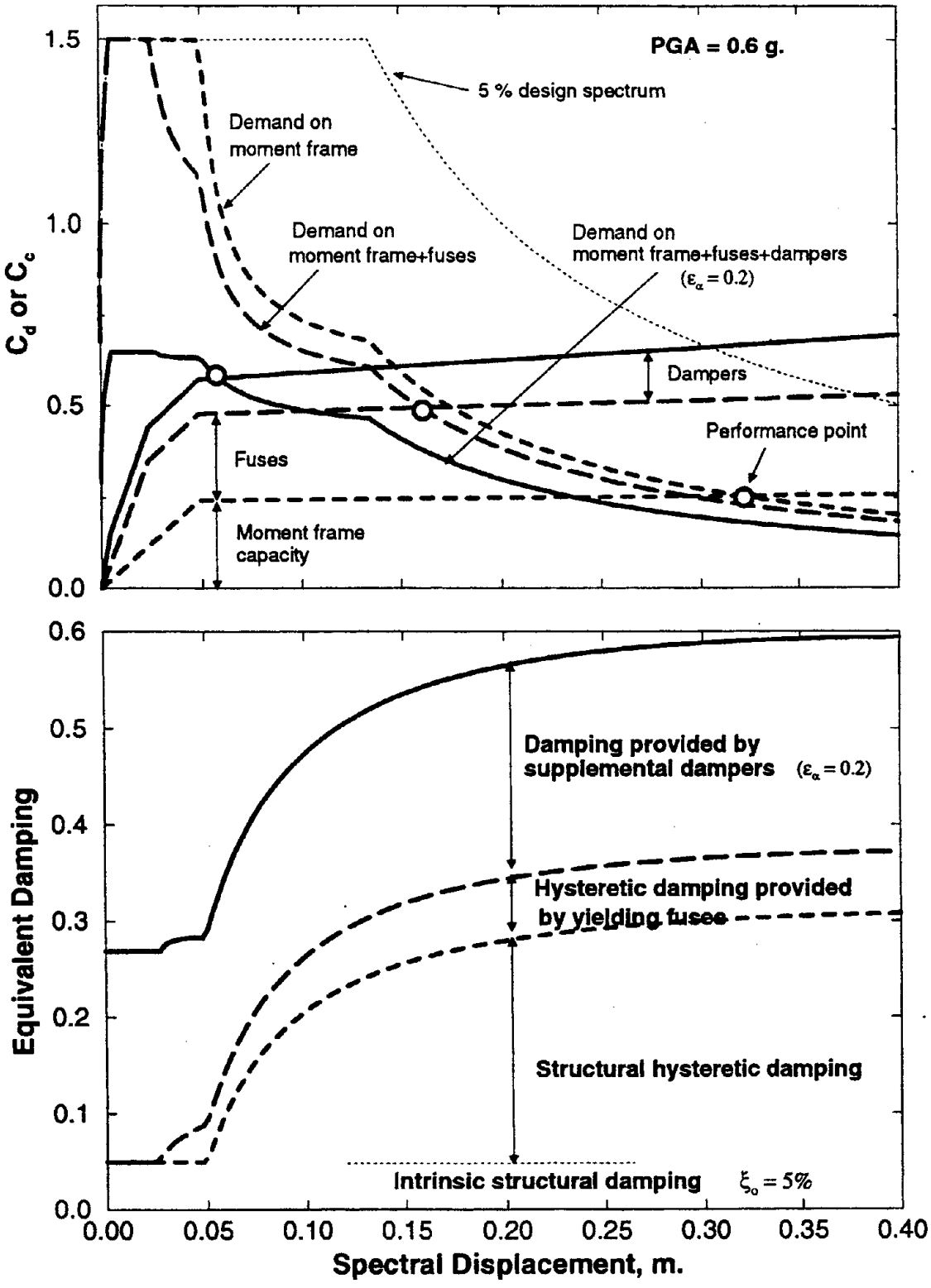

Figure 4-2 Preliminary Retrofit and Design of Supplemental Systems

Equation (4-2) and the corresponding demand curve for one particular damper capacity ε_α = 0.2 (α = 0.2) is plotted for the modified (stiffened) structural capacity (due to added supplemental system stiffness) in figure 4-2. Note that hysteretic damping due to fuse yielding and its stiffness contribution are also presented in this figure. A desired preliminary damper capacity can thus be obtained graphically at the intersection of the corresponding demand curve and the pushover capacity curves.

A step-by-step preliminary design (Phase II) algorithm based on the SDOF idealization and plastic mechanism capacity of the structure (Phase I) is presented in what follows.

4.4.1 SDOF Idealization and Determination of Structural Capacity: PHASE I

Step 0: SDOF Idealization

Determine the equivalent SDOF properties of the structure: effective height, h_e and effective mass, m_e. This can be done by performing a modal analysis. In lieu of such an analysis a code-like approximation can be made which assumes that the first mode shape ($\{\phi_1\}$) is proportional to the story height vector,

$$h_e = \frac{\{h\}^T[M]\{h\}}{\{h\}^T[M]\{1\}} \qquad \textbf{(PI-0a)}$$

$$m_e = \frac{\left(\{h\}^T[M]\{1\}\right)^2}{\{h\}^T[M]\{h\}} \qquad \textbf{(PI-0b)}$$

where $\{h\}$ = story height vector from the base, $[M]$ = diagonal mass matrix of the MDOF structure.

Step 1: Initial Period, T_o

Estimate the initial, elastic period T_o

$$T_o = C_t h_N^{3/4}$$

$$C_t = 0.007 \quad \textit{for R/C MRF} \qquad \textbf{(PI-1a)}$$

$$C_t = 0.005 \quad \textit{for steel MRF}$$

where h_N = height (in meters) above the base to the roof level. Therefore, the elastic structural capacity can be determined as

$$C_{c,el}^{str} = \frac{4\pi^2}{g}\frac{S_d}{T_o^2} = \frac{V_{b,el}}{W_{eff}} \qquad \textit{(PI-1b)}$$

where S_d = displacement response at the effective height h_e.

Step 2: Plastic Mechanism Capacity

Determine the total plastic base shear capacity using equations (2-27) and (2-28)

$$V_{b,pl} = \frac{2\left(n_b(n_{sp}-1)M_{pb}L/L_b + (n_b+1)M_{pc}\right)}{n_{sp}h\left(1-\frac{1}{3}\left(\frac{n_{sp}}{N}\right)^2\right)} \qquad \textit{(PI-2a)}$$

where n_{sp} = is the number of stories participating in the plastic mechanism which can be determined from solving the following cubic equation:

$$\frac{2/3n_{sp}^3}{(1+1/n_b)(L_b/L)(M_{pc}/M_{pb})-1} + n_{sp}^2 - N^2 = 0 \qquad \textit{(PI-2b)}$$

Therefore, plastic mechanism capacity ($C_{c,pl}^{str} = V_{b,pl}/W_{eff}$) and elastic capacity can be used to determine the overall push-over capacity curve with an assumed post yield stiffness ratio α_s. Furthermore, the P-δ effect on the structural capacity can be accounted for as,

$$\Delta C_{P-\delta}^{str} = \frac{\delta}{h_e} = \frac{S_d}{h_e} \qquad \textit{(PI-2c)}$$

The outcome of the procedure described in Steps 1 and 2 to determine the approximate capacity of a structure is graphically shown in figure 2-7.

In order to facilitate further design iterations, a Menegotto-Pinto (1973) model can be used to represent the capacity (pushover) curves of the structure with and/or without various supplemental system configurations as follows,

$$C_c^{str}W = K_1\Delta_s\left(Q + \frac{(1-Q)}{\left(1+\left|\Delta_s/\Delta_y\right|^4\right)^{0.25}}\right) \quad \textbf{(4-3)}$$

in which Q = post yield stiffness ratio, Δ_y = spectral displacement at its theoretical first yield or yield deformation of the supplemental system element, K_1 = initial elastic stiffness based on the first mode period or that of the supplemental system. It must be noted here that these parameters must be replaced with the values corresponding to the damper/fuse properties as will be exemplified later in this section.

4.4.2 Preliminary Design: PHASE II

Step 0: Target Displacement Response

Choose the design structural drift, Θ_{max}. Therefore, the maximum roof displacement is

$$X_{\max}^{roof} = \Theta_{\max} h_N \quad \textbf{(PII-0a)}$$

And the target displacement at the seismic center of mass (effective height) is

$$X_{\max} = \Theta_{\max} h_e \quad \textbf{(PII-0b)}$$

Step 1: Total Effective Damping, ξ_{eff}^{total}

Estimate the total damping ξ_{eff}^{total}, required for the target design displacement X_{max}, and calculate the demand,

$$C_d = \frac{2.5C_a}{B_s} \le \frac{C_v^2 g}{4\pi^2 B_l^2 X_{\max}} \quad \textbf{(PII-1a)}$$

Hence, calculate the effective period, T_e,

$$T_e = 2\pi\sqrt{\frac{X_{\max}}{gC_d}} \quad \textbf{(PII-1b)}$$

Step 2: Required Supplemental System Capacity

Determine the required added capacity due to supplemental system, C_c^{sup},

$$C_c^{\sup} = C_d - C_c^{str} \qquad \textit{(PII-2a)}$$

where C_c^{str} can be read-off the figure 4-2.

Step 3: Damper and Fuse Capacities

Assign the design capacity proportions r_d and r_f, for the dampers and fuses, respectively,

$$C_c^{\sup} = C_c^d + C_c^f \qquad \textit{(PII-3a)}$$

where

$$C_c^d = r_d C_c^{\sup} \qquad \textit{(PII-3b)}$$

$$C_c^f = r_f C_c^{\sup} \qquad \textit{(PII-3c)}$$

in which $r_f + r_d = 1.0$ where r_f and r_d are the proportions of the total load carried by the fuse and dampers respectively. Note a damper-only system may be chosen (r_d =1.0). However, for optimal design it is considered that the fuses and dampers should have a similar capacity thus $r_d = r_f = 0.5$. Such a requirement maximizes passive restraint against wind while maximizing the double-acting nature of the combined fuse and damper system, especially when prestressed to 50% of the yield strength (in case of a system working in tension-only), and therefore minimizes the seismic response.

Step 4: Hysteretic Damping, ξ_{eff}^{str}

Calculate the structural hysteretic damping ξ_{eff}^{str} including the inherent structural damping ξ_o,

$$\xi_{eff}^{str} = \xi_o + \xi_{hy}^{str} = \xi_o + 0.64\eta_s \frac{(1-\alpha_s)(1-\mu_s)}{(1-\alpha_s+\mu_s\alpha_s)} \qquad \textit{(PII-4a)}$$

where η_s = efficiency factor defined as the ratio of the actual area enclosed by the hysteresis loop to that of the assumed bilinear hysteresis (typical values range between

0.2 for concrete and 0.6 for steel structures), and $\mu_s = \frac{X_{\max}}{X_y^{str}}$ is the ductility factor at the target displacement.

Step 5: Hysteretic Damping due to Fuse Yielding, ξ_{hy}^f

Calculate the hysteretic damping due to fuse yielding (if any),

$$\xi_{hy}^f = 0.64\eta_f \frac{(1-\alpha_f)(1-\mu_f)}{(1-\alpha_f+\mu_f\alpha_f)} \qquad \textit{(PII-5a)}$$

where η_f = efficiency factor (a typical value if the fuse is designed to yield at the maximum displacement response is 1/8), $\mu_f = \frac{X_{\max}}{X_y^f}$. It must be noted here that fuse-length should be designed such that

$$X_y^f = \varepsilon_{y,f}\, l_f \qquad \textit{(PII-5b)}$$

in which $\varepsilon_{y,f}$= yield strain of the fuse and X_y^f = corresponding yield deformation. For satisfactory fuse performance, the fuse-length should be designed so that

$$l_f = \frac{X_{\max}}{\varepsilon_{u,f}} \qquad \textit{(PII-5c)}$$

Hence, the constant-design ductility factor for the fuse can be determined as

$$\mu_f = \frac{\varepsilon_{u,f}}{\varepsilon_{y,f}} \qquad \textit{(PII-5d)}$$

Step 6: Added Damping due to Dampers, ξ_d

Calculate the damping due to dampers for the required normalized damper capacity $\varepsilon_{eff}\,(=C_c^d)$ for chosen damper type (that defines power α):

$$\xi_d = \frac{\varepsilon_{eff}}{1+\alpha}\left(\frac{2\pi}{0.75}\right)^{0.15(\alpha-1)} g^{0.5(0.85\alpha+0.15)}\, X_{\max}^{0.5(1.15\alpha-0.15)}\, C_d^{0.5(0.85\alpha-1.85)} \qquad \textit{(PII-6a)}$$

where $\varepsilon_{eff} = C_c^d = \dfrac{c_\alpha \dot{x}_{ref}^{\alpha}}{W_{eff}}$

For ESD when $\alpha = 0.2$ (and g = 9.81 m/s^2), equation (PII-6a) reduces to:

$$\xi_d = 0.93\varepsilon_{eff} \frac{X_{\max}^{0.04}}{C_d^{0.84}}$$

Step 7: Total Effective Damping, ξ_{eff}^{total}

Calculate the total available damping ξ_{eff}^{total},

$$\xi_{eff}^{total} = \xi_{eff}^{str} + \xi_{hy}^{f} + \xi_d \qquad \textit{(PII-7a)}$$

Return to Step 4 until calculated total effective damping ξ_{eff}^{total} is equal or acceptably close to the assumed (previous) value.

Discussion:

At this point it is worth noting that effects of added stiffness and damping are implicitly accounted for in terms of capacities of the components of the supplemental system. Therefore, the preliminary design provides the basic design parameters, namely, required damper as well as fuse (if any) capacities, total required effective damping and corresponding design ground motion demand on the idealized SDOF structure.

In the following sections, a detailed development of the design equations for the two supplemental system configuration introduced by Pekcan et al. (1999), is presented. Thus, design of the supplemental system as part of the MDOF structure can then be undertaken for the desired configuration and the design parameters modified accordingly. A supplementary system should, in general, be designed for a performance deficiency; that is when the structural capacity $C_c^{str}(\xi_{eff}^{str}, X_{\max}, T)$ is less than the demand $C_d(\xi_{eff}^{total}, X_{\max}, T)$:

$$\begin{aligned} &C_c^{str}(\xi_{eff}^{str}, X_{\max}, T) < C_d(\xi_{eff}^{total}, X_{\max}, T) \\ &C_c^{\sup} = C_d - C_c^{str} \end{aligned} \qquad \textbf{(4-4)}$$

where superscripts "*sup*" and "*str*" is used to represent the supplementary system and the bare structure respectively. Although each of the design alternatives has similar conceptual

background from the capacity-demand point of view, design algorithms vary due to supplemental system behavior (as employed in the parent structure). Therefore, two different step-by-step design algorithms are given in the following paragraphs for namely; Damper-Truss Solution (DTR) and Prestressed Tendon-Fuse+Damper Solution (PTDF).

4.5 Damper Placement to Resist Interstory Shear Forces – Truss Solution (DTR)

4.5.1 Design Philosophy

As previously mentioned, building structures primarily respond in their fundamental (first) mode shape. Commonly accepted design approaches are based on sizing the dampers as a function of the interstory deformations due their fundamental modal response along the height of the building structure. It is also desirable that the overall structural deformation pattern follows a uniform distribution of interstory deformations. This, ideally, leads to a linear-triangular maximum response envelope. Moreover, these deformations are particularly dominated by the interstory shear deformations, as would be the case for short/medium height building structures (also a function of aspect ratio H/B). In such cases, damper sizes would be equally distributed as predicated by recent design recommendations (FEMA 273, ATC 40).

However, most experimental research performed to date has shown that the efficiency of dampers on the upper stories diminishes mainly due to the fact that interstory deformations (drift, velocity) are smaller compared to those in the lower stories. Therefore, an efficient distribution of seismic energy dissipation devices is proposed in which devices are sized in proportion to the design story shears. The supplemental devices are placed in the interior load carrying frames mainly for two reasons; a) a desirable moment frame-truss action is attained, b) the gravity load carrying columns of the interior frames have usually reserve axial load capacities which can accommodate additional axial loads due to damper-braces.

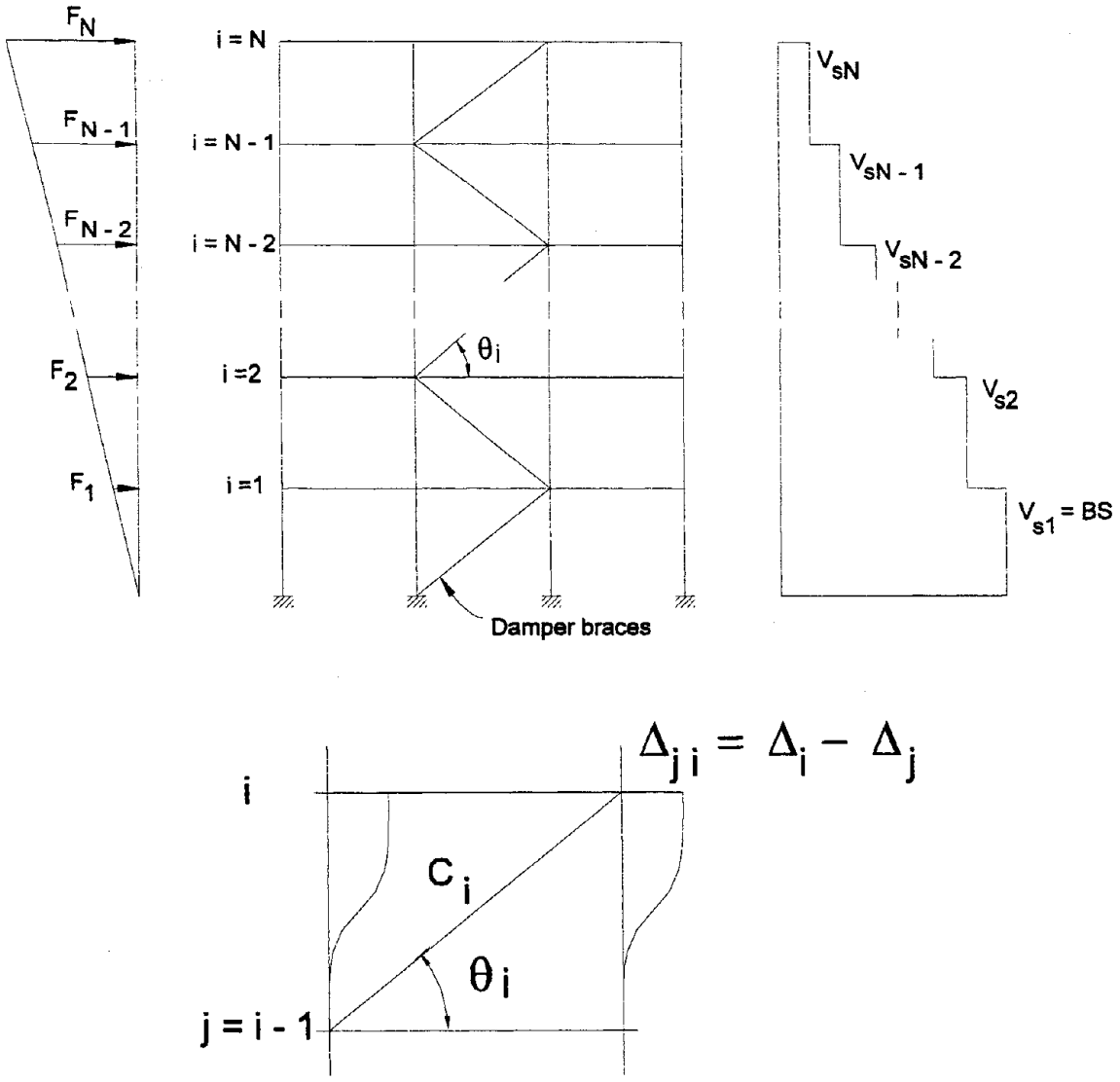

Figure 4-3 Damper Placement to Resist Interstory Shear Forces: Truss Solution

4.5.2 Device Distribution to Resist Interstory Shear Forces

The relationship for the equivalent viscous damping ratio for the MDOF structure shown on figure 4-3 are presented in what follows. Equivalent viscous damping can be formulated as

$$\xi_d = \frac{1}{2}\frac{\sum_i c_i \cos^2\theta_i \Delta_{ri}^2}{\omega_{eff}\sum_i m_i \Delta_i^2} \tag{4-5}$$

in which ω_{eff} = effective frequency, c_i = damper coefficient at the ith floor.

Story deformations Δ_i, are assumed to be proportional to the first mode shape which is then ideally assumed to be proportional to the normalized story height vector $\{\bar{h}\}$. Therefore,

$$\{\Delta_i\} = X_{\max}\{\bar{h}\} \tag{4-6}$$

Equation (3-14) can then be used in equation (4-5) to determined the coefficient for the nonlinear viscous device,

$$\xi_d = \frac{1}{1+\alpha}\left(\frac{2\pi}{T_{eff}}\right)^{\alpha-2}\left(\frac{T_{eff}}{0.75}\right)^{0.15\alpha}\frac{\sum_i c_{\alpha i}(\Delta_{ri}\cos\theta_i)^{1+\alpha}}{\sum_i m_i\Delta_i^2} \tag{4-7}$$

where α = nonlinear damper power assumed to be the same in all floor levels, $c_{\alpha i}$ = nonlinear damper coefficient corrected for the inclination angle θ_i on the ith floor determined as,

$$c_{\alpha i} = \left(\frac{V_{si}}{\sum_j V_{sj}}\right)\frac{c_\alpha\left(\frac{2\pi}{T_{eff}}X_{\max}\right)^\alpha\left(\frac{T_{eff}}{0.75}\right)^{0.15\alpha}}{\left(\frac{2\pi}{T_{eff}}\Delta_{ri}\cos\theta_i\right)^\alpha\left(\frac{T_{eff}}{0.75}\right)^{0.15\alpha}} \qquad i = 1\ldots N \tag{4-8}$$

which can be simplified as,

$$c_{\alpha i} = \left(\frac{V_{si}}{\sum_j V_{sj}}\right)\frac{c_\alpha (X_{\max})^\alpha}{(\Delta_{ri}\cos\theta_i)^\alpha} \qquad i = 1\ldots N$$

in which $c_\alpha = \dfrac{C_c^{sup} W_T}{\dot{x}_{ref}^\alpha}$

Based on the required capacity determined from the preliminary design (section 4.4.2). It must be noted that equation (4-8) ensures the damper size distribution is proportional to the story shear V_{si}.

4.5.3 "Damper-Truss Solution (DTR)" – Design Algorithm: PHASE III-A

Step 0: Damper Coefficient, c_α

Calculate the total damper coefficient c_α from the normalized damper capacity obtained from the preliminary design based on a SDOF idealization described in section 4.4.2,

$$c_\alpha = \frac{C_c^{sup} W_T}{\dot{x}_{ref}^\alpha} \qquad \textit{(PIII-A-0a)}$$

Step 1: Damper Size Distribution

Determine the damper size distribution proportional to the design story shears and correct for the damper brace inclination and design interstory velocity,

$$c_{\alpha i} = \left(\frac{V_{si}}{\sum_j V_{sj}} \right) \frac{c_\alpha (X_{\max})^\alpha}{(\Delta_{ri} \cos\theta_i)^\alpha} \qquad i = 1 \ldots N \qquad \textit{(PIII-A-1a)}$$

in which T_{eff}= is the effective period of vibration of the structure.

If elastomeric spring dampers are to be used, determine the damper properties, i.e. preload P_y, elastomeric stiffness K_2,

$$P_{yi} = c_{\alpha i} \left(\frac{2\pi}{T_{eff}} \Delta_{ri} \cos\theta_i \right)^\alpha \left(\frac{T_{eff}}{0.75} \right)^{0.15\alpha} \qquad \textit{(PIII-A-1b)}$$

The preload in the damper would typically be equal to the maximum damping force, which ensures proper re-centering.

$$x_{yi} = (0.01 \sim 0.05)(\Delta_{ri} \cos\theta_i) \qquad \textit{(PIII-A-1c)}$$

The pseudo yield displacement due to brace (in series) stiffness typically ranges from 1% to 5% of the total maximum stroke capacity of the damper. Therefore initial stiffness K_1,

$$K_1 = \frac{P_{yi}}{x_{yi}} \qquad \textit{(PIII-A-1d)}$$

The elastomeric stiffness K_2 can be taken as 5-10% of the initial stiffness K_1,

$$K_2 = (0.05 \sim 0.10)K_1 \qquad \textit{(PIII-A-1e)}$$

4.6 Damper Placement to Resist Overturning Moments – Load Balancing Prestressed Tendon-Fuse+Damper Solution (PTFD)

4.6.1 Design Philosophy

As mentioned above, the equivalent seismic lateral load distribution typically conforms to the fundamental first mode shape of a structure. For buildings, which possess relatively uniform mass distribution along the height of the structure, this (inertial) load distribution is adequately represented by an inverted triangle. However, in relatively tall building structures the overall response is generally dominated by flexural deformations and higher modes may be significant. Therefore, the lateral load (or resulting displacement) distribution may deviate from the assumed triangular shape. Regardless of the type of lateral distribution, it is contended that the seismic response can be most effectively reduced if these inertial loads are balanced by applying opposing lateral forces. While reducing the story shear demand, this type of load balancing tends to reduce the overturning moment demand on the columns as well.

The concept of load balancing is widely used in post-tensioned prestressed concrete design. The proposed load-balancing supplemental system is an analogous tension-only system composed of two major components; prestressing (post-tensioned) tendons with high axial stiffness and a supplementary damping system (consisting of elastomeric spring dampers and fuse-bars). The draped tendon is anchored at one end (desirably, but not restricted to, the roof) and connected to the supplementary damping system in series at its other end (generally the foundation level). The tendon layout is designed to be piecewise continuous (i.e. in straight line segments), so that each segment diagonally spans between holes bored (or cast in the case of new

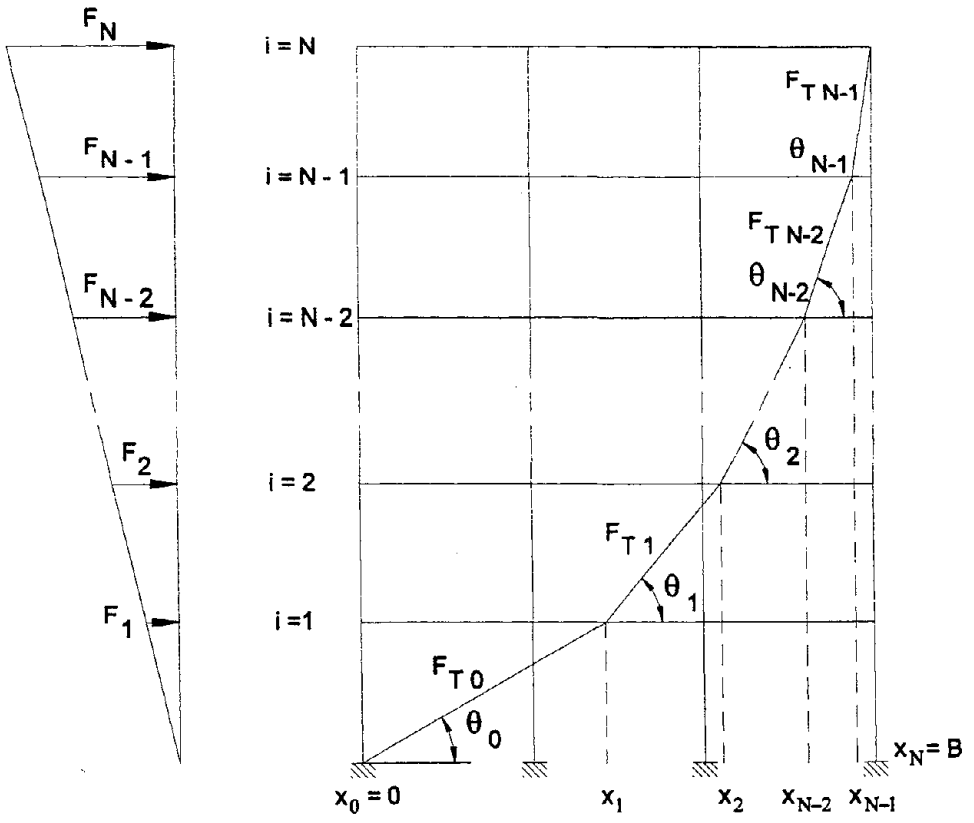

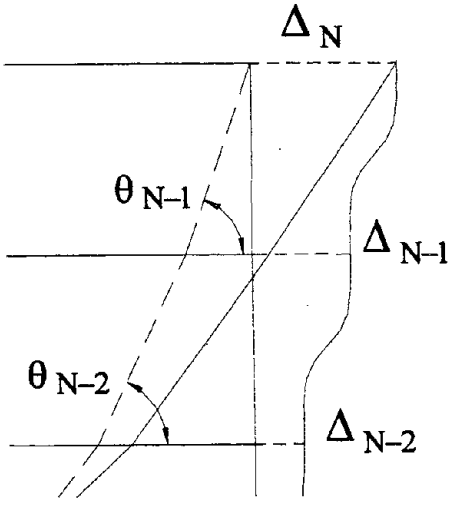

Figure 4-4 Damper Placement to Resist Overturning Moments – Load Balancing Prestressed Tendon-Fuse+Damper Solution (PTFD)

structure) in the floor slab. Tendons are allowed to slide through these holes. The layout is considered to be optimal in that it generates balancing lateral loads whose vertical distribution agree with the shape of the design lateral loads at each floor level. The damping forces are therefore transferred in the horizontal direction by bearing of the tendons to the floor slab/transfer beams.

4.6.2 Damper Deformation and Provided Effective Damping

Once the lateral design loads are determined from the preliminary design stage, the geometry of the tendon layout described above can be determined using the method described by Pekcan et al. (1999).

Deformation of the supplementary system can be determined in terms of the geometry of the tendon layout, interstory deformations, and axial forces in the tendons, as follows:

Interstory deformations, δ_{i+1} between floor levels $i+1$ and i (figure 4-4) can be written as:

$$\delta_{i+1} = \Delta_{i+1} - \Delta_i \qquad i = 0,\ldots,N-1 \tag{4-9}$$

where Δ_i = absolute displacement at floor level i relative to ground.

As can be seen from figure 4-4, deformation of the supplemental system at the foundation level can be written as the sum of all the tendon segment elongations assuming zero tendon stiffness and subtracting the sum of all the actual tendon elongations due to tendon forces, F_{Ti}:

$$X_{sup} = \sum_{i=0}^{N-1}\left\{\left[\left[\sqrt{1-\left[\left(\frac{\delta_{i+1}}{L_i}\right)\sin\theta_i\right]^2} + (\delta_{i+1}/L_i)\cos\theta_i\right] - 1\right]L_i - \frac{F_{Ti}L_i}{A_iE_i}\right\} \tag{4-10}$$

where A_i = cross-sectional area, E_i = Young's Modulus and, $L_i = h_{i+1}/\sin\theta_i$ is the length of tendon segment i.

Finally, it can be shown that the added damping due to dampers can be determined considering the following relationships (section 3):

$$\xi_d = \frac{1}{1+\alpha}\left(\frac{2\pi}{T_k}\right)^{\alpha-2}\left(\frac{T_k}{0.75}\right)^{0.15\alpha}\frac{\sum_i c_{\alpha i}\Delta_{ri}^{1+\alpha}}{\sum_i m_i\Delta_i^2} \qquad \textbf{(4-11)}$$

but $F_{Ti,h} = c_{\alpha i}\Delta_{ri}^{\alpha}\left(\frac{T_k}{0.75}\right)^{0.15\alpha}\left(\frac{2\pi}{T_k}\right)^{\alpha}$ is the horizontal component of the damping force at level i.

Therefore, using the geometry, equation (4-11) can be written as:

$$\xi_d = \left(\frac{1}{1+\alpha}\right)\left(\frac{T_k}{2\pi}\right)^2\frac{\sum_{i=1}^{N-1}(F_{Ti-1}\cos\theta_{i-1} - F_{Ti}\cos\theta_i)\Delta_{ri} + F_{TN}\cos\theta_{N-1}\Delta_{rN}}{\sum_i m_i\Delta_i^2} \qquad \textbf{(4-12)}$$

where F_{Ti} = force in the tendon between floor levels *i-1* and *i*.

4.6.3 "Load Balancing Prestressed Tendon-Fuse+Damper Solution (PTFD)"- Design Algorithm: PHASE III-B

Step 0: Tendon Layout

Determine the tendon layout based on the vertical distribution of the design base shear, solving the tri-diagonal system of linear equations for the system shown on figure 4-4:

$$[R]\{X\} = \{D\} \qquad \textit{(PIII-B-0a)}$$

in which

$$[R] = \begin{bmatrix} -(R_{0,1}+1) & R_{0,1} & 0 & & & \\ 1 & -(R_{1,2}+1) & R_{1,2} & & [0] & \\ & 1 & -(R_{2,3}+1) & R_{2,3} & & \\ & & & \ddots & & \\ & [0] & & 1 & -(R_{N-3,N-2}+1) & R_{N-3,N-2} \\ & & & & 1 & -(R_{N-2,N-1}+1) \end{bmatrix}_{N-1,N-1}$$

is the characteristic vertical load distribution matrix, where $R_{i,i+1} = \sum_{j=i+1} F_j \,/\, \sum_{j=i+2} F_j$, and $\{X\}^T = \{x_1, x_2, \ldots, x_{N-1}\}$ is the unknown column vector of tendon coordinates, and $\{D\}^T = \{0, \ldots, -R_{N-2,N-1}B\}$ (see figure 4-4).

Step 1: Tendon Design

Design the tendons based on the total supplemental system design capacity,

$$\frac{C_c^{\sup} W_T}{\cos\theta_o} \qquad \textit{(PIII-B-1a)}$$

to get the tendon cross-sectional area A_i.

Step 2: Device Deformation Demand

For the design structural displacement, determine the displacement demand on the supplemental devices.

$$X_{\sup} = \sum_{i=0}^{N-1}\left\{\left[\left[\sqrt{1-\left[\left(\frac{\delta_{i+1}}{L_i}\right)\sin\theta_i\right]^2}+\left(\delta_{i+1}/L_i\right)\cos\theta_i\right]-1\right]L_i-\frac{F_{Ti}L_i}{A_iE_i}\right\} \qquad \textit{(PIII-B-2a)}$$

in which $\delta_{i+1} = \Delta_{i+1} - \Delta_i$ and Δ_i = absolute design displacement at floor level i relative to ground.

Step 3: Damper Design

The damper force capacity requirements are based on the required normalized damper capacity $C_c^d = \varepsilon = r_d C_c^{\sup}$ corrected for the tendon layout inclination angle at the foundation level.

$$c_\alpha = \left(\frac{C_c^d W_T}{x_{ref}^\alpha}\right)\frac{1}{\left(\frac{2\pi}{T_{eff}}X_{\sup}\right)^\alpha\left(\frac{T_{eff}}{0.75}\right)^{0.15\alpha}} \qquad \textit{(PIII-B-3a)}$$

in which T_{eff}= is the effective period of vibration of the structure.

If elastomeric spring dampers are used, then determine the damper properties, i.e. preload P_y, elastomeric stiffness K_2,

$$P_y = c_\alpha\left(\frac{2\pi}{T_{eff}}X_{\sup}\right)^\alpha\left(\frac{T_{eff}}{0.75}\right)^{0.15\alpha} \qquad \textit{(PIII-B-3b)}$$

The preload in the damper would typically be equal to the maximum damping force, which ensures proper re-centering.

$$x_y = (0.01 \sim 0.05) X_{\text{sup}} \qquad \textit{(PIII-B-3c)}$$

The pseudo yield displacement due to tendon (in series) stiffness typically ranges from 1% to 5% of the total maximum stroke capacity of the damper. Therefore initial stiffness K_1,

$$K_1 = \frac{P_y}{x_y} \qquad \textit{(PIII-B-3d)}$$

The elastomeric stiffness K_2 can be taken as 5-10% of the initial stiffness K_1,

$$K_2 = (0.05 \sim 0.10) K_1 \qquad \textit{(PIII-B-3e)}$$

Step 4: Fuse Design

Determine the maximum force and corresponding ultimate strength requirements on the fuses,

$$F_{\max,f} = \frac{(1 - r_d) C_c^{\text{sup}} W_T}{\cos\theta_o} \qquad \textit{(PIII-B-4a)}$$

$$F_{fu} = 1.2 F_{\max,f} \qquad \textit{(PIII-B-4b)}$$

Choose Young's Modulus E_f, ultimate strength f_{su}, yield strength f_y, strain at yield ε_y, and ultimate strain ε_u. Calculate the required cross-sectional are A_f,

$$A_f = \frac{F_{fu}}{f_{su}} \qquad \textit{(PIII-B-4c)}$$

and corresponding fuse diameter is then,

$$d_f = \sqrt{\frac{4A_f}{\pi}} \qquad \textit{(PIII-B-4d)}$$

The required fuse length can then be calculated as,

$$l_f = \frac{X_{\sup}}{\varepsilon_u} \qquad \textit{(PIII-B-4e)}$$

4.6.4 Discussion of Load Balancing Approach

As discussed in the previous sections, near-source ground motions may be detrimental for tall-flexible building structures due to high initial pulse in the ground acceleration history. Excessive deformations and most of the yielding tend to concentrate in the lower stories. Furthermore, the supplemental damping devices also become ineffective in mitigating the effects of this type of ground motion. Therefore, other types of supplementary systems should be investigated to ensure that they are effective in mitigating the early high response to impulse type ground motions as well as the following cycles.

In general, stiffness characteristics of the building structure may be improved to mitigate such impulse type ground motion effects. However, uniform stiffening may not be attractive, as the stiffer structure will attract more forces that in turn should be resisted by the structural elements. Needless to say, a system whose stiffness is *controllable* as required, would in such cases be a viable solution. An even better attribute of such a system is if the stiffness of the system can be controlled in such a way that the required amount of opposing force is induced in the system when the seismic impulse hits the building structure. Consequently, a combined fuse+damper system that has the above-mentioned characteristics proposed is considered to be ideal. The sacrificial yielding fuse-bars are used in parallel to the main supplemental damping devices. The fuse-bars provide a high initial stiffness and limit displacements. However, the damping devices are still effective to attenuate the remainder of the response.

The design method of the tendon system utilizes the load-balancing concept as described above. However, it is noted that the level of prestress becomes a more important parameter in designing fuse-bars. In fact, prestressing is desirable to lessen the time when the tendons are slack during the dynamic response. Furthermore, the yielding fuses can be used to enhance the overall system damping characteristics as well. Various levels of prestress and its effects on the structural response will be analytically investigated later in this section. However, it can readily be said that the initial prestress should not exceed the initial pre-load level (if any) of damping devices and the deformation capacity should be carefully ascertained.

4.7 DESIGN VERIFICATION

It is probable that the actual hardware selected for the damper and/or fuse devices do not exactly correspond with the original design target value. It is therefore necessary to check the overall structure performance for the final design layout using the specified mechanical properties for the hardware adopted. This verification stage can be achieved in two phases as discussed in what follows.

4.7.1 Rapid Verification Using SDOF Models: PHASE IV

First, for the chosen solution MDOF can be converted back into an equivalent SDOF system. Hence, expected performance levels can be assessed using a Capacity-Demand Spectral Approach described in Section 2, under the MAE and MCE. If the target displacement objectives are not met then the design should be reviewed. This stage is Phase IV of figure 4-1. The overall capacity of the structure with the supplemental system can be determined by a series of simple analysis described in section 2. The plastic mechanism capacity of the bare structure will be the same. Therefore, the truss action analysis can be used to determine the contributions from the damper braces or supplemental tendons, which are then added to the bare frame capacity, determined in Phase I. The performance point can be identified at the intersection of the capacity and demand curves as shown in figure 4-5, under the MCE. The design process can be advanced to the next phase, if the overall structural deformation is within acceptable limits. However, design of the supplemental system should be revised to accept the imposed deformations by the MCE condition.

A step-by-step algorithm is given for the rapid verification phase in what follows.

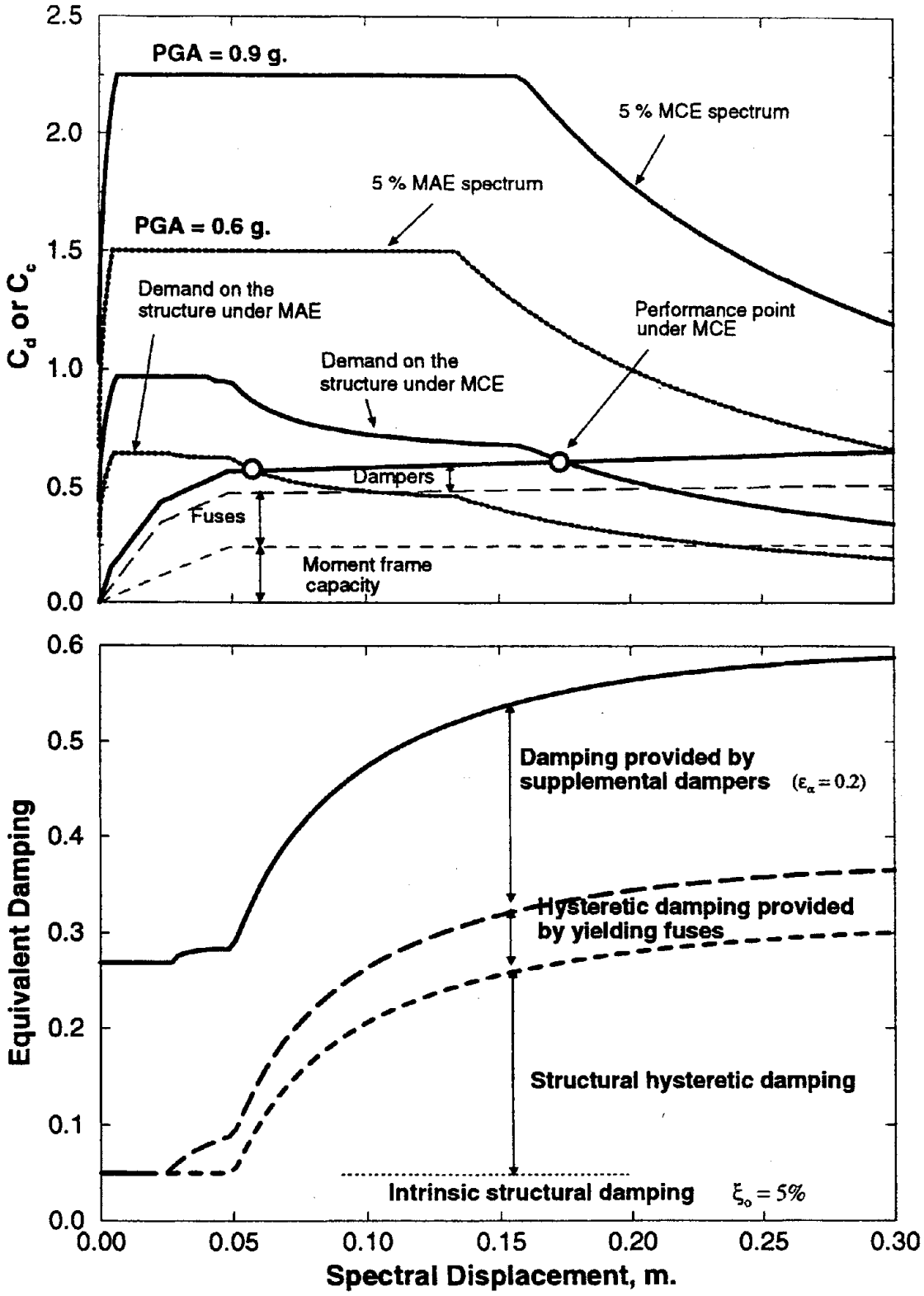

Figure 4-5 Evaluation of the Supplemental System Performance

4.7.1.1 Rapid Design Verification Algorithm

Step 0: Overall Capacity of the Structure

Determine the contribution of the supplemental system to the overall structural capacity in terms of the device and configuration properties using an appropriate analysis method.

It must be noted that the supplemental system is desirably implemented on the interior gravity load carrying frames which consists of beam-column connections that are ideally pin. Therefore, the interior frame together with the supplemental system can be analyzed as a truss as described in section 2. Once the pushover capacity is established for the interior frame and the supplemental system, it can be directly added to the bare structure capacity (Phase I) to determine the overall pushover capacity of the structural system.

Step 1: Demand Imposed by the MCE

Once the 5% demand spectrum for the MCE is determined, overall demand imposed on the structure can be determined as a function of the damping provided by the supplemental system as well as due to yielding as shown in figure 4-5. The performance point can be identified as shown in the figure.

4.7.2 MDOF Evaluation Using Non-linear Time History Analysis: PHASE V

The second part of the design verification process is to conduct a series of non-linear time history analyses for a variety of ground motions that are representative of the MAE and MCE. Structural members should be checked for damage. Also, the supplemental hardware should be checked for its adequacy to accept the deformation demands imposed on it.

Phase V is important, this is because the former verification step (which is based on a SDOF idealization) is unable to ascertain difficulties with higher mode response. However, the non-linear time history analysis of the MDOF idealization accounts for such effects. Moreover the effects of any localized damage can be assessed and addressed in the design.

4.8 SUMMARY AND CONCLUSIONS

A simple, straightforward definition of equivalent damping based on the power consumption equivalence for nonlinear viscous and ESDs was introduced in Section 3. The proposed equivalent linear approach was implemented in analysis and design methods along with an analytical spectral approach to estimate the exact maximum velocity response from the pseudo velocity spectra. It was then noted that near-source ground motions generally have a very undesirable effect on the response, especially for flexible structures. The added damping alone is usually not enough to mitigate such response, which can be characterized with its peak that takes place early in the response history.

In this section, firstly, a straightforward preliminary design methodology is introduced as part of a complete design process. Although this design methodology can be generalized for other supplemental systems, the emphasis is given to the systems that are of [nonlinear] viscous nature. The overall design methodology follows the basic principles of capacity design approach but improves especially the preliminary design phase. The proposed preliminary design phase yields a supplemental system capacity for the equivalent SDOF system which is then adopted in one of the alternative design strategies.

Secondly, a damper distribution (Damper-Truss Solution, DTR) is proposed in which the total design damper size is distributed along the height of the building in proportion to the design story shears. A desired moment frame-truss action can be achieved in which the lateral seismic forces are transferred by the dampers installed on the gravity load carrying interior frames. Design formulations were derived and a step-by-step design algorithm was given.

Finally, an innovative configuration was proposed in which tendons are draped so as to balance the equivalent lateral inertial loads and the supplemental devices are located at either end of the tendon system (Load Balancing Prestressed Tendon-Fuse+Damper Solution, PDTF). Design formulations were derived and step-by-step design algorithms given.

SECTION 5

RETROFIT DESIGN EXAMPLE OF A NINE-STORY FLEXIBLE STEEL BUILDING

5.1 INTRODUCTION

This section presents a retrofit design example of a flexible steel building. The building considered for the verification of the design methodologies introduced in the previous sections is an existing nine-story steel building located in the Los Angeles region. The retrofit design example is carried out for two different configurations; namely, Damper-Truss Solution and Load Balancing Prestressed Fuse+Damper Solution. The performance of the two retrofitted configurations is compared with that of the undamped structure based on the nonlinear time-history analyses and results are discussed.

5.2 DESCRIPTION OF THE EXAMPLE BUILDING AND GENERAL MODELING ASSUMPTIONS

The building considered for the verification of the previously introduced design methodologies is an existing nine-story steel building with square plan and with two axes of symmetry as shown in figure 5-1. Moment resisting frames exist on the perimeter only with pre-Northridge welded moment connections, and all interior beam-column connections are simple connections. Design loads and the structural properties pertinent to the analytical modeling (discussed later) are summarized in table 5-1. The building is located in the Los Angeles region, and according to NEHRP Seismic Hazard maps is located such that the effective peak acceleration coefficient is $C_a = 0.4$ and effective peak velocity coefficient is $C_v = 0.4$.

The example building is currently being studied by researchers throughout the United States as part of a SAC project to investigate various performance issues related to the observed response during the 1994 Northridge earthquake. Therefore, most of the modeling assumptions are in agreement with those recommended by the SAC project-task groups. Since the structural systems in two directions are essentially the same when viewed from the front and side elevations, only the NS direction is chosen for the present study. Furthermore, because of symmetry, only the front-half of the structure is modeled, i.e. one exterior moment frame and two interior gravity-load carrying frames. The building has one basement and that the ground

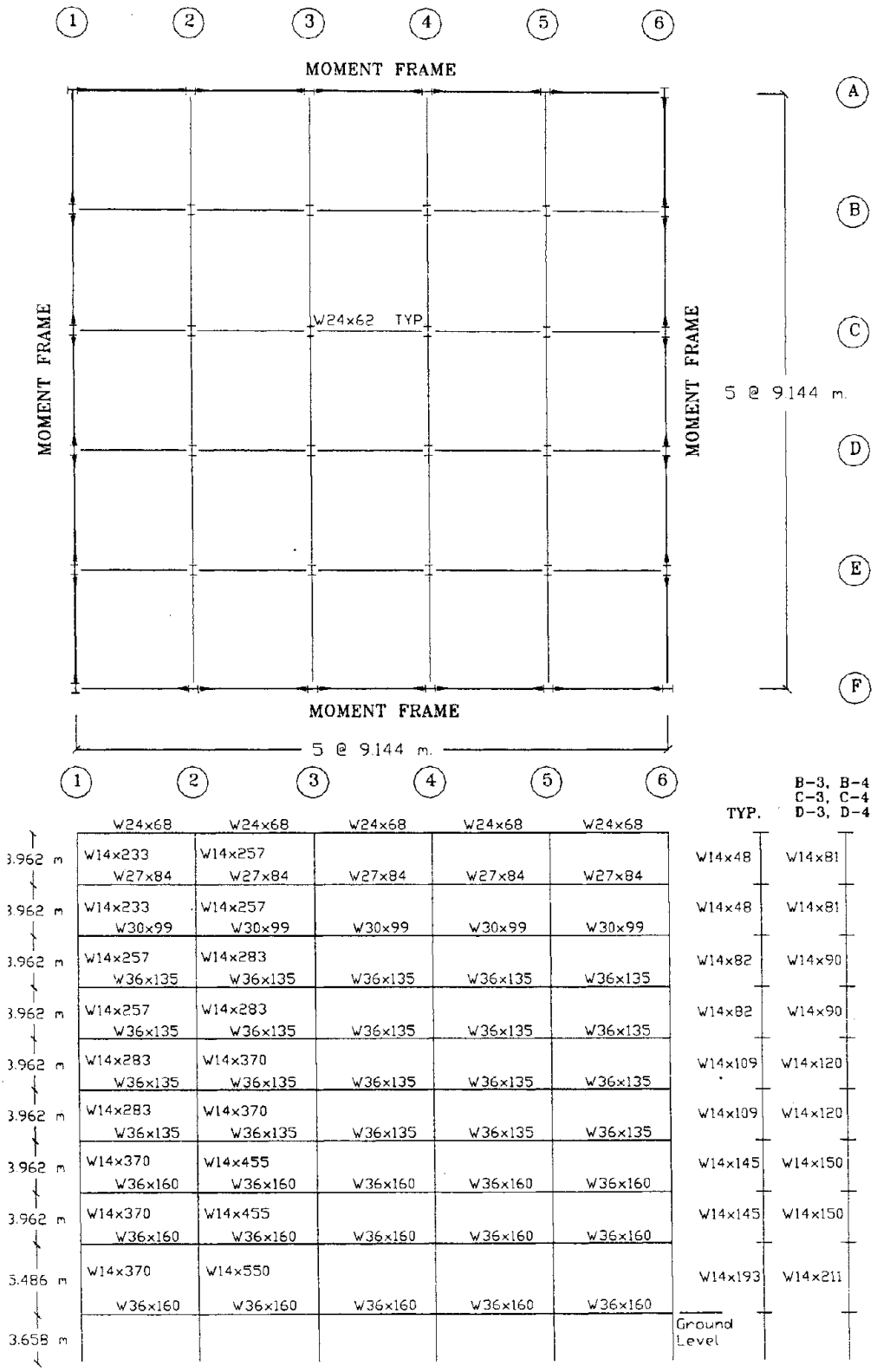

Figure 5-1 Nine-Story Steel Building – Case Study

Table 5-1 Mass and Loading Definitions

Dead Load	
• Floor Slab	= 2.54 kPa
• Ceiling/Flooring	= 0.14 kPa
• Mechanical/Electrical	= 0.34 kPa
• Partitions	
for dead weight	= 0.96 kPa
for seismic mass	= 0.45 kPa
• Steel Framing (assumed)	= 0.62 kPa
• Roofing	= 0.34 kPa
• For penthouse (additional to roof dead load)	= 1.91 kPa
Live Load	
• Typical Floor	= 0.96 kPa
• Roof	= 0.96 kPa
Seismic Mass (Full Structure, Total Weight = 88,395 kN)	
• Roof	= 1.07 Mg
• Floor 3 to Floor 9	= 0.99 Mg
• Floor 2	= 1.01 Mg
• Floor 1	= 0.96 Mg

floor is restrained laterally therefore receives the same ground motion input as the column bases. It is for this reason that only the upper nine stories are modeled in this study.

The following assumptions have been made in the analyses:

(i) The plastic hinges were modeled as point hinges at both ends of the beam and column elements. Structural degradation was not included in the nonlinear models of the elements.

(ii) All the structural elements had 3% strain hardening with bilinear hysteresis properties.

(iii) M-P interaction diagrams were constructed such that plastic moment capacity ($M_p = Z F_y$) is assumed for up to 15% of the axial yield force ($0.15P_y$) and linear thereafter for the strong-axis bending whereas the percentage is assumed to be 40% for the weak-axis bending. Structural steel used in the building had a yield strength, F_y = 50 ksi (345 MPa).

(iv) Interior frame beams were modeled assuming 50% of the real plastic moment capacities to account for the simple beam-to-column connections at their ends.

Table 5-2 Comparison of Mode Shapes

Mode Shapes								
	Exterior Frame Only				Exterior Frame+ 2 Interior Frames			
Mode	1	2	3	4	1	2	3	4
Period (sec.)	2.12	0.80	0.47	0.32	1.78	0.65	0.38	0.26
P. Factor[1]	0.818	0.113	0.041	0.015	0.822	0.109	0.039	0.016
Story 9	1.000	-1.000	-0.965	0.792	1.000	-1.000	-0.965	0.792
8	0.926	-0.536	0.129	-0.778	0.938	-0.582	0.039	-0.676
7	0.823	0.007	0.949	-0.994	0.846	-0.047	0.878	-1.000
6	0.719	0.420	1.000	0.087	0.746	0.388	1.000	-0.022
5	0.609	0.671	0.427	1.000	0.633	0.683	0.481	0.941
4	0.498	0.765	-0.288	0.830	0.518	0.808	-0.231	0.841
3	0.375	0.723	-0.857	-0.124	0.390	0.776	-0.814	-0.085
2	0.262	0.581	-0.998	-0.852	0.269	0.620	-0.965	-0.827
1	0.150	0.357	-0.725	-0.863	0.148	0.371	-0.695	-0.862

[1] Effective modal mass as a fraction of the total mass

(v) The analytical model included one exterior frame and two interior frames. The horizontal degrees of freedoms of the interior frame joints were slaved to corresponding exterior frame joints along each column lines in keeping with the rigid floor assumption.

(vi) Supplemental systems are placed on the interior frame.

5.3 Modal Properties of the Model Building

The inherent viscous damping of the structure is modeled as mass and stiffness proportional (Raleigh) damping. Therefore, viscous damping is assumed to be ξ=2% in the first mode and at $T = 0.2$ in the following relationships:

$$\alpha = \frac{4\pi(T_j\xi_j - T_i\xi_i)}{T_j^2 - T_i^2} \qquad \textit{mass proportion}$$

$$\beta = \frac{T_iT_j(T_j\xi_i - T_i\xi_j)}{T_j^2 - T_i^2} \qquad \textit{stiffness proportion} \qquad \textbf{(5-1)}$$

Half the mass of the building (including live load) is distributed to the horizontal degrees of freedom of the exterior frame. Masses and gravity loads are in general calculated from the corresponding tributary areas shown in figure 5-1. P-δ effects due to gravity loads are included in both the push-over and time history analyses.

Modal analyses were performed on the a) exterior moment frame only and, b) combined system with one exterior moment frame and two interior frames to assess the effect of the interior frames on the initial dynamic properties of the structure as well as the capacity. Mode shapes and corresponding time periods together with the effective modal masses as a fraction of the total mass are summarized in table 5-2. As can be seen from table 5-2, combined structural system has a shorter first mode-elastic period of 1.78 sec. The dynamic response is expected to be governed by the first mode response with contribution from the second mode. Moreover, it is evident from the table that the interior frames have a significant contribution to the overall stiffness of the building. However, mode shapes and corresponding effective masses are similar for the two cases.

5.4 Performance Objectives for the Retrofitted Nine-Story Structure

The general performance criteria adopted in this study is a "no yielding" essentially elastic response of the structural elements under the Maximum Assumed Earthquake (MAE) which has a 10% probability of exceedance in 50 years. The criterion for the Maximum Considered Earthquake (MCE, 2% probability of exceedance in 50 years) however permits up to 0.5% plastic hinge rotation at the beam-ends. This plastic hinge rotation requirement is based on

the findings of many researchers who have studied the performance of typical pre-Northridge welded connections.

The general performance based design objective is to reduce the various response quantities but most importantly to control the interstory drifts so that plastic rotations at the beam ends are within acceptable limits. This plastic hinge rotation criterion (θ_p<0.005 rad) is therefore the most significant and challenging aspect of the retrofit design.

The retrofit design of the example building is given in what follows.

5.5 Determination of the Structural Capacity: PHASE I

Overall capacity of the example structure is determined in two stages; a) elastic-modal analysis, and b) plastic analysis.

Step 1: As was mentioned previously (figure 2-7), linear elastic portion of the push-over curve can be approximated using the first mode period of vibration of the structure (equations (2-17) and (PI-1b)). Elastic stiffness is calculated based on the first mode period of the exterior frame only, T_o = 2.12 sec., since the interior frame beams yield at relatively small drifts,

$$C_{c,el}^{str} = \frac{4\pi^2}{g}\frac{S_d}{T_o^2} = 0.895\Delta_s \qquad \textbf{(PI-1b)}$$

Step 2: Plastic base shear capacity is determined using equations (PI-2a) and (PI-2b). Equation (PI-2a) is plotted in figure 5-2 which has a minimum value at n_{sp} = 6. Hence,

$$C_{c,pl}^{str} = \frac{V_{b,pl}(n_{sp}=6)}{W_T} = 0.302 \qquad \textbf{(PI-2a)}$$

It must be noted here that reduction in the plastic moment capacities of the columns is taken into account for the presence of the gravity loads on the columns. A comparison of Drain-2DX push-over analysis result and simplified analysis is shown in figure 5-3. A 3% percent post yield stiffness ratio is assumed in both analyses.

P-δ effect on the structural capacity is accounted for using equation (PI-2c). Equivalent SDOF height is determined based on the modal analysis results as:

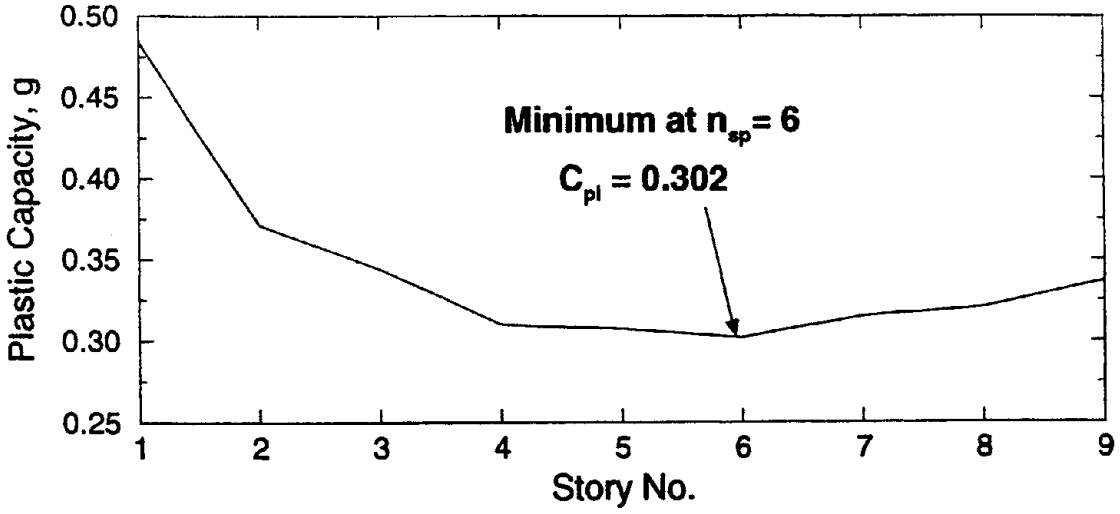

Figure 5-2 Determination of Plastic Capacity from the Number of Stories Participating in the Plastic Mechanism

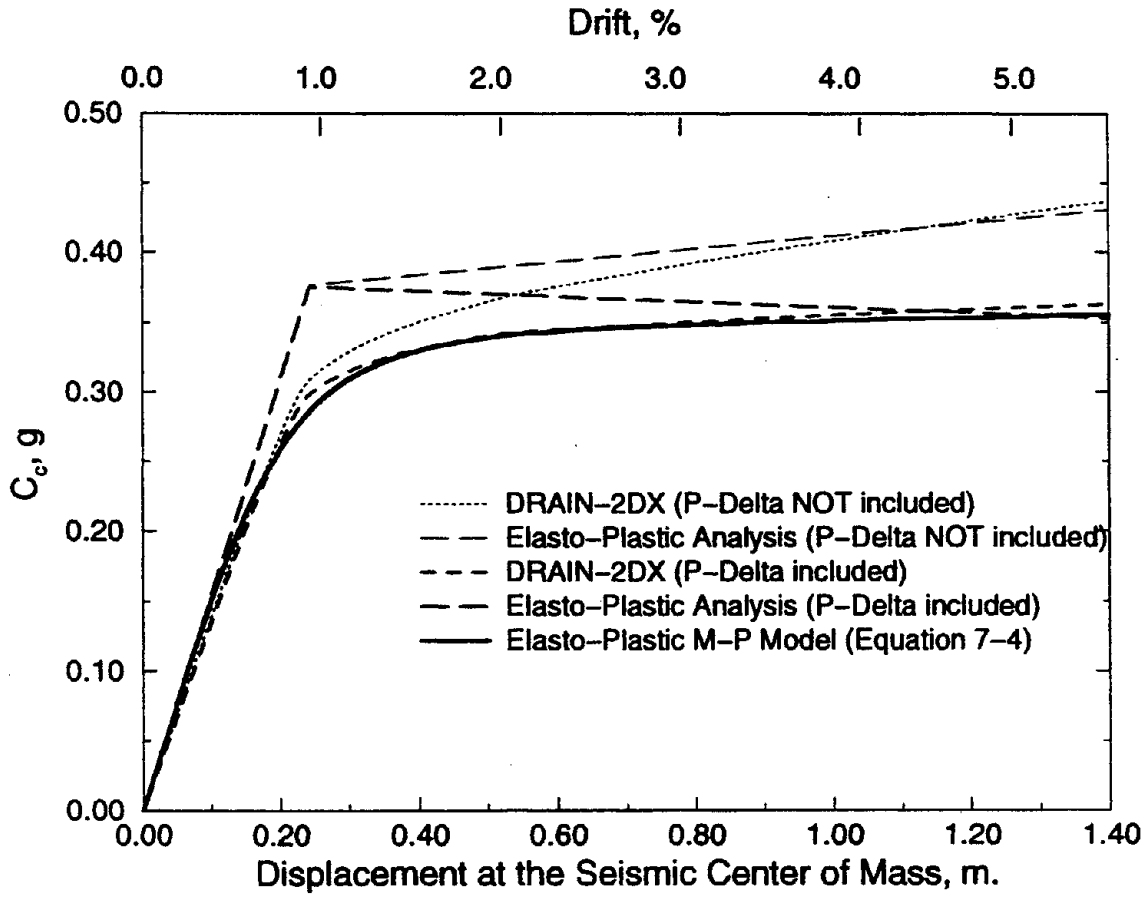

Figure 5-3 Comparison of Push-Over Capacity of the Structure obtained from Drain-2DX and Simplified Elasto-Plastic Analysis

$$\Delta C_{P-\delta}^{str} = \frac{\delta}{h_e} = \frac{\Delta_s}{h_e} = 0.038\Delta_s \qquad \textbf{(PI-2c)}$$

Also shown in figure 5-3 are the Drain-2DX and simplified analyses results including P-δ effects. As can be seen from the figure, simplified analysis provides a very reliable estimate for the structural capacity. In order to facilitate further design iterations, a Menegotto-Pinto model introduced in equation (4-3) is used with a shape factor of R = 4.

$$C_c^{str}W = K_1\Delta_s\left(Q + \frac{(1-Q)}{\left(1+\left|\Delta_s/\Delta_y\right|^4\right)^{0.25}}\right) = 54{,}500\Delta_s\left(0.03 + \frac{0.97}{\left(1+\left|\Delta_s/0.23\right|^4\right)^{0.25}}\right)$$

where initial elastic stiffness K_1 was calculated based on the first mode period

5.6 Preliminary Retrofit Design of the Nine-Story Building: PHASE II

The normalized design capacity of the supplemental system is iteratively determined using the procedure described in section 4.4.2. It must be noted here that the demand C_d is amplified by the factor λ to take uncertainty in the ground motion into account.

Step 0: Target Displacement Response

The target design drift Θ_{max}, at the roof level (or at the effective height, h_e) is chosen to be 0.5% which corresponds to a roof displacement of

$$X_{\max}^{roof} = 0.186\ m.$$

Step 1: Total Effective Damping, ξ_{eff}^{total}

Total effective damping is initially assumed to be 10%. After a few iterations (see section 4.4.2) for a damper only design (i.e. r_d = 1.0), the total effective damping is found to be

$$\xi_{eff}^{total} = 19.2\%$$

for which the reduction factors are

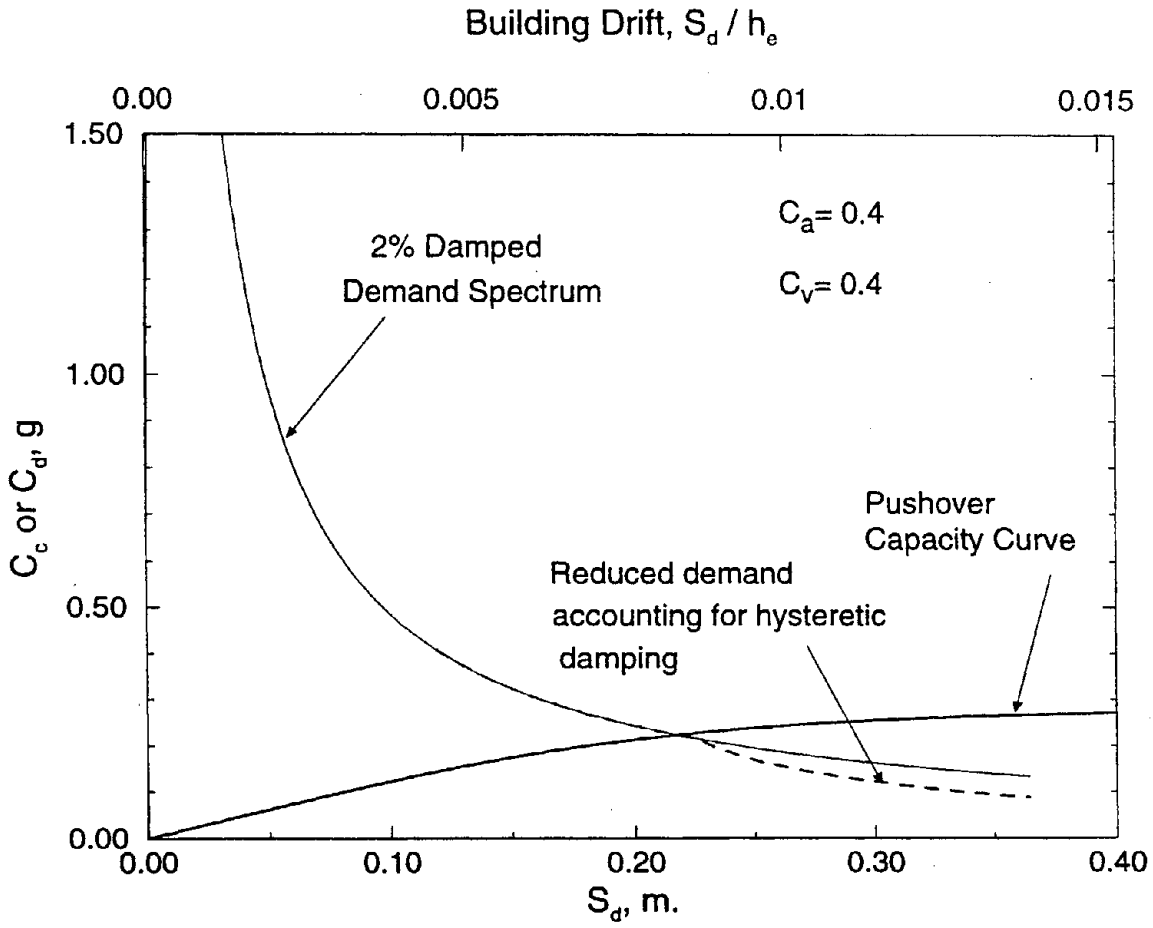

Figure 5-4 Capacity-Demand Spectrum for the Unretrofitted Structure

$$B_s = \left(\frac{\xi_{eff}^{total}}{0.05}\right)^{0.5} = \left(\frac{0.192}{0.05}\right)^{0.5} = 1.995$$

$$B_1 = \left(\frac{\xi_{eff}^{total}}{0.05}\right)^{0.3} = \left(\frac{0.192}{0.05}\right)^{0.3} = 1.513$$

Hence, corresponding ground motion demand,

$$1.5C_d = 1.5\frac{C_v^2 g}{4\pi^2 B_1^2 X_{\max}} = 1.5\frac{0.4^2 \cdot 9.81}{4\pi^2 \cdot 1.515^2 \cdot 0.186} = 0.199$$

Therefore the effective period T_e can be calculated as,

$$T_e = 2\pi\sqrt{\frac{X_{\max}}{gC_d}} = 2\pi\sqrt{\frac{0.186}{9.81 \cdot 0.199}} = 1.94 \text{ sec}$$

Step 2: Required Supplemental System Capacity

Structural capacity corresponding to the target displacement can be either calculated using equation (4-3) or read off the capacity-demand curves shown in figure 5-4,

$$C_c^{str} = 0.145$$

Therefore required supplemental system capacity is,

$$C_c^{sup} = C_d - C_c^{str} = 0.199 - 0.145 = 0.054$$

Also shown in figure 5-4 is the 2% and reduced design demand curve. The response of the unretrofitted structure subjected to design earthquake is expected to be at the intersection of the reduced demand and capacity curves. However, as was mentioned in section 2, variations should be expected due to the uncertainties in the ground motions.

Step 3: Damper and Fuse Capacities

For a damper only design ($r_d = 1.0$, $r_f = 0.0$),

$$C_c^d = r_d C_c^{sup} = 1.0 \cdot 0.054 = 0.054$$

$$C_c^f = r_f C_c^{sup} = 0.0 \cdot 0.054 = 0$$

Step 4: Hysteretic Damping, ξ_{eff}^{str}

Since at the target design displacement, the structure is expected to respond linearly, then the hysteretic damping $\xi_{hy}^{str} = 0$, hence

$$\xi_{eff}^{str} = \xi_o = 2\%$$

Step 5: Hysteretic Damping due to Fuse Yielding, ξ_{hy}^{f}

$$\xi_{hy}^{f} = 0 \qquad (\text{since } r_f = 0)$$

Step 6: Added Damping due to Dampers, ξ_d

The damper power is chosen to be $\alpha = 0.2$, therefore the added damping due to dampers can be calculated as,

$$\xi_d = \frac{C_c^d}{1+\alpha}\left(\frac{2\pi}{0.75}\right)^{0.15(\alpha-1)} g^{0.5(0.85\alpha+0.15)} X_{\max}^{0.5(1.15\alpha-0.15)} C_d^{0.5(0.85\alpha-1.85)}$$

$$= \frac{0.054}{1.+0.2}\cdot\left(\frac{2\pi}{0.75}\right)^{-0.12} \cdot 9.81^{0.16} \cdot 0.186^{0.04} \cdot 0.199^{-0.84}$$

$$= 17.9\%$$

Step 7: Total Effective Damping, ξ_{eff}^{total}

$$\xi_{eff}^{total} = \xi_{eff}^{str} + \xi_{hy}^{f} + \xi_d = 2\% + 0.\% + 17.9\% = 19.9\%$$

which is equal to previous value, therefore the preliminary design is satisfactory.

Design parameters are summarized in table 5-3 for the damper only and damper+fuse design in which equal damper and fuse capacities are chosen ($r_d = r_f = 0.5$).

5.7 Implementation of the Supplemental System: PHASE III

Based on the preliminary design, the normalized damper and/or fuse capacities are calculated. In the third phase of the design, desired supplemental system configuration is chosen and the supplemental system components are detailed together with the chosen system layout. This process for the example structure is given for DTR and PTFD solutions in what follows.

Table 5-3 Summary of Preliminary Design

Target Roof Drift = 0.5%, Damper power, $\alpha = 0.2$												
	ξ_{eff}^{total} %	B_s	B_1	C_d	T_e sec	C_c^{str}	C_c^{sup}	C_c^d	C_c^f	ξ_d %	ξ_{hy}^f %	ξ_{eff}^{str} %
Damper Only	19.9	1.995	1.513	0.199	1.941	0.145	0.054	0.054	0.0	17.9	0.0	2.0
Damper +Fuse	16.9	1.840	1.442	0.219	1.849	0.145	0.074	0.037	0.037	11.4	3.6	2.0

Table 5-4 Summary of DTR Design Parameters

Total equivalent (SDOF) damper coefficient, c = 2,400 kN/(m/sec)$^{0.2}$									
St. No.	**Mode Shape**	**Norm. Inertial Force**	**Norm. Story Shear**	**Interstory Drift %**	**C_α kN/(m/s)$^\alpha$**	**P_y (kN)**	**X_y (mm)**	**K_2 (10^4kN/m)**	**X_{max} (mm)**
9	1.000	1.000	1.00	1.98	900	550	2.7	16	25
8	0.938	0.893	1.89	1.98	1750	1000	2.7	30	25
7	0.846	0.787	2.68	1.98	2500	1450	2.7	43	25
6	0.746	0.680	3.36	1.98	3100	1800	2.7	53	25
5	0.633	0.574	3.93	1.98	3640	2124	2.7	62	25
4	0.518	0.467	4.40	1.98	4100	2400	2.7	70	25
3	0.386	0.361	4.76	1.98	4400	2600	2.7	76	25
2	0.269	0.254	5.02	1.98	4650	2700	2.7	80	25
1	0.148	0.148	5.16	2.74	4550	2800	3.5	63	34

5.7.1 Example DTR Design: PHASE III-A

Elastomeric Spring Dampers with re-centering characteristics are designed for the retrofit of the example building.

Step 0: Damper Coefficient, c_α

Total equivalent (SDOF) damper coefficient is calculated as,

$$c_\alpha = \frac{C_c^{sup} W_T}{\dot{x}_{ref}^{\alpha}} = \frac{0.054 \cdot 44{,}197}{1.0^{0.2}} = 2{,}372 \;\; kN/(m/\sec)^{0.2}$$

Step 1: Damper Size Distribution

Damper size distribution, proportional to the story shears, corrected for the damper brace inclination is determined using equation (PIII-A-1a) and tabulated in table 5-4.

5.7.2 Example PTFD Design: PHASE III-B

Elastomeric Spring Dampers are designed and the tendon layout is determined based on a code lateral force distribution with $k = 1.65$ given in equation (2-1). The design procedure is iterative once the damper tendon layout is determined. The maximum tendon force is updated after the previous iteration (based on the supplemental system capacity), as it equals to the sum of maximum supplemental system capacity and prestress force. This affects the tendon cross-sectional area hence the supplemental system deformation (Equation (PIII-B-2a))

Step 0: Tendon Layout

Tendon layout is determined based on the overturning moments as mentioned above and solving the matrix equation given in equation PIII-B-0a. Scaled tendon layout is shown in figure 5-5

Step 1: Tendon Design

Maximum design force in the tendon is calculated as:

$$\frac{C_c^{sup} W_T}{\cos\theta_o} = \frac{0.054 \cdot 44{,}197}{\cos(31.4^\circ)} = 2{,}800 \quad kN$$

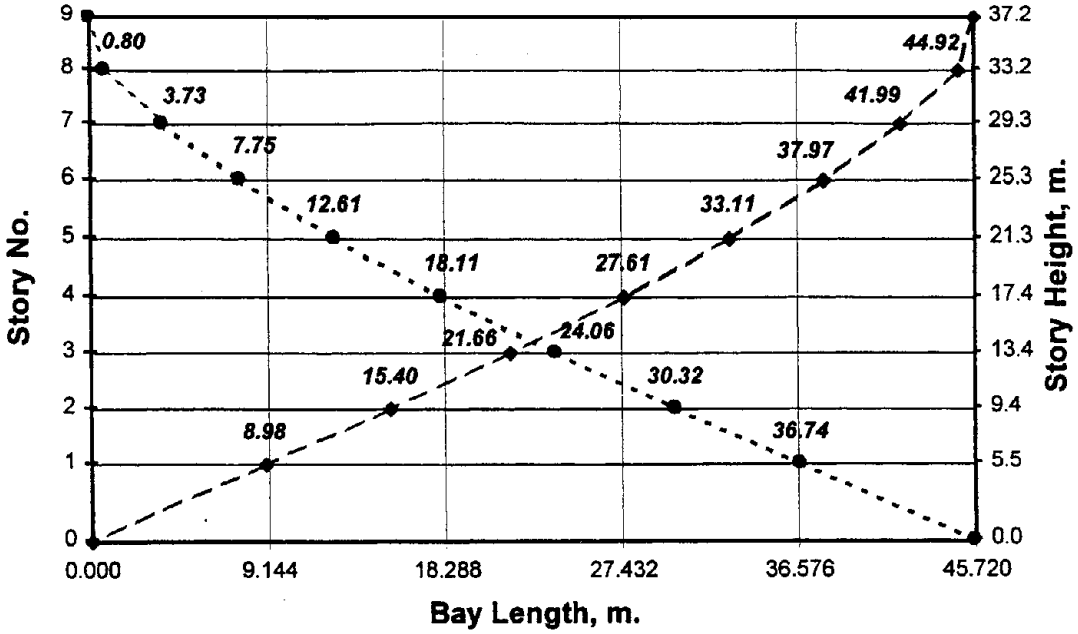

Figure 5-5 Tendon Layout Based on the First Mode Response

Table 5-5 Determination of Supplemental System Deformation

Story No.	Story Displ. (mm)	Interstory Displ (mm)	Tendon Angle	Tendon Length (m)	Tendon Force (kN)	X_{sup} (mm)
9	186	32	68.0	4.27	2083	11
8	154	18	53.5	4.93	2402	11
7	136	18	44.6	5.64	2748	13
6	117	18	39.2	6.27	3056	14
5	98	18	35.8	6.77	3304	15
4	81	18	33.6	7.15	3487	15
3	62	18	32.4	7.40	3608	16
2	44	18	31.7	7.54	3677	15
1	26	26	31.4	10.53	3705	22
					Cumulative X_{sup} =	132

Table 5-6 Summary of PTFD Design Parameters

c_α (kN/(m/s)$^\alpha$)	P_y (kN)	X_y (m)	K_2 (10^4 kN/m)	X_{max} (m)	Max. F. Force[1] (kN)	Fuse Dia. (m)	Fuse Length (m)	Tendon Force (kN)	Initial Prestr. (kN)
2,131	1,852	0.003	3.00	0.20	-	-	-	3,705	925
1,455	1,275	0.003	3.00	0.20	1,915	0.07	1.5	6,376	1,145

[1]For the fuse+damper design, $r_d = r_f = 0.5$

Step 2: Device Deformation

If a prestressing tendon with f_y = 450 MPa is chosen, supplemental system deformation X_{sup} (Equation PIII-B-2a), can be calculated as tabulated in table 5-5.

Step 3: Damper Design (r_d = 1.0)

The damper coefficient can be calculated using equation (PIII-B-3a)

$$c_\alpha = \left(\frac{C_c^d W_T / \cos(\theta_o)}{x_{ref}^\alpha} - F_p \right) \frac{1}{\left(\frac{2\pi}{T_{eff}} X_{sup} \right)^\alpha \left(\frac{T_{eff}}{0.75} \right)^{0.15\alpha}}$$

$$= \left(\frac{0.054 \cdot 44{,}197 / \cos(31.4)}{1.0^{0.2}} - F_p \right) \frac{1}{\left(\frac{2\pi}{1.94} \cdot 13.3 \right)^{0.2} \left(\frac{1.94}{0.75} \right)^{0.15 \cdot 0.2}}$$

$$= 2{,}131.0 \quad kN/(m/s)^{0.2}$$

where F_p = the prestress in the tendons (in the first iteration F_p = 0)

Therefore, ESD should be designed to have preload level P_y,

$$P_y = c_\alpha \left(\frac{2\pi}{T_{eff}} X_{sup} \right)^\alpha \left(\frac{T_{eff}}{0.75} \right)^{0.15\alpha} = 1{,}850 \quad kN$$

Step 4: Fuse and Prestress Design

Based on the above design assumptions, no fuse design is necessary since, r_f = 0. However, at this point of the design process, desired prestress F_p, should be calculated. For this example, a prestress level, which is equal to 50% of the damper preload, is chosen, hence,

$$F_p = \frac{P_y}{2} = \frac{1{,}850}{2} = 925 \quad kN$$

After a few iterations, supplemental system parameters are calculated and listed in table 5-6. Also summarized in the table are the design parameters for the fuse+damper alternative based on the preliminary design parameters given in table 5-3.

5.8 Performance and Evaluation of the Retrofitted Structure with the Supplemental System

The previously introduced enhanced version of nonlinear time history analysis program-DRAIN-2DX was used to evaluate the performance of the example structure subjected to ground motions representative of MAE and MCE earthquakes. Results of the following ground motions are presented: 1940 El Centro S00E, 1972 Taft S69E and 1994 Northridge – Arleta 90°. These ground motions were scaled to peak ground acceleration (PGA) of 0.4g for the MAE. Three ground motions (scaled to PGA=0.60 g) that are representatives of the MCE are 1994 Northridge – Sylmar County Hospital (PGA=0.61 g), 1979 Imperial Valley – Array 5 (PGA=0.59) and 1995 Great Hanshin – Kobe Station (PGA=0.69) were used. Five percent and twenty percent pseudo acceleration response spectra of these ground motions are plotted in figure 5-6, and compared with the corresponding design spectra. Undamped (unretrofitted) response of the structure is compared to those with various supplemental system configurations designed in the previous subsections mainly with reference to above mentioned target design and performance objectives. It must be noted here that the target design objective yields a total effective damping ξ_{eff}^{total} of about 20% for all the design alternatives.

5.8.1 Expected Performance under the MAE and MCE ground motions

The effect of the supplemental system-tendon system on the capacity of the example frame is evaluated after the above design detailing. Figure 5-7 compares the analytically (plastic analysis and Menegotto-Pinto modeling) obtained capacity curves with those obtained from Drain-2DX.

As was previously introduced in section 4, reduced demand curves that account for the added damping due to fuse-bar yielding and dampers are obtained for two configurations and two ground motions. These design curves are shown in figures 5-8 through 5-11. As can be seen from the figures, performance point is defined as where the reduced demand curve intersects corresponding capacity curve. It must be noted however, that these performance points are considered to be mean response. Hence, variations should be expected as discussed in section 2.

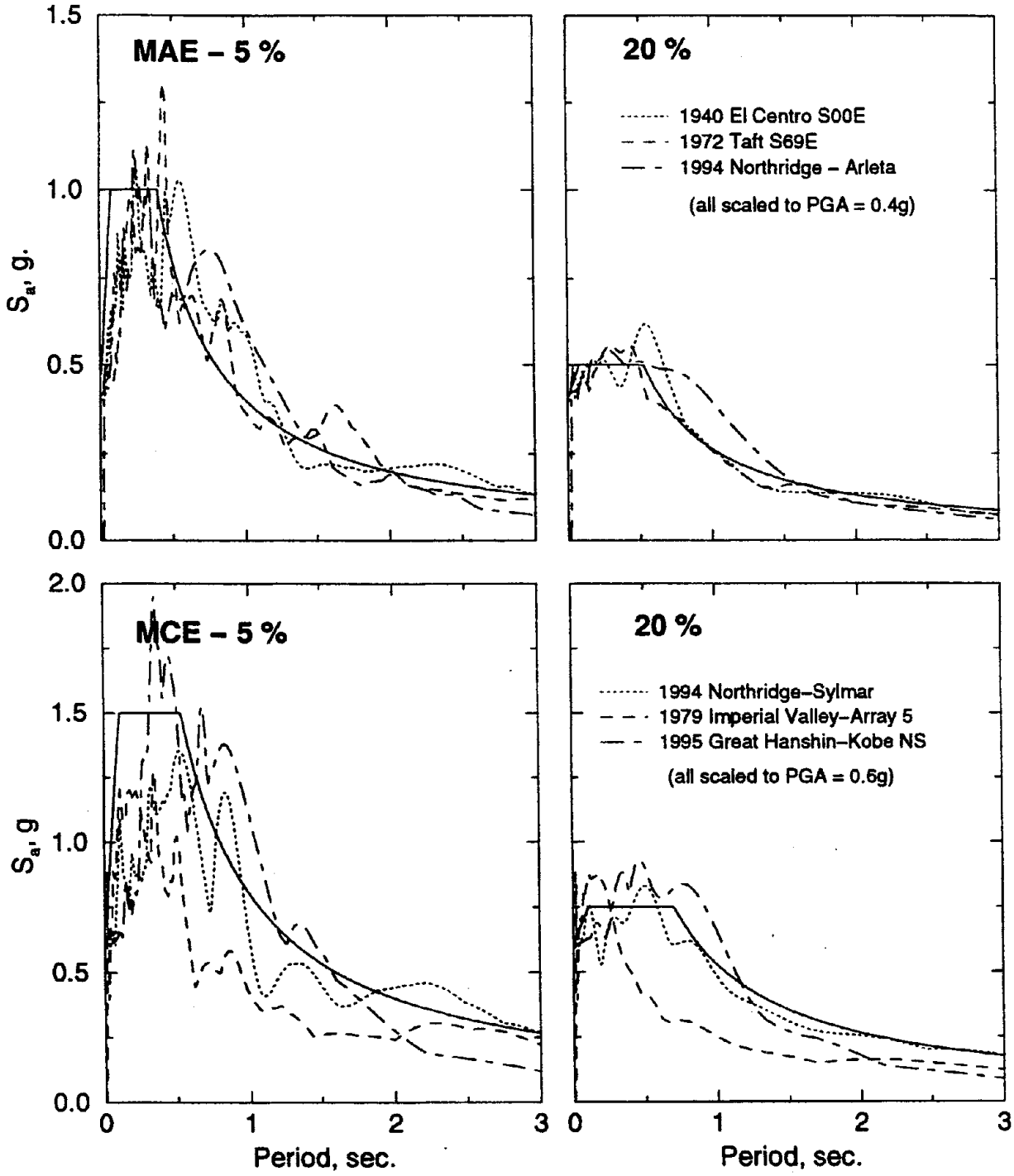

Figure 5-6 Pseudo Acceleration Response Spectra of the Design Ground Motions

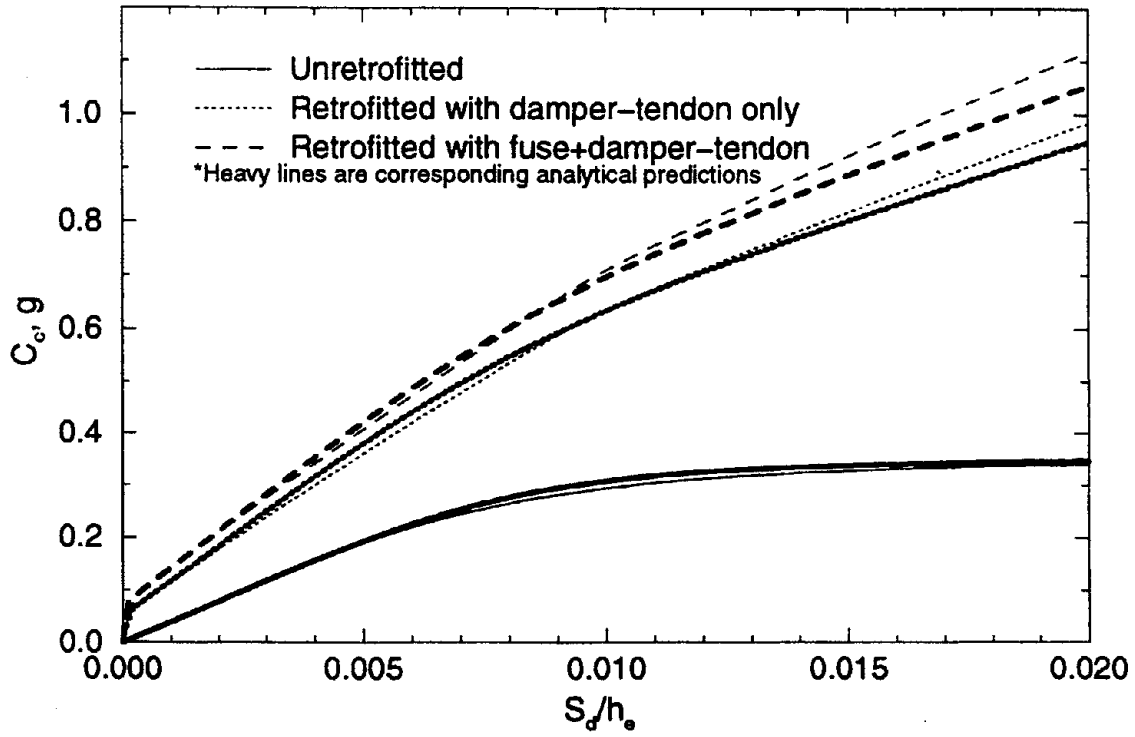

Figure 5-7 Comparison of Pushover Curves Before and After Retrofit

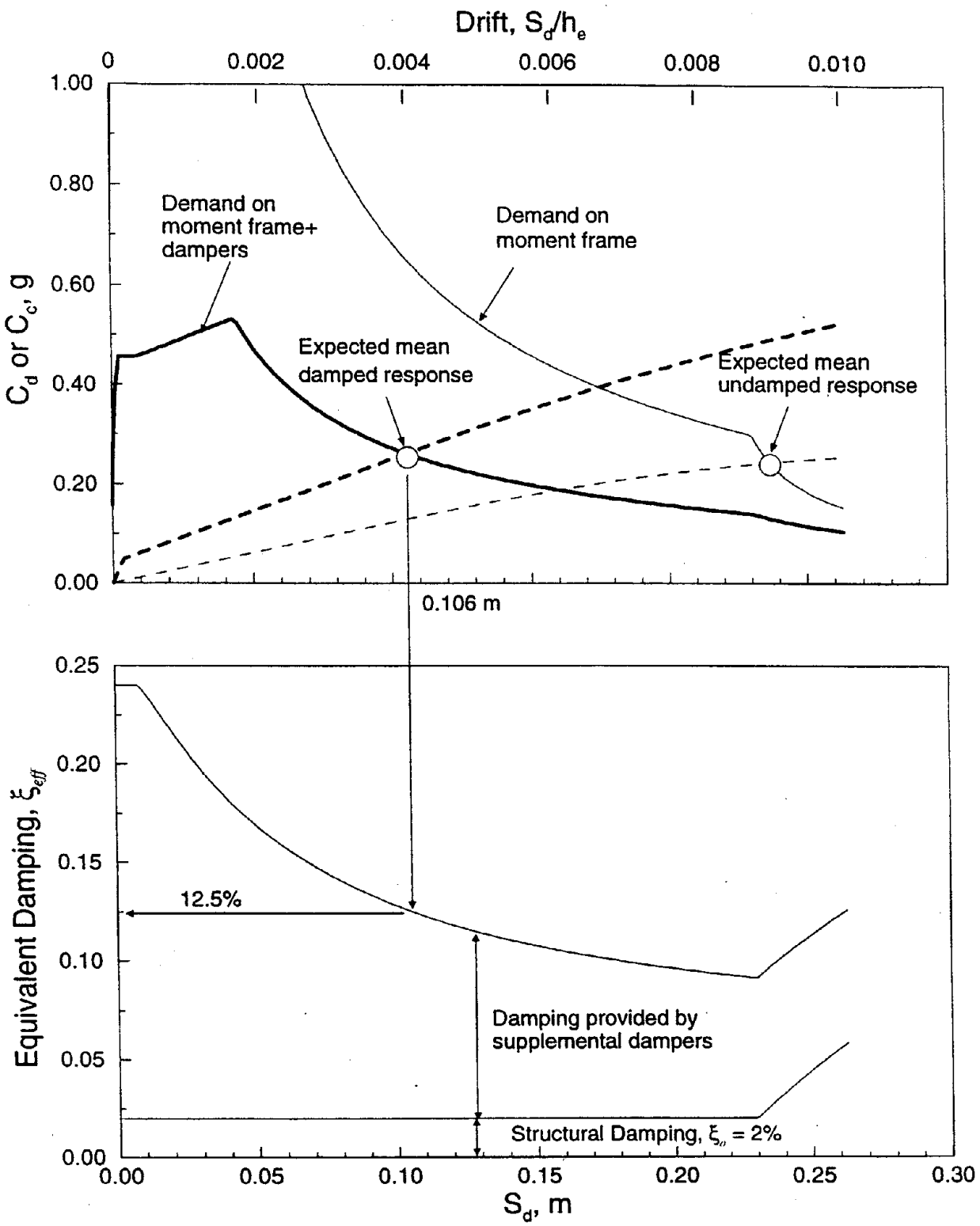

Figure 5-8 Rapid Evaluation of Performance under the MAE – Damper-Tendon Design

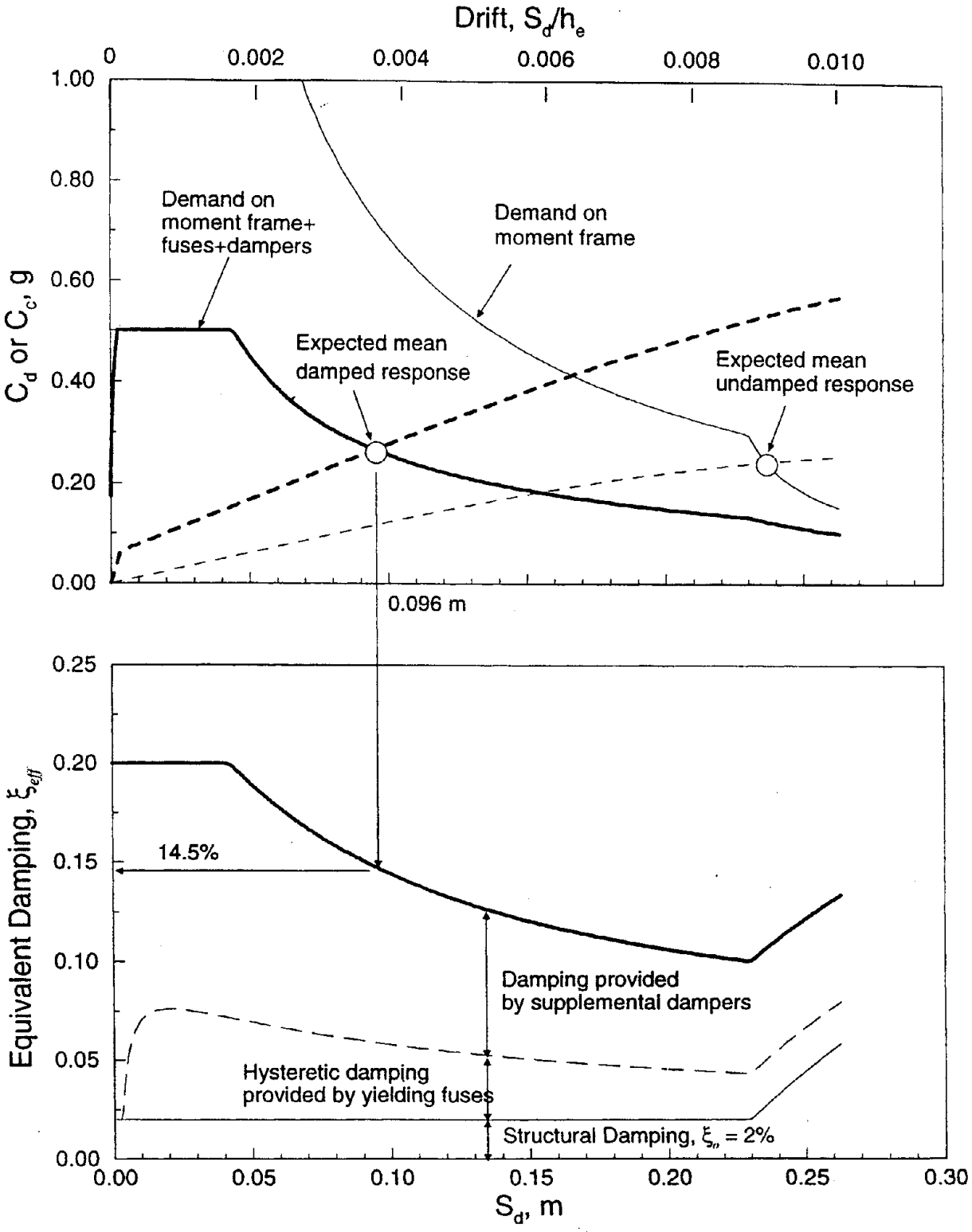

Figure 5-9 Rapid Evaluation of Performance under the MAE – Fuse+Damper-Tendon Design

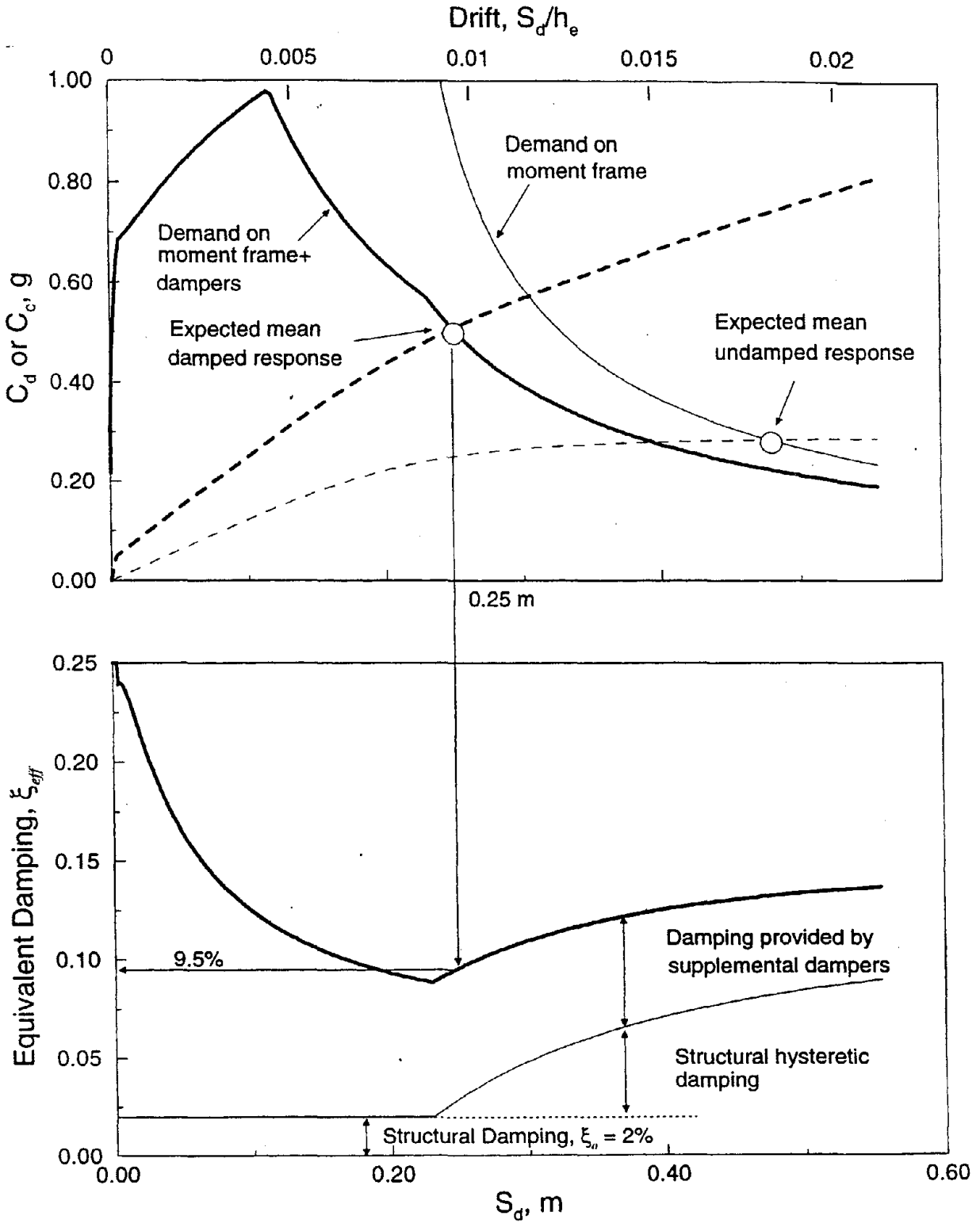

Figure 5-10 Rapid Evaluation of Performance under the MCE – Damper-Tendon Design

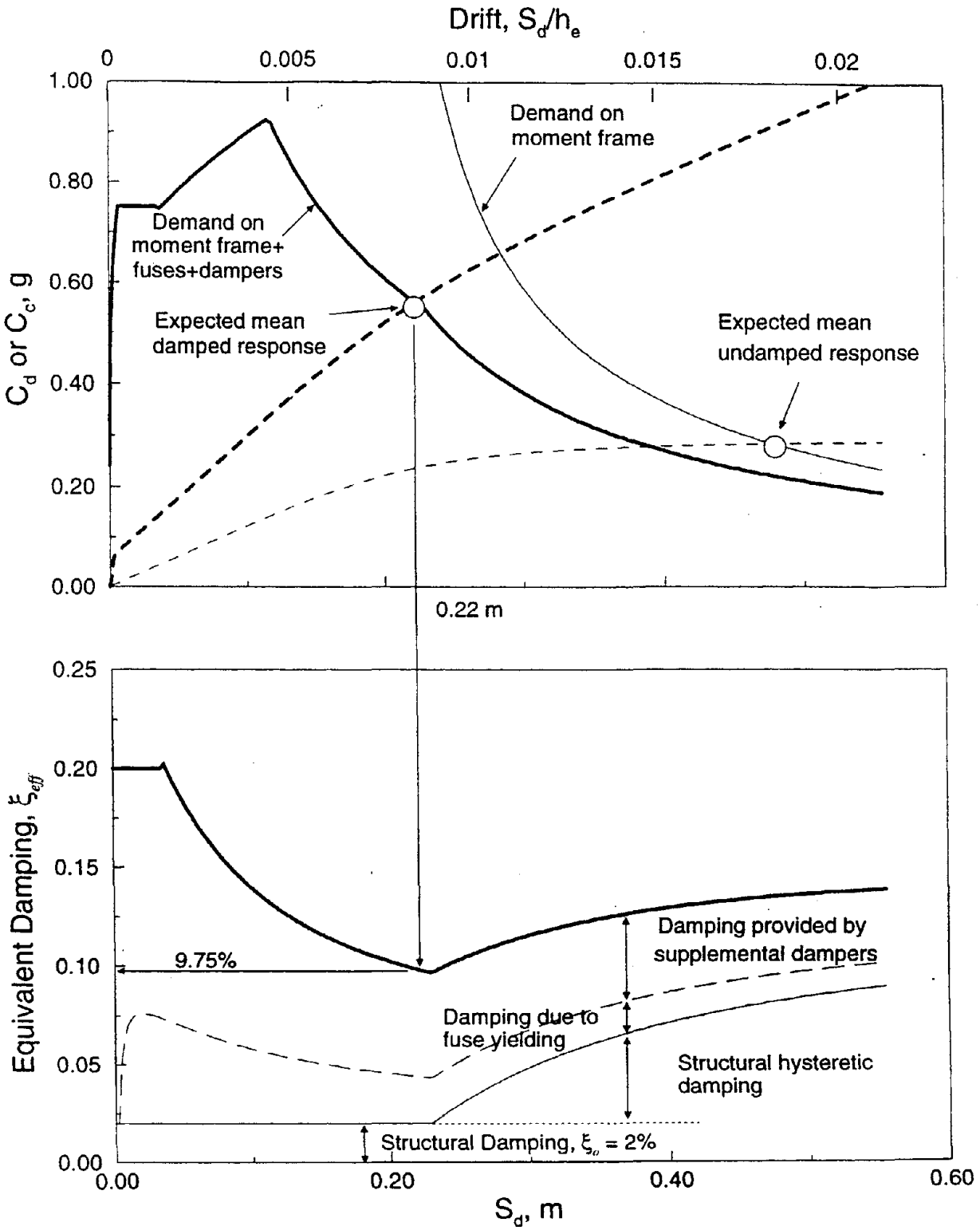

Figure 5-11 Rapid Evaluation of Performance under the MCE – Fuse+Damper-Tendon Design

5.8.2 Undamped and Damped Response Under MAE Ground Motions

Overall response of the example nine-story steel structure is plotted in figures 5-12 and 5-13 for the three MAE ground motions. A general overview of the undamped response (especially under El Centro) reveals the fact that structural system was well designed according to the seismic code requirements. However, as can be seen from figure 5-13a, considerable number of plastic hinges (although generally less than 0.5% radian) form under the scaled Taft ground motion. Moreover, it can be seen from figure 5-12 that large interstory drifts may be expected in the upper four stories. Therefore, as part of the retrofit these stories are braced. Also plotted in figure 5-13b is the performance point of the structure on corresponding pushover capacity curve along with the 5% damped demand curves of the two ground motions.

Maximum response envelopes for the damper tendon and fuse+damper tendon designs are plotted in figures 5-14 through 5-19 in comparison with the undamped response. In general, both designs reduce the maximum response consistently below the elastic limits; hence the structure remained elastic at all times. A uniform interstory profile is obtained. Interstory column shear is reduced and the target design roof displacement is attained. However, overturning moments are amplified. This is because the added supplemental system stiffness as can be seen on figures 5-8 through 5-11. Performance points of the structure are plotted in figure 5-20 on corresponding modified (for the presence of supplemental system) pushover curves along with the 20% damped demand curves of the two ground motions. Variations in the response are attributed to the ground motion variability.

It must be noted here that Arleta ground motion is characteristically different than El Centro and Taft ground motions. The impulsive nature is evident from figure 5-16 as the maximum response occurs early in the time history (first major cycle of response). Moreover, undamped structure response reaches up to about the same level 7 sec. after the first. This is especially an undesirable response type for the damper-tendon as well as fuse+damper-tendon designs since after the fuse yields during the first impulse (response), supplemental system capacity technically relies on that provided by the dampers only.

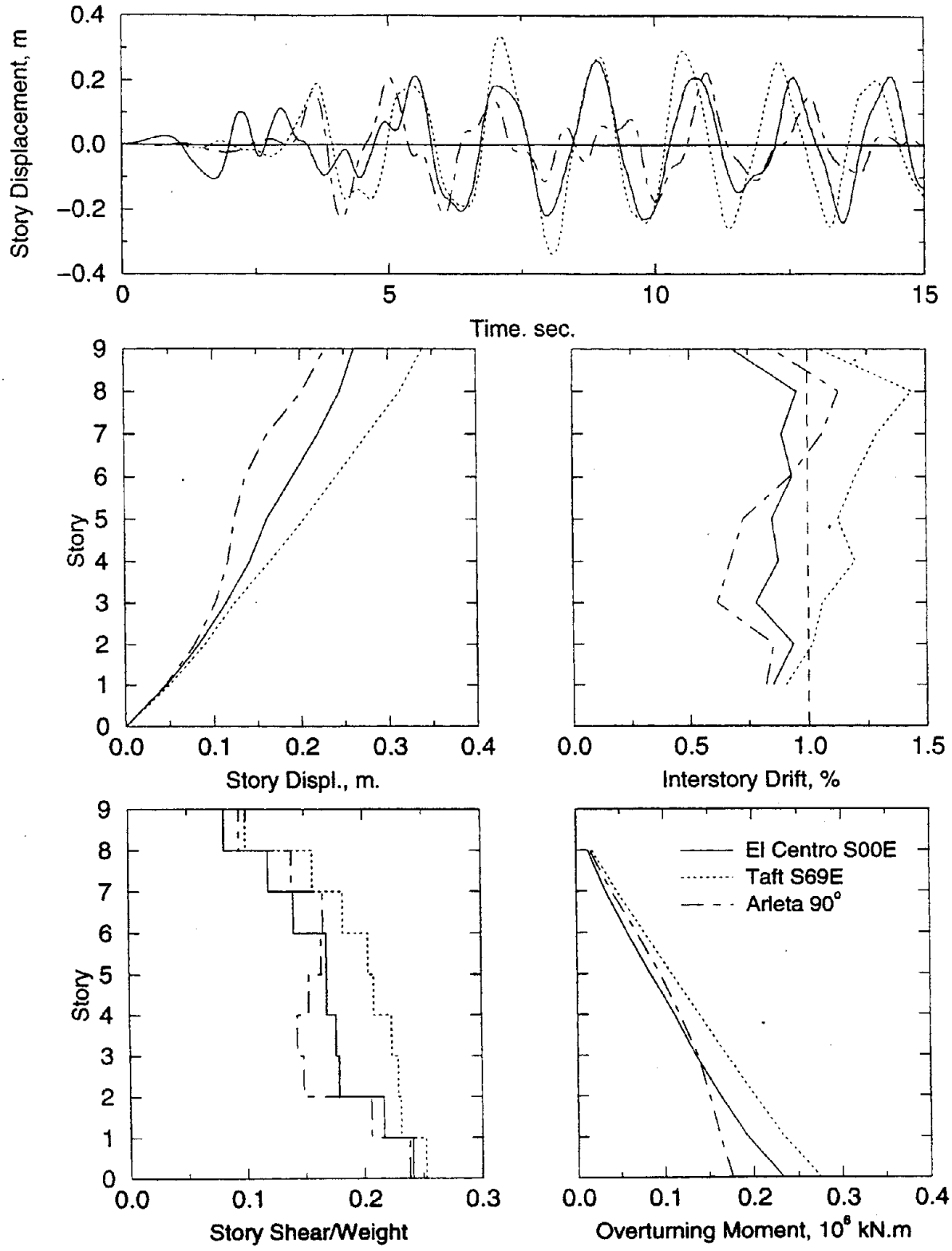

Figure 5-12 Maximum Response Envelopes of Undamped Structure Under MAE Ground Motions

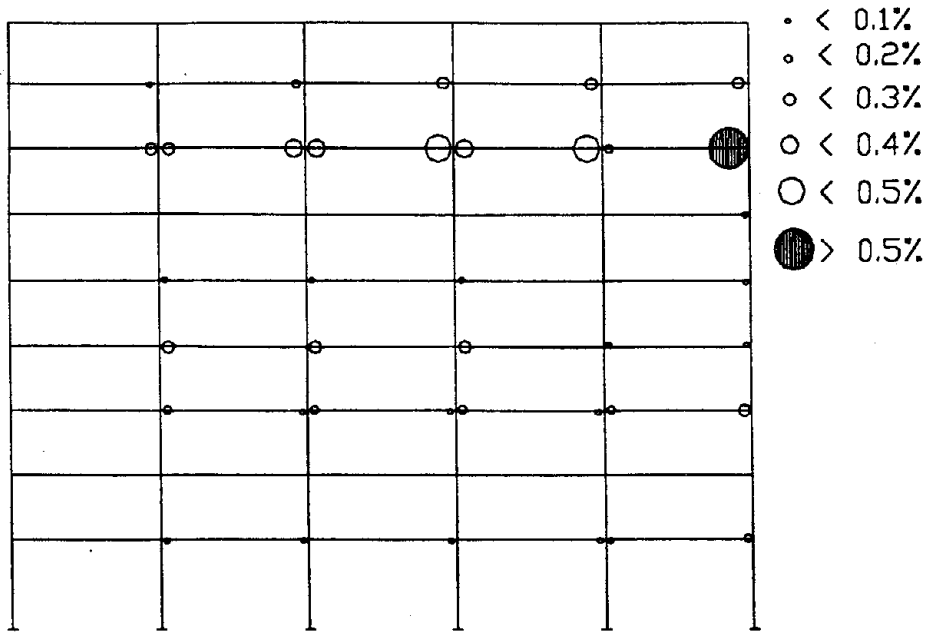

Figure 5-13a Plastic Hinge Locations – Taft S69E – PGA = 0.4g

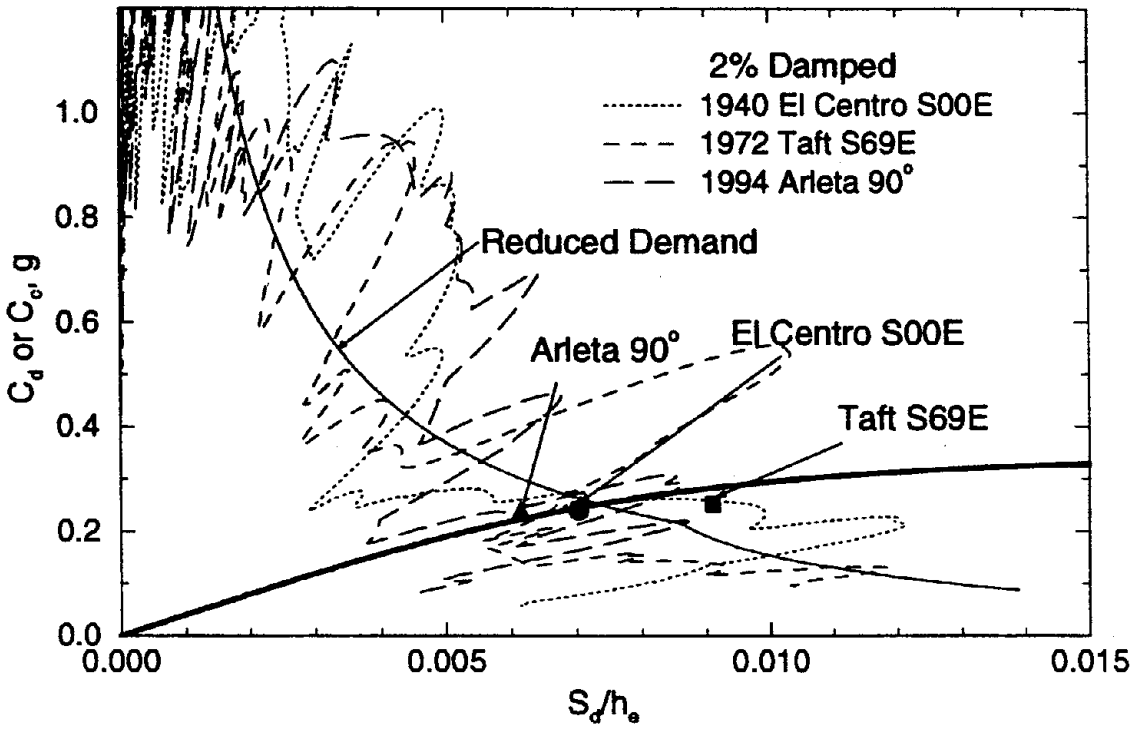

Figure 5-13b Performance of Undamped Structure Under MAE

When comparing the performance of the two design alternatives, one must realize that the size of the damper device needed for the fuse+damper design is about 40% less than that of damper only design. Hence, considerable cost saving is evident.

Both the damper truss solutions namely, proportional distribution and uniform distribution performed within acceptable limits with no significant difference. However, a uniform distribution may be desirable since it provides better control of interstory drifts as shown in figures 5-17 through 5-19.

5.8.3 Undamped and Damped Response Under MCE Ground Motion

As part of the verification phase (PHASE V), example structure was analyzed under 1994 Northridge – Sylmar County Hospital, 1979 Imperial Valley – Array 5 and 1995 Great Hanshin – Kobe ground motions (all scaled to PGA = 0.6 g). These ground motions are thought to be representative of the MCE ground motion, hence according to performance objectives (see section 5.4), supplemental system(s) should not allow any plastic hinge rotations larger than 0.5%.

Maximum response envelopes for the damper tendon and fuse+damper tendon designs are plotted in figures 5-21 through 5-23, in comparison with the undamped response. Although significant yielding can be observed from the figure, the plastic hinge rotations stayed below 0.5% radians at all times except under Lexington Dam ground motion. The distribution of beam/column hinges on the unretrofitted structure for Sylmar case is depicted in figure 5-24. The overall difference between the undamped frame and the damped frame is apparent. While inelastic response is occurring in the damped frame, it is both of lower magnitude and less widespread. However, as can be seen in figure 5-24, although the general response is controlled by the fuse+damper-tendon system under Lexington Dam ground motion, high overturning moments cause plastic rotations to take place even above the permitted limit.

Sample fuse and damper hysteresis are shown in figures 5-25 and 5-26 for Sylmar and Kobe ground motions. As can be seen from these figures, supplemental system is in fact designed for a sufficient deformation capacity (i.e. X_{max} = 0.20 m).

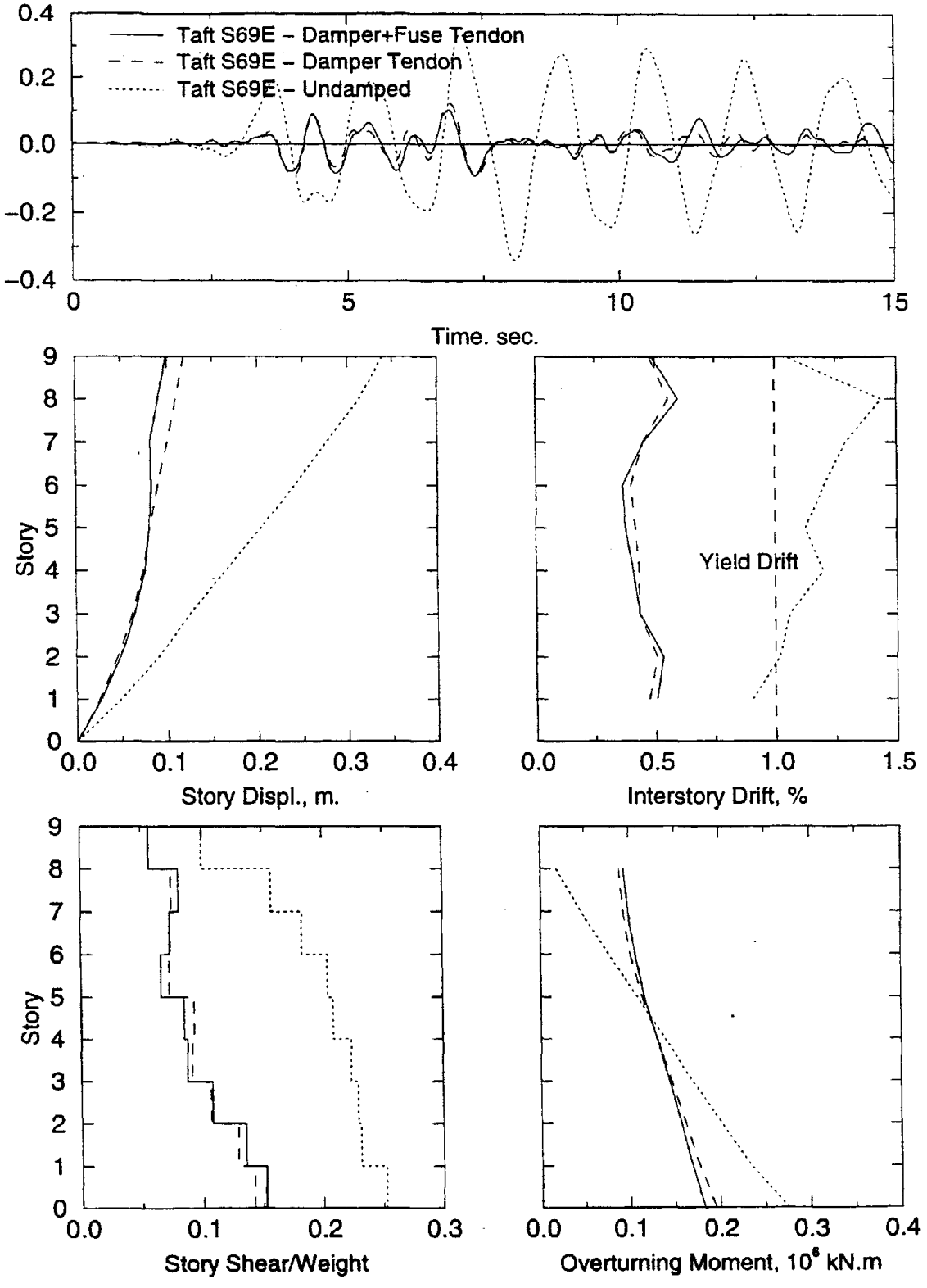

Figure 5-14 Maximum Response Envelopes of Structure with Tendon System Under MAE Ground Motions – Taft S69E

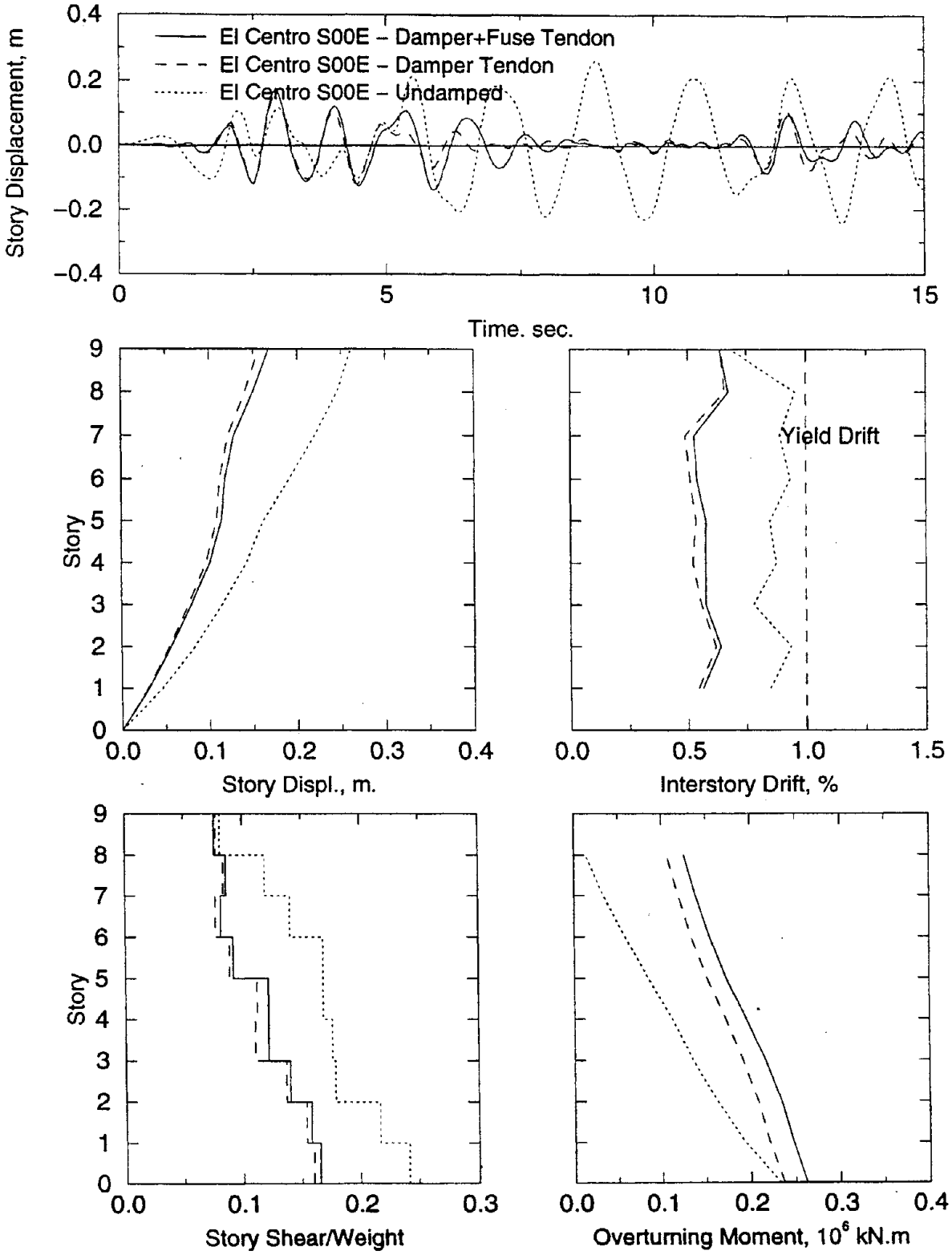

Figure 5-15 Maximum Response Envelopes of Structure with Tendon System Under MAE Ground Motions – El Centro S00E

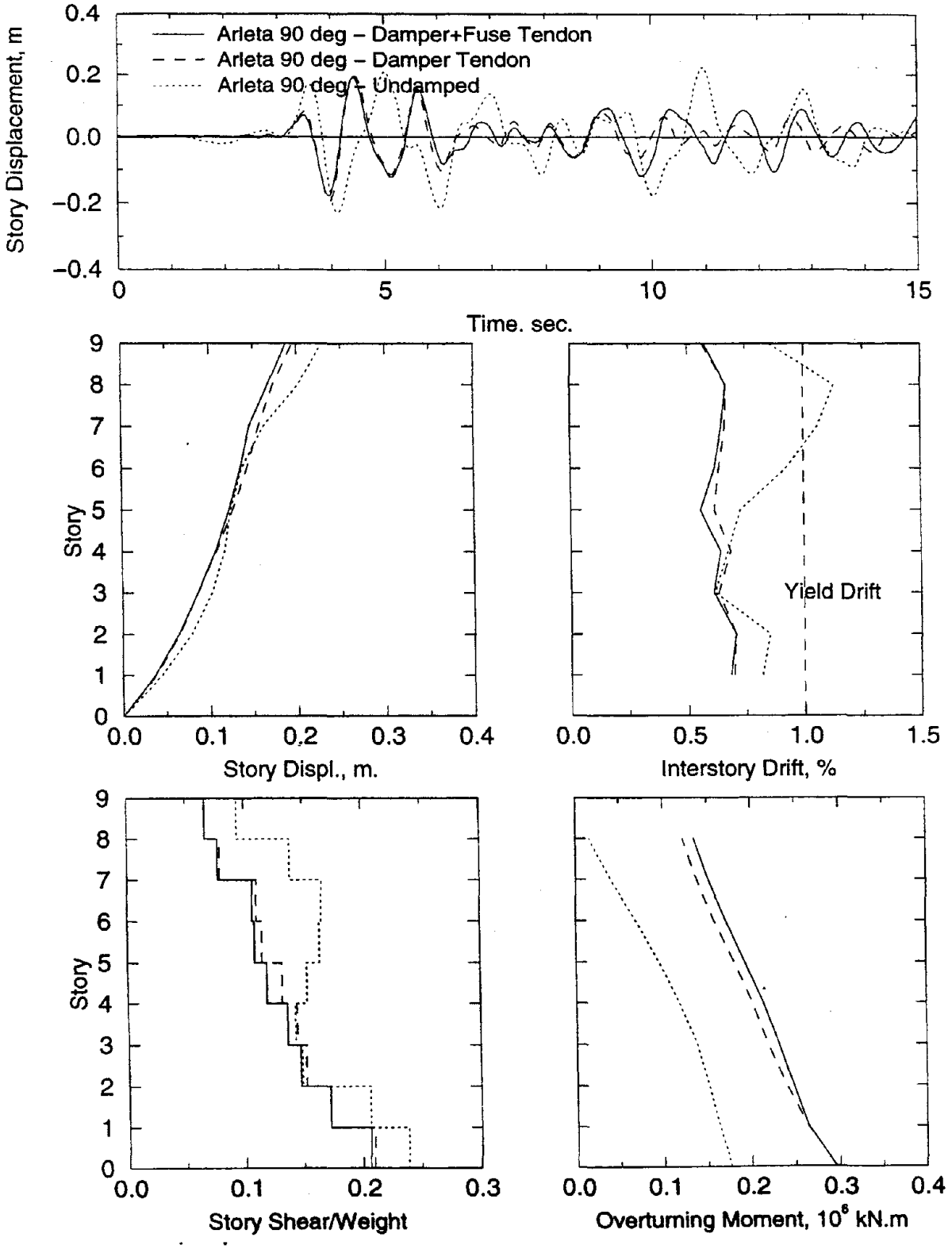

Figure 5-16 Maximum Response Envelopes of Structure with Tendon System Under MAE Ground Motions – Arleta 90°

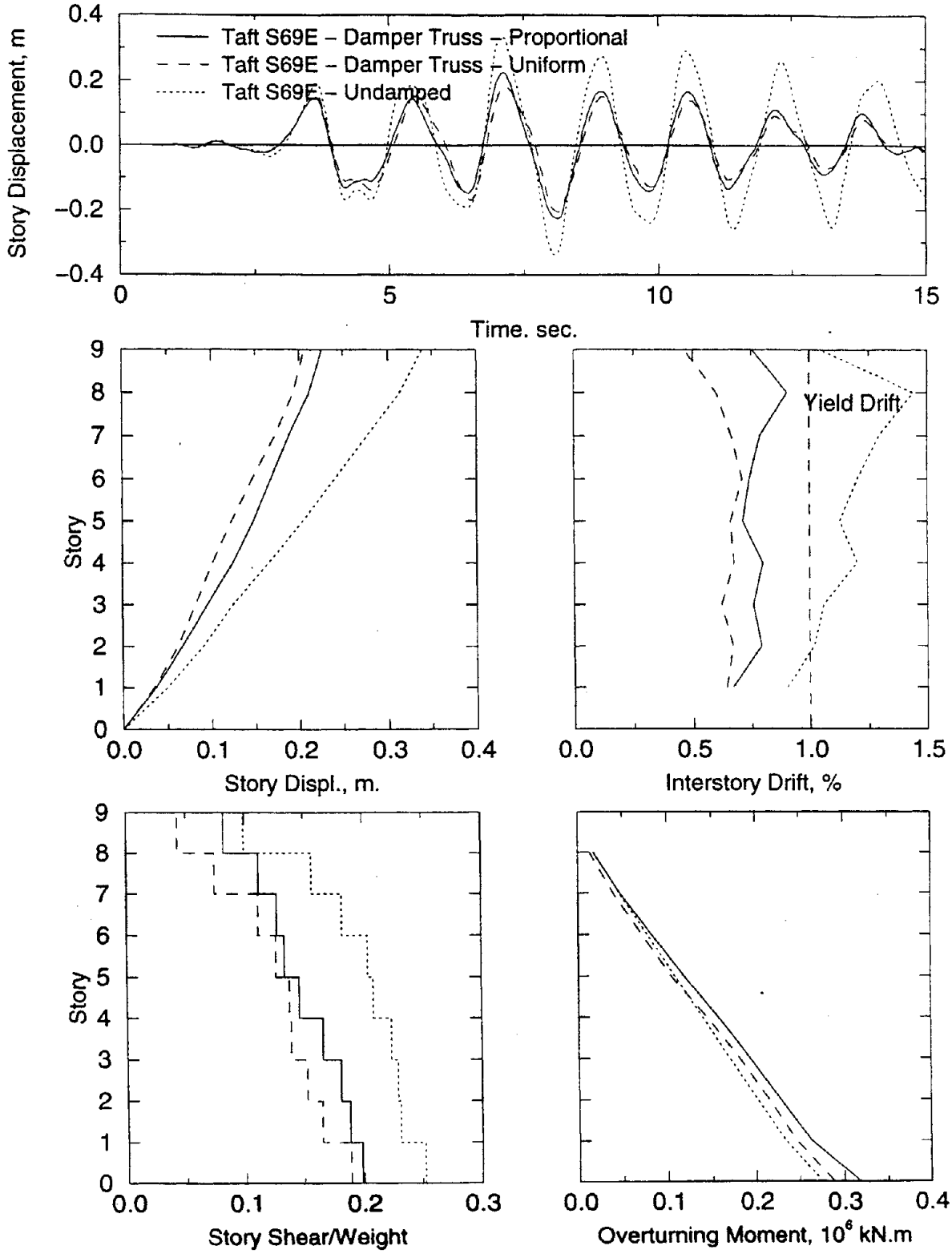

Figure 5-17 Maximum Response Envelopes of Structure with Damper Truss System Under MAE Ground Motions – Taft S69E

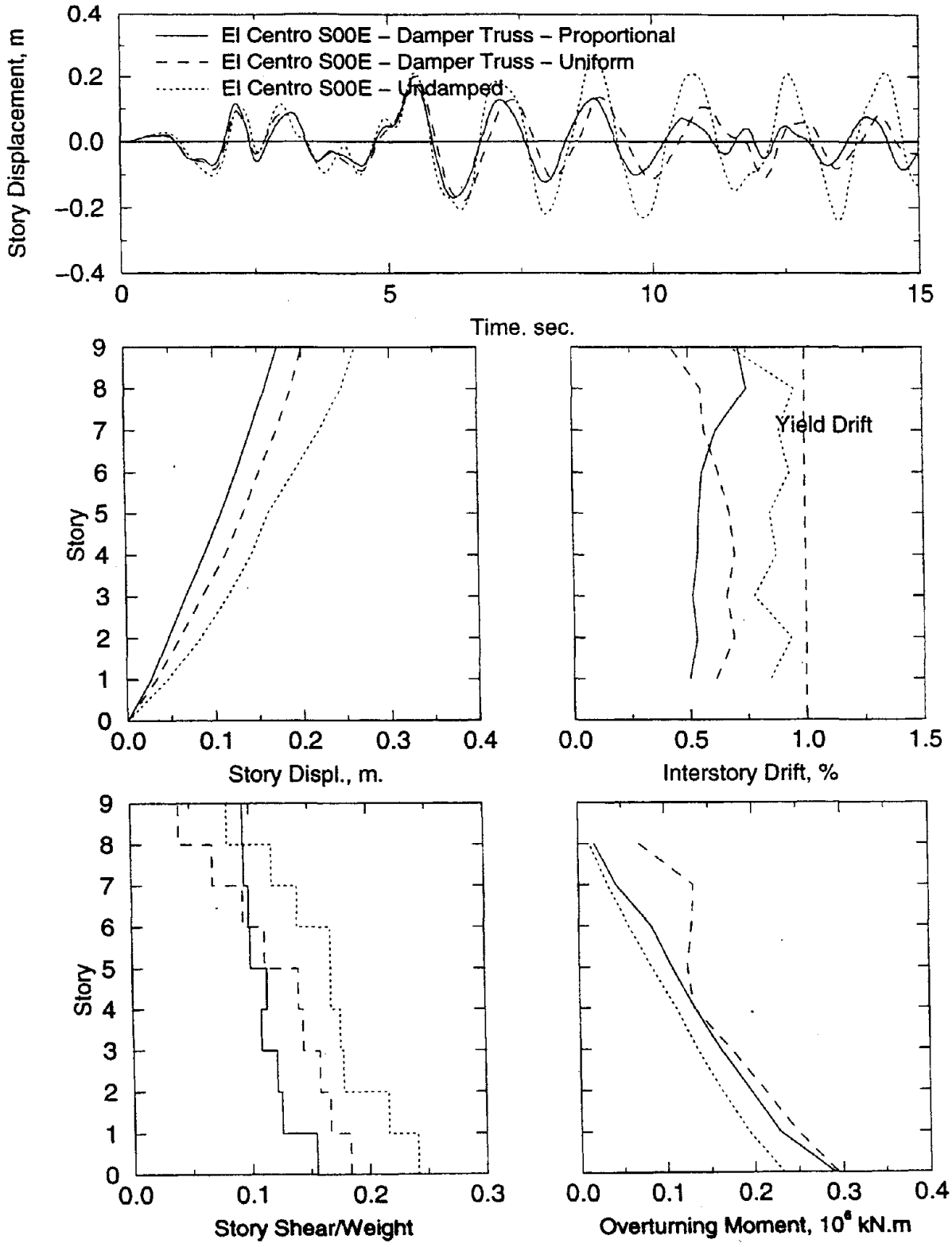

Figure 5-18 Maximum Response Envelopes of Structure with Damper Truss System Under MAE Ground Motions – El Centro S00E

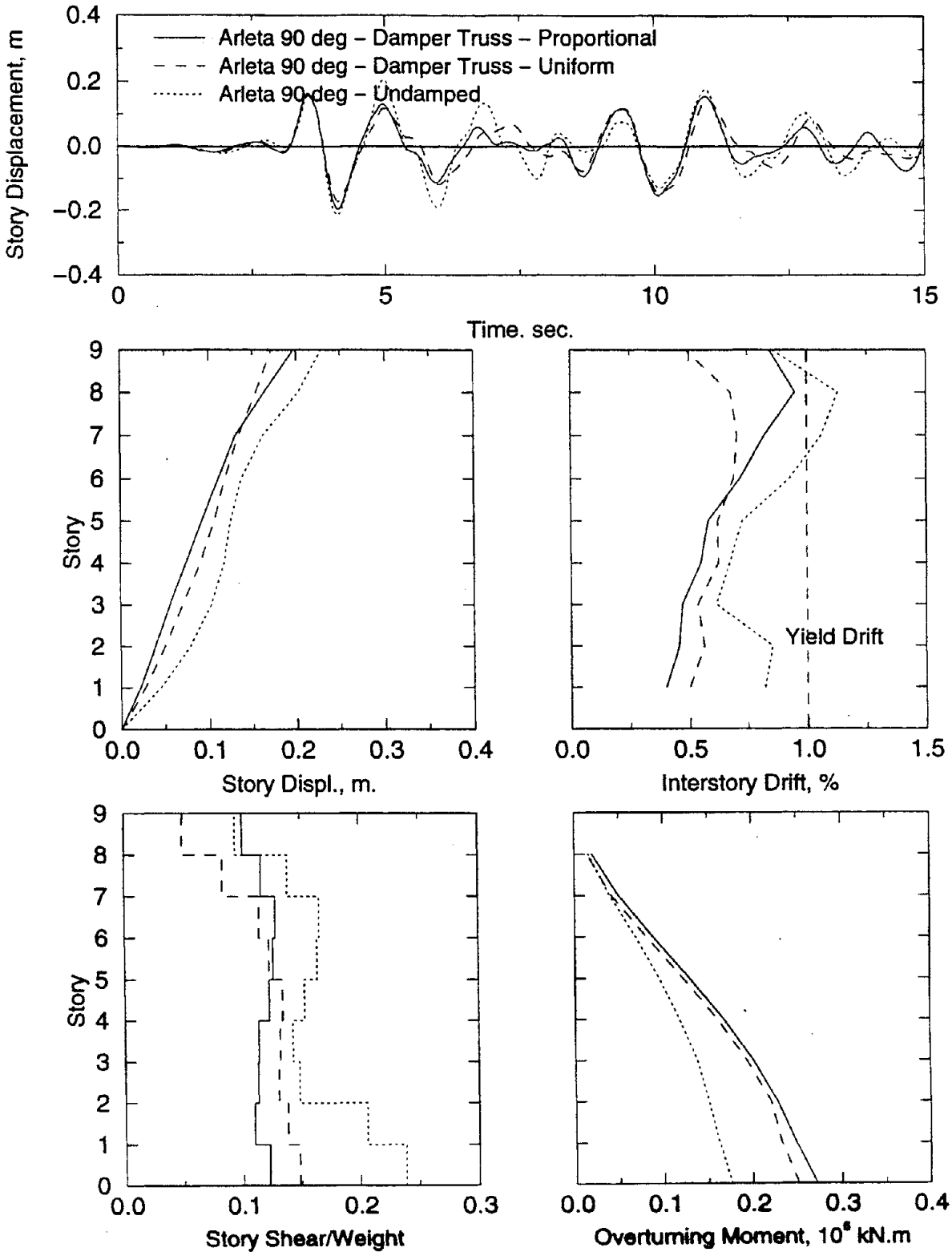

Figure 5-19 Maximum Response Envelopes of Structure with Damper Truss System Under MAE Ground Motions – Arleta 90°

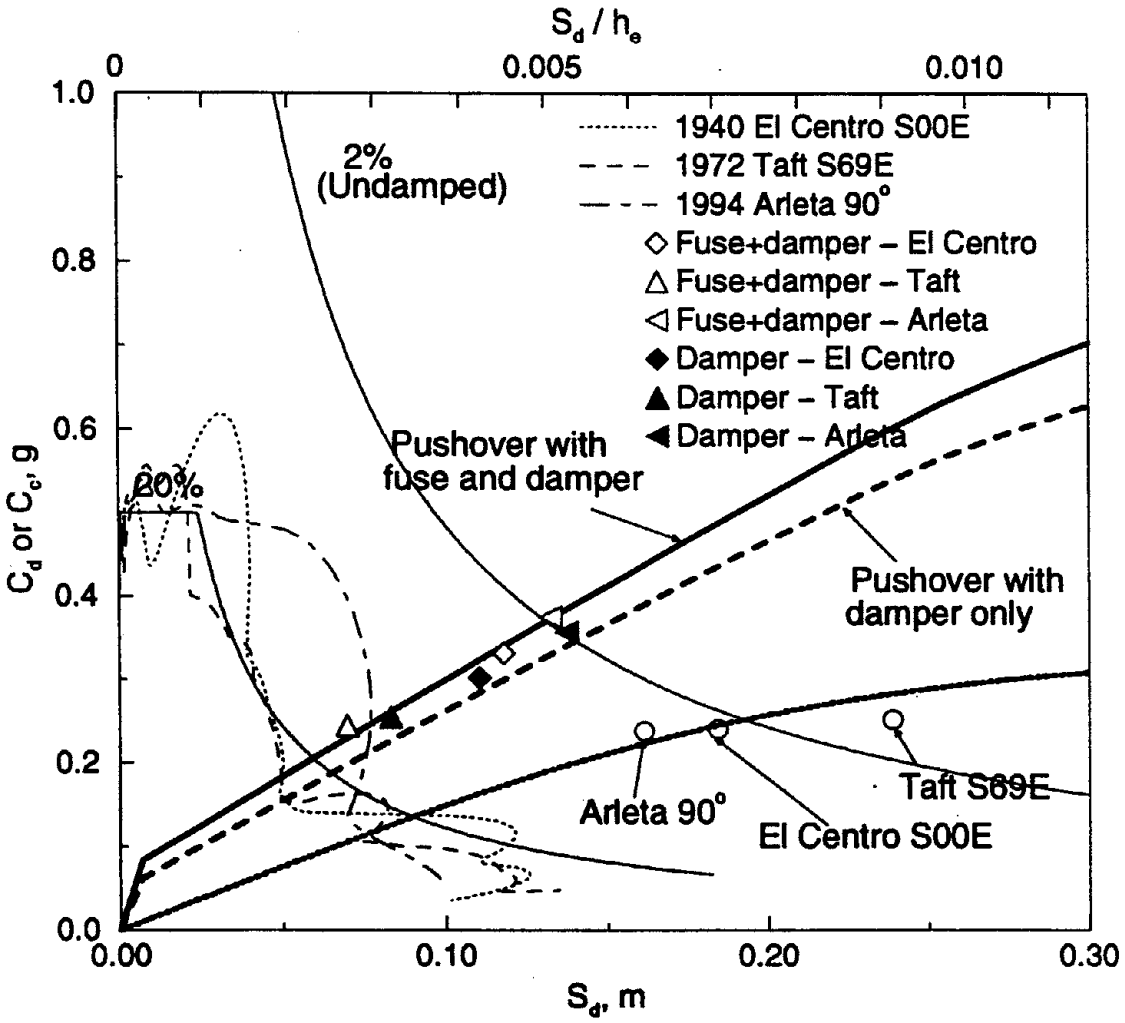

Figure 5-20 Performance of Structure with Tendon Systems Under MAE

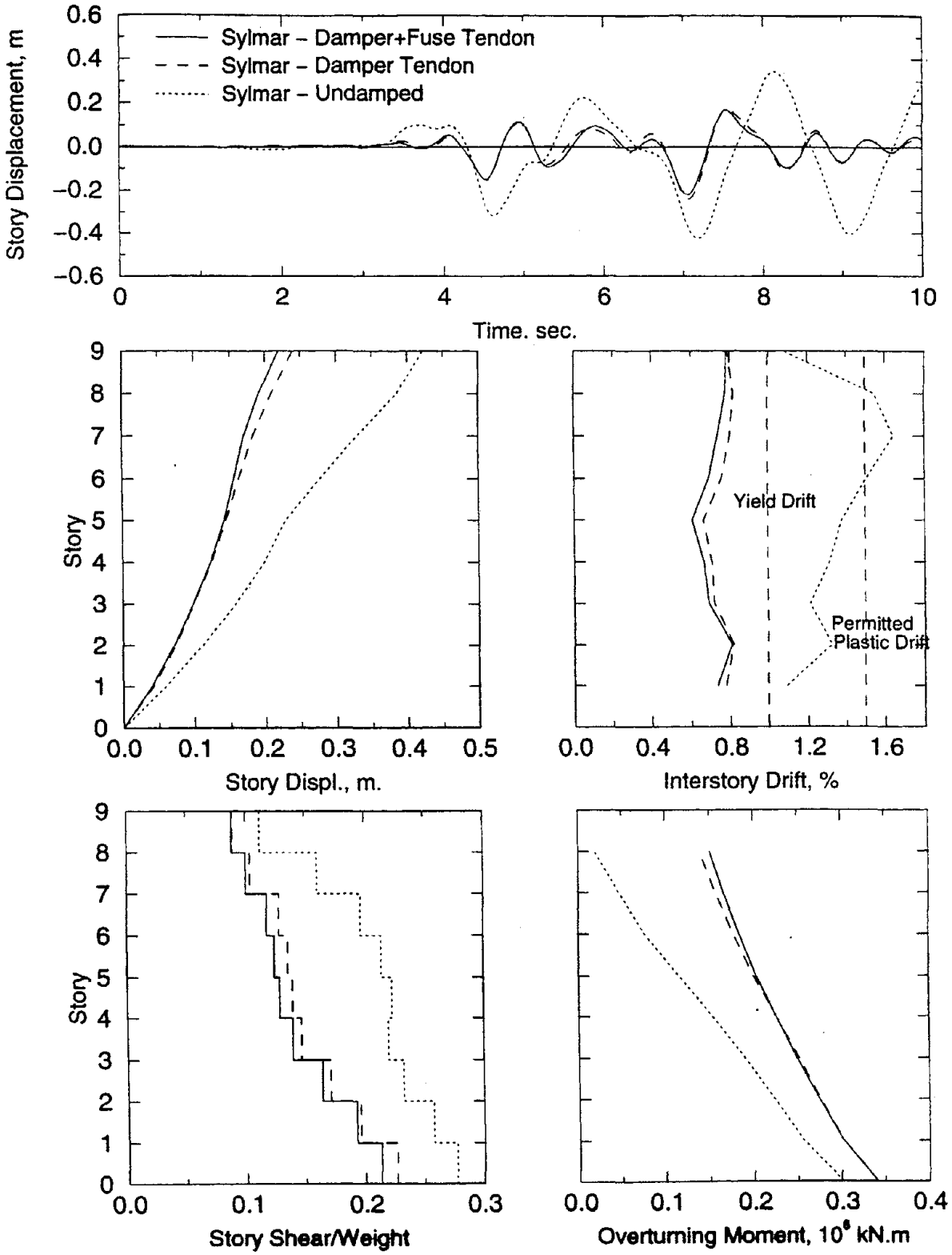

Figure 5-21 Maximum Response Envelopes of Structure with Tendon System Under MCE Ground Motion – Sylmar

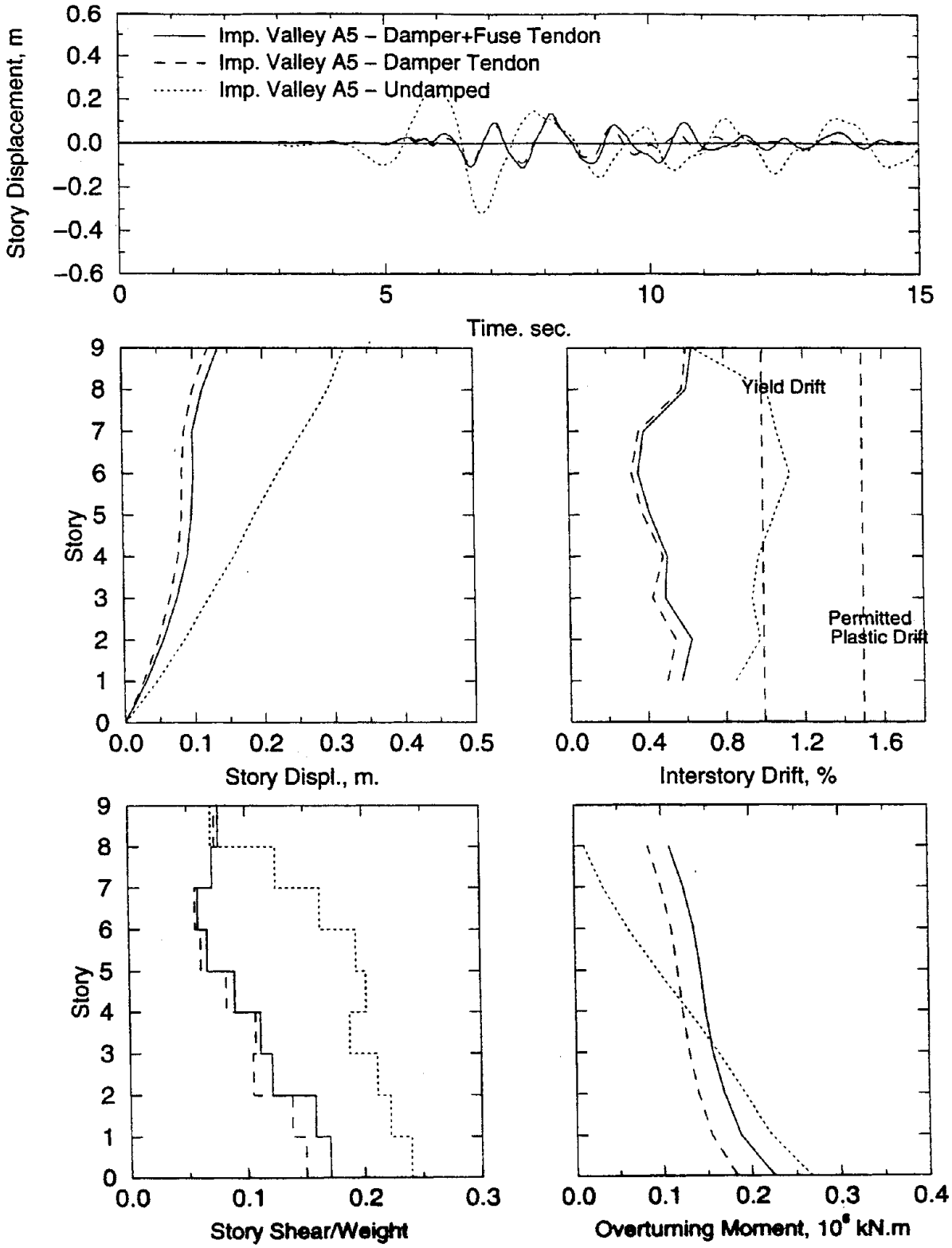

Figure 5-22 Maximum Response Envelopes of Structure with Tendon System Under MCE Ground Motion – Imperial Valley – Array 5

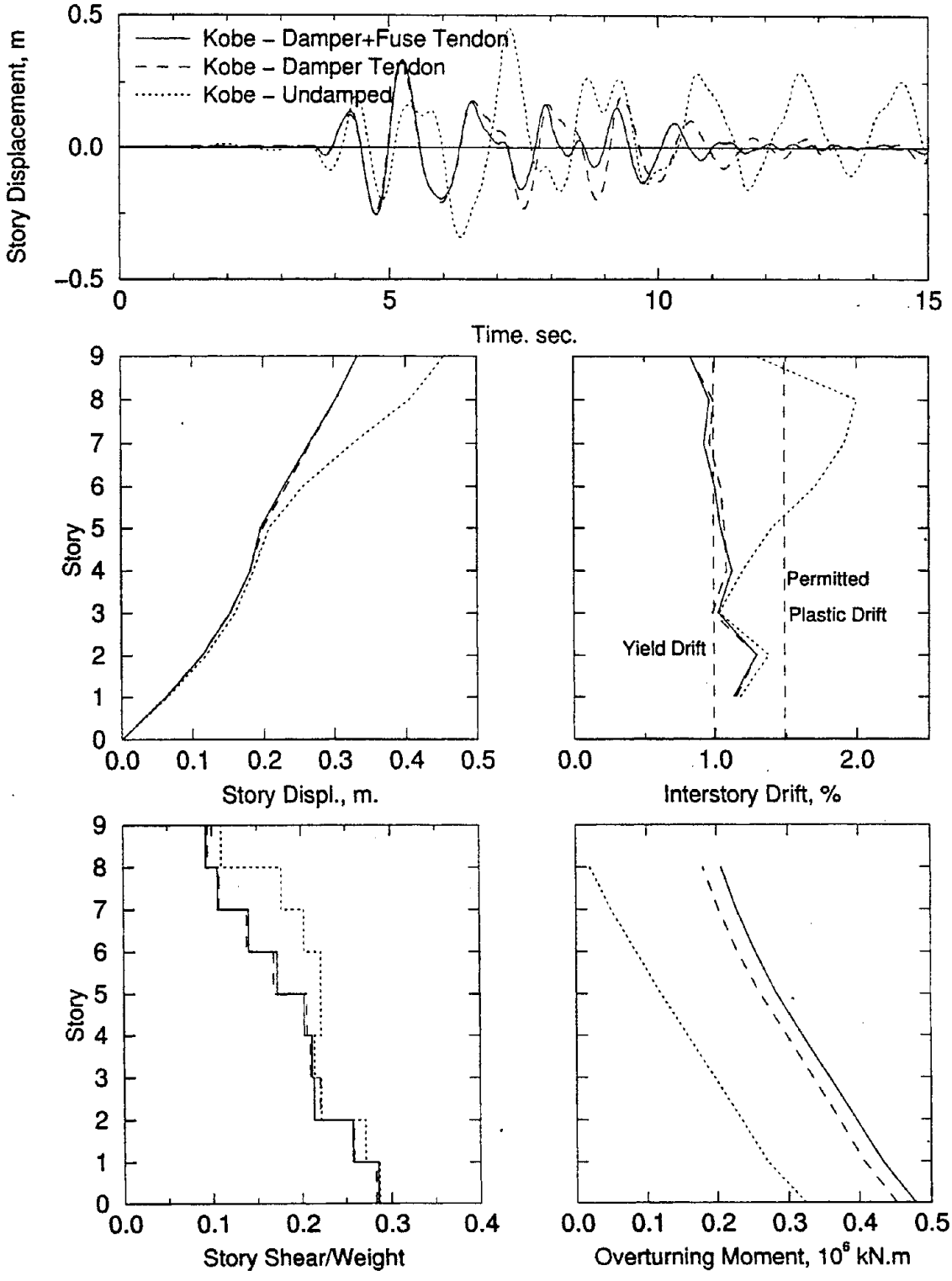

Figure 5-23 Maximum Response Envelopes of Structure with Tendon System Under MCE Ground Motion – Kobe

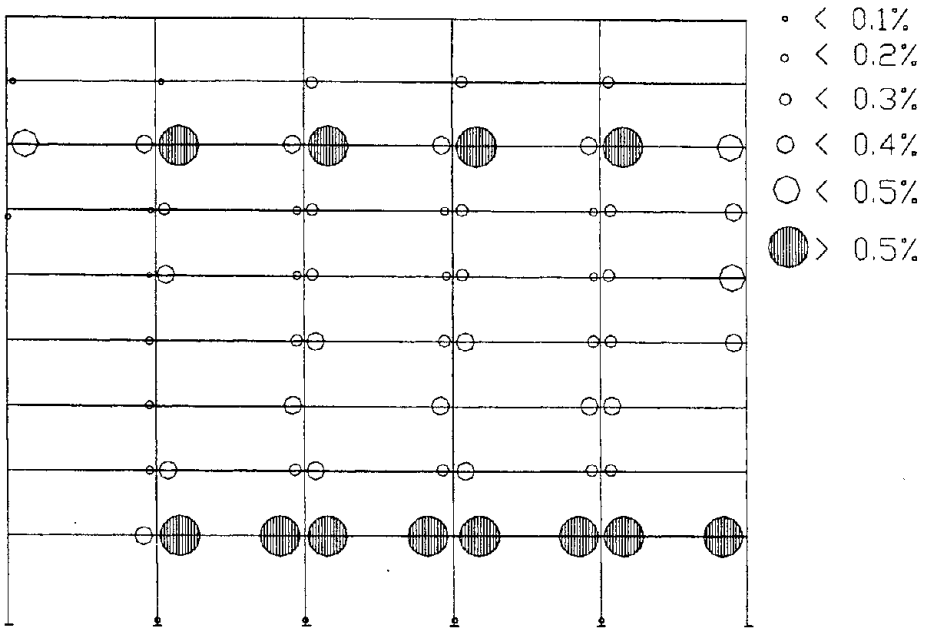

Undamped Structure

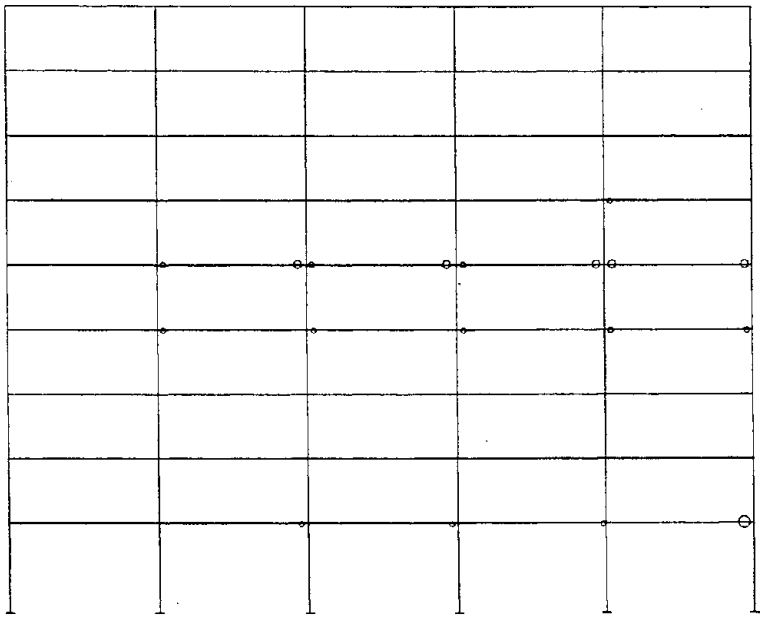

Retrofitted Structure – LPTF+D

Figure 5-24 Plastic Hinge Locations – Sylmar – PGA = 0.6g

Table 5-7 Natural Period of Vibrations and Participation Factors for the Mass Normalized Mode Shapes

Mode	Undamped			Damper Tendon			Fuse+Damper Tendon		
	1st	2nd	3rd	1st	2nd	3rd	1st	2nd	3rd
Period	1.78	0.65	0.26	1.49	0.60	0.35	0.61	0.51	0.35
Part Fact[1]	-1.344	-0.510	0.263	-2.016	-0.719	-0.443	-0.263	9.430	-0.421

[1] Participation factors for the mass normalized mode shapes

5.9 Discussion of the Performance of Proposed Supplemental System

It is evident from the analysis results summarized in the previous subsections that the proposed preliminary design methodology is sufficiently accurate in light of the randomness of ground motion spectra. Moreover, it is suitable for most of the design and retrofit alternatives with supplemental energy dissipating systems. However, since the overall response may be affected by the variations in ground motion characteristics as well as higher mode effects, a comprehensive verification is generally needed to verify the adequacy of the design.

Prestress tendon solutions (damper-tendon and fuse+damper-tendon) characteristically modify the structural dynamic properties (dominant mode shape etc.). Since the determination and detailing of the tendon layout is initially based on the undamped response of the structure, balanced inertial loads on the damped structure are in fact different than those initially considered. First three natural periods and corresponding participation factors are summarized in table 5-7 for the two alternative designs. It can be seen from table that while modifying the mode shapes, the tendon layout also alters the respective participation factors, hence increasing the higher mode contributions on the overall response. The expected damping forces (hence damping) cannot be attained fully, merely due to fact that the inertial loads that the design is based on, are not in fact balanced effectively. Consequently, although it may not be possible to design a 100% optimal layout, an iterative procedure should be adopted which would close in upon a "near optimum" layout. Finally, due to high variations in structural system characteristics, each problem should be treated on its own merits.

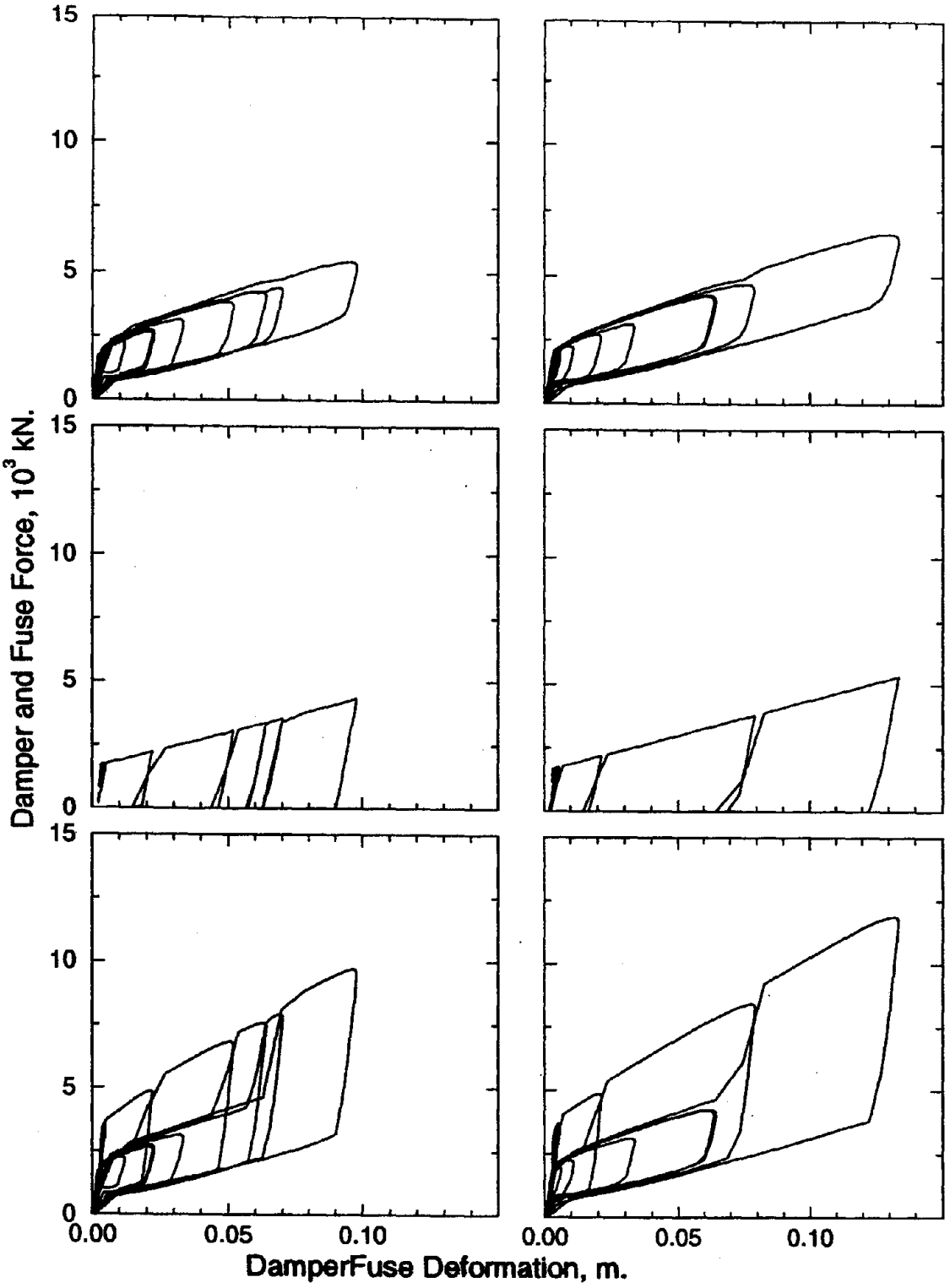

Figure 5-25 Sample Supplemental System Hysteresis - Sylmar

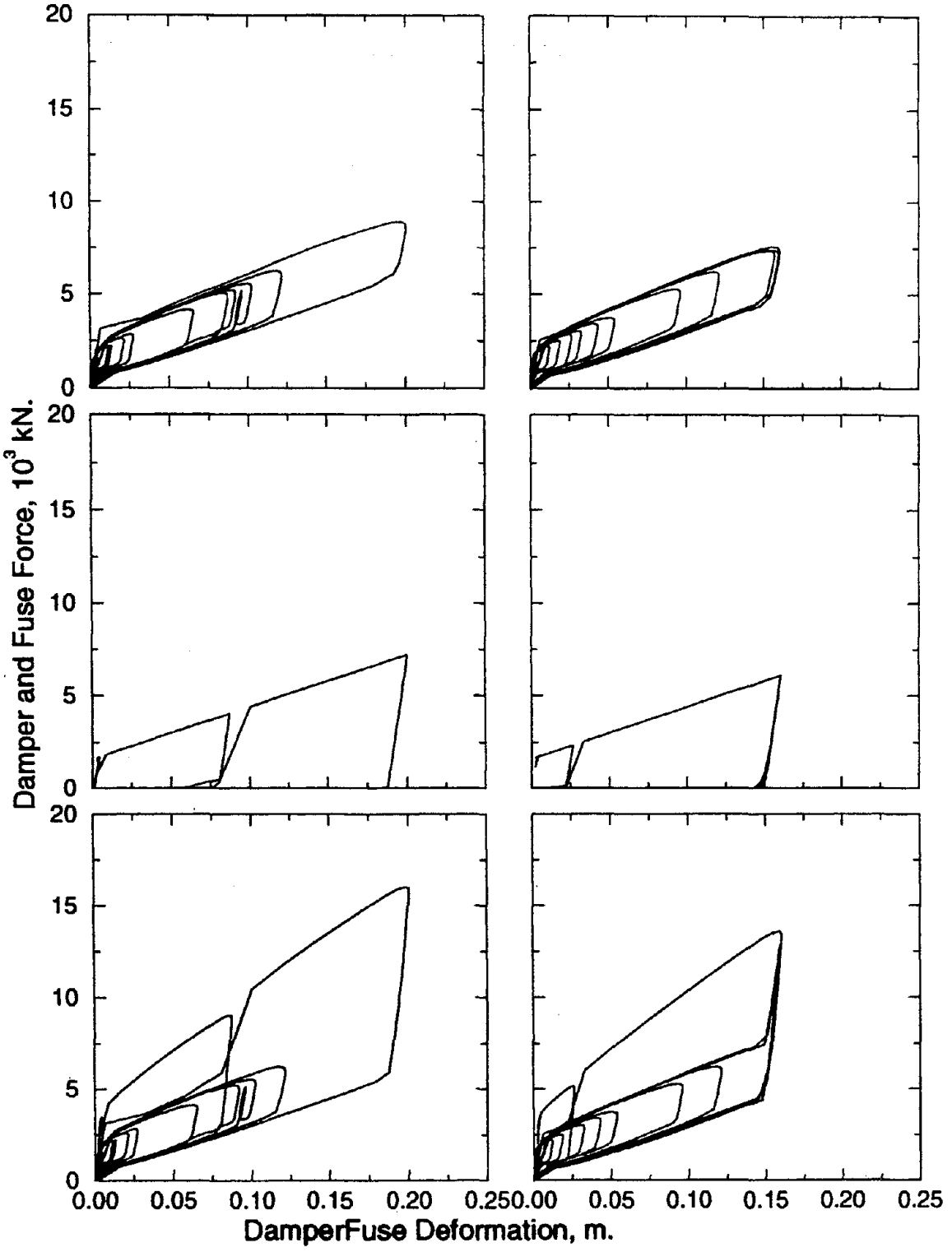

Figure 5-26 Sample Supplemental System Hysteresis - Kobe

As can be seen from the overall response comparisons, target design (performance objective) can be more efficiently attained with a fuse+damper combined supplemental system. The maximum response of the structure is reduced below the desired limits with both designs. However, it can readily be said that fuse+damper design provides a more economical design. Although column shear forces are reduced by about 20-30% at the base level, overturning moments are not significantly (as expected) reduced due to the extra stiffening introduced and the consequence of possible higher mode effects. If the inertial loads were truly balanced, a significant reduction in both the displacement and member forces could be expected. Finally, in general prestress losses were in the order of 5% of the initial level.

5.10 SUMMARY AND CONCLUSIONS

A retrofit design example of a nine-story flexible steel building structure was presented. An innovative configuration was proposed in which tendons are draped so as to balance the equivalent lateral inertial loads and the supplemental devices are located at either end of the tendon system (Load Balancing Prestressed Tendon-Fuse+Damper Solution, PDTF). Design formulations were derived and step-by-step design algorithms given in section 4. Because of the manner in which damping forces are transferred, the second alternative design and configuration is considered to be preferable. However, it was also noted that the tendon layout should be determined by an iterative process in which the change in system stiffness (hence mode shapes etc.) is accounted for. Furthermore, it was pointed out that the proposed fuse-damper system might be especially effective under pulse type ground motions. It was noted that the fuse-bars provide high initial stiffness and therefore are desirable also under service conditions (wind loads etc.).

It is noted that the variations in the seismic response (for which the structure/supplemental system is designed) should be expected as was pointed out previously in section 2.

SECTION 6

SUMMARY, CONCLUSIONS AND RECOMMENDATIONS

6.1 SUMMARY

In this study, various factors that have an effect on the development of seismic design of reinforced concrete and steel structures were studied. It was realized that in developing simplified design methodologies, straightforward and accurate idealizations are needed. One form of idealization is to linearize the actual nonlinear device properties. The most commonly accepted and employed linearization technique is based on the amount of dissipated *energy* by a viscous device in one cycle of response. However, a linearized model based on *power consumption equivalence* between a linear and nonlinear viscous device yields an accurate and simple relationship. To satisfactorily use any linearized method, exact spectral velocities should be used in design formulations. For this purpose, a set of 36 strong ground motions (characteristically near-source ground motions) and their components were used to generate the customary pseudo velocity and also *actual-velocity* spectra. Empirical expressions were obtained to enable transformations between pseudo and actual velocities as a function of damping and period. These relationships were then simplified to permit their use in design formulations. Hence, simplified velocity transformations were used in the proposed equivalent power consumption approach to determine the equivalent properties of nonlinear viscous dampers.

To further facilitate the simplified design methodology, the notion of a *normalized damper capacity* ε, was introduced. This parameter (ε) was used in the preliminary design formulations in which a SDOF idealization was used along with the capacity-demand spectral design approach. This design approach lends itself to a simplified hand analysis by means of an elasto-plastic representation of capacity (lateral strength, pushover) curve for the MDOF system.

On the basis of analyzing the 36 ground motions, it was concluded that the main source of design uncertainty is due to the random variability in the ground motion demand on the structures. Therefore, an attempt was made to quantify these uncertainties through statistical analysis. This analysis was performed on the above-mentioned set of scaled ground motions. Consequently, standard log-normal dispersion factors (β) were proposed for the assessment of

variability within the short (β_s = 0.2) and long (β_l = 0.5) period ranges of the spectral acceleration curves.

Finally, the results of the above-mentioned studies were addressed and implemented in the preliminary design and detailing of the proposed supplemental system configurations. A retrofit design example of a nine-story flexible steel building, located in Los Angeles area, was presented. Based on a preliminary design using capacity-demand nonlinear static procedures, time-history analyses were conducted to assess whether the design objectives were met. Results from this analysis showed that although the dynamic response could be reduced, some variability in interstory drift as well as forces is to be expected due to the effects of ground motion variability and also higher mode response.

6.2 CONCLUSIONS

The important conclusions drawn and observations made on the implications for design and practical applications are summarized. Concluding remarks are made regarding the simplified design methodology and various other issues investigated. Finally, conclusions related to the analytical study are given.

6.2.1 Design Implications and Methodology

1. The Capacity-Demand spectral design approach can be efficiently employed in the preliminary as well as final design stages provided that a reliable SDOF idealization of the actual MDOF system is used.

2. Rigorous pushover analysis is often considered to be a more realistic way to determine the structures' lateral capacity. However, it must be understood that any pushover analysis is in fact a step-by-step plastic analysis. Therefore, a nonlinear pushover analysis can be effectively replaced (without losing accuracy) by a two-stage elasto-plastic analysis for regular structures. The first stage gives the elastic stiffness (and hence natural period), the second stage the plastic strength (limit) capacity.

3. The amount of damping due to supplemental systems that are of [nonlinear] viscous nature can be quantified in terms of equivalent linear damping by an equivalent power consumption approach. This approach provides a simple, straightforward relationship that can be efficiently included in the design process.

4. Damping calculations may be quite sensitive to the velocity response of nonlinear dampers. In fact, it should be kept in mind that the traditional approximation of the actual maximum structural velocity by pseudo velocity is not a good approximation, especially for short and long period response and particularly at higher damping levels. Although it is non-trivial to find a precise relationship between pseudo and actual velocities, a straightforward empirical rule-based transformation has been proposed which is a function of both the damping level and natural period.

5. As part of the preliminary design, normalized damper capacity is introduced based on the equivalent linear damping formulation that used the above-mentioned velocity transformation. When written in terms of spectral quantities, the normalized damper capacity can be efficiently used along with the SDOF idealization.

6. Among many other sources of uncertainties involved in the seismic design in general, those that are associated with the ground motions (demand) are the most challenging to quantify. A statistical approach, however, yields two distinct log-normal standard deviations from the mean response for the short ($\beta_s = 0.2$) and long period ranges ($\beta_l = 0.5$).

7. Finally, it must be noted that the proposed design methodology starts with a structure which may be designed for gravity loads only.

6.2.2 Case Study- Design Example

A real 9 story steel building that suffered damage in the 1994 Northridge earthquake was used as the basis for a case study for retrofit design.

1. The computational model developed for the analytical evaluation of the ESD devices proved to be dependable and accurate. The model captured the main characteristics of the nonlinear-velocity dependent behavior of these devices. The computational model was implemented into a general purpose-nonlinear time history analysis program, (Drain-2DX) and validated against experimental results obtained from testing the 1/3 scale concrete and 1/4 scale steel buildings.

2. The proposed preliminary design procedure for idealized SDOF provides good estimates for the supplemental system capacity when MDOF distribution of the damping forces are taken into account by proper transformations.

3. Plastic methods of pushover analysis (including P-Δ effects) provide a simple but

accurate way to estimate the structural capacity.

4. The draped tendon layout used in the load balancing approach should be iteratively determined as the higher mode effects may significantly reduce the effectiveness of the supplemental system. Code-based distributions (first mode dominant response) of the inertial forces can be used as an initial approximation.

5. In case of maximum considered earthquake ground motions for which structures are permitted a limited amount of yielding, dominant modal properties change during the response. As a result, the effectiveness of the load balancing tendon solution may diminish, but not significantly. This can be observed from the time history analyses results obtained; the performance points when plotted on the capacity-demand spectra do not always correspond well with the SDOF prediction. However, response variations are within the expected range due to ground motion variability.

6. Although design objectives are achieved for the maximum roof displacement response, it is difficult to obtain a uniform interstory drift profile. This is because of higher mode effects on the efficiency of the tendon layout as the balanced inertial loads may in fact be different than those the system is designed for.

7. Fuse-bars can be used in series with the damper devices for a more economical design as the required damper size is reduced by about 40% (for the analyzed structure) from the damper-only design to a fuse + damper design.

8. High levels of accelerations (and floor inertia forces) may be expected especially at the upper stories, but the overall base shear is still reduced by about 30-40%. However, overturning moment demands are generally increased for the stiffened structure.

9. Prestress level has no effect on the initial capacity of the structure and it does not significantly affect the overall response. However, a prestress level of at least 50% of the maximum expected supplemental system force response should be chosen in order to prevent the tendons from becoming slack. This ensures the effectiveness of the system for low amplitude earthquakes.

6.3 Future Research Recommendations

1. The Capacity-Demand spectrum approach in the design of structures discussed earlier is a deterministic approach. In evaluating the seismic response of structures, it is assumed that both the capacity and demand curves are known a priori without any associated uncertainty.

However, in a real scenario, such an assumption may lead to serious inaccuracy in the final design stage since both the capacity and demand will have some form of probabilistic variations as mentioned in Section 2. If this is neglected, then the design will be one among many possibilities from a probabilistic point of view. Alternatively, if the probabilistic variations in both capacity and demand are known in the form of some distribution, then the expected response can be ascertained within certain limits of confidence. Probabilistic versus deterministic response predictions should be assessed.

2. In general, the uncertainty associated with the final design will result from uncertainty in both the demand and capacity or some combination of the two. The uncertainty in demand is because at a given location, there can be an array of ground motions with associated response spectra, which are being generalized to follow a code-specified spectrum. Hence, a statistical study was undertaken to probabilistically quantify this type of uncertainty. However, similar studies should be performed by carefully selecting the set of ground motions that can be characterized according to the site conditions. Uncertainties in the capacity arise from the i) uncertainty inherent in the method of analysis – approximations, assumptions etc., and ii) uncertainty associated with the randomness of material properties (concrete/steel strength, detailing etc.) Once various components of uncertainty are identified and assessed, they can be combined in to groups that take different types of structural system configurations into account. Hence, the final design and/or analysis can be represented probabilistically. Consequently, systematic analyses should be performed with the aid of computational tools to reliably quantify these uncertainties.
3. Three-dimensional response of structures with load balancing tendons may pose important problems if it is not carefully considered in the design. Fuse-bars are designed to yield under major ground motion shaking. Hence, after the first major peak response, stiffness characteristics and distribution in the structure will be modified due to yielding of the fuse-bars. This difference in stiffness is likely to promote torsional response. Therefore, the overall supplemental system should be designed to accommodate the undesired torsional effects. Moreover, three-dimensional nonlinear analysis tools should be developed and used in the analytical investigation of this phenomenon.

SECTION 7

REFERENCES

Atalik T.S. and, Utku S., (1976), "Stochastic linearization of multi-degree-of-freedom nonlinear systems," *International Journal of Earthquake Engineering and Structural Dynamics*, V.4, pp. 411-420.

ATC-40, (1996), "Seismic Evaluation and Retrofit of Concrete Buildings," Applied Technology Council.

Chaughey, T.K., (1959a), "Response of a nonlinear string to random loading," *Journal of Applied Mechanics*, V.26, pp. 341-344.

Chaughey, T.K., (1959b), "Response of Van de Pol's oscillator to random excitation," *Journal of Applied Mechanics*, V.26, pp. 345-344.

Cheng, C.T., (1997), "New Paradigms for Seismic Design and Retrofit of Bridge Piers," Ph.D. Dissertation, State University of New York at Buffalo.

Chopra. A.K., (1995), "Dynamics of Structures", Prentice Hall, Inc.

Clough, R.W., and Penzien, J., (1993), "Dynamics of Structures," McGraw-Hill, Inc., 2nd Edition, New York, USA.

Constantinou, M.C., Soong, T.T., and Dargush, G.F., (Editors), (1998), *Passive Energy Dissipation Systems for Structural Design and Retrofit*, Monograph Series –1, Multidisciplinary Center for Earthquake Engineering Research, Buffalo, New York.

FEMA 273, (1998) "NEHRP Guidelines for the Seismic Rehabilitation of Buildings," *Federal Emergency Management Agency.*

FEMA 274, (1998) "NEHRP Commentary on the Guidelines for the Seismic Rehabilitation of Buildings," *Federal Emergency Management Agency.*

Freeman, S.A., (1994), "The Capacity Spectrum Method for Determining the Demand Displacement," *Technical Session: Displacement Considerations in Design of Earthquake-Resisting buildings*, ACI 1994 Spring Convention.

Foster, E.T., (1968), "Semi-linear random vibrations in discrete systems," *Journal of Applied Mechanics, Transactions of ASME*, V.35, pp. 560-564.

Gluck, N., Reinhorn, A.M., Gluck, J., and Levy, R., (1996), "Design of Supplemental Dampers for Control of Structures," *Journal of Structural Engineering, ASCE,* Vol. 122, No.12, pp.1394-1399.

Iwan, W.D., and Gates, N.C., (1979), "Estimating Earthquake Response of Simple Hysteretic Structures," *Journal of the Engineering Mechanics Division, ASCE*, Vol. 105, No. EM3, pp. 391-405.

Iwan, W.D., and Yang, I.M., (1972), "Application of Statistical Linearization techniques to nonlinear MDOF systems," *Journal of Applied Mechanics, Transactions of ASME*, V.39, pp. 545-550.

Jacobsen, L.S., (1930), "Steady Forced Vibration as Influenced by Damping," *Transactions, ASME,* Vol. 52, Part 1, pp. APM 169-181.

Kircher, C., (1993a, b), "Status Report of Structural Engineers Association of California (SEAOC) - Ad-Hoc Ground Motion committee," *Presentations at SEAOC Annual Convention*, Scottsdale.

Mahaney, J.A., Paret, T.F., Kehoe, B.E., and Freeman, S.A., (1993), "The Capacity Spectrum Method for Evaluations Structural Response During Loma Prieta Earthquake," *Proceedings, 1993 National Earthquake Conference.*

Newmark, N.M., and W.J. Hall, (1982), "Earthquake Spectra and Design," *Earthquake Engineering Research Institute*, Oakland, California.

Park, Y.J., and Ang, A.H.S., (1985), "Mechanistic Seismic Damage Model for Reinforced Concrete," *Journal of Structural Engineering, ASCE*, Vol.111, No.4, pp. 722-739.

Pekcan, G., Mander, J.B., and Chen, S.S., (1995a), " The Seismic Response of a 1:3 Scale R.C. Structure with Elastomeric Spring Dampers," *Earthquake Spectra*, Vol. 11, No.2, pp. 249-267.

Pekcan, G., Mander, J.B., and Chen, S.S., (1995b), " Experimental Performance and Analytical Study of a Non-Ductile Reinforced Concrete Frame Structure Retrofitted with

Elastomeric Spring Dampers,". *Technical Report NCEER-95-0010*, National Center for Earthquake Engineering Research, SUNY at Buffalo, July.

Pekcan, G., Mander, J.B., and Chen, S.S., (1999a), "Experimental Investigation and Computational Modeling of Seismic Response of a 1:4 Scale Model Steel Structure with a Load Balancing Supplemental Damping System," *Technical Report MCEER-99-0006*, Multidisciplinary Center. for Earthquake Engineering Research, Buffalo, N.Y.

Pekcan G., Mander, J.B., and Chen, S.S., (1999b), "Fundamental Considerations for the Design of Nonlinear Viscous Dampers," *Earthquake Engineering and Structural Dynamics*, Vol. 28, No.11, pp. 1405-1425.

Pekcan G., Mander, J.B., and Chen, S.S., (2000), "Experiments on a Steel MRF Building with a Supplemental Tendon System." *Journal of Structural Engineering*, ASCE, Vol. 126, No.4.

Prakash, V., Powell, G.H., and Filippou, F.C., (1992), "Drain-2DX: Base Program User Guide," *Report No. UCB/SEMM-92/29*, University of California at Berkeley, December.

SAC, (1997), Interim Guidelines: Evaluation, Repair, Modification and Design of Steel Moment Frames, Report No. SAC-95-02, California, USA.

Shen. K.L., and Soong, T.T., (1996), "Design of Energy Dissipation Devices Based on Concept of Damage Control," *Journal of Structural Engineering*, Vol. 122, No.1, pp. 76-82.

Soong, T.T. and Constantionu, M.C., (Editors), (1994), "Passive and Active Structural Vibration Control in Civil Engineering," Springer-Verlag, Wien, New York.

Whittaker, A.S., Bertero, V.V., Thompson, C.L., and Alonso, L.J., (1991), "Seismic Testing of Steel Plate Energy Dissipation Devices," *Earthquake Spectra, 7(4)*, EERI, November, pp. 563-604.

Whittaker, A.S., (1992), "Tentative General Requirements for the Design and Construction of Structures Incorporating Discrete Passive Energy Dissipation Devices," *Proceedings of the Fifth U.S.-Japan Workshop on the Improvement of Building Structural Design and Construction Practices*, ATC-15-4, San Diego, CA.

Multidisciplinary Center for Earthquake Engineering Research
List of Technical Reports

The Multidisciplinary Center for Earthquake Engineering Research (MCEER) publishes technical reports on a variety of subjects related to earthquake engineering written by authors funded through MCEER. These reports are available from both MCEER Publications and the National Technical Information Service (NTIS). Requests for reports should be directed to MCEER Publications, Multidisciplinary Center for Earthquake Engineering Research, State University of New York at Buffalo, Red Jacket Quadrangle, Buffalo, New York 14261. Reports can also be requested through NTIS, 5285 Port Royal Road, Springfield, Virginia 22161. NTIS accession numbers are shown in parenthesis, if available.

NCEER-87-0001 "First-Year Program in Research, Education and Technology Transfer," 3/5/87, (PB88-134275, A04, MF-A01).

NCEER-87-0002 "Experimental Evaluation of Instantaneous Optimal Algorithms for Structural Control," by R.C. Lin, T.T. Soong and A.M. Reinhorn, 4/20/87, (PB88-134341, A04, MF-A01).

NCEER-87-0003 "Experimentation Using the Earthquake Simulation Facilities at University at Buffalo," by A.M. Reinhorn and R.L. Ketter, to be published.

NCEER-87-0004 "The System Characteristics and Performance of a Shaking Table," by J.S. Hwang, K.C. Chang and G.C. Lee, 6/1/87, (PB88-134259, A03, MF-A01). This report is available only through NTIS (see address given above).

NCEER-87-0005 "A Finite Element Formulation for Nonlinear Viscoplastic Material Using a Q Model," by O. Gyebi and G. Dasgupta, 11/2/87, (PB88-213764, A08, MF-A01).

NCEER-87-0006 "Symbolic Manipulation Program (SMP) - Algebraic Codes for Two and Three Dimensional Finite Element Formulations," by X. Lee and G. Dasgupta, 11/9/87, (PB88-218522, A05, MF-A01).

NCEER-87-0007 "Instantaneous Optimal Control Laws for Tall Buildings Under Seismic Excitations," by J.N. Yang, A. Akbarpour and P. Ghaemmaghami, 6/10/87, (PB88-134333, A06, MF-A01). This report is only available through NTIS (see address given above).

NCEER-87-0008 "IDARC: Inelastic Damage Analysis of Reinforced Concrete Frame - Shear-Wall Structures," by Y.J. Park, A.M. Reinhorn and S.K. Kunnath, 7/20/87, (PB88-134325, A09, MF-A01). This report is only available through NTIS (see address given above).

NCEER-87-0009 "Liquefaction Potential for New York State: A Preliminary Report on Sites in Manhattan and Buffalo," by M. Budhu, V. Vijayakumar, R.F. Giese and L. Baumgras, 8/31/87, (PB88-163704, A03, MF-A01). This report is available only through NTIS (see address given above).

NCEER-87-0010 "Vertical and Torsional Vibration of Foundations in Inhomogeneous Media," by A.S. Veletsos and K.W. Dotson, 6/1/87, (PB88-134291, A03, MF-A01). This report is only available through NTIS (see address given above).

NCEER-87-0011 "Seismic Probabilistic Risk Assessment and Seismic Margins Studies for Nuclear Power Plants," by Howard H.M. Hwang, 6/15/87, (PB88-134267, A03, MF-A01). This report is only available through NTIS (see address given above).

NCEER-87-0012 "Parametric Studies of Frequency Response of Secondary Systems Under Ground-Acceleration Excitations," by Y. Yong and Y.K. Lin, 6/10/87, (PB88-134309, A03, MF-A01). This report is only available through NTIS (see address given above).

NCEER-87-0013 "Frequency Response of Secondary Systems Under Seismic Excitation," by J.A. HoLung, J. Cai and Y.K. Lin, 7/31/87, (PB88-134317, A05, MF-A01). This report is only available through NTIS (see address given above).

 Preceding Page Blank

NCEER-87-0014 "Modelling Earthquake Ground Motions in Seismically Active Regions Using Parametric Time Series Methods," by G.W. Ellis and A.S. Cakmak, 8/25/87, (PB88-134283, A08, MF-A01). This report is only available through NTIS (see address given above).

NCEER-87-0015 "Detection and Assessment of Seismic Structural Damage," by E. DiPasquale and A.S. Cakmak, 8/25/87, (PB88-163712, A05, MF-A01). This report is only available through NTIS (see address given above).

NCEER-87-0016 "Pipeline Experiment at Parkfield, California," by J. Isenberg and E. Richardson, 9/15/87, (PB88-163720, A03, MF-A01). This report is available only through NTIS (see address given above).

NCEER-87-0017 "Digital Simulation of Seismic Ground Motion," by M. Shinozuka, G. Deodatis and T. Harada, 8/31/87, (PB88-155197, A04, MF-A01). This report is available only through NTIS (see address given above).

NCEER-87-0018 "Practical Considerations for Structural Control: System Uncertainty, System Time Delay and Truncation of Small Control Forces," J.N. Yang and A. Akbarpour, 8/10/87, (PB88-163738, A08, MF-A01). This report is only available through NTIS (see address given above).

NCEER-87-0019 "Modal Analysis of Nonclassically Damped Structural Systems Using Canonical Transformation," by J.N. Yang, S. Sarkani and F.X. Long, 9/27/87, (PB88-187851, A04, MF-A01).

NCEER-87-0020 "A Nonstationary Solution in Random Vibration Theory," by J.R. Red-Horse and P.D. Spanos, 11/3/87, (PB88-163746, A03, MF-A01).

NCEER-87-0021 "Horizontal Impedances for Radially Inhomogeneous Viscoelastic Soil Layers," by A.S. Veletsos and K.W. Dotson, 10/15/87, (PB88-150859, A04, MF-A01).

NCEER-87-0022 "Seismic Damage Assessment of Reinforced Concrete Members," by Y.S. Chung, C. Meyer and M. Shinozuka, 10/9/87, (PB88-150867, A05, MF-A01). This report is available only through NTIS (see address given above).

NCEER-87-0023 "Active Structural Control in Civil Engineering," by T.T. Soong, 11/11/87, (PB88-187778, A03, MF-A01).

NCEER-87-0024 "Vertical and Torsional Impedances for Radially Inhomogeneous Viscoelastic Soil Layers," by K.W. Dotson and A.S. Veletsos, 12/87, (PB88-187786, A03, MF-A01).

NCEER-87-0025 "Proceedings from the Symposium on Seismic Hazards, Ground Motions, Soil-Liquefaction and Engineering Practice in Eastern North America," October 20-22, 1987, edited by K.H. Jacob, 12/87, (PB88-188115, A23, MF-A01). This report is available only through NTIS (see address given above).

NCEER-87-0026 "Report on the Whittier-Narrows, California, Earthquake of October 1, 1987," by J. Pantelic and A. Reinhorn, 11/87, (PB88-187752, A03, MF-A01). This report is available only through NTIS (see address given above).

NCEER-87-0027 "Design of a Modular Program for Transient Nonlinear Analysis of Large 3-D Building Structures," by S. Srivastav and J.F. Abel, 12/30/87, (PB88-187950, A05, MF-A01). This report is only available through NTIS (see address given above).

NCEER-87-0028 "Second-Year Program in Research, Education and Technology Transfer," 3/8/88, (PB88-219480, A04, MF-A01).

NCEER-88-0001 "Workshop on Seismic Computer Analysis and Design of Buildings With Interactive Graphics," by W. McGuire, J.F. Abel and C.H. Conley, 1/18/88, (PB88-187760, A03, MF-A01). This report is only available through NTIS (see address given above).

NCEER-88-0002 "Optimal Control of Nonlinear Flexible Structures," by J.N. Yang, F.X. Long and D. Wong, 1/22/88, (PB88-213772, A06, MF-A01).

NCEER-88-0003 "Substructuring Techniques in the Time Domain for Primary-Secondary Structural Systems," by G.D. Manolis and G. Juhn, 2/10/88, (PB88-213780, A04, MF-A01).

NCEER-88-0004 "Iterative Seismic Analysis of Primary-Secondary Systems," by A. Singhal, L.D. Lutes and P.D. Spanos, 2/23/88, (PB88-213798, A04, MF-A01).

NCEER-88-0005 "Stochastic Finite Element Expansion for Random Media," by P.D. Spanos and R. Ghanem, 3/14/88, (PB88-213806, A03, MF-A01).

NCEER-88-0006 "Combining Structural Optimization and Structural Control," by F.Y. Cheng and C.P. Pantelides, 1/10/88, (PB88-213814, A05, MF-A01).

NCEER-88-0007 "Seismic Performance Assessment of Code-Designed Structures," by H.H-M. Hwang, J-W. Jaw and H-J. Shau, 3/20/88, (PB88-219423, A04, MF-A01). This report is only available through NTIS (see address given above).

NCEER-88-0008 "Reliability Analysis of Code-Designed Structures Under Natural Hazards," by H.H-M. Hwang, H. Ushiba and M. Shinozuka, 2/29/88, (PB88-229471, A07, MF-A01). This report is only available through NTIS (see address given above).

NCEER-88-0009 "Seismic Fragility Analysis of Shear Wall Structures," by J-W Jaw and H.H-M. Hwang, 4/30/88, (PB89-102867, A04, MF-A01).

NCEER-88-0010 "Base Isolation of a Multi-Story Building Under a Harmonic Ground Motion - A Comparison of Performances of Various Systems," by F-G Fan, G. Ahmadi and I.G. Tadjbakhsh, 5/18/88, (PB89-122238, A06, MF-A01). This report is only available through NTIS (see address given above).

NCEER-88-0011 "Seismic Floor Response Spectra for a Combined System by Green's Functions," by F.M. Lavelle, L.A. Bergman and P.D. Spanos, 5/1/88, (PB89-102875, A03, MF-A01).

NCEER-88-0012 "A New Solution Technique for Randomly Excited Hysteretic Structures," by G.Q. Cai and Y.K. Lin, 5/16/88, (PB89-102883, A03, MF-A01).

NCEER-88-0013 "A Study of Radiation Damping and Soil-Structure Interaction Effects in the Centrifuge," by K. Weissman, supervised by J.H. Prevost, 5/24/88, (PB89-144703, A06, MF-A01).

NCEER-88-0014 "Parameter Identification and Implementation of a Kinematic Plasticity Model for Frictional Soils," by J.H. Prevost and D.V. Griffiths, to be published.

NCEER-88-0015 "Two- and Three- Dimensional Dynamic Finite Element Analyses of the Long Valley Dam," by D.V. Griffiths and J.H. Prevost, 6/17/88, (PB89-144711, A04, MF-A01).

NCEER-88-0016 "Damage Assessment of Reinforced Concrete Structures in Eastern United States," by A.M. Reinhorn, M.J. Seidel, S.K. Kunnath and Y.J. Park, 6/15/88, (PB89-122220, A04, MF-A01). This report is only available through NTIS (see address given above).

NCEER-88-0017 "Dynamic Compliance of Vertically Loaded Strip Foundations in Multilayered Viscoelastic Soils," by S. Ahmad and A.S.M. Israil, 6/17/88, (PB89-102891, A04, MF-A01).

NCEER-88-0018 "An Experimental Study of Seismic Structural Response With Added Viscoelastic Dampers," by R.C. Lin, Z. Liang, T.T. Soong and R.H. Zhang, 6/30/88, (PB89-122212, A05, MF-A01). This report is available only through NTIS (see address given above).

NCEER-88-0019 "Experimental Investigation of Primary - Secondary System Interaction," by G.D. Manolis, G. Juhn and A.M. Reinhorn, 5/27/88, (PB89-122204, A04, MF-A01).

NCEER-88-0020 "A Response Spectrum Approach For Analysis of Nonclassically Damped Structures," by J.N. Yang, S. Sarkani and F.X. Long, 4/22/88, (PB89-102909, A04, MF-A01).

NCEER-88-0021 "Seismic Interaction of Structures and Soils: Stochastic Approach," by A.S. Veletsos and A.M. Prasad, 7/21/88, (PB89-122196, A04, MF-A01). This report is only available through NTIS (see address given above).

NCEER-88-0022 "Identification of the Serviceability Limit State and Detection of Seismic Structural Damage," by E. DiPasquale and A.S. Cakmak, 6/15/88, (PB89-122188, A05, MF-A01). This report is available only through NTIS (see address given above).

NCEER-88-0023 "Multi-Hazard Risk Analysis: Case of a Simple Offshore Structure," by B.K. Bhartia and E.H. Vanmarcke, 7/21/88, (PB89-145213, A05, MF-A01).

NCEER-88-0024 "Automated Seismic Design of Reinforced Concrete Buildings," by Y.S. Chung, C. Meyer and M. Shinozuka, 7/5/88, (PB89-122170, A06, MF-A01). This report is available only through NTIS (see address given above).

NCEER-88-0025 "Experimental Study of Active Control of MDOF Structures Under Seismic Excitations," by L.L. Chung, R.C. Lin, T.T. Soong and A.M. Reinhorn, 7/10/88, (PB89-122600, A04, MF-A01).

NCEER-88-0026 "Earthquake Simulation Tests of a Low-Rise Metal Structure," by J.S. Hwang, K.C. Chang, G.C. Lee and R.L. Ketter, 8/1/88, (PB89-102917, A04, MF-A01).

NCEER-88-0027 "Systems Study of Urban Response and Reconstruction Due to Catastrophic Earthquakes," by F. Kozin and H.K. Zhou, 9/22/88, (PB90-162348, A04, MF-A01).

NCEER-88-0028 "Seismic Fragility Analysis of Plane Frame Structures," by H.H-M. Hwang and Y.K. Low, 7/31/88, (PB89-131445, A06, MF-A01).

NCEER-88-0029 "Response Analysis of Stochastic Structures," by A. Kardara, C. Bucher and M. Shinozuka, 9/22/88, (PB89-174429, A04, MF-A01).

NCEER-88-0030 "Nonnormal Accelerations Due to Yielding in a Primary Structure," by D.C.K. Chen and L.D. Lutes, 9/19/88, (PB89-131437, A04, MF-A01).

NCEER-88-0031 "Design Approaches for Soil-Structure Interaction," by A.S. Veletsos, A.M. Prasad and Y. Tang, 12/30/88, (PB89-174437, A03, MF-A01). This report is available only through NTIS (see address given above).

NCEER-88-0032 "A Re-evaluation of Design Spectra for Seismic Damage Control," by C.J. Turkstra and A.G. Tallin, 11/7/88, (PB89-145221, A05, MF-A01).

NCEER-88-0033 "The Behavior and Design of Noncontact Lap Splices Subjected to Repeated Inelastic Tensile Loading," by V.E. Sagan, P. Gergely and R.N. White, 12/8/88, (PB89-163737, A08, MF-A01).

NCEER-88-0034 "Seismic Response of Pile Foundations," by S.M. Mamoon, P.K. Banerjee and S. Ahmad, 11/1/88, (PB89-145239, A04, MF-A01).

NCEER-88-0035 "Modeling of R/C Building Structures With Flexible Floor Diaphragms (IDARC2)," by A.M. Reinhorn, S.K. Kunnath and N. Panahshahi, 9/7/88, (PB89-207153, A07, MF-A01).

NCEER-88-0036 "Solution of the Dam-Reservoir Interaction Problem Using a Combination of FEM, BEM with Particular Integrals, Modal Analysis, and Substructuring," by C-S. Tsai, G.C. Lee and R.L. Ketter, 12/31/88, (PB89-207146, A04, MF-A01).

NCEER-88-0037 "Optimal Placement of Actuators for Structural Control," by F.Y. Cheng and C.P. Pantelides, 8/15/88, (PB89-162846, A05, MF-A01).

NCEER-88-0038 "Teflon Bearings in Aseismic Base Isolation: Experimental Studies and Mathematical Modeling," by A. Mokha, M.C. Constantinou and A.M. Reinhorn, 12/5/88, (PB89-218457, A10, MF-A01). This report is available only through NTIS (see address given above).

NCEER-88-0039 "Seismic Behavior of Flat Slab High-Rise Buildings in the New York City Area," by P. Weidlinger and M. Ettouney, 10/15/88, (PB90-145681, A04, MF-A01).

NCEER-88-0040 "Evaluation of the Earthquake Resistance of Existing Buildings in New York City," by P. Weidlinger and M. Ettouney, 10/15/88, to be published.

NCEER-88-0041 "Small-Scale Modeling Techniques for Reinforced Concrete Structures Subjected to Seismic Loads," by W. Kim, A. El-Attar and R.N. White, 11/22/88, (PB89-189625, A05, MF-A01).

NCEER-88-0042 "Modeling Strong Ground Motion from Multiple Event Earthquakes," by G.W. Ellis and A.S. Cakmak, 10/15/88, (PB89-174445, A03, MF-A01).

NCEER-88-0043 "Nonstationary Models of Seismic Ground Acceleration," by M. Grigoriu, S.E. Ruiz and E. Rosenblueth, 7/15/88, (PB89-189617, A04, MF-A01).

NCEER-88-0044 "SARCF User's Guide: Seismic Analysis of Reinforced Concrete Frames," by Y.S. Chung, C. Meyer and M. Shinozuka, 11/9/88, (PB89-174452, A08, MF-A01).

NCEER-88-0045 "First Expert Panel Meeting on Disaster Research and Planning," edited by J. Pantelic and J. Stoyle, 9/15/88, (PB89-174460, A05, MF-A01).

NCEER-88-0046 "Preliminary Studies of the Effect of Degrading Infill Walls on the Nonlinear Seismic Response of Steel Frames," by C.Z. Chrysostomou, P. Gergely and J.F. Abel, 12/19/88, (PB89-208383, A05, MF-A01).

NCEER-88-0047 "Reinforced Concrete Frame Component Testing Facility - Design, Construction, Instrumentation and Operation," by S.P. Pessiki, C. Conley, T. Bond, P. Gergely and R.N. White, 12/16/88, (PB89-174478, A04, MF-A01).

NCEER-89-0001 "Effects of Protective Cushion and Soil Compliancy on the Response of Equipment Within a Seismically Excited Building," by J.A. HoLung, 2/16/89, (PB89-207179, A04, MF-A01).

NCEER-89-0002 "Statistical Evaluation of Response Modification Factors for Reinforced Concrete Structures," by H.H-M. Hwang and J-W. Jaw, 2/17/89, (PB89-207187, A05, MF-A01).

NCEER-89-0003 "Hysteretic Columns Under Random Excitation," by G-Q. Cai and Y.K. Lin, 1/9/89, (PB89-196513, A03, MF-A01).

NCEER-89-0004 "Experimental Study of `Elephant Foot Bulge' Instability of Thin-Walled Metal Tanks," by Z-H. Jia and R.L. Ketter, 2/22/89, (PB89-207195, A03, MF-A01).

NCEER-89-0005 "Experiment on Performance of Buried Pipelines Across San Andreas Fault," by J. Isenberg, E. Richardson and T.D. O'Rourke, 3/10/89, (PB89-218440, A04, MF-A01). This report is available only through NTIS (see address given above).

NCEER-89-0006 "A Knowledge-Based Approach to Structural Design of Earthquake-Resistant Buildings," by M. Subramani, P. Gergely, C.H. Conley, J.F. Abel and A.H. Zaghw, 1/15/89, (PB89-218465, A06, MF-A01).

NCEER-89-0007 "Liquefaction Hazards and Their Effects on Buried Pipelines," by T.D. O'Rourke and P.A. Lane, 2/1/89, (PB89-218481, A09, MF-A01).

NCEER-89-0008 "Fundamentals of System Identification in Structural Dynamics," by H. Imai, C-B. Yun, O. Maruyama and M. Shinozuka, 1/26/89, (PB89-207211, A04, MF-A01).

NCEER-89-0009 "Effects of the 1985 Michoacan Earthquake on Water Systems and Other Buried Lifelines in Mexico," by A.G. Ayala and M.J. O'Rourke, 3/8/89, (PB89-207229, A06, MF-A01).

NCEER-89-R010 "NCEER Bibliography of Earthquake Education Materials," by K.E.K. Ross, Second Revision, 9/1/89, (PB90-125352, A05, MF-A01). This report is replaced by NCEER-92-0018.

NCEER-89-0011 "Inelastic Three-Dimensional Response Analysis of Reinforced Concrete Building Structures (IDARC-3D), Part I - Modeling," by S.K. Kunnath and A.M. Reinhorn, 4/17/89, (PB90-114612, A07, MF-A01). This report is available only through NTIS (see address given above).

NCEER-89-0012 "Recommended Modifications to ATC-14," by C.D. Poland and J.O. Malley, 4/12/89, (PB90-108648, A15, MF-A01).

NCEER-89-0013 "Repair and Strengthening of Beam-to-Column Connections Subjected to Earthquake Loading," by M. Corazao and A.J. Durrani, 2/28/89, (PB90-109885, A06, MF-A01).

NCEER-89-0014 "Program EXKAL2 for Identification of Structural Dynamic Systems," by O. Maruyama, C-B. Yun, M. Hoshiya and M. Shinozuka, 5/19/89, (PB90-109877, A09, MF-A01).

NCEER-89-0015 "Response of Frames With Bolted Semi-Rigid Connections, Part I - Experimental Study and Analytical Predictions," by P.J. DiCorso, A.M. Reinhorn, J.R. Dickerson, J.B. Radziminski and W.L. Harper, 6/1/89, to be published.

NCEER-89-0016 "ARMA Monte Carlo Simulation in Probabilistic Structural Analysis," by P.D. Spanos and M.P. Mignolet, 7/10/89, (PB90-109893, A03, MF-A01).

NCEER-89-P017 "Preliminary Proceedings from the Conference on Disaster Preparedness - The Place of Earthquake Education in Our Schools," Edited by K.E.K. Ross, 6/23/89, (PB90-108606, A03, MF-A01).

NCEER-89-0017 "Proceedings from the Conference on Disaster Preparedness - The Place of Earthquake Education in Our Schools," Edited by K.E.K. Ross, 12/31/89, (PB90-207895, A012, MF-A02). This report is available only through NTIS (see address given above).

NCEER-89-0018 "Multidimensional Models of Hysteretic Material Behavior for Vibration Analysis of Shape Memory Energy Absorbing Devices, by E.J. Graesser and F.A. Cozzarelli, 6/7/89, (PB90-164146, A04, MF-A01).

NCEER-89-0019 "Nonlinear Dynamic Analysis of Three-Dimensional Base Isolated Structures (3D-BASIS)," by S. Nagarajaiah, A.M. Reinhorn and M.C. Constantinou, 8/3/89, (PB90-161936, A06, MF-A01). This report has been replaced by NCEER-93-0011.

NCEER-89-0020 "Structural Control Considering Time-Rate of Control Forces and Control Rate Constraints," by F.Y. Cheng and C.P. Pantelides, 8/3/89, (PB90-120445, A04, MF-A01).

NCEER-89-0021 "Subsurface Conditions of Memphis and Shelby County," by K.W. Ng, T-S. Chang and H-H.M. Hwang, 7/26/89, (PB90-120437, A03, MF-A01).

NCEER-89-0022 "Seismic Wave Propagation Effects on Straight Jointed Buried Pipelines," by K. Elhmadi and M.J. O'Rourke, 8/24/89, (PB90-162322, A10, MF-A02).

NCEER-89-0023 "Workshop on Serviceability Analysis of Water Delivery Systems," edited by M. Grigoriu, 3/6/89, (PB90-127424, A03, MF-A01).

NCEER-89-0024 "Shaking Table Study of a 1/5 Scale Steel Frame Composed of Tapered Members," by K.C. Chang, J.S. Hwang and G.C. Lee, 9/18/89, (PB90-160169, A04, MF-A01).

NCEER-89-0025 "DYNA1D: A Computer Program for Nonlinear Seismic Site Response Analysis - Technical Documentation," by Jean H. Prevost, 9/14/89, (PB90-161944, A07, MF-A01). This report is available only through NTIS (see address given above).

NCEER-89-0026 "1:4 Scale Model Studies of Active Tendon Systems and Active Mass Dampers for Aseismic Protection," by A.M. Reinhorn, T.T. Soong, R.C. Lin, Y.P. Yang, Y. Fukao, H. Abe and M. Nakai, 9/15/89, (PB90-173246, A10, MF-A02). This report is available only through NTIS (see address given above).

NCEER-89-0027 "Scattering of Waves by Inclusions in a Nonhomogeneous Elastic Half Space Solved by Boundary Element Methods," by P.K. Hadley, A. Askar and A.S. Cakmak, 6/15/89, (PB90-145699, A07, MF-A01).

NCEER-89-0028 "Statistical Evaluation of Deflection Amplification Factors for Reinforced Concrete Structures," by H.H.M. Hwang, J-W. Jaw and A.L. Ch'ng, 8/31/89, (PB90-164633, A05, MF-A01).

NCEER-89-0029 "Bedrock Accelerations in Memphis Area Due to Large New Madrid Earthquakes," by H.H.M. Hwang, C.H.S. Chen and G. Yu, 11/7/89, (PB90-162330, A04, MF-A01).

NCEER-89-0030 "Seismic Behavior and Response Sensitivity of Secondary Structural Systems," by Y.Q. Chen and T.T. Soong, 10/23/89, (PB90-164658, A08, MF-A01).

NCEER-89-0031 "Random Vibration and Reliability Analysis of Primary-Secondary Structural Systems," by Y. Ibrahim, M. Grigoriu and T.T. Soong, 11/10/89, (PB90-161951, A04, MF-A01).

NCEER-89-0032 "Proceedings from the Second U.S. - Japan Workshop on Liquefaction, Large Ground Deformation and Their Effects on Lifelines, September 26-29, 1989," Edited by T.D. O'Rourke and M. Hamada, 12/1/89, (PB90-209388, A22, MF-A03).

NCEER-89-0033 "Deterministic Model for Seismic Damage Evaluation of Reinforced Concrete Structures," by J.M. Bracci, A.M. Reinhorn, J.B. Mander and S.K. Kunnath, 9/27/89, (PB91-108803, A06, MF-A01).

NCEER-89-0034 "On the Relation Between Local and Global Damage Indices," by E. DiPasquale and A.S. Cakmak, 8/15/89, (PB90-173865, A05, MF-A01).

NCEER-89-0035 "Cyclic Undrained Behavior of Nonplastic and Low Plasticity Silts," by A.J. Walker and H.E. Stewart, 7/26/89, (PB90-183518, A10, MF-A01).

NCEER-89-0036 "Liquefaction Potential of Surficial Deposits in the City of Buffalo, New York," by M. Budhu, R. Giese and L. Baumgrass, 1/17/89, (PB90-208455, A04, MF-A01).

NCEER-89-0037 "A Deterministic Assessment of Effects of Ground Motion Incoherence," by A.S. Veletsos and Y. Tang, 7/15/89, (PB90-164294, A03, MF-A01).

NCEER-89-0038 "Workshop on Ground Motion Parameters for Seismic Hazard Mapping," July 17-18, 1989, edited by R.V. Whitman, 12/1/89, (PB90-173923, A04, MF-A01).

NCEER-89-0039 "Seismic Effects on Elevated Transit Lines of the New York City Transit Authority," by C.J. Costantino, C.A. Miller and E. Heymsfield, 12/26/89, (PB90-207887, A06, MF-A01).

NCEER-89-0040 "Centrifugal Modeling of Dynamic Soil-Structure Interaction," by K. Weissman, Supervised by J.H. Prevost, 5/10/89, (PB90-207879, A07, MF-A01).

NCEER-89-0041 "Linearized Identification of Buildings With Cores for Seismic Vulnerability Assessment," by I-K. Ho and A.E. Aktan, 11/1/89, (PB90-251943, A07, MF-A01).

NCEER-90-0001 "Geotechnical and Lifeline Aspects of the October 17, 1989 Loma Prieta Earthquake in San Francisco," by T.D. O'Rourke, H.E. Stewart, F.T. Blackburn and T.S. Dickerman, 1/90, (PB90-208596, A05, MF-A01).

NCEER-90-0002 "Nonnormal Secondary Response Due to Yielding in a Primary Structure," by D.C.K. Chen and L.D. Lutes, 2/28/90, (PB90-251976, A07, MF-A01).

NCEER-90-0003 "Earthquake Education Materials for Grades K-12," by K.E.K. Ross, 4/16/90, (PB91-251984, A05, MF-A05). This report has been replaced by NCEER-92-0018.

NCEER-90-0004 "Catalog of Strong Motion Stations in Eastern North America," by R.W. Busby, 4/3/90, (PB90-251984, A05, MF-A01).

NCEER-90-0005 "NCEER Strong-Motion Data Base: A User Manual for the GeoBase Release (Version 1.0 for the Sun3)," by P. Friberg and K. Jacob, 3/31/90 (PB90-258062, A04, MF-A01).

NCEER-90-0006 "Seismic Hazard Along a Crude Oil Pipeline in the Event of an 1811-1812 Type New Madrid Earthquake," by H.H.M. Hwang and C-H.S. Chen, 4/16/90, (PB90-258054, A04, MF-A01).

NCEER-90-0007 "Site-Specific Response Spectra for Memphis Sheahan Pumping Station," by H.H.M. Hwang and C.S. Lee, 5/15/90, (PB91-108811, A05, MF-A01).

NCEER-90-0008 "Pilot Study on Seismic Vulnerability of Crude Oil Transmission Systems," by T. Ariman, R. Dobry, M. Grigoriu, F. Kozin, M. O'Rourke, T. O'Rourke and M. Shinozuka, 5/25/90, (PB91-108837, A06, MF-A01).

NCEER-90-0009 "A Program to Generate Site Dependent Time Histories: EQGEN," by G.W. Ellis, M. Srinivasan and A.S. Cakmak, 1/30/90, (PB91-108829, A04, MF-A01).

NCEER-90-0010 "Active Isolation for Seismic Protection of Operating Rooms," by M.E. Talbott, Supervised by M. Shinozuka, 6/8/9, (PB91-110205, A05, MF-A01).

NCEER-90-0011 "Program LINEARID for Identification of Linear Structural Dynamic Systems," by C-B. Yun and M. Shinozuka, 6/25/90, (PB91-110312, A08, MF-A01).

NCEER-90-0012 "Two-Dimensional Two-Phase Elasto-Plastic Seismic Response of Earth Dams," by A.N. Yiagos, Supervised by J.H. Prevost, 6/20/90, (PB91-110197, A13, MF-A02).

NCEER-90-0013 "Secondary Systems in Base-Isolated Structures: Experimental Investigation, Stochastic Response and Stochastic Sensitivity," by G.D. Manolis, G. Juhn, M.C. Constantinou and A.M. Reinhorn, 7/1/90, (PB91-110320, A08, MF-A01).

NCEER-90-0014 "Seismic Behavior of Lightly-Reinforced Concrete Column and Beam-Column Joint Details," by S.P. Pessiki, C.H. Conley, P. Gergely and R.N. White, 8/22/90, (PB91-108795, A11, MF-A02).

NCEER-90-0015 "Two Hybrid Control Systems for Building Structures Under Strong Earthquakes," by J.N. Yang and A. Danielians, 6/29/90, (PB91-125393, A04, MF-A01).

NCEER-90-0016 "Instantaneous Optimal Control with Acceleration and Velocity Feedback," by J.N. Yang and Z. Li, 6/29/90, (PB91-125401, A03, MF-A01).

NCEER-90-0017 "Reconnaissance Report on the Northern Iran Earthquake of June 21, 1990," by M. Mehrain, 10/4/90, (PB91-125377, A03, MF-A01).

NCEER-90-0018 "Evaluation of Liquefaction Potential in Memphis and Shelby County," by T.S. Chang, P.S. Tang, C.S. Lee and H. Hwang, 8/10/90, (PB91-125427, A09, MF-A01).

NCEER-90-0019 "Experimental and Analytical Study of a Combined Sliding Disc Bearing and Helical Steel Spring Isolation System," by M.C. Constantinou, A.S. Mokha and A.M. Reinhorn, 10/4/90, (PB91-125385, A06, MF-A01). This report is available only through NTIS (see address given above).

NCEER-90-0020 "Experimental Study and Analytical Prediction of Earthquake Response of a Sliding Isolation System with a Spherical Surface," by A.S. Mokha, M.C. Constantinou and A.M. Reinhorn, 10/11/90, (PB91-125419, A05, MF-A01).

NCEER-90-0021 "Dynamic Interaction Factors for Floating Pile Groups," by G. Gazetas, K. Fan, A. Kaynia and E. Kausel, 9/10/90, (PB91-170381, A05, MF-A01).

NCEER-90-0022 "Evaluation of Seismic Damage Indices for Reinforced Concrete Structures," by S. Rodriguez-Gomez and A.S. Cakmak, 9/30/90, PB91-171322, A06, MF-A01).

NCEER-90-0023 "Study of Site Response at a Selected Memphis Site," by H. Desai, S. Ahmad, E.S. Gazetas and M.R. Oh, 10/11/90, (PB91-196857, A03, MF-A01).

NCEER-90-0024 "A User's Guide to Strongmo: Version 1.0 of NCEER's Strong-Motion Data Access Tool for PCs and Terminals," by P.A. Friberg and C.A.T. Susch, 11/15/90, (PB91-171272, A03, MF-A01).

NCEER-90-0025 "A Three-Dimensional Analytical Study of Spatial Variability of Seismic Ground Motions," by L-L. Hong and A.H.-S. Ang, 10/30/90, (PB91-170399, A09, MF-A01).

NCEER-90-0026 "MUMOID User's Guide - A Program for the Identification of Modal Parameters," by S. Rodriguez-Gomez and E. DiPasquale, 9/30/90, (PB91-171298, A04, MF-A01).

NCEER-90-0027 "SARCF-II User's Guide - Seismic Analysis of Reinforced Concrete Frames," by S. Rodriguez-Gomez, Y.S. Chung and C. Meyer, 9/30/90, (PB91-171280, A05, MF-A01).

NCEER-90-0028 "Viscous Dampers: Testing, Modeling and Application in Vibration and Seismic Isolation," by N. Makris and M.C. Constantinou, 12/20/90 (PB91-190561, A06, MF-A01).

NCEER-90-0029 "Soil Effects on Earthquake Ground Motions in the Memphis Area," by H. Hwang, C.S. Lee, K.W. Ng and T.S. Chang, 8/2/90, (PB91-190751, A05, MF-A01).

NCEER-91-0001 "Proceedings from the Third Japan-U.S. Workshop on Earthquake Resistant Design of Lifeline Facilities and Countermeasures for Soil Liquefaction, December 17-19, 1990," edited by T.D. O'Rourke and M. Hamada, 2/1/91, (PB91-179259, A99, MF-A04).

NCEER-91-0002 "Physical Space Solutions of Non-Proportionally Damped Systems," by M. Tong, Z. Liang and G.C. Lee, 1/15/91, (PB91-179242, A04, MF-A01).

NCEER-91-0003 "Seismic Response of Single Piles and Pile Groups," by K. Fan and G. Gazetas, 1/10/91, (PB92-174994, A04, MF-A01).

NCEER-91-0004 "Damping of Structures: Part 1 - Theory of Complex Damping," by Z. Liang and G. Lee, 10/10/91, (PB92-197235, A12, MF-A03).

NCEER-91-0005 "3D-BASIS - Nonlinear Dynamic Analysis of Three Dimensional Base Isolated Structures: Part II," by S. Nagarajaiah, A.M. Reinhorn and M.C. Constantinou, 2/28/91, (PB91-190553, A07, MF-A01). This report has been replaced by NCEER-93-0011.

NCEER-91-0006 "A Multidimensional Hysteretic Model for Plasticity Deforming Metals in Energy Absorbing Devices," by E.J. Graesser and F.A. Cozzarelli, 4/9/91, (PB92-108364, A04, MF-A01).

NCEER-91-0007 "A Framework for Customizable Knowledge-Based Expert Systems with an Application to a KBES for Evaluating the Seismic Resistance of Existing Buildings," by E.G. Ibarra-Anaya and S.J. Fenves, 4/9/91, (PB91-210930, A08, MF-A01).

NCEER-91-0008 "Nonlinear Analysis of Steel Frames with Semi-Rigid Connections Using the Capacity Spectrum Method," by G.G. Deierlein, S-H. Hsieh, Y-J. Shen and J.F. Abel, 7/2/91, (PB92-113828, A05, MF-A01).

NCEER-91-0009 "Earthquake Education Materials for Grades K-12," by K.E.K. Ross, 4/30/91, (PB91-212142, A06, MF-A01). This report has been replaced by NCEER-92-0018.

NCEER-91-0010 "Phase Wave Velocities and Displacement Phase Differences in a Harmonically Oscillating Pile," by N. Makris and G. Gazetas, 7/8/91, (PB92-108356, A04, MF-A01).

NCEER-91-0011 "Dynamic Characteristics of a Full-Size Five-Story Steel Structure and a 2/5 Scale Model," by K.C. Chang, G.C. Yao, G.C. Lee, D.S. Hao and Y.C. Yeh," 7/2/91, (PB93-116648, A06, MF-A02).

NCEER-91-0012 "Seismic Response of a 2/5 Scale Steel Structure with Added Viscoelastic Dampers," by K.C. Chang, T.T. Soong, S-T. Oh and M.L. Lai, 5/17/91, (PB92-110816, A05, MF-A01).

NCEER-91-0013 "Earthquake Response of Retaining Walls; Full-Scale Testing and Computational Modeling," by S. Alampalli and A-W.M. Elgamal, 6/20/91, to be published.

NCEER-91-0014 "3D-BASIS-M: Nonlinear Dynamic Analysis of Multiple Building Base Isolated Structures," by P.C. Tsopelas, S. Nagarajaiah, M.C. Constantinou and A.M. Reinhorn, 5/28/91, (PB92-113885, A09, MF-A02).

NCEER-91-0015 "Evaluation of SEAOC Design Requirements for Sliding Isolated Structures," by D. Theodossiou and M.C. Constantinou, 6/10/91, (PB92-114602, A11, MF-A03).

NCEER-91-0016 "Closed-Loop Modal Testing of a 27-Story Reinforced Concrete Flat Plate-Core Building," by H.R. Somaprasad, T. Toksoy, H. Yoshiyuki and A.E. Aktan, 7/15/91, (PB92-129980, A07, MF-A02).

NCEER-91-0017 "Shake Table Test of a 1/6 Scale Two-Story Lightly Reinforced Concrete Building," by A.G. El-Attar, R.N. White and P. Gergely, 2/28/91, (PB92-222447, A06, MF-A02).

NCEER-91-0018 "Shake Table Test of a 1/8 Scale Three-Story Lightly Reinforced Concrete Building," by A.G. El-Attar, R.N. White and P. Gergely, 2/28/91, (PB93-116630, A08, MF-A02).

NCEER-91-0019 "Transfer Functions for Rigid Rectangular Foundations," by A.S. Veletsos, A.M. Prasad and W.H. Wu, 7/31/91, to be published.

NCEER-91-0020 "Hybrid Control of Seismic-Excited Nonlinear and Inelastic Structural Systems," by J.N. Yang, Z. Li and A. Danielians, 8/1/91, (PB92-143171, A06, MF-A02).

NCEER-91-0021 "The NCEER-91 Earthquake Catalog: Improved Intensity-Based Magnitudes and Recurrence Relations for U.S. Earthquakes East of New Madrid," by L. Seeber and J.G. Armbruster, 8/28/91, (PB92-176742, A06, MF-A02).

NCEER-91-0022 "Proceedings from the Implementation of Earthquake Planning and Education in Schools: The Need for Change - The Roles of the Changemakers," by K.E.K. Ross and F. Winslow, 7/23/91, (PB92-129998, A12, MF-A03).

NCEER-91-0023 "A Study of Reliability-Based Criteria for Seismic Design of Reinforced Concrete Frame Buildings," by H.H.M. Hwang and H-M. Hsu, 8/10/91, (PB92-140235, A09, MF-A02).

NCEER-91-0024 "Experimental Verification of a Number of Structural System Identification Algorithms," by R.G. Ghanem, H. Gavin and M. Shinozuka, 9/18/91, (PB92-176577, A18, MF-A04).

NCEER-91-0025 "Probabilistic Evaluation of Liquefaction Potential," by H.H.M. Hwang and C.S. Lee," 11/25/91, (PB92-143429, A05, MF-A01).

NCEER-91-0026 "Instantaneous Optimal Control for Linear, Nonlinear and Hysteretic Structures - Stable Controllers," by J.N. Yang and Z. Li, 11/15/91, (PB92-163807, A04, MF-A01).

NCEER-91-0027 "Experimental and Theoretical Study of a Sliding Isolation System for Bridges," by M.C. Constantinou, A. Kartoum, A.M. Reinhorn and P. Bradford, 11/15/91, (PB92-176973, A10, MF-A03).

NCEER-92-0001 "Case Studies of Liquefaction and Lifeline Performance During Past Earthquakes, Volume 1: Japanese Case Studies," Edited by M. Hamada and T. O'Rourke, 2/17/92, (PB92-197243, A18, MF-A04).

NCEER-92-0002 "Case Studies of Liquefaction and Lifeline Performance During Past Earthquakes, Volume 2: United States Case Studies," Edited by T. O'Rourke and M. Hamada, 2/17/92, (PB92-197250, A20, MF-A04).

NCEER-92-0003 "Issues in Earthquake Education," Edited by K. Ross, 2/3/92, (PB92-222389, A07, MF-A02).

NCEER-92-0004 "Proceedings from the First U.S. - Japan Workshop on Earthquake Protective Systems for Bridges," Edited by I.G. Buckle, 2/4/92, (PB94-142239, A99, MF-A06).

NCEER-92-0005 "Seismic Ground Motion from a Haskell-Type Source in a Multiple-Layered Half-Space," A.P. Theoharis, G. Deodatis and M. Shinozuka, 1/2/92, to be published.

NCEER-92-0006 "Proceedings from the Site Effects Workshop," Edited by R. Whitman, 2/29/92, (PB92-197201, A04, MF-A01).

NCEER-92-0007 "Engineering Evaluation of Permanent Ground Deformations Due to Seismically-Induced Liquefaction," by M.H. Baziar, R. Dobry and A-W.M. Elgamal, 3/24/92, (PB92-222421, A13, MF-A03).

NCEER-92-0008 "A Procedure for the Seismic Evaluation of Buildings in the Central and Eastern United States," by C.D. Poland and J.O. Malley, 4/2/92, (PB92-222439, A20, MF-A04).

NCEER-92-0009 "Experimental and Analytical Study of a Hybrid Isolation System Using Friction Controllable Sliding Bearings," by M.Q. Feng, S. Fujii and M. Shinozuka, 5/15/92, (PB93-150282, A06, MF-A02).

NCEER-92-0010 "Seismic Resistance of Slab-Column Connections in Existing Non-Ductile Flat-Plate Buildings," by A.J. Durrani and Y. Du, 5/18/92, (PB93-116812, A06, MF-A02).

NCEER-92-0011 "The Hysteretic and Dynamic Behavior of Brick Masonry Walls Upgraded by Ferrocement Coatings Under Cyclic Loading and Strong Simulated Ground Motion," by H. Lee and S.P. Prawel, 5/11/92, to be published.

NCEER-92-0012 "Study of Wire Rope Systems for Seismic Protection of Equipment in Buildings," by G.F. Demetriades, M.C. Constantinou and A.M. Reinhorn, 5/20/92, (PB93-116655, A08, MF-A02).

NCEER-92-0013 "Shape Memory Structural Dampers: Material Properties, Design and Seismic Testing," by P.R. Witting and F.A. Cozzarelli, 5/26/92, (PB93-116663, A05, MF-A01).

NCEER-92-0014 "Longitudinal Permanent Ground Deformation Effects on Buried Continuous Pipelines," by M.J. O'Rourke, and C. Nordberg, 6/15/92, (PB93-116671, A08, MF-A02).

NCEER-92-0015 "A Simulation Method for Stationary Gaussian Random Functions Based on the Sampling Theorem," by M. Grigoriu and S. Balopoulou, 6/11/92, (PB93-127496, A05, MF-A01).

NCEER-92-0016 "Gravity-Load-Designed Reinforced Concrete Buildings: Seismic Evaluation of Existing Construction and Detailing Strategies for Improved Seismic Resistance," by G.W. Hoffmann, S.K. Kunnath, A.M. Reinhorn and J.B. Mander, 7/15/92, (PB94-142007, A08, MF-A02).

NCEER-92-0017 "Observations on Water System and Pipeline Performance in the Limón Area of Costa Rica Due to the April 22, 1991 Earthquake," by M. O'Rourke and D. Ballantyne, 6/30/92, (PB93-126811, A06, MF-A02).

NCEER-92-0018 "Fourth Edition of Earthquake Education Materials for Grades K-12," Edited by K.E.K. Ross, 8/10/92, (PB93-114023, A07, MF-A02).

NCEER-92-0019 "Proceedings from the Fourth Japan-U.S. Workshop on Earthquake Resistant Design of Lifeline Facilities and Countermeasures for Soil Liquefaction," Edited by M. Hamada and T.D. O'Rourke, 8/12/92, (PB93-163939, A99, MF-E11).

NCEER-92-0020 "Active Bracing System: A Full Scale Implementation of Active Control," by A.M. Reinhorn, T.T. Soong, R.C. Lin, M.A. Riley, Y.P. Wang, S. Aizawa and M. Higashino, 8/14/92, (PB93-127512, A06, MF-A02).

NCEER-92-0021 "Empirical Analysis of Horizontal Ground Displacement Generated by Liquefaction-Induced Lateral Spreads," by S.F. Bartlett and T.L. Youd, 8/17/92, (PB93-188241, A06, MF-A02).

NCEER-92-0022 "IDARC Version 3.0: Inelastic Damage Analysis of Reinforced Concrete Structures," by S.K. Kunnath, A.M. Reinhorn and R.F. Lobo, 8/31/92, (PB93-227502, A07, MF-A02).

NCEER-92-0023 "A Semi-Empirical Analysis of Strong-Motion Peaks in Terms of Seismic Source, Propagation Path and Local Site Conditions, by M. Kamiyama, M.J. O'Rourke and R. Flores-Berrones, 9/9/92, (PB93-150266, A08, MF-A02).

NCEER-92-0024 "Seismic Behavior of Reinforced Concrete Frame Structures with Nonductile Details, Part I: Summary of Experimental Findings of Full Scale Beam-Column Joint Tests," by A. Beres, R.N. White and P. Gergely, 9/30/92, (PB93-227783, A05, MF-A01).

NCEER-92-0025 "Experimental Results of Repaired and Retrofitted Beam-Column Joint Tests in Lightly Reinforced Concrete Frame Buildings," by A. Beres, S. El-Borgi, R.N. White and P. Gergely, 10/29/92, (PB93-227791, A05, MF-A01).

NCEER-92-0026 "A Generalization of Optimal Control Theory: Linear and Nonlinear Structures," by J.N. Yang, Z. Li and S. Vongchavalitkul, 11/2/92, (PB93-188621, A05, MF-A01).

NCEER-92-0027 "Seismic Resistance of Reinforced Concrete Frame Structures Designed Only for Gravity Loads: Part I - Design and Properties of a One-Third Scale Model Structure," by J.M. Bracci, A.M. Reinhorn and J.B. Mander, 12/1/92, (PB94-104502, A08, MF-A02).

NCEER-92-0028 "Seismic Resistance of Reinforced Concrete Frame Structures Designed Only for Gravity Loads: Part II - Experimental Performance of Subassemblages," by L.E. Aycardi, J.B. Mander and A.M. Reinhorn, 12/1/92, (PB94-104510, A08, MF-A02).

NCEER-92-0029 "Seismic Resistance of Reinforced Concrete Frame Structures Designed Only for Gravity Loads: Part III - Experimental Performance and Analytical Study of a Structural Model," by J.M. Bracci, A.M. Reinhorn and J.B. Mander, 12/1/92, (PB93-227528, A09, MF-A01).

NCEER-92-0030 "Evaluation of Seismic Retrofit of Reinforced Concrete Frame Structures: Part I - Experimental Performance of Retrofitted Subassemblages," by D. Choudhuri, J.B. Mander and A.M. Reinhorn, 12/8/92, (PB93-198307, A07, MF-A02).

NCEER-92-0031 "Evaluation of Seismic Retrofit of Reinforced Concrete Frame Structures: Part II - Experimental Performance and Analytical Study of a Retrofitted Structural Model," by J.M. Bracci, A.M. Reinhorn and J.B. Mander, 12/8/92, (PB93-198315, A09, MF-A03).

NCEER-92-0032 "Experimental and Analytical Investigation of Seismic Response of Structures with Supplemental Fluid Viscous Dampers," by M.C. Constantinou and M.D. Symans, 12/21/92, (PB93-191435, A10, MF-A03). This report is available only through NTIS (see address given above).

NCEER-92-0033 "Reconnaissance Report on the Cairo, Egypt Earthquake of October 12, 1992," by M. Khater, 12/23/92, (PB93-188621, A03, MF-A01).

NCEER-92-0034 "Low-Level Dynamic Characteristics of Four Tall Flat-Plate Buildings in New York City," by H. Gavin, S. Yuan, J. Grossman, E. Pekelis and K. Jacob, 12/28/92, (PB93-188217, A07, MF-A02).

NCEER-93-0001 "An Experimental Study on the Seismic Performance of Brick-Infilled Steel Frames With and Without Retrofit," by J.B. Mander, B. Nair, K. Wojtkowski and J. Ma, 1/29/93, (PB93-227510, A07, MF-A02).

NCEER-93-0002 "Social Accounting for Disaster Preparedness and Recovery Planning," by S. Cole, E. Pantoja and V. Razak, 2/22/93, (PB94-142114, A12, MF-A03).

NCEER-93-0003 "Assessment of 1991 NEHRP Provisions for Nonstructural Components and Recommended Revisions," by T.T. Soong, G. Chen, Z. Wu, R-H. Zhang and M. Grigoriu, 3/1/93, (PB93-188639, A06, MF-A02).

NCEER-93-0004 "Evaluation of Static and Response Spectrum Analysis Procedures of SEAOC/UBC for Seismic Isolated Structures," by C.W. Winters and M.C. Constantinou, 3/23/93, (PB93-198299, A10, MF-A03).

NCEER-93-0005 "Earthquakes in the Northeast - Are We Ignoring the Hazard? A Workshop on Earthquake Science and Safety for Educators," edited by K.E.K. Ross, 4/2/93, (PB94-103066, A09, MF-A02).

NCEER-93-0006 "Inelastic Response of Reinforced Concrete Structures with Viscoelastic Braces," by R.F. Lobo, J.M. Bracci, K.L. Shen, A.M. Reinhorn and T.T. Soong, 4/5/93, (PB93-227486, A05, MF-A02).

NCEER-93-0007 "Seismic Testing of Installation Methods for Computers and Data Processing Equipment," by K. Kosar, T.T. Soong, K.L. Shen, J.A. HoLung and Y.K. Lin, 4/12/93, (PB93-198299, A07, MF-A02).

NCEER-93-0008 "Retrofit of Reinforced Concrete Frames Using Added Dampers," by A. Reinhorn, M. Constantinou and C. Li, to be published.

NCEER-93-0009 "Seismic Behavior and Design Guidelines for Steel Frame Structures with Added Viscoelastic Dampers," by K.C. Chang, M.L. Lai, T.T. Soong, D.S. Hao and Y.C. Yeh, 5/1/93, (PB94-141959, A07, MF-A02).

NCEER-93-0010 "Seismic Performance of Shear-Critical Reinforced Concrete Bridge Piers," by J.B. Mander, S.M. Waheed, M.T.A. Chaudhary and S.S. Chen, 5/12/93, (PB93-227494, A08, MF-A02).

NCEER-93-0011 "3D-BASIS-TABS: Computer Program for Nonlinear Dynamic Analysis of Three Dimensional Base Isolated Structures," by S. Nagarajaiah, C. Li, A.M. Reinhorn and M.C. Constantinou, 8/2/93, (PB94-141819, A09, MF-A02).

NCEER-93-0012 "Effects of Hydrocarbon Spills from an Oil Pipeline Break on Ground Water," by O.J. Helweg and H.H.M. Hwang, 8/3/93, (PB94-141942, A06, MF-A02).

NCEER-93-0013 "Simplified Procedures for Seismic Design of Nonstructural Components and Assessment of Current Code Provisions," by M.P. Singh, L.E. Suarez, E.E. Matheu and G.O. Maldonado, 8/4/93, (PB94-141827, A09, MF-A02).

NCEER-93-0014 "An Energy Approach to Seismic Analysis and Design of Secondary Systems," by G. Chen and T.T. Soong, 8/6/93, (PB94-142767, A11, MF-A03).

NCEER-93-0015 "Proceedings from School Sites: Becoming Prepared for Earthquakes - Commemorating the Third Anniversary of the Loma Prieta Earthquake," Edited by F.E. Winslow and K.E.K. Ross, 8/16/93, (PB94-154275, A16, MF-A02).

NCEER-93-0016 "Reconnaissance Report of Damage to Historic Monuments in Cairo, Egypt Following the October 12, 1992 Dahshur Earthquake," by D. Sykora, D. Look, G. Croci, E. Karaesmen and E. Karaesmen, 8/19/93, (PB94-142221, A08, MF-A02).

NCEER-93-0017 "The Island of Guam Earthquake of August 8, 1993," by S.W. Swan and S.K. Harris, 9/30/93, (PB94-141843, A04, MF-A01).

NCEER-93-0018 "Engineering Aspects of the October 12, 1992 Egyptian Earthquake," by A.W. Elgamal, M. Amer, K. Adalier and A. Abul-Fadl, 10/7/93, (PB94-141983, A05, MF-A01).

NCEER-93-0019 "Development of an Earthquake Motion Simulator and its Application in Dynamic Centrifuge Testing," by I. Krstelj, Supervised by J.H. Prevost, 10/23/93, (PB94-181773, A-10, MF-A03).

NCEER-93-0020 "NCEER-Taisei Corporation Research Program on Sliding Seismic Isolation Systems for Bridges: Experimental and Analytical Study of a Friction Pendulum System (FPS)," by M.C. Constantinou, P. Tsopelas, Y-S. Kim and S. Okamoto, 11/1/93, (PB94-142775, A08, MF-A02).

NCEER-93-0021 "Finite Element Modeling of Elastomeric Seismic Isolation Bearings," by L.J. Billings, Supervised by R. Shepherd, 11/8/93, to be published.

NCEER-93-0022 "Seismic Vulnerability of Equipment in Critical Facilities: Life-Safety and Operational Consequences," by K. Porter, G.S. Johnson, M.M. Zadeh, C. Scawthorn and S. Eder, 11/24/93, (PB94-181765, A16, MF-A03).

NCEER-93-0023 "Hokkaido Nansei-oki, Japan Earthquake of July 12, 1993, by P.I. Yanev and C.R. Scawthorn, 12/23/93, (PB94-181500, A07, MF-A01).

NCEER-94-0001 "An Evaluation of Seismic Serviceability of Water Supply Networks with Application to the San Francisco Auxiliary Water Supply System," by I. Markov, Supervised by M. Grigoriu and T. O'Rourke, 1/21/94, (PB94-204013, A07, MF-A02).

NCEER-94-0002 "NCEER-Taisei Corporation Research Program on Sliding Seismic Isolation Systems for Bridges: Experimental and Analytical Study of Systems Consisting of Sliding Bearings, Rubber Restoring Force Devices and Fluid Dampers," Volumes I and II, by P. Tsopelas, S. Okamoto, M.C. Constantinou, D. Ozaki and S. Fujii, 2/4/94, (PB94-181740, A09, MF-A02 and PB94-181757, A12, MF-A03).

NCEER-94-0003 "A Markov Model for Local and Global Damage Indices in Seismic Analysis," by S. Rahman and M. Grigoriu, 2/18/94, (PB94-206000, A12, MF-A03).

NCEER-94-0004 "Proceedings from the NCEER Workshop on Seismic Response of Masonry Infills," edited by D.P. Abrams, 3/1/94, (PB94-180783, A07, MF-A02).

NCEER-94-0005 "The Northridge, California Earthquake of January 17, 1994: General Reconnaissance Report," edited by J.D. Goltz, 3/11/94, (PB193943, A10, MF-A03).

NCEER-94-0006 "Seismic Energy Based Fatigue Damage Analysis of Bridge Columns: Part I - Evaluation of Seismic Capacity," by G.A. Chang and J.B. Mander, 3/14/94, (PB94-219185, A11, MF-A03).

NCEER-94-0007 "Seismic Isolation of Multi-Story Frame Structures Using Spherical Sliding Isolation Systems," by T.M. Al-Hussaini, V.A. Zayas and M.C. Constantinou, 3/17/94, (PB193745, A09, MF-A02).

NCEER-94-0008 "The Northridge, California Earthquake of January 17, 1994: Performance of Highway Bridges," edited by I.G. Buckle, 3/24/94, (PB94-193851, A06, MF-A02).

NCEER-94-0009 "Proceedings of the Third U.S.-Japan Workshop on Earthquake Protective Systems for Bridges," edited by I.G. Buckle and I. Friedland, 3/31/94, (PB94-195815, A99, MF-A06).

NCEER-94-0010 "3D-BASIS-ME: Computer Program for Nonlinear Dynamic Analysis of Seismically Isolated Single and Multiple Structures and Liquid Storage Tanks," by P.C. Tsopelas, M.C. Constantinou and A.M. Reinhorn, 4/12/94, (PB94-204922, A09, MF-A02).

NCEER-94-0011 "The Northridge, California Earthquake of January 17, 1994: Performance of Gas Transmission Pipelines," by T.D. O'Rourke and M.C. Palmer, 5/16/94, (PB94-204989, A05, MF-A01).

NCEER-94-0012 "Feasibility Study of Replacement Procedures and Earthquake Performance Related to Gas Transmission Pipelines," by T.D. O'Rourke and M.C. Palmer, 5/25/94, (PB94-206638, A09, MF-A02).

NCEER-94-0013 "Seismic Energy Based Fatigue Damage Analysis of Bridge Columns: Part II - Evaluation of Seismic Demand," by G.A. Chang and J.B. Mander, 6/1/94, (PB95-18106, A08, MF-A02).

NCEER-94-0014 "NCEER-Taisei Corporation Research Program on Sliding Seismic Isolation Systems for Bridges: Experimental and Analytical Study of a System Consisting of Sliding Bearings and Fluid Restoring Force/Damping Devices," by P. Tsopelas and M.C. Constantinou, 6/13/94, (PB94-219144, A10, MF-A03).

NCEER-94-0015 "Generation of Hazard-Consistent Fragility Curves for Seismic Loss Estimation Studies," by H. Hwang and J-R. Huo, 6/14/94, (PB95-181996, A09, MF-A02).

NCEER-94-0016 "Seismic Study of Building Frames with Added Energy-Absorbing Devices," by W.S. Pong, C.S. Tsai and G.C. Lee, 6/20/94, (PB94-219136, A10, A03).

NCEER-94-0017 "Sliding Mode Control for Seismic-Excited Linear and Nonlinear Civil Engineering Structures," by J. Yang, J. Wu, A. Agrawal and Z. Li, 6/21/94, (PB95-138483, A06, MF-A02).

NCEER-94-0018 "3D-BASIS-TABS Version 2.0: Computer Program for Nonlinear Dynamic Analysis of Three Dimensional Base Isolated Structures," by A.M. Reinhorn, S. Nagarajaiah, M.C. Constantinou, P. Tsopelas and R. Li, 6/22/94, (PB95-182176, A08, MF-A02).

NCEER-94-0019 "Proceedings of the International Workshop on Civil Infrastructure Systems: Application of Intelligent Systems and Advanced Materials on Bridge Systems," Edited by G.C. Lee and K.C. Chang, 7/18/94, (PB95-252474, A20, MF-A04).

NCEER-94-0020 "Study of Seismic Isolation Systems for Computer Floors," by V. Lambrou and M.C. Constantinou, 7/19/94, (PB95-138533, A10, MF-A03).

NCEER-94-0021 "Proceedings of the U.S.-Italian Workshop on Guidelines for Seismic Evaluation and Rehabilitation of Unreinforced Masonry Buildings," Edited by D.P. Abrams and G.M. Calvi, 7/20/94, (PB95-138749, A13, MF-A03).

NCEER-94-0022 "NCEER-Taisei Corporation Research Program on Sliding Seismic Isolation Systems for Bridges: Experimental and Analytical Study of a System Consisting of Lubricated PTFE Sliding Bearings and Mild Steel Dampers," by P. Tsopelas and M.C. Constantinou, 7/22/94, (PB95-182184, A08, MF-A02).

NCEER-94-0023 "Development of Reliability-Based Design Criteria for Buildings Under Seismic Load," by Y.K. Wen, H. Hwang and M. Shinozuka, 8/1/94, (PB95-211934, A08, MF-A02).

NCEER-94-0024 "Experimental Verification of Acceleration Feedback Control Strategies for an Active Tendon System," by S.J. Dyke, B.F. Spencer, Jr., P. Quast, M.K. Sain, D.C. Kaspari, Jr. and T.T. Soong, 8/29/94, (PB95-212320, A05, MF-A01).

NCEER-94-0025 "Seismic Retrofitting Manual for Highway Bridges," Edited by I.G. Buckle and I.F. Friedland, published by the Federal Highway Administration (PB95-212676, A15, MF-A03).

NCEER-94-0026 "Proceedings from the Fifth U.S.-Japan Workshop on Earthquake Resistant Design of Lifeline Facilities and Countermeasures Against Soil Liquefaction," Edited by T.D. O'Rourke and M. Hamada, 11/7/94, (PB95-220802, A99, MF-E08).

NCEER-95-0001 "Experimental and Analytical Investigation of Seismic Retrofit of Structures with Supplemental Damping: Part 1 - Fluid Viscous Damping Devices," by A.M. Reinhorn, C. Li and M.C. Constantinou, 1/3/95, (PB95-266599, A09, MF-A02).

NCEER-95-0002 "Experimental and Analytical Study of Low-Cycle Fatigue Behavior of Semi-Rigid Top-And-Seat Angle Connections," by G. Pekcan, J.B. Mander and S.S. Chen, 1/5/95, (PB95-220042, A07, MF-A02).

NCEER-95-0003 "NCEER-ATC Joint Study on Fragility of Buildings," by T. Anagnos, C. Rojahn and A.S. Kiremidjian, 1/20/95, (PB95-220026, A06, MF-A02).

NCEER-95-0004 "Nonlinear Control Algorithms for Peak Response Reduction," by Z. Wu, T.T. Soong, V. Gattulli and R.C. Lin, 2/16/95, (PB95-220349, A05, MF-A01).

NCEER-95-0005 "Pipeline Replacement Feasibility Study: A Methodology for Minimizing Seismic and Corrosion Risks to Underground Natural Gas Pipelines," by R.T. Eguchi, H.A. Seligson and D.G. Honegger, 3/2/95, (PB95-252326, A06, MF-A02).

NCEER-95-0006 "Evaluation of Seismic Performance of an 11-Story Frame Building During the 1994 Northridge Earthquake," by F. Naeim, R. DiSulio, K. Benuska, A. Reinhorn and C. Li, to be published.

NCEER-95-0007 "Prioritization of Bridges for Seismic Retrofitting," by N. Basöz and A.S. Kiremidjian, 4/24/95, (PB95-252300, A08, MF-A02).

NCEER-95-0008 "Method for Developing Motion Damage Relationships for Reinforced Concrete Frames," by A. Singhal and A.S. Kiremidjian, 5/11/95, (PB95-266607, A06, MF-A02).

NCEER-95-0009 "Experimental and Analytical Investigation of Seismic Retrofit of Structures with Supplemental Damping: Part II - Friction Devices," by C. Li and A.M. Reinhorn, 7/6/95, (PB96-128087, A11, MF-A03).

NCEER-95-0010 "Experimental Performance and Analytical Study of a Non-Ductile Reinforced Concrete Frame Structure Retrofitted with Elastomeric Spring Dampers," by G. Pekcan, J.B. Mander and S.S. Chen, 7/14/95, (PB96-137161, A08, MF-A02).

NCEER-95-0011 "Development and Experimental Study of Semi-Active Fluid Damping Devices for Seismic Protection of Structures," by M.D. Symans and M.C. Constantinou, 8/3/95, (PB96-136940, A23, MF-A04).

NCEER-95-0012 "Real-Time Structural Parameter Modification (RSPM): Development of Innervated Structures," by Z. Liang, M. Tong and G.C. Lee, 4/11/95, (PB96-137153, A06, MF-A01).

NCEER-95-0013 "Experimental and Analytical Investigation of Seismic Retrofit of Structures with Supplemental Damping: Part III - Viscous Damping Walls," by A.M. Reinhorn and C. Li, 10/1/95, (PB96-176409, A11, MF-A03).

NCEER-95-0014 "Seismic Fragility Analysis of Equipment and Structures in a Memphis Electric Substation," by J-R. Huo and H.H.M. Hwang, (PB96-128087, A09, MF-A02), 8/10/95.

NCEER-95-0015 "The Hanshin-Awaji Earthquake of January 17, 1995: Performance of Lifelines," Edited by M. Shinozuka, 11/3/95, (PB96-176383, A15, MF-A03).

NCEER-95-0016 "Highway Culvert Performance During Earthquakes," by T.L. Youd and C.J. Beckman, available as NCEER-96-0015.

NCEER-95-0017 "The Hanshin-Awaji Earthquake of January 17, 1995: Performance of Highway Bridges," Edited by I.G. Buckle, 12/1/95, to be published.

NCEER-95-0018 "Modeling of Masonry Infill Panels for Structural Analysis," by A.M. Reinhorn, A. Madan, R.E. Valles, Y. Reichmann and J.B. Mander, 12/8/95.

NCEER-95-0019 "Optimal Polynomial Control for Linear and Nonlinear Structures," by A.K. Agrawal and J.N. Yang, 12/11/95, (PB96-168737, A07, MF-A02).

NCEER-95-0020 "Retrofit of Non-Ductile Reinforced Concrete Frames Using Friction Dampers," by R.S. Rao, P. Gergely and R.N. White, 12/22/95, (PB97-133508, A10, MF-A02).

NCEER-95-0021 "Parametric Results for Seismic Response of Pile-Supported Bridge Bents," by G. Mylonakis, A. Nikolaou and G. Gazetas, 12/22/95, (PB97-100242, A12, MF-A03).

NCEER-95-0022 "Kinematic Bending Moments in Seismically Stressed Piles," by A. Nikolaou, G. Mylonakis and G. Gazetas, 12/23/95.

NCEER-96-0001 "Dynamic Response of Unreinforced Masonry Buildings with Flexible Diaphragms," by A.C. Costley and D.P. Abrams," 10/10/96.

NCEER-96-0002 "State of the Art Review: Foundations and Retaining Structures," by I. Po Lam, to be published.

NCEER-96-0003 "Ductility of Rectangular Reinforced Concrete Bridge Columns with Moderate Confinement," by N. Wehbe, M. Saiidi, D. Sanders and B. Douglas, 11/7/96, (PB97-133557, A06, MF-A02).

NCEER-96-0004 "Proceedings of the Long-Span Bridge Seismic Research Workshop," edited by I.G. Buckle and I.M. Friedland, to be published.

NCEER-96-0005 "Establish Representative Pier Types for Comprehensive Study: Eastern United States," by J. Kulicki and Z. Prucz, 5/28/96, (PB98-119217, A07, MF-A02).

NCEER-96-0006 "Establish Representative Pier Types for Comprehensive Study: Western United States," by R. Imbsen, R.A. Schamber and T.A. Osterkamp, 5/28/96, (PB98-118607, A07, MF-A02).

NCEER-96-0007 "Nonlinear Control Techniques for Dynamical Systems with Uncertain Parameters," by R.G. Ghanem and M.I. Bujakov, 5/27/96, (PB97-100259, A17, MF-A03).

NCEER-96-0008 "Seismic Evaluation of a 30-Year Old Non-Ductile Highway Bridge Pier and Its Retrofit," by J.B. Mander, B. Mahmoodzadegan, S. Bhadra and S.S. Chen, 5/31/96.

NCEER-96-0009 "Seismic Performance of a Model Reinforced Concrete Bridge Pier Before and After Retrofit," by J.B. Mander, J.H. Kim and C.A. Ligozio, 5/31/96.

NCEER-96-0010 "IDARC2D Version 4.0: A Computer Program for the Inelastic Damage Analysis of Buildings," by R.E. Valles, A.M. Reinhorn, S.K. Kunnath, C. Li and A. Madan, 6/3/96, (PB97-100234, A17, MF-A03).

NCEER-96-0011 "Estimation of the Economic Impact of Multiple Lifeline Disruption: Memphis Light, Gas and Water Division Case Study," by S.E. Chang, H.A. Seligson and R.T. Eguchi, 8/16/96, (PB97-133490, A11, MF-A03).

NCEER-96-0012 "Proceedings from the Sixth Japan-U.S. Workshop on Earthquake Resistant Design of Lifeline Facilities and Countermeasures Against Soil Liquefaction, Edited by M. Hamada and T. O'Rourke, 9/11/96, (PB97-133581, A99, MF-A06).

NCEER-96-0013 "Chemical Hazards, Mitigation and Preparedness in Areas of High Seismic Risk: A Methodology for Estimating the Risk of Post-Earthquake Hazardous Materials Release," by H.A. Seligson, R.T. Eguchi, K.J. Tierney and K. Richmond, 11/7/96.

NCEER-96-0014 "Response of Steel Bridge Bearings to Reversed Cyclic Loading," by J.B. Mander, D-K. Kim, S.S. Chen and G.J. Premus, 11/13/96, (PB97-140735, A12, MF-A03).

NCEER-96-0015 "Highway Culvert Performance During Past Earthquakes," by T.L. Youd and C.J. Beckman, 11/25/96, (PB97-133532, A06, MF-A01).

NCEER-97-0001 "Evaluation, Prevention and Mitigation of Pounding Effects in Building Structures," by R.E. Valles and A.M. Reinhorn, 2/20/97, (PB97-159552, A14, MF-A03).

NCEER-97-0002 "Seismic Design Criteria for Bridges and Other Highway Structures," by C. Rojahn, R. Mayes, D.G. Anderson, J. Clark, J.H. Hom, R.V. Nutt and M.J. O'Rourke, 4/30/97, (PB97-194658, A06, MF-A03).

NCEER-97-0003 "Proceedings of the U.S.-Italian Workshop on Seismic Evaluation and Retrofit," Edited by D.P. Abrams and G.M. Calvi, 3/19/97, (PB97-194666, A13, MF-A03).

NCEER-97-0004 "Investigation of Seismic Response of Buildings with Linear and Nonlinear Fluid Viscous Dampers," by A.A. Seleemah and M.C. Constantinou, 5/21/97, (PB98-109002, A15, MF-A03).

NCEER-97-0005 "Proceedings of the Workshop on Earthquake Engineering Frontiers in Transportation Facilities," edited by G.C. Lee and I.M. Friedland, 8/29/97, (PB98-128911, A25, MR-A04).

NCEER-97-0006 "Cumulative Seismic Damage of Reinforced Concrete Bridge Piers," by S.K. Kunnath, A. El-Bahy, A. Taylor and W. Stone, 9/2/97, (PB98-108814, A11, MF-A03).

NCEER-97-0007 "Structural Details to Accommodate Seismic Movements of Highway Bridges and Retaining Walls," by R.A. Imbsen, R.A. Schamber, E. Thorkildsen, A. Kartoum, B.T. Martin, T.N. Rosser and J.M. Kulicki, 9/3/97.

NCEER-97-0008 "A Method for Earthquake Motion-Damage Relationships with Application to Reinforced Concrete Frames," by A. Singhal and A.S. Kiremidjian, 9/10/97, (PB98-108988, A13, MF-A03).

NCEER-97-0009 "Seismic Analysis and Design of Bridge Abutments Considering Sliding and Rotation," by K. Fishman and R. Richards, Jr., 9/15/97, (PB98-108897, A06, MF-A02).

NCEER-97-0010 "Proceedings of the FHWA/NCEER Workshop on the National Representation of Seismic Ground Motion for New and Existing Highway Facilities," edited by I.M. Friedland, M.S. Power and R.L. Mayes, 9/22/97.

NCEER-97-0011 "Seismic Analysis for Design or Retrofit of Gravity Bridge Abutments," by K.L. Fishman, R. Richards, Jr. and R.C. Divito, 10/2/97, (PB98-128937, A08, MF-A02).

NCEER-97-0012 "Evaluation of Simplified Methods of Analysis for Yielding Structures," by P. Tsopelas, M.C. Constantinou, C.A. Kircher and A.S. Whittaker, 10/31/97, (PB98-128929, A10, MF-A03).

NCEER-97-0013 "Seismic Design of Bridge Columns Based on Control and Repairability of Damage," by C-T. Cheng and J.B. Mander, 12/8/97.

NCEER-97-0014 "Seismic Resistance of Bridge Piers Based on Damage Avoidance Design," by J.B. Mander and C-T. Cheng, 12/10/97.

NCEER-97-0015 "Seismic Response of Nominally Symmetric Systems with Strength Uncertainty," by S. Balopoulou and M. Grigoriu, 12/23/97, (PB98-153422, A11, MF-A03).

NCEER-97-0016 "Evaluation of Seismic Retrofit Methods for Reinforced Concrete Bridge Columns," by T.J. Wipf, F.W. Klaiber and F.M. Russo, 12/28/97.

NCEER-97-0017 "Seismic Fragility of Existing Conventional Reinforced Concrete Highway Bridges," by C.L. Mullen and A.S. Cakmak, 12/30/97, (PB98-153406, A08, MF-A02).

NCEER-97-0018 "Loss Asssessment of Memphis Buildings," edited by D.P. Abrams and M. Shinozuka, 12/31/97.

NCEER-97-0019 "Seismic Evaluation of Frames with Infill Walls Using Quasi-static Experiments," by K.M. Mosalam, R.N. White and P. Gergely, 12/31/97, (PB98-153455, A07, MF-A02).

NCEER-97-0020 "Seismic Evaluation of Frames with Infill Walls Using Pseudo-dynamic Experiments," by K.M. Mosalam, R.N. White and P. Gergely, 12/31/97.

NCEER-97-0021 "Computational Strategies for Frames with Infill Walls: Discrete and Smeared Crack Analyses and Seismic Fragility," by K.M. Mosalam, R.N. White and P. Gergely, 12/31/97, (PB98-153414, A10, MF-A02).

NCEER-97-0022 "Proceedings of the NCEER Workshop on Evaluation of Liquefaction Resistance of Soils," edited by T.L. Youd and I.M. Idriss, 12/31/97.

MCEER-98-0001 "Extraction of Nonlinear Hysteretic Properties of Seismically Isolated Bridges from Quick-Release Field Tests," by Q. Chen, B.M. Douglas, E.M. Maragakis and I.G. Buckle, 5/26/98.

MCEER-98-0002 "Methodologies for Evaluating the Importance of Highway Bridges," by A. Thomas, S. Eshenaur and J. Kulicki, 5/29/98.

MCEER-98-0003 "Capacity Design of Bridge Piers and the Analysis of Overstrength," by J.B. Mander, A. Dutta and P. Goel, 6/1/98.

MCEER-98-0004 "Evaluation of Bridge Damage Data from the Loma Prieta and Northridge, California Earthquakes," by N. Basoz and A. Kiremidjian, 6/2/98.

MCEER-98-0005 "Screening Guide for Rapid Assessment of Liquefaction Hazard at Highway Bridge Sites,"by T. L. Youd, 6/16/98.

MCEER-98-0006 "Structural Steel and Steel/Concrete Interface Details for Bridges," by P. Ritchie, N. Kauhl and J. Kulicki, 7/13/98.

MCEER-98-0007 "Capacity Design and Fatigue Analysis of Confined Concrete Columns," by A. Dutta and J.B. Mander, 7/14/98.

MCEER-98-0008 "Proceedings of the Workshop on Performance Criteria for Telecommunication Services Under Earthquake Conditions," edited by A.J. Schiff, 7/15/98.

MCEER-98-0009 "Fatigue Analysis of Unconfined Concrete Columns," by J.B. Mander, A. Dutta and J.H. Kim, 9/12/98.

MCEER-98-0010 "Centrifuge Modeling of Cyclic Lateral Response of Pile-Cap Systems and Seat-Type Abutments in Dry Sands," by A.D. Gadre and R. Dobry, 10/2/98.

MCEER-98-0011 "IDARC-BRIDGE: A Computational Platform for Seismic Damage Assessment of Bridge Structures," by A.M. Reinhorn, V. Simeonov, G. Mylonakis and Y. Reichman, 10/2/98.

MCEER-98-0012 "Experimental Investigation of the Dynamic Response of Two Bridges Before and After Retrofitting with Elastomeric Bearings," by D.A. Wendichansky, S.S. Chen and J.B. Mander, 10/2/98.

MCEER-98-0013 "Design Procedures for Hinge Restrainers and Hinge Sear Width for Multiple-Frame Bridges," by R. Des Roches and G.L. Fenves, 11/3/98, (PB99-140477, A13, MF-A03).

MCEER-98-0014 "Response Modification Factors for Seismically Isolated Bridges," by M.C. Constantinou and J.K. Quarshie, 11/3/98, (PB99-140485, A14, MF-A03).

MCEER-98-0015 "Proceedings of the U.S.-Italy Workshop on Seismic Protective Systems for Bridges," edited by I.M. Friedland and M.C. Constantinou, 11/3/98.

MCEER-98-0016 "Appropriate Seismic Reliability for Critical Equipment Systems: Recommendations Based on Regional Analysis of Financial and Life Loss," by K. Porter, C. Scawthorn, C. Taylor and N. Blais, 11/10/98.

MCEER-98-0017 "Proceedings of the U.S. Japan Joint Seminar on Civil Infrastructure Systems Research," edited by M. Shinozuka and A. Rose, 11/12/98.

MCEER-98-0018 "Modeling of Pile Footings and Drilled Shafts for Seismic Design," by I. PoLam, M. Kapuskar and D. Chaudhuri, 12/21/98.

MCEER-99-0001 "Seismic Evaluation of a Masonry Infilled Reinforced Concrete Frame by Pseudodynamic Testing," by S.G. Buonopane and R.N. White, 2/16/99.

MCEER-99-0002 "Response History Analysis of Structures with Seismic Isolation and Energy Dissipation Systems: Verification Examples for Program SAP2000," by J. Scheller and M.C. Constantinou, 2/22/99.

MCEER-99-0003 "Experimental Study on the Seismic Design and Retrofit of Bridge Columns Including Axial Load Effects," by A. Dutta, T. Kokorina and J.B. Mander, 2/22/99.

MCEER-99-0004 "Experimental Study of Bridge Elastomeric and Other Isolation and Energy Dissipation Systems with Emphasis on Uplift Prevention and High Velocity Near-source Seismic Excitation," by A. Kasalanati and M. C. Constantinou, 2/26/99.

MCEER-99-0005 "Truss Modeling of Reinforced Concrete Shear-flexure Behavior," by J.H. Kim and J.B. Mander, 3/8/99.

MCEER-99-0006 "Experimental Investigation and Computational Modeling of Seismic Response of a 1:4 Scale Model Steel Structure with a Load Balancing Supplemental Damping System," by G. Pekcan, J.B. Mander and S.S. Chen, 4/2/99.

MCEER-99-0007 "Effect of Vertical Ground Motions on the Structural Response of Highway Bridges," by M.R. Button, C.J. Cronin and R.L. Mayes, 4/10/99.

MCEER-98-0008 "Seismic Reliability Assessment of Critical Facilities: A Handbook, Supporting Documentation, and Model Code Provisions," by G.S. Johnson, R.E. Sheppard, M.D. Quilici, S.J. Eder and C.R. Scawthorn, 4/12/99

MCEER-99-0009 "Impact Assessment of Selected MCEER Highway Project Research on the Seismic Design of Highway Structures," by C. Rojahn, R. Mayes, D.G. Anderson, J.H. Clark, D'Appolonia Engineering, S. Gloyd and R.V. Nutt, 4/14/99.

MCEER-99-0010 "Site Factors and Site Categories in Seismic Codes," by R. Dobry, R. Ramos and M.S. Power, 7/19/99.

MCEER-99-0011 "Restrainer Design Procedures for Multi-Span Simply-Supported Bridges," by M.J. Randall, M. Saiidi, E. Maragakis and T. Isakovic, 7/20/99.

MCEER-99-0012 "Property Modification Factors for Seismic Isolation Bearings," by M.C. Constantinou, P. Tsopelas, A. Kasalanati and E. Wolff, 7/20/99.

MCEER-99-0013 "Critical Seismic Issues for Existing Steel Bridges," by P. Ritchie, N. Kauhl and J. Kulicki, 7/20/99.

MCEER-99-0014 "Nonstructural Damage Database," by A. Kao, T.T. Soong and A. Vender, 7/24/99, (PB2000-101407, A06, MF-A01).

MCEER-99-0015 "Guide to Remedial Measures for Liquefaction Mitigation at Existing Highway Bridge Sites," by H.G. Cooke and J. K. Mitchell, 7/26/99, (PB2000-101703, A11, MF-A03).

MCEER-99-0016 "Proceedings of the MCEER Workshop on Ground Motion Methodologies for the Eastern United States," edited by N. Abrahamson and A. Becker, 8/11/99.

MCEER-99-0017 "Quindío, Colombia Earthquake of January 25, 1999: Reconnaissance Report," by A.P. Asfura and P.J. Flores, 10/4/99.

MCEER-99-0018 "Hysteretic Models for Cyclic Behavior of Deteriorating Inelastic Structures," by M.V. Sivaselvan and A.M. Reinhorn, 11/5/99.

MCEER-99-0019 "Proceedings of the 7th U.S.- Japan Workshop on Earthquake Resistant Design of Lifeline Facilities and Countermeasures Against Soil Liquefaction," edited by T.D. O'Rourke, J.P. Bardet and M. Hamada, 11/19/99.

MCEER-99-0020 "Development of Measurement Capability for Micro-Vibration Evaluations with Application to Chip Fabrication Facilities," by G.C. Lee, Z. Liang, J.W. Song, J.D. Shen and W.C. Liu, 12/1/99.

MCEER-99-0021 "Design and Retrofit Methodology for Building Structures with Supplemental Energy Dissipating Systems," by G. Pekcan, J.B. Mander and S.S. Chen, 12/31/99.